https://doi.org/10.15388/vu.thesis.768
https://orcid.org/0000-0003-1994-2121

VILNIUS UNIVERSITY
CENTER FOR PHYSICAL SCIENCES AND TECHNOLOGY

Liepa Pastarnokienė

Development and Research of Advanced Eco-Friendly Anti-Corrosion Epoxy Coatings

DOCTORAL DISSERTATION

Natural Sciences,
Chemistry (N 003)

VILNIUS 2025

The dissertation was prepared between 2020 and 2024 at Vilnius University. The research was supported by Research Council of Lithuania.

Academic supervisor:
Assoc. Prof. Dr. Tatjana Kochanė (Vilnius University, Natural Sciences, Chemistry – N 003).
Academic consultant:
Prof. Dr. Ričardas Makuška (Vilnius University, Natural Sciences, Chemistry – N 003).

Chairman – Assoc. Prof. Dr. Vaidas Klimkevičius (Vilnius University, Natural Sciences, Chemistry – N 003).
Members:
Assoc. Prof. Dr. Eglė Fataraitė-Urbonienė (Kaunas Technology University, Technological Sciences, Materials Engineering – T 008),
Dr. Tatjana Kavleiskaja (Vilnius University, Natural Sciences, Chemistry – N 003),
Dr. Teresė Rauckytė-Žak (University of Science and Technology in Bydgoszcz, Natural Sciences, Chemistry – N 003)
Assoc. Prof. Dr. Denis Sokol (Vilnius University, Natural Sciences, Chemistry – N 003).

The dissertation shall be defended at a public meeting of the Dissertation Defence Panel at 2 p. m. on 13th of June 2025 in Inorganic Chemistry Auditorium of the Institute of Chemistry of the Faculty of Chemistry and Geosciences (Vilnius University). Address: Naugarduko Str. 24, 141, Vilnius, Lithuania, phone: +370 (5) 219 3105; e-mail: info@chgf.vu.lt.

The text of this dissertation can be accessed at the **Vilnius University library**, as well as on the website of Vilnius University:
www.vu.lt/lt/naujienos/ivykiu-kalendorius

https://doi.org/10.15388/vu.thesis.768
https://orcid.org/0000-0003-1994-2121

VILNIAUS UNIVERSITETAS
FIZINIŲ IR TECHNOLOGIJOS MOKSLŲ CENTRAS

Liepa Pastarnokienė

Pažangių ekologiškų antikorozinių epoksidinių dangų kūrimas ir tyrimas

DAKTARO DISERTACIJA

Gamtos mokslai,
Chemija (N 003)

VILNIUS 2025

Disertacija rengta 2020–2024 metais, Vilniaus universitete.
Mokslinius tyrimus rėmė Lietuvos mokslo taryba.

Mokslinė vadovė
Doc. dr. Tatjana Kochanė (Vilniaus universitetas, gamtos mokslai, chemija – N 003).
Mokslinis konsultantas
Prof. dr. Ričardas Makuška (Vilniaus universitetas, gamtos mokslai, chemija – N 003).

Gynimo taryba:
Pirmininkas – doc. dr. Vaidas Klimkevičius (Vilniaus universitetas, gamtos mokslai, chemija – N 003).
Nariai:
doc. dr. Eglė Fataraitė-Urbonienė (Kauno technologijos universitetas, technologijos mokslai, medžiagų inžinerija – T 008),
dr. Tatjana Kavleiskaja (Vilniaus universitetas, gamtos mokslai, chemija – N 003),
dr. Teresė Rauckytė-Žak (Bydgoščiaus Jono ir Andriaus Sniadeckių technikos ir gamtos mokslų universitetas, gamtos mokslai, chemija – N 003),
doc. dr. Denis Sokol (Vilniaus universitetas, gamtos mokslai, chemija – N 003).

Disertacija ginama viešame Gynimo tarybos posėdyje 2025 m. birželio 13 d. 14.00 val. Vilniaus universiteto Chemijos ir geomokslų fakulteto Chemijos instituto Neorganinės chemijos auditorijoje. Adresas: Naugarduko g. 24, 141, Vilnius, Lietuva, tel. +370 (5) 219 3105; el. paštas info@chgf.vu.lt.

Disertaciją galima peržiūrėti Vilniaus universiteto bibliotekoje ir VU interneto svetainėje adresu:
https://www.vu.lt/naujienos/ivykiu-kalendorius

LIST OF ABBREVATIONS

ΔT	Cure interval/Kietėjimo temperatūros intervalas
ΔH_R	Total reaction heat (enthalpy)/Kietėjimo reakcijos entalpija
3ITT	Three-interval thixotropy test
AGE	C12-C14 alkyl glycidyl ether/C12-C14 alkilglicidileteris
AHEW	Active hydrogen equivalent weight
BDGE	1,4-Butanediol diglycidyl ether/1,4-Butanedioldiglicidileteris
CHDGE	Cyclohexandiol diglycidyl ether
CNSL	Cashew nutshell liquid/Anakardžių riešutų kevalų skystis
CO_2	Carbon dioxide
DETA	Diethylenetriamine
DGA	Diglycidyl aniline
DMAPA	Dimethylaminopropylamine/Dimetilaminopropilaminas
DMDC	4,4'-Methylenebis(2-methylcyclohexylamine)
DMP	2,4,6-Tris[(dimethylamino)methyl]phenol/2,4,6-Tri[(dimetilamino)metil] fenolis
DSC	Differential scanning calorimetry/Diferencinė skenuojamoji kalorimetrija
EDA	1,2-Ethanediamine/1,2-Etandiaminas
EEW	Epoxy equivalent weight
FT-IR	Fourier-transform infrared spectroscopy
G'	Storage modulus/Kaupimo modulis
G''	Loss modulus/Nuostolių modulis
GA	Gum Arabic/Gumarabikas
GPTE	Glycerol propoxylate triglycidyl ether/Glicerolio propoksilatriglicidileteris
η	Dinamic viscosity
HDE	1,6-Hexandiol diglycidyl ether/1,6-Heksandioldiglicidileteris
HDI	Hexamethylene diisocyanate
IPDI	Isophorone diisocyanate/Izoforondiizocianatas
M_w	Molecular weight
MXDA	m-Xylylenediamine/m-Ksililendiaminas
OM	Optical microscope/Optinis mikroskopas
ρ	Density
PA	Part A (in this work epoxy part of the composition)
PAAE	Polyaspartic acid ester/Poliasparto rūgšties esteris
PACM	para-Diaminodicyclohexylmethane
PB	Part B (in this work amine part of the composition)
PCL	Polycaprolactone
PhA	Phenalkamine/Fenalkaminai

phr	Parts per hundred
PMMA	Polymethylmethacrylate
PU	Polyurea/Poliurėja
PUF	Poly(urea-formaldehyde)
PUR	Polyurethane
PVA	Polyvinyl alcohol/Polivinilalkoholis
RD	Reactive diluent/Reaktyvūs skiedikliai
SDBS	Sodium dodecylbenzenesulfonate/Natrio dodecilbenzensulfonatas
SEM	Scanning electron microscope/Skenuojantis elektroninis mikroskopas
SMA	Styrene-maleic anhydride copolymer
SNR	Signal-to-noise ratio/Signalo ir triukšmo santykis
tanδ	Loss factor/Nuostolių faktorius
TCCM	True color confocal microscope
TDCB	Tapered double cantilever beam
TEPA	Tetraethylenepentamine/Tetraetilenpentaminas
TETA	Triethylenetetramine/Trietilentetraminas
T_g	Glass transition temperature/Stiklėjimo temperatūra
TGA	Thermogravimetric analysis
T_i	Initial curing temperature/Pradinė reakcijos temperatūra
TIPTP	Tris(4-isocyanato phenyl)thiophosphate/Tri(4-izocianato fenil)tiofosfatas
TMD	2,2,4-Trimethylhexane-1,6-diamine/2,2,4-Trimetilheksan-1,6-diaminas
TMGE	Trimethylpropane glycidyl ether
T_p	Peak curing temperature
T_t	Terminal curing temperature
UV	Ultraviolet radiation
VOC	Volatile organic compound/Lakūs organiniai junginiai
W/O/W	Water-in-oil-in-water

CONTENTS

INTRODUCTION

Corrosion is a pervasive issue that poses significant challenges to the longevity and structural integrity of metallic substrates. To combat this phenomenon, anti-corrosion coatings are employed worldwide to mitigate the deterioration caused by moisture, chemicals, and environmental salts. These coatings play a vital role in extending the service life of metals by forming a protective barrier that inhibits the penetration of corrosive agents. The formulations of these coatings often include polymers such as polyurethanes, alkyds, acrylics, epoxies, and aspartic acid esters, which contribute to their effectiveness and versatility (Fig. 1). The global market for anti-corrosion coatings is substantial, with an estimated value ranging between \$30 and \$40 billion USD, driven by consistent annual growth [1].

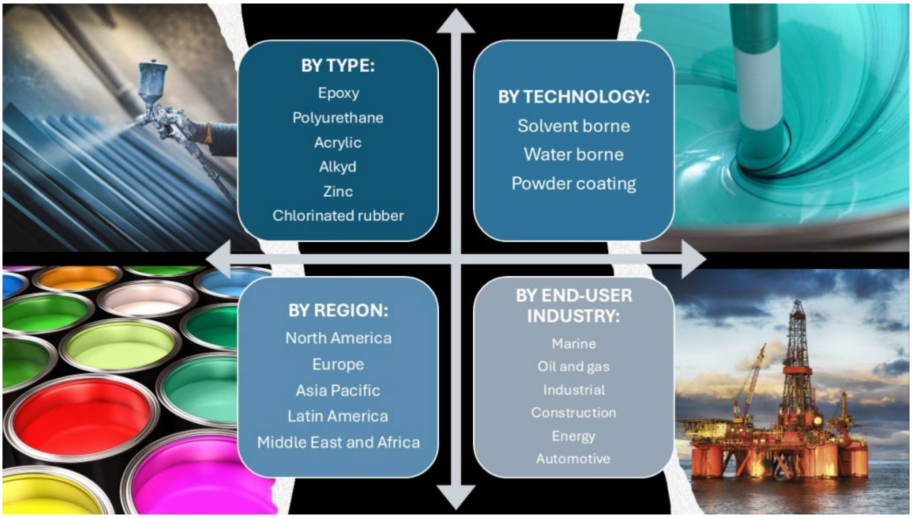

Fig. 1. Global anti-corrosion coating market

Among these coatings, epoxy-based systems stand out due to their multifaceted protective capabilities. Epoxy coatings not only offer robust corrosion resistance but can also be tailored for enhanced mechanical and environmental performance. Depending on their formulation, these coatings can exhibit elasticity for impact resistance, hardness for superior abrasion and weather resistance, or hydrophobic properties to repel moisture and pollutants [2–4]. Additionally, epoxy coatings are known for their remarkable chemical and thermal stability, with the ability to cure at subzero temperatures while maintaining their functional properties [5, 6]. Advanced formulations can endure prolonged exposure, ensuring durability and service life of up to 15–20 years without significant degradation.

The evolving regulatory landscape, driven by heightened environmental awareness, has placed increased emphasis on reducing the ecological and health impacts of paints and coatings. The primary toxic substances in epoxy coating formulations are low molecular weight amines, which are used as hardeners. As an alternative, less toxic hardeners are being introduced – bio-based phenalkamines (PhA) synthesized from substances found in renewable natural sources, such as cashew nutshell liquid (CNSL) [7, 8]. Cardanol-based PhA hardeners exhibit hydrophobic properties and the ability to cure epoxy resins even at low temperatures and in humid climate conditions [8–10].

Additionally, manufacturers are adapting to stringent regulations by developing formulations that minimize or eliminate volatile organic compounds (VOC) [11–13]. A prominent trend in this context is the shift toward high-solids coatings, which incorporate minimal or no volatile components, thereby reducing environmental harm. These coatings often utilize reactive diluents (RD) as a substitute for traditional solvents. RD not only facilitate the reduction of viscosity but also contribute to the solid content of the composition by undergoing chemical reactions, ensuring that they remain within the cured coating [14–16].

Amidst these advancements, smart self-healing coatings have gained considerable attention for their potential to reduce material waste and extend product lifespans. Various self-healing mechanisms have been investigated, including the release of encapsulated healing agents, the formation of reversible chemical bonds, and the use of nanoparticles with migration capabilities [17, 18]. Of these, the release of healing agents has emerged as a leading strategy, offering a well-documented and practical approach to addressing the challenges of durability and sustainability in modern coatings [19].

Novelty and originality of this work.

This study introduces innovative approaches to sustainable epoxy coatings by exploring novel bio-based materials and advanced self-healing technologies.

To harden epoxy resins, low molecular weight amines derived from petroleum compounds, which are highly toxic and harmful not only to the environment but also to human health, are commonly used. In order to reduce toxicity and improve environmental sustainability, the effectiveness of phenalkamine-based bio-derived amines in curing bisphenol A-based epoxy resins was evaluated. Kinetic studies of the reactions between bisphenol A and low molecular weight amines, as well as PhA-based curing agents, were conducted for the first time to determine and compare their thermal efficiency, degree of curing, and pot-life using differential scanning calorimetry (DSC) and rheological methods.

Volatile organic compounds are often used in epoxy coating formulations due to their ability to reduce costs and viscosity of epoxy-based coatings. However, these volatile components evaporate, increasing air pollution and posing health risks. To reduce the VOC content in coatings, a new emerging alternative – reactive diluents – was explored. Due to the presence of epoxy functional groups, RDs can react with amine-based hardeners intended for epoxy systems, remaining chemically bound within the coating during formation. To assess the impact of RDs on epoxy formulations and their curing process, the gelation and vitrification times of the forming coatings were examined, and the viscosity was determined using a rotational rheometer. Additionally, mechanical tests were performed to evaluate the influence of RDs on the properties of the cured coatings.

One of the key achievements of this work is the development of a novel microencapsulation technology, which enabled the synthesis of polyaspartic acid ester (PAAE) microcapsules with a wall formed under ultraviolet (UV) light. This method is applied for the first time in the encapsulation of PAAE. UV polymerization for microcapsule formation provides a significant advantage due to the very rapid synthesis process. The encapsulation process of isophorone diisocyanate (IPDI) into a polyurea (PU) shell was improved, resulting in a high encapsulated material content. To optimize the efficiency of PAAE and IPDI microcapsule production, the Taguchi experimental design method was employed – a technique particularly useful for optimizing synthesis conditions yet rarely seen in publications related to microcapsule synthesis. Finally, a dual microcapsule system was developed, and these microcapsules were incorporated into epoxy coating formulations to create advanced self-healing coatings.

The aim of this work was to develop zero VOC based anticorrosive coatings using environmentally less harmful curing agents, reactive diluents, and to investigate the use of a dual microcapsule system for the production of self-healing coatings. The tasks to achieve the main goal were formulated as follows:

1. Evaluate the effect of bio-based phenalkamine hardeners on curing kinetics of anti-corrosion epoxy coatings.
2. Evaluate the effect of reactive diluents on curing and properties of anti-corrosion epoxy coating.

3. Optimize the encapsulation process of polyaspartic acid ester in UV curable polyacrylate shell using the Taguchi method of experimental design.
4. Optimize the encapsulation process of isophorone diisocyanate into polyurea shell using the Taguchi method of experimental design.
5. Develop smart self-healing anti-corrosion epoxy coatings using dual microcapsule system.

1. LITERATURE OVERVIEW

1.1. Anti-corrosion coatings

Anti-corrosion coatings are engineered to endure diverse environmental conditions, including UV radiation, chemically intensive industrial zones, exposure to precipitation and fertilizers, subterranean environments with bacterial activity, high humidity, and immersion in oceanic conditions characterized by wave impact, wind forces, and elevated salinity. The specific requirements and classifications for anti-corrosion coatings across various environmental contexts are defined in the international standard ISO 12944:2019, titled *"Coatings and Varnishes – Corrosion Protection of Steel Structures by Protective Coating Systems"* [20]. Based on the range of exposures encountered, anti-corrosion coatings are categorized into six distinct corrosivity classes, as outlined in Table 1.

Table 1. Corrosivity categories by environmental impact

Corrosion category	**Steel corrosion rate (First year)**	**Interior**	**Exterior**
C1 Very Low	<1.3 µm	Heated buildings with clean atmosphere: office, shop, hotel, school	-
C2 Low	1.3-25 µm	Unheated buildings, where condensation can occur: sports hall, depots	Atmospheres with low levels of pollution. Mostly rural areas
C3 Medium	25-50 µm	Production rooms with high humidity, and air pollution: laundry, breweries, dairies	Urban and industrial atmospheres, moderate sulfur dioxide pollution, coastal areas with low salinity
C4 High	50-80 µm	Chemical plants, swimming pools, coastal ships and boatyards	Industrial areas and coastal areas with moderate salinity
C5 Very High	80-200 µm	Buildings or areas with almost permanent condensation and high pollution	Industrial areas with high humidity and aggressive atmosphere. Coastal areas with high salinity
CX Extreme	200-700 µm	Industrial areas with extreme air humidity and aggressive atmosphere	Offshore areas with high salinity and industrial areas with extreme air humidity subtropical and tropical atmosphere.

Anti-corrosion coatings are typically classified based on the mechanisms by which they prevent corrosion on metal surfaces. These coatings employ three fundamental protective mechanisms [21]:

- Barrier protection. Corrosion protection is achieved by applying a coating system that restricts the penetration of corrosive species into the substrate surface through its low permeability to liquids, gases, and ions.
- Substrate surface passivation (inhibitive effect). Protection can be accomplished through the formation of a chemical conversion layer or by incorporating inhibitive pigments into the coating.
- Sacrificial protection (galvanic effect). This mechanism of protection is widely used in metallic, organic, and inorganic coatings, and involves protecting the substrate by the sacrificial corrosion of a more electrochemically active metal that is in electrical contact with the substrate.

An anti-corrosion coating system typically comprises multiple layers of coatings, each designed with specific properties and functions. Depending on the performance requirements, these layers may consist of metallic, inorganic, or organic coatings [21].

In highly corrosive marine environments, a standard anti-corrosion system usually includes a primer, one or more intermediate coats, and a topcoat (Fig. 2) [22].

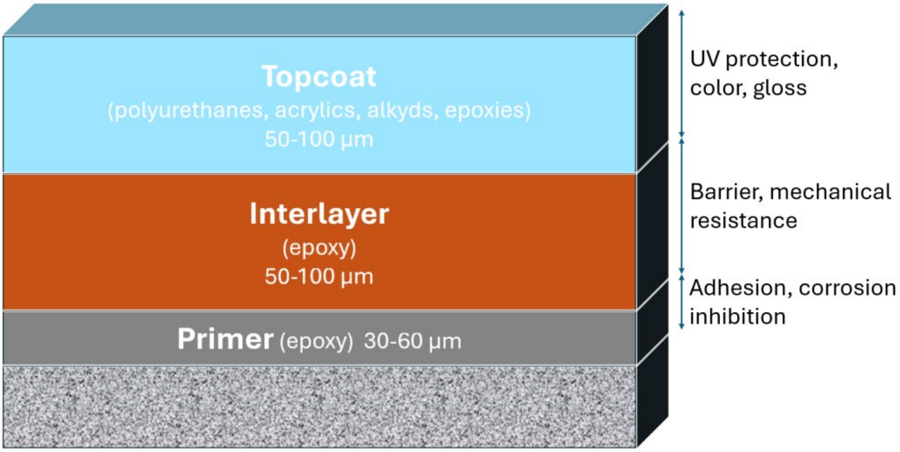

Fig. 2. Anti-corrosion coating system

The primary function of the primer is to protect the substrate from corrosion and ensure strong adhesion. For this purpose, metallic zinc or corrosion-inhibitive pigments are often incorporated into primers, especially for structures located in splash zones or atmospheric conditions [23], [24], [25].

The intermediate coat serves to build up the coating system's thickness and acts as a barrier to prevent the penetration of corrosive species to the substrate. It also ensures good adhesion between the primer and the topcoat [26].

The topcoat, which is directly exposed to the external environment, must provide the desired color and gloss while offering protection against varying weather conditions and physical impacts. Additionally, the topcoat requires high resistance to UV radiation. Environmental factors such as moisture, temperature fluctuations, and UV radiation can lead to degradation of the coating, ultimately reducing its lifespan [21, 27].

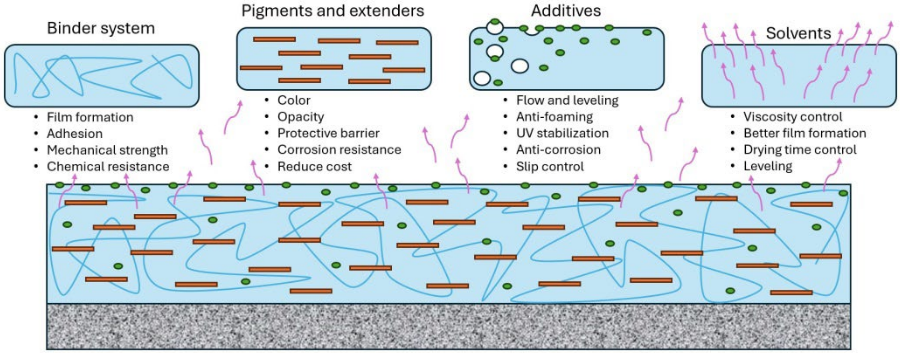

Fig. 3. Components in coating

The appropriate selection and combination of components and process steps can result in an anti-corrosion coating system that provides long-lasting protection against environmental elements while maintaining aesthetic qualities. Coatings can be formulated using a diverse range of chemicals and materials or combinations thereof, with each component serving a specific function. The primary categories of components in coatings include pigments, binders, extenders, additives, and solvents (Fig. 3) [28].

1.1.1.Epoxy-amine coatings

Epoxy resins, the principal component of epoxy coatings, represent a versatile class of materials characterized by their high reactivity and excellent mechanical, electrical, chemical, thermal, and anti-corrosion properties [29, 30]. These attributes make epoxy resins suitable for a broad range of applications, including paints and coatings [31–33], adhesives [34–37], industrial tooling [38–40], aerospace components [41–43], electronic materials [44–46], and biomaterials [47–49].

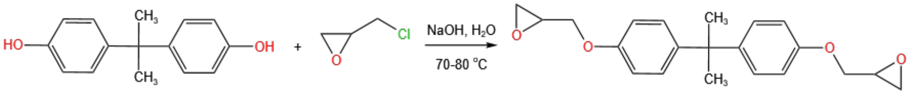

Fig. 4. Formation of epoxy resin

Epoxy resins are synthesized via a condensation reaction between diphenyl propane derivatives and epichlorohydrin (Fig. 4) [50]. The most used precursor to produce solvent-borne epoxy resins is bisphenol A, which results from the reaction of phenols with acetone. Other precursors, such as bisphenol F (formed from phenols and formaldehyde), and modified epoxy resins, including epoxy esters and epoxy-functional silanes, have been developed to address specific application requirements. For particularly aggressive environments, epoxy novolac resins are preferred due to their superior chemical resistance (Fig. 5) [2]. This enhanced resistance is attributed to the higher density of epoxy groups per molecule in novolac resins compared to bisphenol A or bisphenol F epoxy resins, resulting in a more tightly crosslinked and durable coating.

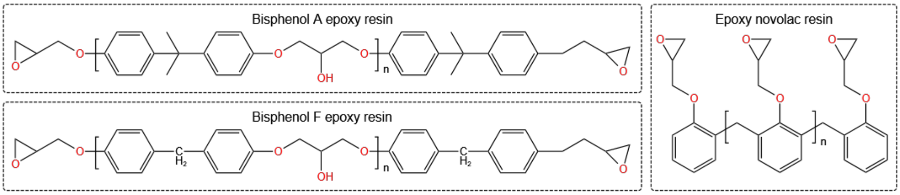

Fig. 5. Types of epoxy resins

Due to their high reactivity, epoxy resin pre-polymers or polymers containing epoxide groups can react with a variety of co-reactants, including high and low molecular weight aliphatic and aromatic amines, acid derivatives, amides, anhydrides, esters, and thiols, forming cross-linked structures [2]. Cycloaliphatic amines have traditionally been used as curing agents for epoxy resins due to their excellent corrosion resistance, though their availability is decreasing. Alternatives such as polyamines and amides, often used in combination, are becoming more common to optimize film formation and improve coating properties. The toxicity associated with amine curing agents has led manufacturers to develop coatings where an initial amine-epoxy adduct is formed, with additional epoxy resin required to complete the curing process [51].

PhA is a relatively new class of curing agents for epoxy resins, widely used in protective coatings. Advantages of these curing agents are related to low/room temperature curing applications, good moisture tolerance and good surface appearance of the coatings [8–10]. PhA are bio-based amines synthesized from cardanol refined from renewable material, CNSL (Fig. 6) [7, 8].

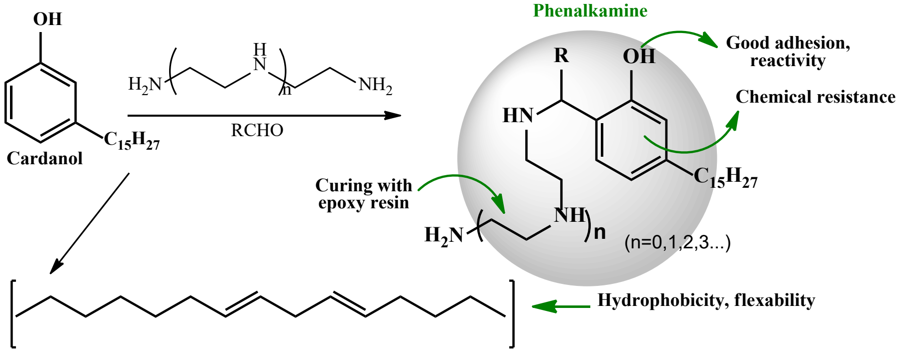

Fig. 6. The synthesis and structure–property relationship of phenalkamines [52]

The distinctive structure of PhA has some effect on properties of the resulting paints and coatings. Due to the long aliphatic alkyl side chain of cardanol, PhA-containing paints are characterized by lower viscosity and surface tension, and improved wetting properties; resulting coatings possess good flexibility and hydrophobicity, and improved water resistance. The aromatic backbone of PhA gives excellent chemical resistance. Side chains of PhA containing amino- and iminogroups, react easily with the epoxy groups giving highly cross-linked products. High activity of PhA even at ambient temperature as well as good adhesion is related to the presence of the phenolic hydroxyl group. Furthermore, PhA hardeners are known for low toxicity, which makes them eco-friendly [10, 53].

Curing low-molecular-weight epoxy resins with amine hardeners typically results in tightly cross-linked materials with a high glass transition temperature (T_g) [54]. PhA can be effectively used as an eco-friendly solution to reduce the brittleness and T_g of cured epoxy resins. The curing mechanism and properties of the epoxy coatings depend on the PhA structure, molecular weight and the amount of amine groups.

1.1.2.Solvent-free coatings

Solvent-borne coatings are a vital part of the coating industry and are widely used in various segments [55–58]. Formulations for such coatings contain organic solvents, most of them with relatively low boiling point, which are referred to as VOC [58]. VOC are unsafe, harmful to the human body, and cause environmental pollution. Since environmental requirements are increasing, a demand for the coating's formulations with very low VOC and for the solvent-free coating systems is becoming essential. Solvent-free epoxy resin coatings not only solve environmental issues but also improve some coatings properties like stability and strength [59, 60].

To avoid problems associated with VOC, the use of RDs in solvent-borne coatings instead of organic solvents was proposed and realized [61]. RDs are substances that contain reactive groups and take part in reactions with a hardener becoming integral part of a coating during curing [62]. The essential requirements to RD are low viscosity, compatibility with the base resin, low volatility, non-toxicity, and the ability to participate in the curing process [63–65]. The addition of RD reduces viscosity of resins, allows the addition of more fillers, improves the wetting behavior, and facilitates film-forming process. RDs are categorized as monofunctional and polyfunctional.

Most monofunctional RDs are excellent in reducing viscosity but cause a decrease in the crosslink density of the resin, which affects mechanical properties of the coatings. Reaction behavior of polyfunctional RD is considered to be similar to that of the basic epoxy components, which means that they do not affect the crosslink density [66–68]. Among the RDs, those with epoxy groups are the most important for VOC-free (or very low VOC) epoxy coatings. Usually, they are compatible with the base resin, do not produce VOC during curing, and therefore are more environmentally friendly than non-reactive diluents [69].

The effect of difunctional RD 1,4-butanediol diglycidyl ether (BDGE), cyclohexandiol diglycidyl ether (CHDGE), and diglycidyl aniline (DGA) on epoxy systems was studied by differential scanning calorimetry (DSC) [70–73]. It was determined that the presence of DGA decreased the apparent activation energy of the curing process. Contrarily, the addition of BDGE increased the value of E_a and the reaction exponent. Moreover, the addition of BDGE increased the efficiency of the curing process, curing degree, and T_g of the cured coatings [72].

In order to evaluate the effect of functionality of RD, rheological behavior and curing of RD containing epoxy resins, as well as mechanical and physical properties of epoxy coatings were investigated [66]. As additives to epoxy resin formulations, three RD were used: monofunctional C12-C14 alkyl glycidyl ether (AGE), difunctional 1,6-hexandiol diglycidyl ether (HDE) and trifunctional trimethyl propane glycidyl ether (TMGE). The highest viscosity was characteristic for the epoxy resin mixture containing trifunctional TMGE while the viscosity of the mixtures containing AGE or HDE was similar and lower. Addition of RD improved workability and usually increased pot-life (the period of time during which mixed coating formulation remains usable, usually considered as time until which the viscosity of a paint doubles) of the epoxy resins; in some cases, addition of the trifunctional TMGE slightly reduced pot-life of the system. The longest pot-life of the epoxy system was obtained using monofunctional AGE. The presence of difunctional HDE and trifunctional TMGE significantly increased compressive and flexural strength of the epoxy coatings. Addition of RD irrespective of their functionality decreased adhesion of the epoxy coatings.

The same RD were used in another study [63] evaluating their effect on viscosity of the epoxy resins, and physical and mechanical properties of the epoxy coatings. The epoxy mixture containing trifunctional TMGE exhibited the fastest curing and the shortest film drying time. The best mechanical properties of the epoxy coatings were obtained using epoxy mixtures containing 12% RD, irrespective of functionality. The presence of difunctional HDE increased molecular chain flexibility and impact strength of the coatings, while the presence of TMGE increased brittleness and decreased impact resistance of the coatings.

1.2. Self-healing coatings

Polymeric coatings are utilized as barrier layers to protect substrates from environmental impacts. For effective protection, the coating must maintain its adhesion, structural integrity, and resist degradation under operational conditions, such as mechanical stress, wear, pH variations, surface tension, and temperature changes [74, 75]. However, over time, these factors can lead to scratches, surface and internal microcracks, or even delamination, prompting the search for solutions to mitigate environmental interactions [75, 76]. Self-healing coatings possess the ability to autonomously or externally stimulate "repair" damage, either fully or partially, which extends their service life and reduces maintenance costs [77, 78].

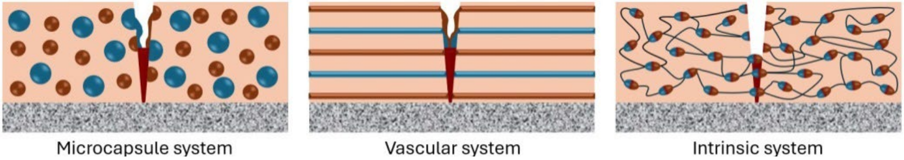

Fig. 7. Self-healing systems

Contemporary self-healing polymer technologies offer the potential to develop safer, more durable, and resilient materials for various industries, including coatings, electronics, and energy applications [77]. Self-healing systems can be categorized into three main types: capsule-based systems, vascular systems, and intrinsic self-healing systems (Fig. 7) [77].

In capsule-based systems self-healing of materials can occur when capsules containing an active agent are embedded within the material [75, 79, 80]. When the material, along with the embedded capsules, is damaged, the active component inside the capsules is released and reacts at the damage site with active substances either present in the material itself or in other types of capsules. After healing, the entire content of the capsule is consumed, and it cannot be replenished.

A similar mechanism operates in vascular systems using capillaries: hollow capillaries filled with an active agent can be incorporated into the matrix, creating one-dimensional, two-dimensional, or three-dimensional self-healing materials [79]. When a capillary is damaged, and the active component is used up for healing, it can be replenished externally. Moreover, if further damage occurs, the active agent from another intact capillary within the network can be utilized for healing.

In systems employing intrinsic self-healing, no active healing agent is present. These systems exhibit what is termed latent self-healing, which is activated either by material damage or by external stimulation (e.g., heating, UV irradiation, etc.). The healing process in these materials can occur through mechanisms such as reversible polymerization, the melting of thermoplastic phases, formation of ionic or hydrogen bonds, or the reorganization of a flexible polymeric network [77, 81, 82].

The primary objective of any self-healing system is to achieve 100% healing efficiency. Each self-healing methodology includes at least one example system that has successfully reached this goal. However, the range of damage volumes that can be effectively healed varies significantly depending on the approach (Table 2). Most intrinsic systems require minimal damage volumes for efficient repair, as intrinsic rebonding mechanisms necessitate close proximity between damaged surfaces. Capsule-based systems are capable of addressing small to moderate damage volumes, constrained by the limited volumetric fraction of the encapsulated healing agent. Vascular systems, by contrast, can deliver healing agents to both small and large damage zones, with the lower limit determined by damage dimensions sufficient to intersect the vascular network. Since vascular networks are replenishable, it is hypothesized that their upper damage volume limit significantly exceeds that of capsule-based systems [77].

Table 2. Comparison of self-healing system efficiencies

Material	Healing system	Chemistry	Maximum healing efficiency (%) / Evaluation method	Ref.
Epoxy coating	Dual etched glass microcapsules	Epoxy-amine	93% Tapered double cantilever beam (TDCB) test	[83]
Epoxy coating	Dual PMMA microcapsules	Epoxy-amine	84.5% TDCB	[84]
PUR coating	Intrinsic disulfide bonds	PCL-HM	92% Tensile test	[85]
Epoxy coating	Dual MF microcapsules	PEA-IPDI	93% True color confocal microscope (TCCP)	[81]
PCL network	Intrinsic disulfide bonds	PCL with disulfide	92% Tensile test	[86]
Epoxy coating	Microvascular network	Epoxy-amine	> 60% Scanning electron microscopy (SEM)	[87]
Epoxy coating	Microcapsule-microvascular system	Epoxy-amine; HEMA-HEA	100% Seal testing of impact specimens	[88]
Epoxy composite	Microvascular glass fiber system	Epoxy-anhydride	69% Tensile test	[89]
Epoxy coating	Microvascular network	Epoxy-thiol	100% Mode-I fracture test	[90]
PUR coating	Intrinsic Diels-Alder	Furan-polydopamine; maleimide-PUR	93% Tensile test	[91]
PUR composite	Intrinsic Diels-Alder	Polydopamine particles; PUR-isocyanate	96% Tensile test	[92]

1.2.1. Microcapsule systems

The capsule-based system is the most extensively studied and widely used. Although it has limitations – such as allowing only a single healing event at a specific location and posing challenges in achieving uniform capsule distribution throughout the substrate – it remains dominant due to its technological simplicity compared to other self-healing systems [93]. There are several types of self-healing capsule systems:

- Single microcapsule system;
- Microcapsule and dispersed catalyst system;
- Dual microcapsule system.

In the single microcapsule system, the active substance is encapsulated, and in the event of coating damage, it can react with functional groups within the material [94].

Healing can be initiated by light or environmental moisture in this system. UV light-curable polyurethane acrylate and a 2-hydroxy-2-methyl-phenylacetone initiator were encapsulated within a methylether-melamine-formaldehyde shell to protect the core material from high temperatures and sunlight. When incorporated into a bitumen sample at just 3 % concentration, these microcapsules facilitated the self-healing of microcracks under UV light, forming a waterproof layer [95]. Isocyanates such as hexamethylene diisocyanate (HDI) and isophorone diisocyanate (IPDI) are considered ideal candidates for moisture-triggered self-healing systems. These compounds react with water to produce amines, which subsequently interact with unreacted isocyanates to form a crosslinked polymer network. This crosslinking process results in the formation of a robust protective barrier, effectively enhancing the coating's integrity and durability [96].

In the microcapsule and dispersed catalyst system, self-healing occurs when the active agent released from the capsule upon damage reacts with a catalyst dispersed in the matrix [97]. In such systems, Grubbs' catalyst is utilized in conjunction with PUF (poly(urea-formaldehyde)) microcapsules containing dicyclopentadiene. Upon the formation of a crack, the microcapsules rupture, releasing the encapsulated healing agent. The released dicyclopentadiene interacts with Grubbs' catalyst, initiating a ring-opening polymerization reaction that effectively seals and cures the crack. Wax was used to create a protective layer for Grubbs’ catalyst as well as improve incorporation into epoxy-amine system [98].

The dual microcapsule system encapsulates two separate healing agents, which react with each other when the capsules are damaged. This system is versatile and can be applied to both thermosetting and thermoplastic polymer systems [99]. Numerous dual microcapsule systems have been reported, with epoxy-amine systems being the most extensively studied. A thermally stable healing system based on epoxy-amine chemistry was developed, where one type of microcapsule contained polyamine, prepared through vacuum infiltration into hollow polymeric microcapsules. The second set of microcapsules was fabricated by forming a urea-formaldehyde wall around epoxy resin via interfacial polymerization. The healing performance of such a system, measured using SEM was up to 84% [100].

Microcapsules with active agent have been successfully produced using various techniques such as interfacial polymerization, *in situ* polymerization, coacervation, meltable dispersion, or physical wall formation [101]. Core-shell microcapsules have also been prepared by inverse emulsion (w/o), Pickering stabilization [102–105], inverse Pickering stabilization [106–108], and multiple emulsions [101], etc.

These microcapsules contain healing agents such as epoxy resins [109–111], amines [112, 113], isocyanates [114–118] and various kinds of oils [119–121]. If the coating is damaged, either through mechanical force or its inclination to shrink and crack, the microcapsules release healing agents into the affected area. This action forms a new barrier against the environment and seals the damaged area.

The correct choice of wall material is very important since it influences the encapsulation efficiency and stability of the microcapsules. The ideal wall material should have good compatibility with coating formulation, chemical non-reactivity with the active core materials, ability to seal and hold the active material within its structure during processing or storage, ability to provide maximum protection to the active material against oxygen, heat, light, and humidity, and other environmental conditions [122]. Numerous polymer materials are appropriate for creating the shells of capsules. The most popular shells for microcapsules formation are poly(urea formaldehyde) [121, 123–127], poly(melamine formaldehyde) [128–130], poly(urea melamine formaldehyde) [129, 131], polyurethane [132], polyurea [133–135], poly(methyl methacrylate) [136–138], and others.

Among others, UV curable materials are promising to be used for encapsulation of active compounds. UV curable shell of microcapsules can be formed from various materials subject to the specific requirements of an application. UV-curable resins or polymers, such as acrylates, epoxies, or urethanes, can be used to form the shell. These materials are designed to undergo polymerization and cross-linking upon exposure to UV light, resulting in a solid and durable shell. A microfluidic device was employed to produce monodisperse water-in-oil-in-water (W/O/W) double-emulsion droplets of controllable size [123]. Under UV irradiation, ethoxylated trimethylolpropane triacrylate prepolymer was cross-linked to form the shell of microcapsules [139]. Tung oil as a self-healing agent was encapsulated into photo-crosslinkable polyacrylic shell [140]. The oil phase contained tung oil, photopolymerization monomer glycidyl methacrylate, and crosslinker 1,6-hexanediol diacrylate. Upon UV irradiation, glycidyl methacrylate and 1,6-hexanediol diacrylate were polymerized along the inner side of the oil droplets, leading to the formation of cross-linked poly(glycidyl methacrylate) shell. The microcapsules exhibited good mechanical properties, allowing them to maintain their integrity even under high shear forces encountered during agitation and further dispersion within water-based epoxy coating

[140]. Photopolymerization technology combined with solvent evaporation technique was employed to prepare microcapsules containing linseed oil as an active agent for self-healing purposes [124]. Polyurethane acrylate with four active sites was used for shell formation. The initial emulsion was directly irradiated by UV light for the polymerization of UV-curable prepolymer of polyurethane acrylate, and then the co-solvent was removed to prepare microcapsules. Water-borne epoxy coatings formulated with microcapsules exhibited good self-healing properties, enabling full recovery of scratches with a microcapsule concentration of 15 wt % [141].

PAAE represent a relatively recent advancement in coating technologies. PAAEs are essential for the development of polyaspartic coatings. PAAE is used as co-reactants in the two-component PU system, along with an isocyanate component [125]. During NCO-amine reaction, a crosslinked PU network is formed, providing the coating unique properties, such as exceptional chemical resistance, abrasion resistance, flexibility, and fast curing. Due to fast reaction with isocyanates, PAAE can be used for the development of microcapsules for self-healing coatings. Since the PAAE are relatively new, there are very few published works using PAAE as a healing agent in microcapsule systems. In a limited number of studies investigating the feasibility of utilizing PAAE as a self-healing agent, PAAE was encapsulated within a poly(melamine-formaldehyde) shell through an in-situ polymerization process [126]. It was determined, however, that the reaction between the amino groups of PAAE and hydroxyl groups of the melamine-formaldehyde prepolymer occurred during the shell formation leading to reduced size of microcapsules [127]. It was reported that smaller microcapsules were less likely to rupture during the scratch process providing worse self-healing properties to the coating [126].

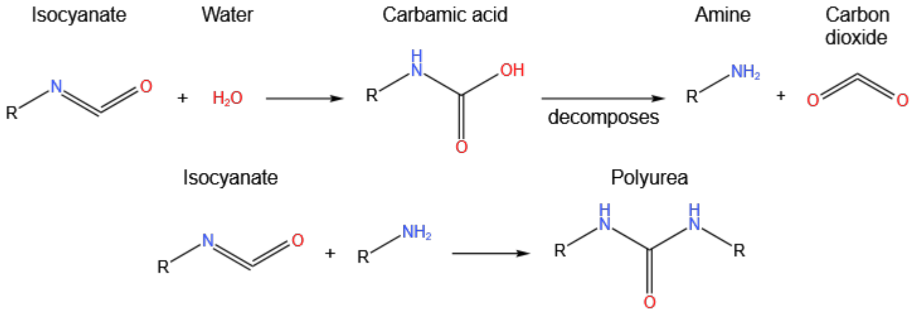

Fig. 8. Isocyanate reaction with water

Isocyanates have been extensively studied in the context of self-healing systems due to their high reactivity with polyols, amines, and aspartic acid esters [142–144]. They can also form coatings independently through partial hydrolysis to amines under humid conditions. Isocyanate reaction with water proceeds in two distinct steps. Initially, the isocyanate group reacts with water to generate an amine group and carbon dioxide (CO_2) [145].

Subsequently, the newly formed amine group reacts with remaining isocyanate groups, leading to the formation of a PU polymer while releasing additional CO_2 (Fig. 8). The resulting PU can form a continuous film, effectively sealing the crack without requiring additional reactants or components.

1.3. Taguchi experimental design

The successful microencapsulation process depends on numerous controlled and uncontrolled parameters within the preparation process, which are interconnected in a synergistic manner. Taguchi method was developed by Dr. Genchi Taguchi, a Japanese scientist in early years of 20th century. Taguchi's techniques have been used widely in engineering design. The Taguchi method contains system design, parameter design, and tolerance design procedures to achieve a robust process and result for the best product quality [146]. Taguchi experimental design method utilizes two major tools: orthogonal array for experiment design and analysis of data using signal-to-noise ratio (SNR).

Experiment	**P1**	**P2**	**P3**	**P4**
E1	1	1	1	1
E2	1	2	2	2
E3	1	3	3	3
E4	2	1	2	3
E5	2	2	3	1
E6	2	3	1	2
E7	3	1	3	2
E8	3	2	1	3
E9	3	3	2	1

Fig. 9. Example of orthogonal array L9 four parameters: P1 – voltage, P2 – temperature, P3 – pressure, P4 – humidity; and three levels: 1 – high, 2 – medium, 3 – low.

The Taguchi orthogonal array is a robust and systematic experimental design technique used to minimize the impact of uncontrollable factors and identify the optimal combination of process parameters. This approach helps reduce both the time and cost of experimentation. These arrays were created using an algorithm developed by Taguchi, ensuring that each variable and setting is tested equally [147].

For example, if we have four parameters (e.g., voltage, temperature, pressure, and humidity) and three levels (high, medium, low), the appropriate array is L9 (Fig. 9).

Taguchi method uses statistical measure of performance called SNR. The SNR indicates the sensitivity of signal (characteristic of quality) to noise (deviation in factors). The SNR is mainly used as an objective function to determine the most optimum set of operating conditions. There are three main types of SNRs used in the Taguchi method: smaller-the-better (used when the goal is to minimize the response), larger-the-better (used when the goal is to maximize the response) and nominal-the-best (used when the aim is to achieve a target value for the response) (Fig. 10) [148].

$$\frac{S}{N} = -10 \cdot log\left(\frac{1}{n}\sum y^2\right)$$

Smaller-the-better

$$\frac{S}{N} = -10 \cdot log\left(\frac{1}{n}\sum \frac{1}{y^2}\right)$$

Larger-the-better

$$\frac{S}{N} = -10 \cdot log\frac{\bar{y}^2}{s^2}$$

Nominal-the-best

y – the measured value
n – the number of measurements in a trial
s – the nominal value

Fig. 10. The standard SNR ratios

Two characteristics such as higher loading and optimal size of microcapsules are the most desirable for optimization of encapsulation processes. Different parameters can be varied in obtaining both characteristics. Usually, such parameters as agitation speed, surfactant type and concentration, reaction time, reaction temperature, and core to shell ratio are chosen as affecting loading and size of microcapsules [136, 149–152].

The Taguchi design tool can be applied across various research domains, including the development of self-healing materials. While this methodology has been relatively underutilized, the study applied the Taguchi design to develop hybrid self-healing coatings containing linseed oil nanocapsules [153]. In this work, 16 samples were prepared, varying in the amounts of linseed oil nanocapsules, anti-corrosion agents, paint type, and the type of anti-corrosion agent used. Another study applied the Taguchi design to investigate the influence of several process parameters – such as surfactant concentration, core-to-shell ratio in the initial feed, temperature, and agitation speed – on the core content of epoxy-loaded polymethylmethacrylate (PMMA) microcapsules [154]. Optimal parameters for microcapsule formation were identified, resulting in a high core content of 66.53% epoxy within the PMMA shell.

To summarize the literature review, the development of environmentally friendly protective coatings is one of the most important areas for extending the service life of metallic structures. The search for new alternatives to classical toxic materials has great prospects for the development of advanced anti-corrosion coatings. Phenalkamines, amines from renewable sources, can be used as less toxic hardeners for epoxy systems. However, the use of phenalkamines in coatings is comparatively limited and it is therefore essential to investigate their rheological behavior, curing kinetics and film formation characteristics in order to maintain high environmental requirements. Reactive diluents are materials that contain reactive groups and chemically react with the curing agent, becoming a permanent part of the coating once cured. Their incorporation helps lower the resin's viscosity, enables the addition of more fillers, enhances wetting properties, and aids in the film formation process. Consistent and systematic research on reactive diluents is essential for the development of low or VOC-free coatings.

A self-healing two-capsule system coating is an advanced smart coating engineered to autonomously repair damage, such as scratches or cracks, without the need for external intervention. This area is currently the focus of extensive research, with scientists continually exploring new active materials for encapsulation and developing innovative shell structures – efforts that are driving the creation of next-generation self-healing coating systems.

2. EXPERIMENTAL

2.1. Coating development materials

Commercial epoxy resins and amine hardeners, typically used in anti-corrosion epoxy-based coatings, were employed.

The epoxy resins used in formulations (Table 3) were bisphenol-A with the commercial names Araldite GY-240 and Araldite GY-2600, bisphenol-A/-F and novolac epoxy resins with commercial names Araldite GY 783 and Araldite GY 289, respectively, and reactive epoxy diluents Araldite DY-L – trifunctional RD based on glycerol propoxylate triglycidyl ether (GPTE), Araldite DY-D and Araldite DY-H – difunctional RD based on BDGE and HDE, and Araldite DY-E – monofunctional RD based on AGE. These chemicals were kindly donated by Huntsman Co.

Table 3. Epoxy resins and reactive diluents

Name	Resin/RD	Parameters	Basic chemical formula
Araldite® GY 240	Resin Bisphenol A	EEW = 180-183 g/eq $\rho = 1.17$ g/cm^3 $\eta = 7\text{-}9$ Pa·s	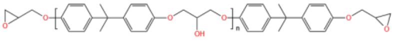
Araldite® GY 2600	Resin Bisphenol A	EEW = 184-189 g/eq $\rho = 1.17$ g/cm^3 $\eta = 12\text{-}14$ Pa·s	
Araldite® GY 289	Resin Phenol novolac	EEW = 167-175 g/eq $\rho = 1.19$ g/cm^3 $\eta = 9\text{-}11$ Pa·s	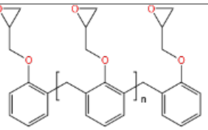
Araldite® GY 783	Resin Bisphenol A/F with reactive diluent	EEW = 189-200 g/eq $\rho = 1.13$ g/cm^3 $\eta = 0.8\text{-}1.1$ Pa·s	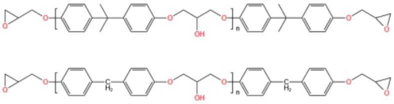
Araldite® DY-L	Trifunctional reactive diluent	EEW = 606-800 g/eq $\rho = 1.06$ g/cm^3 $\eta = 0.16\text{-}0.24$ Pa·s	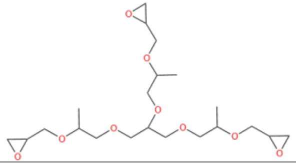
Araldite® DY-E	Monofunctional reactive diluent	EEW = 278-317 g/eq $\rho = 0.89$ g/cm^3 $\eta = 0.004\text{-}0.012$ Pa·s	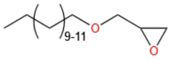
Araldite® DY-D	Difunctional reactive diluent	EEW = 118-125 g/eq $\rho = 1.08$ g/cm^3 $\eta = 0.015\text{-}0.025$ Pa·s	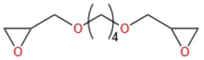
Araldite® DY-H	Difunctional reactive diluent	EEW = 143 g/eq $\rho = 1.06$ g/cm^3 $\eta = 0.021\text{-}0.031$ Pa·s	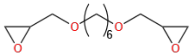

The amine hardeners (Table 4) low-molecular-weight amines such as 1,2-ethanediamine (EDA), triethylenetetramine (TETA), and diethylenetriamine (DETA), an amine-terminated polyoxypropylene glycol (polyetheramine) commercially known as Jeffamine D-230, polyamidoamine Aradur 450 and low viscosity co-hardener (accelerator) based on 2,4,6-tris[(dimethylamino) methyl]phenol (DMP) Accelerator 960-1 were provided by Huntsman Co. Other amine hardeners Luna-cure PACM-20 based on para-diaminodicyclohexylmethane (PACM) and Luna-cure MACM-F based on 4,4'-methylenebis(2-methylcyclohexylamine) (DMDC) were obtained from DKSH. Additionally, cardanol-based PhA containing Cardolite Lite-2002, Cardolite GX-6004 and Cardolite NX-6019 were generously supplied by Cardolite Co (Table 5).

Table 4. Amine curing agents

Name	Type	Parameters	Basic chemical formula
EDA	Aliphatic amine	AHEW = 15 g/eq $\rho = 0.90$ g/cm^3 $\eta = 0.002$ Pa·s	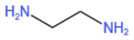
DETA	Aliphatic amine	AHEW = 21 g/eq $\rho = 0.95$ g/cm^3 $\eta = 0.007$ Pa·s	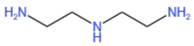
TETA	Aliphatic amine	AHEW = 24 g/eq $\rho = 0.98$ g/cm^3 $\eta = 0.014$ Pa·s	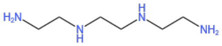
Jeffamine D-230	Polyether amine	AHEW = 60 g/eq $\rho = 0.97$ g/cm^3 $\eta = 0.009$ Pa·s	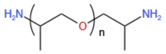
Aradur 450	Polyamidoamine	AHEW = 115 g/eq $\rho = 1.01$ g/cm^3 $\eta = 1\text{-}2$ Pa·s	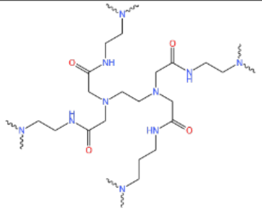
Luna-cure PACM-20	Cycloaliphatic amine	AHEW = 52 g/eq $\rho = 0.96$ g/cm^3 $\eta = 0.05\text{-}0.1$ Pa·s	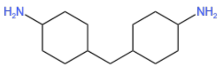
Luna-cure MACM-F	Cycloaliphatic amine	AHEW = 60 g/eq $\rho = 0.95$ g/cm^3 $\eta = 0.08\text{-}0.15$ Pa·s	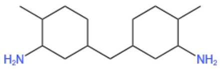
Accelerator 960-1	Accelerator/ curing agent	$\rho = 1\text{-}1.1$ g/cm^3 $\eta = 0.05\text{-}0.5$ Pa·s	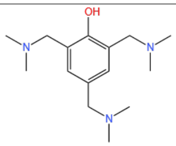

Table 5. The compositions of cardanol-based commercial phenalkamines*

Components	Cardolite		
	Lite-2002, % (AHEW = 104 eq/g)	**GX-6004, %** (AHEW = 76 eq/g)	**NX-6019, %** (AHEW = 133 eq/g)
Cardanol-based phenalkamine 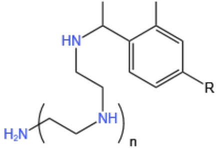	72-78	50-62	68-75
m-Xylylenediamine (MXDA) 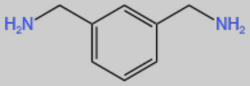	18-22	15-23	18-21
Cashew nutshell extract, decarboxylated	-	16-20	18-21
Tetraethylenepentamine (TEPA) 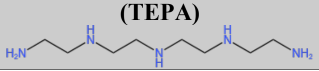	4-6	-	-
2,2,4-Trimethylhexane-1,6-diamine (TMD) 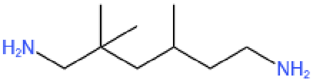	-	~7	-
2,4,6-Tris[(dimethylamino) methyl]phenol (DMP) 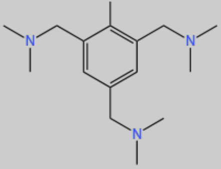	-	-	3-4
Dimethylaminopropylamine (DMAPA) 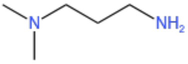	-	-	2-3
Phenol	-	-	0.6-0.9
Ethylenediamine (EDA) 	-	-	0.6-0.9

* From the material safety data sheets of phenalkamines

2.2. Microencapsulation materials

The UV printing photopolymer resin Anycubic Colored UV Resin containing mixture of acrylate monomers and photoinitiator ethyl phenyl(2,4,6-trimethylbenzoyl)phosphinate was purchased from ANYCUBIC

3D Printing. The acrylic UV resin is characterized by low viscosity (0.15-0.25 Pa·s at 25 ºC), short curing time, low shrinkage after curing, and appropriate hardness. PAAE with commercial name of Desmophen® NH 1220, IPDI (NCO content 37.5%) and polyisocyanate under commercial name Desmodur RFE (27% solution of tris(4-isocyanato phenyl)thiophosphate (TIPTP) in ethyl acetate, NCO content of 7.2%) was purchased from Covestro AG. TETA was supplied by Huntsman Co. Xylene was supplied by Eurochemicals, ethyl lactate was obtained from TCI, and sodium dodecylbenzenesulfonate (SDBS) was acquired from Eurochemicals. Gum arabic (GA) was purchased from Thermo Fisher Scientific, while styrene-maleic anhydride copolymer (SMA, M_w ~7000 g/mol, 13% in water) and polyvinyl alcohol (PVA, M_w ~85000-124000 g/mol, deacetylation degree 85%) were obtained from Sigma-Aldrich.

2.3. Coating formulation

Cured coating samples for testing were made by mixing epoxy resin or resin mixture with RD and the corresponding amount of amine hardener or amine hardener mixture (Tables 6, 7).

Table 6. Compositions of epoxy resins and reactive diluents (PA)

Epoxy system	PA1, % EEW=184	PA2, % EEW= 178	PA3, % EEW=163	PA4, % EEW=167
Araldite® GY 783	15	15	15	15
Araldite® GY 289	75	75	75	75
Araldite® DY-L	10	-	-	-
Araldite® DY-E	-	10	-	-
Araldite® DY-D	-	-	10	-
Araldite® DY-H	-	-	-	10

Table 7. Compositions of amine hardeners (PB)

Hardener system	PB1, % AHEW=66.2 g/eq	PB2, % AHEW=67.9 g/eq
Aradur 450	52	70
PACM-20	33	20
MACM-F	9	-
DETA	6	5
Accelerator 960-1	-	5

The mixing ratio of epoxy resin to a curing agent was stoichiometric. Amine hydrogen equivalent weight (AHEW) of amine blends, epoxy equivalent weight (EEW) of epoxy blends, and weight of curing agent per 100 parts of epoxy resin (phr) are calculated using equations (1) – (3).

$$AHEW\ of\ Amine\ Blend = \frac{Total\ Weight\ of\ Amine\ Blend}{\frac{Weight\ A}{AHEW_A} + \frac{Weight\ B}{AHEW_B} + \cdots} \tag{1}$$

$$EEW\ of\ Epoxy\ Resin\ Blend = \frac{Total\ Weight\ of\ Epoxy\ Blend}{\frac{Weight\ A}{EEW_A} + \frac{Weight\ B}{EEW_B} + \cdots} \tag{2}$$

$$phr = \frac{AHEW\ of\ Amine\ Blend}{EEW\ of\ Epoxy\ Resin\ Blend} \times 100 \tag{3}$$

EEW and AHEW were determined using equations (1) and (2), with the calculated values presented in Tables 6 and 7, respectively. To prepare coating samples of PA+PB composition, a fixed amount of 100 g of component PA was used. The required amount of component PB was then calculated based on the phr formula, as described in equation (3). For instance, in the case of the PA1+PB2 system, the phr calculation is as follows:

$$\frac{66.2\ g/eq\ (AHEW\ of\ PB1)}{184\ g/eq\ (EEW\ of\ PA1)} \times 100 = \ 35.97g \tag{4}$$

That means that for 100 g PA1, 35.97 g of PB1 was used to cure composition and prepare samples for the tests.

2.3.1. Evaluation of coating curing by DSC

A calorimeter Perkin Elmer DSC8500 was used to study curing of epoxy resins by amines. A non-isothermal DSC test was performed under nitrogen atmosphere (rate 40 mL/min). A sealed empty aluminum pan was used as a reference. Samples of 3–5 mg were heated from -60 to 200 °C at the rates of 5, 10, 15 and 20 °C/min and then kept at this temperature for an additional 10 min. The heat flow curves were recorded, and the thermal data were further processed to determine the initial curing temperature (T_i), peak curing temperature (T_p), terminal curing temperature (T_t) and reaction enthalpy (ΔH_R). For determination of the T_g of the fully cured systems, mixed epoxy-amine samples were cured at room temperature for 2 weeks, and then, nonisothermal DSC test was performed heating from 0 to 200 °C at the rate of 10 °C/min.

2.3.2. Evaluation of coating curing by rheological measurements

A rheometer Anton Paar MCR302 was used to study the initial stage of curing and for the determination of pot-life of the curing system. The pot-life is defined as the amount of time it takes for the product's initial mixed viscosity to double. The measurements were performed at 25 °C with a parallel-plate of diameter 50 mm; a distance between the parallel plate and the base mount of 1 mm; the shear rate was kept constant at 0.25 s^{-1}. The viscosity (in mPa·s) was measured every 5 s.

Rheological properties of the epoxy/amine mixtures during isothermal curing at 50 ºC were studied by the oscillatory shear measurements using a rheometer MCR302 (Anton Paar). Parallel-plate measuring system with a diameter of 25 mm and a gap between measuring plates of 0.5 mm was used to perform the shear oscillation sweep test. All experiments were carried out with amplitude of oscillation 0.1% and an angular frequency of 1 Hz, 2 Hz, and 4 Hz. Sinusoidal stress was used in all experiments, which is the basis for calculating the storage modulus (G') the loss modulus (G''), and the loss factor ($\tan\delta$). Components of PA and PB were used as received and carefully mixed at the stoichiometric ratio. After preparing the sample, it was immediately placed in the plate–plate geometry assembly and quickly heated (60 ºC/min) to the target curing temperature (50 ºC).

The three-interval thixotropy test (3ITT) was performed to determine the thixotropic behavior of the mixed compositions PA + PB as well as compositions with added microcapsules using a rheometer MCR302 (Anton Paar). Parallel-plate measuring system with a diameter of 50 mm with a gap between measuring plates of 1 mm and constant 25 ºC temperature was used to perform the 3ITT test. The low-high-low shear test regime of 3ITT test closely resembles brush/roller/spray loading, brushing/rolling/spraying, and subsequent drying of paint, respectively [155]. During the first interval, the sample was subjected to low shear rate (0.1 s^{-1}) for 50 s, and then, for 5 s, a higher (1000 s^{-1}) shear rate is applied and finally back to low shear rate for 200 s. The low–high–low shear rate test of 3ITT resembles the application process of composition. During this process, the internal structure of composition is broken down using high shear rates and the recovery pre- and post-application of high shear was measured by tracking the change in viscosity. The recovery rate of viscosity at given time after removal of high shear was used to predict the sagging and leveling characteristics of coating systems [156].

2.3.3. Anti-sagging test

Anti-sagging properties were determined according to ASTM D4400 using a BYK Sag Meter. The multiple notched applicators with varying clearances spanning medium range (3-12 mils) and high range (4-24 mils) were used. For the measurements, approximately 10 mL of the mixed composition PA+PB were transferred onto a flexible smooth metal plate. The multiple notch applicator was drawn down across the metal plate, which formed a series of evenly spaced stripes. The plate was then quickly hung vertically and left to dry in room conditions. The coating samples were monitored visually after drying and rated for an anti-sagging measure. The anti-sagging index was defined as the thickest thickness (mm) of dry coating stripe remained without sagging.

2.4. Evaluation of mechanical properties of coatings

2.4.1. Coating sample preparation

PA and PB were mixed at stoichiometric ratio, and three different metal substrates were coated immediately by the curing epoxy resins (Table 8). The steel smooth plates were used for hardness and impact resistance tests, aluminum coated flexible plates for flexibility tests and blasted plates of high roughness for adhesion tests.

Table 8. Metal substrates used for mechanical tests

Substrate type	**Steel plates, smooth surface, thickness 1 mm**	**Aluminum coated flexible plates**	**Blasted plates, roughness 50 to 85 µm, thickness 5 mm**
Coating method	Automatic, BYK byko-drive XL, thickness 200 µm, speed 3 mm/s	Automatic, BYK byko-drive XL, thickness 200 µm, speed 3 mm/s	Coating by hand with spatula
Mechanical tests	Coating hardness (BYK Pendulum Hardness Tester), direct impact resistance (TQC Impact Tester)	Coating flexibility (BYK Conical Mandrel Tester)	Adhesion, resistance to abrasion (PosiTest AT-A Automatic)

The steel smooth plates and flexible aluminum coated plates were coated using BYK byko-drive XL and a film applicator with 4 gaps from 50 to 200 µm. The thickness chosen for the coating application was 200 µm and the applicator was pushed at 3 mm/s speed to assure good coating spread. The blasted plates were coated by hand using spatula, spreading and levelling the coating across the plate surface.

2.4.2.Hardness test

Hardness of the epoxy coatings was evaluated by the König pendulum method according to ASTM D4366 (BYK König Pendulum Hardness Tester). The test was performed on a coating with a thickness of 200 μm on a steel surface. The pendulum hardness of the coating surface was measured with respect to the pendulum oscillation time from 6° to 3° at relative humidity 23±1 °C and 50±2 %. The number of oscillations is recorded. Three replicates were made for each treatment group.

2.4.3.Direct impact test

Coatings resistance to cracking or peeling from the metal substrate was evaluated according to ISO 6272-1:2011 using the impact resistance testing device TQC. The test was performed on coatings with a thickness of 200 μm on a steel surface. The minimum height of fall for 20 mm diameter 1 kg weight was measured under normalized conditions, in order to damage tested coatings. Impact resistance is defined as the impact energy (J) that a coating can withstand without visual damage. Three replicates were made for each treatment group.

2.4.4.Flexibility test

Flexibility of coatings with the thickness 200 μm on a flexible aluminum plate was evaluated according to ASTM D5221. The coating on the plate was cut into even pieces every 2 cm. Conical mandrel bend tests were performed by bending the coated panels on a conical mandrel tester (BYK Conical Mandrel Tester) up to 135° over a period of 3 seconds. For the test, three coated aluminum specimens from each coating with dimensions of 150 × 100 × 0.5 mm^3 were used. The diameter of the cone varied from 38 mm to 3 mm. The coating was considered flexible if there was no crack on its surface on all three coated samples.

2.4.5.Adhesion test

Determination of the adhesion to a metal surface was performed according to ATSM D4541 using a PosiTest® AT-A (DeFelsko). The pull-off test was carried out by gluing 14 mm diameter dollies to the abrased with sandpaper coating using a two-part epoxy glue. After 24 h a pull-off test was conducted by applying a tensile stress perpendicular to the surface. The tensile stress was applied until the coating was torn from the metal surface and the magnitude of the stress measured was recorded in N/mm^2 (MPa). On completion of the test, the dolly was visually examined to determine if the failure had occurred at the interface (cohesion) or in the substrate (adhesion). Three replicates were made for each treatment group, and the average results were reported.

2.4.6. Abrasion test

The abrasion resistance of the coatings was determined according to ASTM D4060 using Taber Abrasion Tester. In a Taber test, a coating is mounted on a turntable platform that rotates on a vertical axis at a fixed speed. Two standard CS17 Taber abrasive wheels, each applied with 1000 g load, are lowered onto the specimen surface. 1000 cycles of abrasive wear action were produced. The reducing of the coating weight (mg) after abrasion was evaluated. Two replicates were made for each treatment group, and the average results were reported.

2.5. Microencapsulation methods

2.5.1. Encapsulation of polyaspartic acid ester

Microcapsules containing PAAE were obtained by an oil-in-water emulsion photopolymerization method by initiating shell formation using UV light. General procedures and an example of the material used are presented below. To make microcapsules EA1, the oil phase was prepared by mixing UV curable acrylic resin (1.67 g), PAAE Desmophen NH 1220 (1.67 g), and solvent ethyl lactate (1.67 g). An emulsifier solution was prepared by dissolving and stirring overnight PVA (3.00 g) and GA (4.50 g) in deionized water (142.50 g) to make PVA 2% / GA 3% solution. The oil phase (5.00 g) was then added to 150 g of aqueous emulsifier solution and stirred at a given speed by Ultra Turrax homogenizer for 10 min. The resulting emulsion was subjected to photo-irradiation with 48 W UV light for 3 min at a distance of 10 cm. The microcapsules obtained were washed with deionized water and separated by lyophilization.

2.5.2.Encapsulation of IPDI into PU shell

Microcapsules containing IPDI with PU shell were obtained by an oil-in-water emulsion interfacial polymerization method. The shell formation was achieved by adding TETA into isocyanate-water emulsion. To prepare microcapsules No IE1 solution of the emulsifiers PVA 2% / GA 3% was prepared by dissolving PVA (3.0 g) and GA (4.5 g) in deionized water (142.5g) and stirring overnight. The oil phase was prepared by mixing IPDI (13.3 g) with the solution of Desmodur RFE (15.6 g). The oil phase (28.9 g) was then added to the emulsifier solution (150 g) and stirred at 3000 rpm for 5 min. The resulting emulsion was set to stir at the constant speed of 1000 rpm while the temperature was increased up to 60 °C. When the temperature reached the intended value, TETA was slowly added to the emulsion, and the emulsion was stirred at 1000 rpm for 30 min. To remove unreacted materials, the obtained microcapsules were washed with deionized water 4-5 times. Finally, microcapsules were separated by lyophilization at -55 °C and 0.2 mbar.

2.5.3.Characterization of microcapsules

The assessment of average microcapsule size, size distribution, and stability was conducted using an optical microscope Nikon Eclipse LV100ND. Further characterization of microcapsule size, morphology, and rupture was performed utilizing a scanning electron microscope (SEM) Hitachi TM3000. The analysis of the microcapsules using Fourier-transform infrared spectroscopy (FT-IR) spectra within the range of 550-4000 cm^{-1} was carried out by Jasco FT-IR 4600 spectrometer. The determination of the PAAE as well as IPDI content within the microcapsules was executed through thermogravimetric analysis (TGA) using a Hitachi STA200 instrument. The TGA involved a heating rate of 40 °C/min until reaching 150 °C, followed by 10 °C/min until 550 °C, all under a nitrogen gas flow.

2.5.4.Design of experiment by Taguchi method

In preliminary investigation it was identified that five pivotal parameters have the biggest potential to influence the core content, size of microcapsules and microcapsule yield. These parameters are core-to-shell ratio, agitation speed, type and quantity of emulsifier, type and quantity of solvent and reaction time. The chosen parameters and their respective levels are given in

Tables 9-11, with the range of levels determined through preliminary experimental assessments.

The Taguchi design methodology was employed to find the optimal process parameters using SNR analysis [152]. The larger-the-better criterion was used to determine optimal conditions to achieve maximum microcapsule core content and maximum reaction yield. Simultaneously, the nominal-the-better criterion was used to identify conditions conducive to the production of microcapsules with a size of 50 μm.

Table 9. Taguchi design parameters for PAAE – ethyl lactate encapsulation

Parameter, units	**Levels**			
	1	2	3	4
Core-to-shell ratio	2:1	3:1	4:1	5:1
Agitation speed, rpm	500	750	1000	3000
Emulsifier and its concentration, %	PVA 2 / GA 3	PVA 1 / GA 1.5	SDBS 1	PVA 2 / SDBS 1
Ethyl lactate, % of the core content	50	25	10	–

Table 10. Taguchi design parameters for PAAE – xylene encapsulation

Parameter, units	**Levels**			
	1	2	3	4
Core-to-shell ratio	2:1	3:1	4:1	5:1
Agitation speed, rpm	500	750	1000	3000
Emulsifier and its concentration, %	PVA 2 / GA 3	PVA 1 / GA 1.5	SDBS 1	SMA 1
Xylene, % of the core content	–	10	25	50

Table 11. Taguchi design parameters for IPDI encapsulation

Parameter, units	**Levels**			
	1	2	3	4
Core-to-shell ratio	2:1	3:1	4:1	5:1
Agitation speed, rpm	3000	4000	5000	6000
Emulsifier and its concentration, %	PVA 2 / GA 3	PVA 1 / GA 1.5	SDBS 1	GA 7
Reaction time, min	30	45	60	90

2.6. Evaluation of self-healing of coatings

To evaluate the self-healing performance, microcapsules containing PAAE (EA8) and IPDI (IA4) were mixed together by equal amounts and incorporated into an epoxy coating formulation at concentrations of 5 % (2.5%

of each type), 10 % (5% of each type), and 15 % (7.5% of each type) by weight. The prepared formulations were applied to freshly blasted metal substrates at 400 µm thickness using a coating blade and allowed to cure for one day. Twenty-four hours after application, cross-incisions were made in the hardened coating using a blade with an approximate width of 100 µm, ensuring full penetration through the coating to the metal substrate. The samples were then subjected to self-healing conditions, either at room temperature for 24 hours or at 80 °C for 1 hour.

After the healing process, the coatings were evaluated through visual inspection and optical microscopy (OM) to determine the extent of self-healing. Subsequently, the performance of the self-healed coatings was further evaluated by subjecting the damaged samples to a salt spray chamber for 7 days. After exposure, the damaged areas of the coatings – both with and without microcapsules – were analyzed and compared visually and using OM to assess corrosion resistance and healing efficiency.

3. RESULTS AND DISCUSSION

3.1. Development of epoxy anti-corrosion coatings

3.1.1.Curing of epoxy resins by bio-based phenalkamines

PhA represent a relatively new class of amine curing agents, alleged to offer several advantages over traditional low-molecular-weight amines. These advantages include the ability to cure at low temperatures (reported to be as low as 5 °C), a bio-based origin derived from renewable sources like CNSL, extended pot-life, inherent hydrophobicity, and superior corrosion resistance [9, 52, 53]. However, to verify these claims and evaluate their practical applicability, systematic experimental investigations under real conditions were necessary. Such evaluations are critical for determining the extent to which these properties translate into measurable performance benefits in epoxy resin systems.

To analyze the differences in the epoxy resin curing process, two bisphenol A-based resins, Araldite GY-240 and Araldite GY-2600, were selected**.** While these resins exhibit similar fundamental properties**,** their key differentiating factor is molecular weight – Araldite GY-240 has a lower molecular weight compared to Araldite GY-2600.

For an evaluation of curing agents, several low molecular weight amines – TETA, EDA, and polyetheramine (Jeffamine D-230) – were selected for testing. Furthermore, to assess the potential benefits of using commercially available amines, the PhA-based compounds Cardolite Lite-2002, Cardolite GX-6004, and Cardolite NX-6019 were specifically chosen for comparison. All three Cardolite products are comprised of 50-78% cardanol-based PhA, 0-21% of CNSL extract and 22-30% of smaller amines – MXDA, TEPA, TMD, EDA, DMP and DMAPA. The approximate compositions of these commercial PhA-based hardeners are provided in Table 5.

Curing of epoxy resins by bio-based PhA containing hardeners and, for comparison, by low-molecular-weight amines was studied by DSC and rheological measurements. DSC tests of curing epoxy compositions are very important since they provide several parameters characterizing curing process: initial reaction temperature (T_i) indicates which of curing agents has the potential to be used for curing at low temperature, temperature cure interval (ΔT) correlates with the reaction rate, and the ΔH_R of the curing reaction presents thermal effect of the curing process. In turn, rheological measurements help to determine pot-life of the curing system, which is defined as the time required for the viscosity of the epoxy-amine system to double.

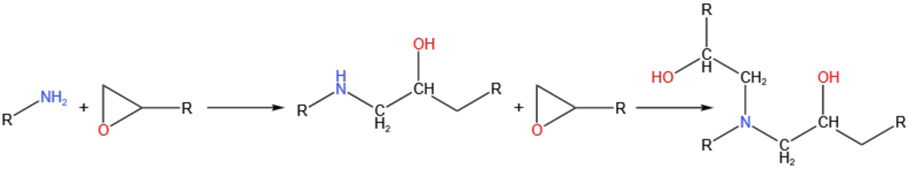

Fig. 11. Reaction of epoxy resin with amine hardener

Evidently, the curing reaction (Fig. 11) is an exothermic process which is represented by one exothermic peak (Fig. 12). From the curing curves, T_i, peak curing temperature (T_p), terminal curing temperature (T_t) [157], ΔT, and ΔH_R of the curing reaction were obtained and listed in Table 12. The T_i did not depend on the type of the epoxy resin but was dependent on the type of the hardener being the lowest for the PhA-based hardeners NX-6019 and GX-6004 (Table 12). PhA-based hardener NX-6019 contains tertiary amines DMP and DMAPA which are used as accelerators in epoxy-amines curing systems and greatly increase reaction speed as well as lower T_i of reaction. Curing by Jeffamine D-230 was evidently late, which was reflected in higher values of T_i, T_p, and T_t. T_p obtained by using other hardeners including PhA-based hardeners was similar and close to 100 °C.

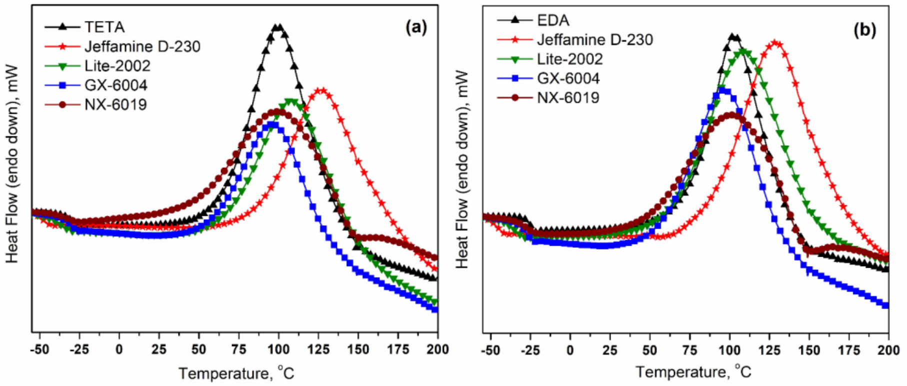

Fig. 12. DSC curing of epoxy resins GY-240 (a) or GY-2600 (b) by different amines

ΔH_R of the cure reaction of the epoxy resin GY-240 by various hardeners was slightly higher compared to that of GY-2600. Curing of the epoxy resins by low-molecular-weight amines TETA and Jeffamine D-230 was accompanied by the highest exothermic effect (ΔH_R about 386-431 J/g).

Table 12. Characteristic parameters of DSC curing of epoxy resins by different amines

Amine hardener	T_i, °C	T_p, °C	T_t, °C	ΔT,°C*	ΔH_R, J/g	T_g
Epoxy resin GY-240						
EDA	72.6	100.9	132.7	60.1	-	76
TETA	64.7	100.0	142.7	78.0	431.4	-
Jeffamine D-230	85.2	126.5	188.9	103.7	386.0	80
Lite-2002	64.2	108.9	161.3	97.1	363.9	73
NX-6019	48.2	99.9	146.0	97.8	344.9	50
GX-6004	55.0	96.8	136.0	81.0	308.5	85
Epoxy resin GY-2600						
EDA	71.5	103.1	141.4	69.9	312.4	53
TETA	62.9	94.7	142.4	79.5	-	98
Jeffamine D-230	83.2	127.7	186.1	102.9	397.9	71
Lite-2002	63.9	108.9	158.0	94.1	335.1	76
NX-6019	47.1	103.0	146.9	99.8	276.8	53
GX-6004	55.5	96.8	137.2	81.7	291.4	82

*$\Delta T = T_t - T_i$, °C

The smallest ΔT were characteristic of the epoxy resins cured by low-molecular-weight amines EDA and TETA which indicates the highest cure rate. Curing by these hardeners started at 63–73 °C, and the ΔT was relatively narrow and ranged 60–80 °C. Surprisingly, curing of the epoxy resins by polyetheramine Jeffamine D-230 proceeded at a significantly higher temperature and full cure was reached at about 190 °C.

The ΔH_R of curing of the epoxy resins by PhA-based hardeners Lite-2002, GX-6004, or NX-6019 was lower (ΔH_R 277–364 J/g). In these cases, the cure process started earlier (at about 47–64 °C), and the ΔT was broader (about 80–100 °C). Since all PhA-based hardeners had lower T_i in comparison to low molecular weight amines, it can be concluded that they start reacting at lower temperatures. In comparison, GX-6004 appears to be the most active PhA-based hardener among all those investigated, as it exhibited the shortest ΔT. This phenomenon can be attributed to highly reactive TMD [158] present in the composition of this PhA-based hardener.

T_g of the cured epoxy resins is associated with crosslinking density of the system (Fig. 13). T_g of the cured epoxy resins varied from 50 °C to 98 °C and was dependent on the type of hardener (Table 12). The highest T_g (98 °C) was characteristic for the epoxy resin GY-2600 cured by TETA. Likely, tightly crosslinked network was formed in this case due to high functionality of TETA and short distances between active centers.

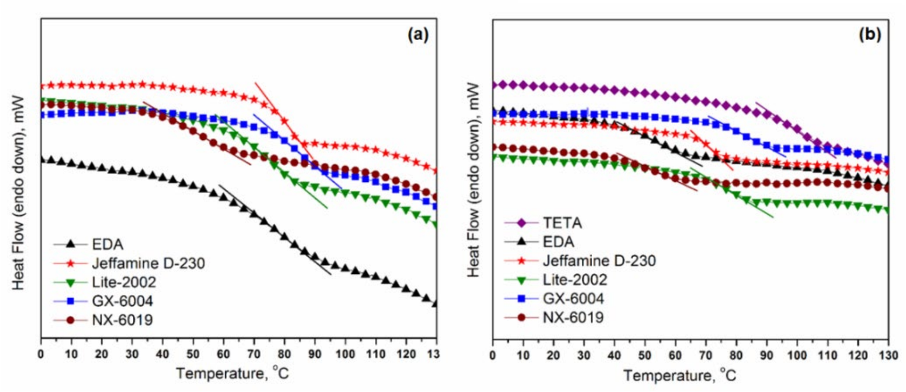

Fig. 13. DSC curves of the epoxy resins GY-240 (a) and GY-2600 (b) cured using different amines (second heating)

Lower values of T_g were characteristic for the epoxy resins cured by EDA and Jeffamine D-230. The crosslinking density in the cured epoxy resins is expected to be lower in these cases due to lower functionality of these hardeners. Lower T_g of the epoxy resins cured by PhA-based hardener NX-6019 and Lite-2002 (50-76 °C) could be attributed to the long alkyl chains present in the PhA, which increase flexibility and chain mobility in the cured system. Slightly higher T_g (82-85 °C) was characteristic of the epoxy resins cured by PhA-based hardener GX-6004. This correlates well with higher reactivity of this hardener demonstrated by DSC studies.

Changes in viscosity of the curing epoxy resins at room temperature during 1-2 hours after mixing were evaluated by rotational rheometer. The curing of epoxy resins by amine hardeners results in consistent increase in viscosity of the system. The rate of the viscosity changes could be an indicator of activity of the reacting components during initial stage of the curing. Pot-life of the curing system was considered to be quantitative parameter reflecting the rate of the cure process (Table 13). The curves presenting changes in viscosity of the epoxy resins GY-240 and GY-2600 mixed with various amines show similar trends (Fig. 14). The initial viscosity of the epoxy resins mixed with low-molecular-weight amines EDA and TETA, and PhA-based hardener Lite-2002 doubles in approx. 25-35 min. Pot-life of the epoxy resins mixed with Jeffamine D-230 is more than 120 min. This indicates that the activity of Jeffamine D-230 at room temperature is very low. Nevertheless, this amine could be used as a hardener for epoxy resins at higher temperatures, as it was shown by DSC studies. The shortest pot-life (less than 20 min) was characteristic for the systems comprising epoxy resins and PhA-based hardeners NX-6019 and GX-6004. A high reactivity of the PhA-based hardener GX-6004 in curing epoxy resins was determined also by DSC studies (Table 12).

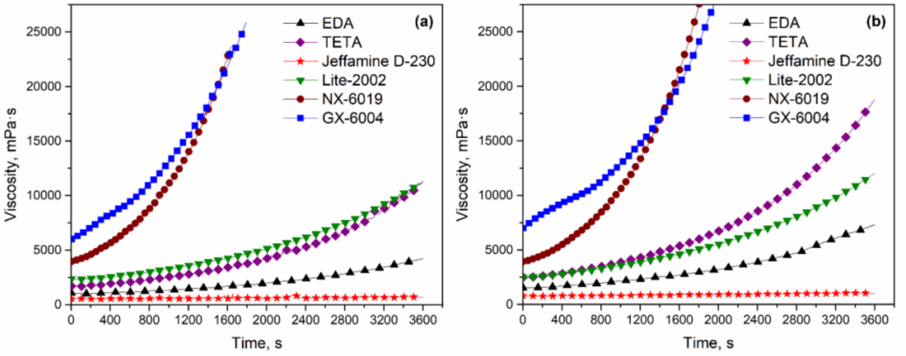

Fig. 14. Changes in dynamic viscosity of the epoxy resins GY-240 (a) and GY-2600 (b) after mixing with various amine hardeners

A short pot-life of the systems containing epoxy resins and PhA-based hardener NX-6019 correlates well with the lowest T_i (at about 48 °C) (Table 12), which means that energetic barrier to start curing reactions is low due to accelerators (DMP and DMAPA) used in the system. Thus, DSC curing of epoxy resins by PhA-based hardener NX-6019 starts earlier and, regardless of the lower curing rate, reaches full curing in approximately the same time as by using the most reactive PhA-based hardener GX-6004.

Table 13. Dynamic viscosity and pot-life of epoxy resins under curing by various amine hardeners

Amine hardener	Initial viscosity, mPa·s	Pot-life, min	Initial viscosity, mPa·s	Pot-life, min
	Epoxy resin GY-240		**Epoxy resin GY-2600**	
EDA	1050	35.5	1500	30
TETA	1680	26.5	2490	24.5
Jeffamine D-230	530	>120	790	>120
Lite-2002	2320	30	2510	30
NX-6019	3960	12	3900	12.5
GX-6004	6010	15	7000	19

Curing of bisphenol A based epoxy resins Araldite GY-2600 and Araldite GY-240 by low-molecular-weight amines EDA, TETA, and Jeffamine D-230, and bio-based PhA containing hardeners Cardolite NX-6019, Cardolite Lite-2002, and Cardolite GX-6004 were studied by DSC and rheology measurements. DSC analysis revealed that epoxy resins cured with PhA-based hardeners initiated curing at a lower temperature, exhibited a broader curing temperature range, and had slightly slower curing rates compared to those cured with low-molecular-weight amine hardeners. These differences highlight the distinct curing behavior of PhA-based systems, which may influence the final properties of the epoxy network. Curing of epoxy resins by the PhA-based hardener NX-6019 was characterised by the lowest T_i and the shortiest pot-life while curing by the PhA-based hardener GX-6004 started later but proceeded with the highest rate. In PhA-based hardeners this is achieved using only a fraction of compositions (22-30%) as small molecular weight amines (MXDA, TMD, TEPA, EDA) and accelerators (DMP, DMAPA). T_g of the cured epoxy resins depended on the type of hardener and varied from 50 °C to 98 °C. Slightly lower T_g of the epoxy resins cured by PhA-based hardeners is related to the long alkyl chains present in the composition of the PhA, which increases flexibility and chain mobility in the cured system. Nevertheless, the use of the most reactive PhA-based hardener GX-6004 containing ~7% of highly reactive TMD provided a possibility to increase T_g of the cured epoxy resins to 80–85 °C.

In conclusion, this study highlights the numerous benefits of using PhA-based hardeners for epoxy coatings. PhA are bio-based, derived from renewable sources, and have a lower environmental impact due to their reduced toxicity. Their low T_i allows for curing at lower temperatures, which extends the workable time across the cold seasons. Epoxy resins cured by PhA-based hardeners achieve T_g values comparable to those cured with pure low-molecular-weight amines. Moreover, the long aliphatic chains in PhA could contribute to enhanced flexibility, improved hydrophobicity, reduced shrinkage, and the potential for better mechanical properties in the cured epoxy coatings.

3.1.2. The effect of reactive diluents on curing and properties of the epoxy coatings

RDs are recognized for their potential to reduce VOC content while maintaining the mechanical performance of coatings. By replacing VOC with RD, it is possible to reduce viscosity, increase pigment loading, and enhance mechanical properties such as flexibility, hardness, adhesion, and scratch resistance, while simultaneously reducing the harmfulness of the composition since RDs react with amine hardeners and stay in coating (Fig. 15). However, existing literature on the effects of RD on the properties of epoxy resins and coatings is limited and, in some cases, inconsistent.

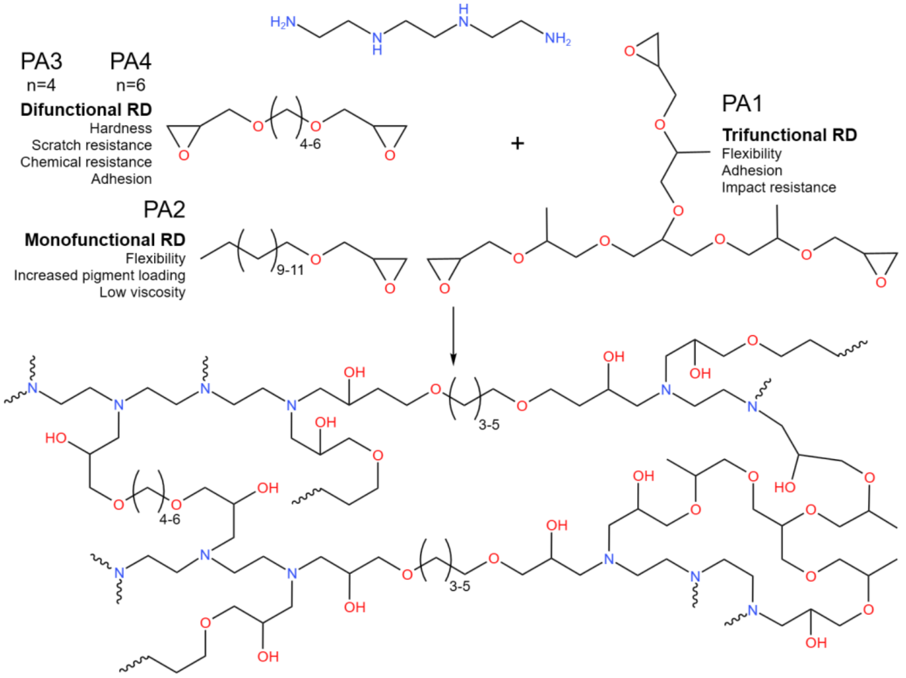

Fig. 15. Reactive diluents in epoxy coating

In this work four epoxy-based compositions were mixed each containing bisphenol-A/-F resin (15 %) by commercial name of Araldite® 783, novolac resin (75 %) Araldite® 289 and 10 % of tested RDs. The RDs chosen for the experiment were trifunctional RD based on GPTE used in PA1 formulation, monofunctional RD based on AGE in PA2 formulation and difunctional RDs based on BDGE in PA3 and HDE in PA4 formulations. Additionally, two different hardeners were employed, PB1 and PB2 with the main difference being DMP tertiary amine accelerator used in PB2 formulation, to test how RDs work with different curing agents. The full PA and PB compositions are given in Tables 6 and 7.

The primary objective was to compare the effect of different RDs on the gelation and vitrification times of the curing systems. Additionally, the effect of RD on the cured epoxy coatings was examined by determining the T_g of the cured systems. Finally, the effect of RD functionality on the mechanical properties of cured epoxy coatings with and without fillers, such as hardness, impact resistance, adhesion, and abrasion resistance, was systematically assessed.

Understanding the viscoelastic properties of materials is vital for product development. Oscillatory shear measurements are performed in controlled strain mode. The given deformation and the measured time-delayed shear stress response are used to calculate the storage modulus G′ and loss modulus G″. G′ measures the energy retained during deformation, indicating the material's stiffness and resistance to shape change. G″ measures the energy lost as heat during deformation, reflecting the material's damping capabilities. The relationship between G′ and G″ is important: if G″ exceeds G′, the material acts like a liquid; if G′ is greater, it behaves like a solid. This relationship is quantified by the loss tangent $\tan\delta$, which helps in understanding the damping characteristics of viscoelastic materials [159].

Evolution and trend of the parameters of G′, G″ and $\tan\delta$ during curing of epoxy resins present important information about the cure process, more specifically, provides gelation and vitrification times. Gelation refers to the formation of three-dimensional crosslinked network that increases viscosity of the material exponentially to infinity [160]. The most generally accepted criterion for gelation is the crossover point of the shear G′ and G″[161]. For other, more complicated networks, the gel point can be found by detecting $\tan\delta$ at different frequencies and determining their crossover point during cure [161–165].

Vitrification time is defined as the point at which the molecular weight or cross-link density of the curing polymer exceeds that which is thermodynamically stable as a rubber to a glass, at which point the reaction dramatically slows due to the reduced mobility of the reactants [166]. Vitrification can be determined from the maximum $\tan\delta$ peak at 1 Hz, the maximum G″ peak at 1 Hz, the onset of frequency dependence in G′, and with the end of frequency dependence in G′[167].

In this study, gelation time of the curing epoxy systems was determined by crossover of the parameters G′ and G″, and crossover of $\tan\delta$ at different frequencies, and vitrification time was determined from the maximum $\tan\delta$ peak at 1 Hz and the maximum G″ peak at 1 Hz. The gelation and vitrification values were summarized in Table 14.

The tested epoxy-amine systems behave like solids at the beginning of the curing process (G′ > G″) due to entrapped air bubbles during mixing of the epoxy system and a curing agent together. After 10-15 min, the G″ becomes larger than the G′ since the system shows liquid type behavior.

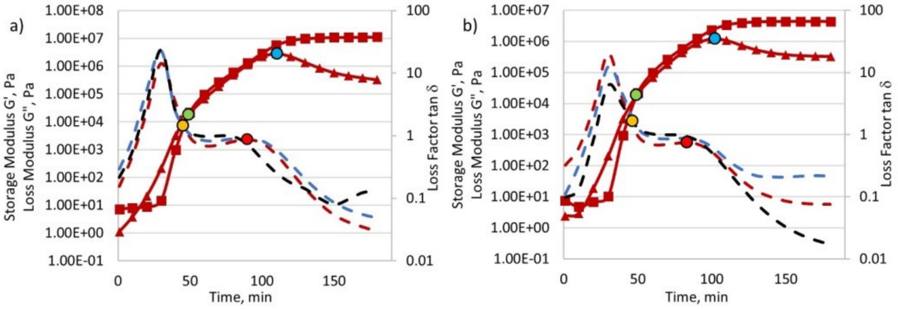

Fig. 16. Evolution of storage modulus G′ (-■-) and loss modulus G″ (-▲-) (angular frequency 1 Hz), and loss factor tanδ (---) (angular frequencies 1 Hz (---); 2 Hz (---); 4 Hz (---)) during curing of the epoxy system PA4 by amine hardeners PB1 (a) and PB2 (b) at 50 °C. Filled circles indicate tanδ crossover (●), crossover of G′ and G″ (●), peak of G″ (●), and second peak of tanδ at 1 Hz (●).

As the reaction proceeds, both G′ and G″ increase and at a certain time intersect; the crossover point indicates equilibrium between viscous and elastic behavior. In this zone gelation occurs. Later-on, when curing reaction progresses and elastic behavior dominates, G′ becomes larger than G″ and tends to approach its maximum value whereas G″ reaches a peak and starts to decrease. In this zone vitrification occurs (Fig. 16).

Gelation time and vitrification time determined by tanδ crossover and tanδ peak, respectively, are shorter compared to those determined by G′ and G″ crossover, and G″ peak, respectively (Table 14). More reliable data are received from the dependencies of tanδ [158–162].

Table 14. Gelation and vitrification time of the curing epoxy resins

Epoxy/amine system	**Gelation time, min**		**Vitrification time, min**	
	tanδ crossover, 1 Hz, 2 Hz, 4 Hz	G′ and G″ crossover, 1 Hz	tanδ peak, 1 Hz	G″ peak, 1 Hz
PA1/PB1	111	132	120	152
PA1/PB2	51	59	88	112
PA2/PB1	85	90	140	173
PA2/PB2	49	59	100	126
PA3/PB1	67	75	110	134
PA3/PB2	45	49	90	111
PA4/PB1	66	76	120	147
PA4/PB2	45	49	83	102

It is evident from Table 14, that gelation time and vitrification time of the epoxy system under curing by the accelerator-containing hardener PB2 were significantly shorter compared to those received under curing by the accelerator-free hardener PB1. This confirms that curing of epoxy systems in the presence of the accelerator proceeds much faster.

Gelation time is affected by the type of the epoxy system, more specifically, by the used RD. The shortest gelation time is characteristic for the epoxy systems PA3/PB1(PB2) and PA4/PB1(PB2) containing difunctional RDs BDGE and HDE (Table 14). Higher reactivity of difunctional RDs in curing reactions could be related to lower epoxy equivalents and low molecular weight of these RDs compared to monofunctional and trifunctional RDs (Table 3). Epoxy systems containing monofunctional AGE (PA2) and trifunctional GPTE (PA1) were less reactive. Monofunctional AGE has a long aliphatic chain of C12-C14 and only one epoxy group, which makes it less reactive and impeding crosslinking reactions. Trifunctional GPTE has the highest molecular weight and branched structure, which could reduce flexibility of the compound and make some reactive groups inaccessible.

Vitrification time of the epoxy systems containing difunctional BDGE and HDE (PA3 and PA4) and trifunctional GPTE (PA1) is very close (Table 14). The presence of monofunctional AGE (PA2) makes vitrification time longer; this could be related to plasticizing effect of this RD containing long aliphatic chain.

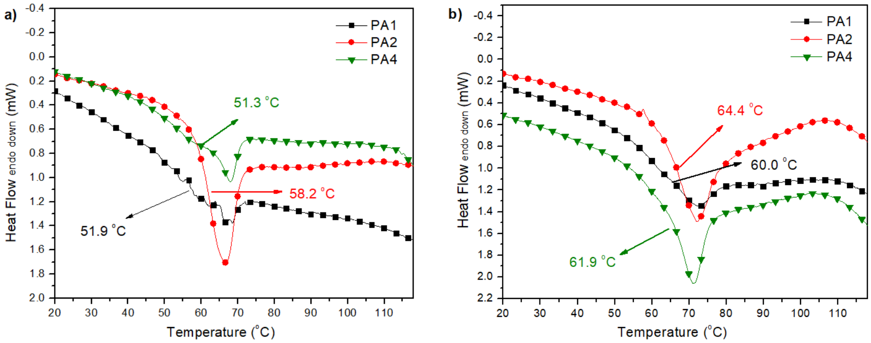

Fig. 17. DSC curves of the epoxy resins PA1, PA2 and PA4 cured by the amine hardeners PB1 (a) and PB2 (b)

DSC curves of the epoxy systems containing various RDs and cured by two hardeners are presented in Fig. 17. DSC curves show endothermic transition at about 60–75 °C. This transition appears like a part of an endothermic peak which is caused by the thermal history of the cured epoxy systems and should be ignored [168, 169]. T_g of the cured epoxy resins depends on the type of hardener being higher for the systems cured by the accelerator-containing hardener PB2 (Table 15). It is related to a higher degree of crosslinking taking place in the presence of tertiary amine DMP. T_g of the cured epoxy resins containing difunctional HDE and trifunctional GPTE (PA4 and PA1, respectively) are very close. Monofunctional AGE (PA2) had more remarkable effect on the T_g raising its value by 3–7 °C. This could be attributed to the lower viscosity of the epoxy system PA2 (Table 16), which makes it easier for network structure to form and create higher crosslinking during formation of the coatings. Nevertheless, differences in T_g of the cured epoxy resins containing RD of different functionality are rather small and hardly deserve attention.

Table 15. Properties of the cured epoxy coatings containing reactive diluents of various functionality

Epoxy resin	**PA1**		**PA2**		**PA3**		**PA4**	
Hardener	PB1	PB2	PB1	PB2	PB1	PB2	PB1	PB2
T_g, °C	51.9	60.0	58.2	64.4	-	-	51.3	61.9
Hardness, Osc	88	103	83	96	101	104	102	103
Adhesion, MPa	20.3	19.8	19.7	22.1	17.3	23.3	23.0	19.8
Impact resistance, J	4.5	4.5	5.0	4.5	6.0	5.5	6.0	5.0

Mechanical properties of the naked epoxy coatings (without fillers and various additives) prepared from the epoxy resin mixtures containing RD and cured by the hardeners with and without accelerator are listed in Table 15. The hardness of the coatings is rather high, about 100 Osc. Slightly higher hardness is characteristic for the coatings containing difunctional BDGE and HDE (PA3 and PA4) and cured by the hardener containing an accelerator DMP (PB2). This could be predetermined by rather short aliphatic chains between epoxy groups in BDGE and HDE, which creates tighter crosslinking of the coatings.

Slightly higher impact resistance is characteristic for the coatings containing difunctional RDs BDGE and HDE (PA3 and PA4) (Fig. 18). Curing of the coatings by the hardener containing DMP accelerator (PB2) slightly reduces impact resistance. This correlates to the T_g parameter as well as hardness, since higher T_g and hardness shows more cross-linked matrix which results in less deformative/flexible coatings with reduced impact resistance.

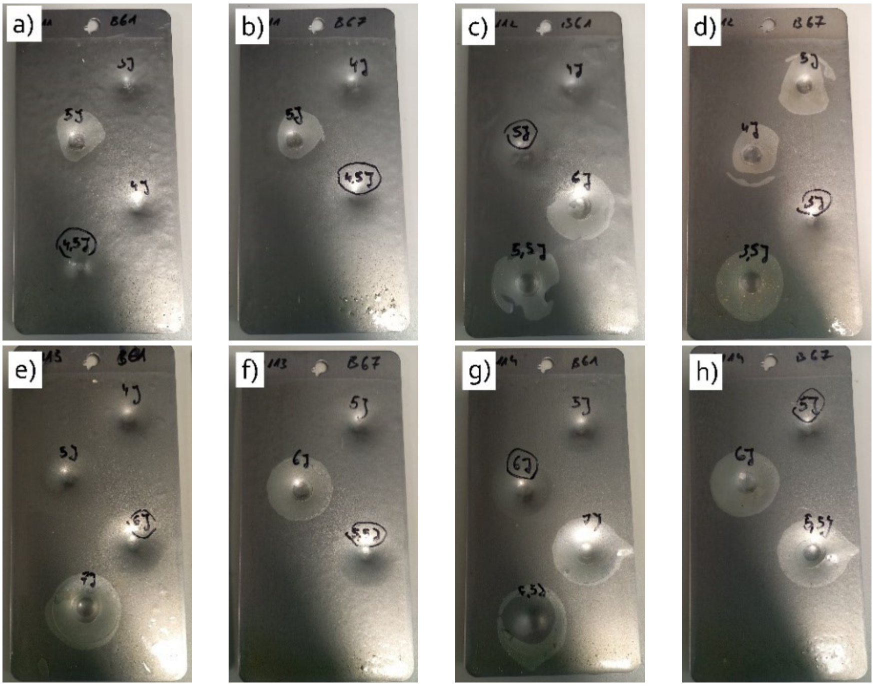

Fig. 18. Impact resistance of different coating systems: a) PA1+PB1; b) PA1+PB2; c) PA2+PB1; d) PA2+PB2; e) PA3+PB1; f) PA3+PB2; g) PA4+PB1; h) PA4+PB2

The adhesion of the coatings is good and does not seem to depend on the used RD and amine hardeners (Fig. 19).

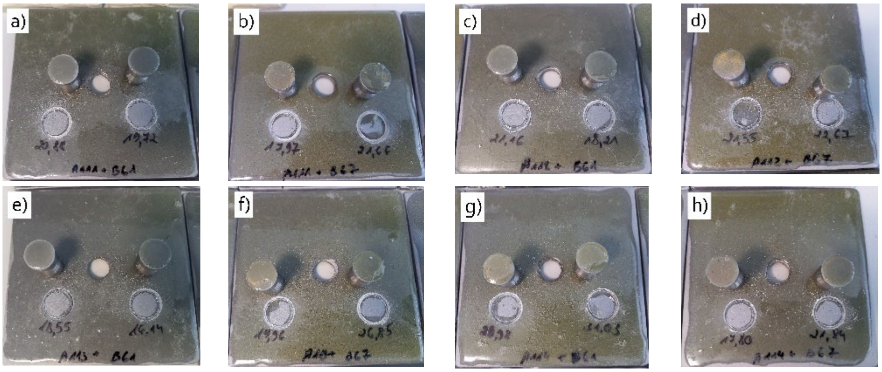

Fig. 19. Adhesion test of different coating systems: a) PA1+PB1; b) PA1+PB2; c) PA2+PB1; d) PA2+PB2; e) PA3+PB1; f) PA3+PB2; g) PA4+PB1; h) PA4+PB2

Table 16 presents properties of anti-corrosion epoxy coatings containing not only RD but also fillers and various additives. Coatings containing fillers and various additives were used to evaluate the effect of RD on properties of coatings in real formulations. It should be noted that the content of fillers and additives is the same in all compositions. The compositions included various additives: glass flakes, quartz and silicon carbide to enhance mechanical resistance, hardness, scratch resistance, and impact resistance; strontium aluminum polyphosphate hydrate for corrosion protection; titanium dioxide for color and opacity; dispersion agents to improve pigment loading; rheology modifiers to enhance anti-sagging properties; and silicon-based additives to provide anti-foaming, leveling, and wetting properties. The hardness and adhesion of the filled coatings are comparable to those of unfilled and do not depend on RD.

Impact resistance of the filled epoxy coatings is much higher due to special fillers used in formulation such as glass flakes and quartz but also do not depend on RD. The filled coatings are characterized by very high abrasion resistance, especially those containing difunctional BDGE and HDE (PA3 and PA4) RDs due to tighter crosslinking of the coatings. The use of the amine hardener containing a DMP accelerator (PB2) also increases abrasion resistance.

Table 16. Properties of the cured epoxy coatings containing various reactive diluents, fillers and additives

Epoxy resin	**PA1**		**PA2**		**PA3**		**PA4**	
Hardener	PB1	PB2	PB1	PB2	PB1	PB2	PB1	PB2
Viscosity at shear rate 0.1 cm^{-1}, Pa·s	60.3	40.3	45.1	30.2	40.1	26.7	43.5	27.8
Viscosity at shear rate 1000 cm^{-1}, Pa·s	2.65	3.47	1.69	2.42	1.89	2.63	2.24	2.65
Hardness, Osc	94	95	93	97	90	105	97	107
Abrasion resist., mg	39	34	52	25	23	20	19	15
Adhesion, MPa	21.9	21.2	21.4	24.2	19.3	19.8	19.3	20.6
Impact resistance, J	7	9	8	10	7	8	9	9

A very important characteristic of the mixed epoxy compositions is dynamic viscosity at low shear rate (0.1 s^{-1}) mimicking storage state, and at high shear rate (1000 s^{-1}) mimicking airless spray (Table 16). The low viscosity of the mixed compositions is desirable since it requires easier application methods as well as gives better coating formation and leveling. Dynamic viscosity of the mixed compositions at high shear rates was in correlation with the viscosity of RD. The highest viscosity is characteristic for the composition containing trifunctional GPTE (PA1). The viscosities at high and low shear rates of the compositions containing difunctional and monofunctional RDs are significantly lower. Mixing with the hardener containing an accelerator DMP (PB2) reduces viscosity at a low shear rate but evidently increases viscosity of the compositions at high shear rate.

The influence of RDs with different functionalities on the curing of epoxy resins is evident but minimal. Epoxy resins containing difunctional RD exhibit the shortest gelation time during curing. The vitrification time of cured epoxy resins with difunctional BDGE, HDE and trifunctional GPTE is nearly identical, whereas the inclusion of monofunctional AGE extends the vitrification time. The data obtained from DSC analysis suggest that the use of monofunctional reactive diluent had more remarkable effect on the T_g raising its value by 3–7 °C. Reactive epoxy diluents had some effect on properties of the cured naked and filled epoxy coatings. Monofunctional AGE reduced the viscosity of epoxy formulations at high shear rates. Difunctional BDGE and HDE had the most significant impact, reducing the viscosity of epoxy formulations while enhancing the hardness and abrasion resistance of the filled coatings. This study demonstrated that RDs can not only replace traditional VOCs to reduce viscosity but also improve the mechanical properties of coatings without introducing toxic side effects.

3.2. Optimization of encapsulation of reactive compounds for self-healing anti-corrosion epoxy coatings

Dual-component microcapsules are widely employed to achieve effective self-healing properties. Amines are an attractive choice for healing materials due to their ability to react with epoxies and isocyanates. Unfortunately, amines are generally hydrophilic, highly reactive and possess a high pH, which makes encapsulation via oil-in-water methods particularly difficult [113]. In this work, a dual microcapsule system was selected for testing: one microcapsule containing PAAE as the healing agent encapsulated in a UV-curable shell, and the other containing IPDI as the healing agent enclosed within a PU shell.

PAAE was selected as the healing agent due to its high reactivity with isocyanates and its compatibility with the coating matrix. However, the use of PAAE as a healing agent remains relatively unexplored, primarily due to its novelty and the challenges associated with its encapsulation. The more hydrophobic nature of PAAE in comparison to other amines allows it to be emulsified in water, making oil-in-water encapsulation techniques feasible [81, 140]. This study introduces a novel approach to encapsulating PAAE within a UV-curable shell. This method offers significant advantages, including faster encapsulation times, higher microcapsule yields, and represents an area that has not been extensively studied.

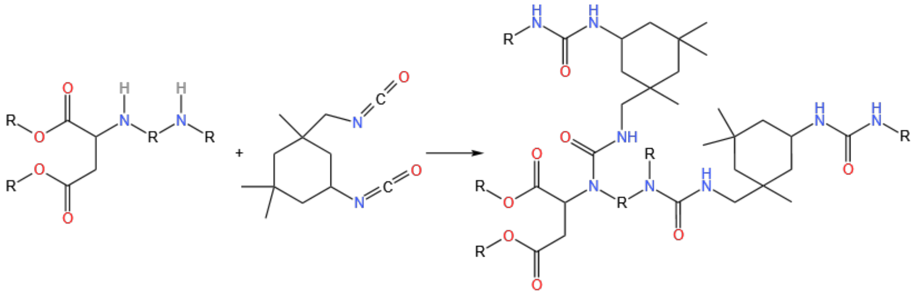

Fig. 20. PAAE reaction with IPDI

To complement the dual-microcapsule system, IPDI was selected as the isocyanate component due to its compatibility and reactivity with PAAE. IPDI is a cycloaliphatic diisocyanate, characterized by two isocyanate groups with differing reactivities (primary and secondary -NCO groups), enabling selective interactions with hydroxyl-functionalized compounds. This unique reactivity profile has made IPDI a common choice in the synthesis of polyurethane foams [170–173] and polyurethane coatings [174–176]. The reaction between PAAE and IPDI (Fig. 20) results in PU which offers numerous advantages, such as good leveling performance, alkali and acid resistance, water and wear resistance.

3.2.1.Encapsulation of PAAE into UV curable shell

Successful encapsulation depends on many factors, with emulsification being the primary and most influential factor. Emulsification depends on the selected emulsifier, agitation speed, temperature, and duration of the process. The emulsifier ensures generation of new oil droplets in the dispersed phase and subsequent stabilization of these droplets. Polymeric and charge-containing emulsifiers (stabilizers) were used for stabilization of the emulsions. Mixture of PVA-GA, a copolymer of SMA or SDBS were used as stabilizers. GA demonstrated good stabilization ability in many studies on microencapsulation [177, 178]. Combining two polymeric stabilizers, PVA and GA, gave even better results, increasing efficiency of microencapsulation. SMA was also often used for stabilization of emulsions containing encapsulating materials [179]. Hydrolyzed SMA possesses hydrophilic carboxyl groups alongside hydrophobic aryl groups, enabling it to self-assemble into a dual-layered structure. This emulsifier combines both polymeric and ionic stabilization. Low molecular weight charge-containing emulsifier SDBS exhibits good stabilization by the formation of micellar layer on hydrophobic droplets.

Table 17. Results of microencapsulation of PAAE in UV-curing resin (first series – ethyl lactate as a solvent)

No	Core: shell	Agitation speed, rpm	Emulsifier and its concentration, %	Ethyl lactate in core, %	Core content, %	Microcapsule size range, µm	Average microcapsule size, µm
EA1	2:1	500	PVA 2 / GA 3	50	40.3	30-270	70
EA2	3:1	750	PVA 1 / GA 1.5	25	51.2	20-260	130
EA3	4:1	1000	SDBS 1	10	21.0	5-160	50
EA4	5:1	3000	PVA 2 / SDBS 1	-	19.0	5-100	30
EA5	2:1	750	SDBS 1	-	47.6	10-1110	100
EA6	3:1	1000	PVA 2 / SDBS 1	50	10.3	5-110	40
EA7	4:1	3000	PVA 2 / GA 3	25	41.7	15-100	50
EA8	5:1	500	PVA 1 / GA 1.5	10	71.1	70-400	130
EA9	2:1	1000	PVA 2 / GA 3	10	37.5	10-140	70
EA10	3:1	3000	PVA 1 / GA 1.5	-	51.6	10-120	70
EA11	4:1	500	SDBS 1	50	43.7	30-280	70
EA12	5:1	750	PVA 2 / SDBS 1	25	14.2	5-150	60
EA13	2:1	3000	SDBS 1	25	13.2	5-110	10
EA14	3:1	500	PVA 2 / SDBS 1	10	58.1	20-330	100
EA15	4:1	750	PVA 2 / GA 3	-	63.7	40-180	80
EA16	5:1	1000	PVA 1 / GA 1.5	50	46.4	10-150	70

Table 18. Data of microencapsulation of PAAE in UV-curing resin: second series – xylene as a solvent

No	Core: shell	Agitation speed, rpm	Emulsifier and its concentration, %	Xylene in core, %	Core content, %	Microcapsule size range, µm	Average microcapsule size, µm
XA1	2:1	500	PVA 2 / GA 3	-	54.3	18-500	60
XA2	3:1	750	PVA 1 / GA 1.5	10	53.1	11-620	60
XA3	4:1	1000	SDBS 1	25	48.5	21-53	50
XA4	5:1	3000	SMA 1	50	6	9-28	15
XA5	2:1	750	SDBS 1	50	28.5	38-70	20
XA6	3:1	1000	SMA 1	-	57.4	18-280	70
XA7	4:1	3000	PVA 2 / GA 3	10	17.3	5-50	30
XA8	5:1	500	PVA 1 / GA 1.5	25	68.7	20-150	50
XA9	2:1	1000	PVA 2 / GA 3	25	15.6	8-25	20
XA10	3:1	3000	PVA 1 / GA 1.5	50	40.8	15-60	25
XA11	4:1	500	SDBS 1	-	63.1	30-390	230
XA12	5:1	750	SMA 1	10	56.8	16-240	50
XA13	2:1	3000	SDBS 1	10	29.8	9-130	22
XA14	3:1	500	SMA 1	25	54.8	23-210	60
XA15	4:1	750	PVA 2 / GA 3	50	23.5	5-35	15
XA16	5:1	1000	PVA 1 / GA 1.5	-	62.7	10-140	40

It is known that increasing size of microcapsules usually worsens their mechanical properties but improves healing efficiency [96]. Obviously, there is an optimal microcapsule size that can effectively balance both properties. When the size of microcapsules approaches the thickness of a coating, it leads to compromised mechanical and visual characteristics of the coating [180].

In the present study, obtaining of microcapsules with the size of 50 µm was projected, since microcapsules of such dimensions are appropriate for the coatings with the thickness of 200-500 µm.

Two series of experiments were carried out to synthesize microcapsules differing in size and core content. Four key parameters such as core-to-shell ratio, agitation speed, emulsifier type and concentration, and amount of solvents ethyl lactate or xylene were chosen to govern core content and size of microcapsules. The microcapsules were created using water in oil emulsification method described in 2.5.1 (Scheme 1).

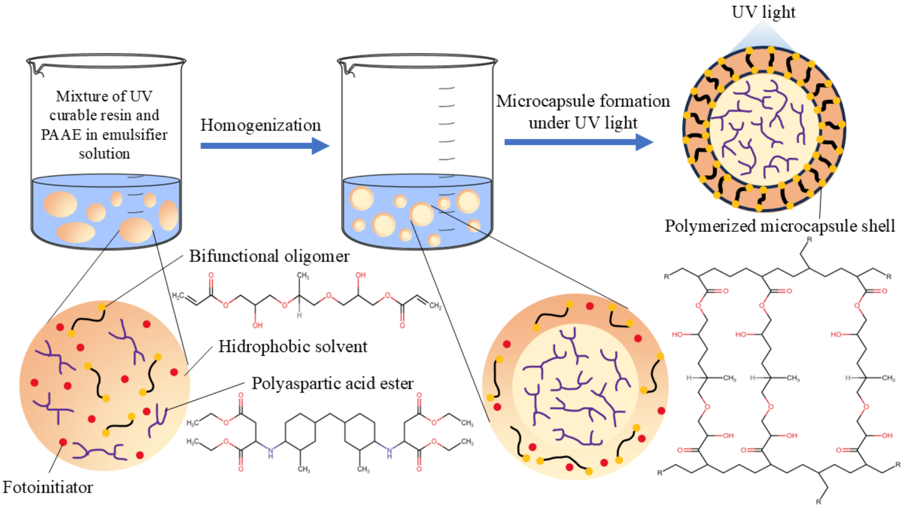

Scheme 1. PAAE encapsulation into UV cured polyacrylate shell.

PAAE and UV curable acrylic resin were mixed and subsequently added to water-emulsifier solution to create an oil-in-water emulsion. A homogenizer was employed to achieve the desired oil droplet size. After preparing the emulsion, UV light was used in combination with a photoinitiator present in the UV resin mixture to initiate a radical polymerization reaction. The photoinitiator used (ethyl phenyl(2,4,6-trimethylbenzoyl)phosphinate) absorbed the UV light, generating reactive free radicals that triggered the polymerization of the C=C double bonds in the UV-curable resin comprised of monomers, leading to the formation of the microcapsule shell (Fig. 21).

In the first series (Table 17), solvent for the oil phase ethyl lactate was used to enhance layer separation during emulsification. Ethyl lactate is a biodegradable solvent with high solvency power, low vapor pressure, low surface tension and high boiling point.

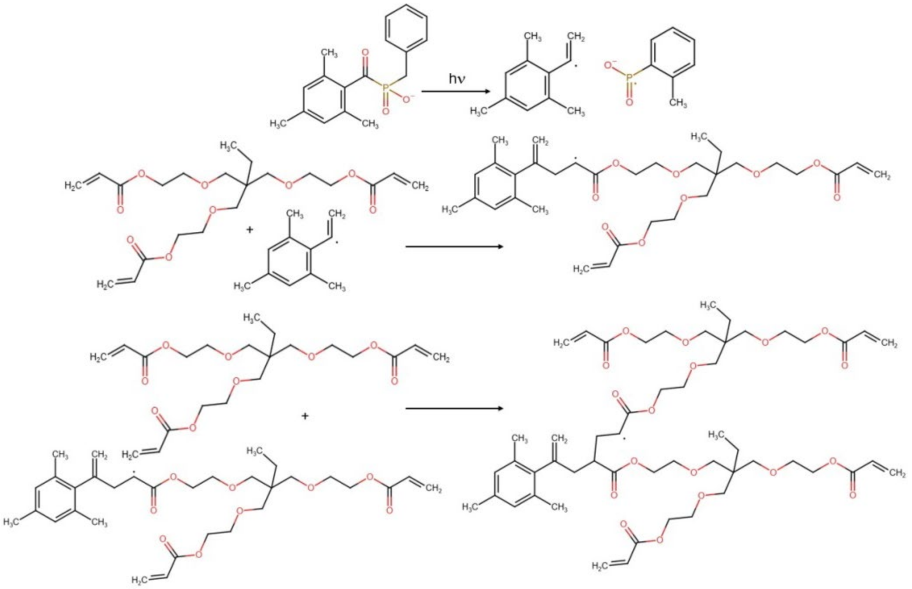

Fig. 21. Photopolymerization reaction of microcapsule shell formation

The substitution of solvents like toluene or acetone with ethyl lactate has led to a notably safer working environment [181]. In the second series (Table 18), the solvent for the oil phase ethyl lactate was replaced by xylene, and the emulsifier mixture PVA / SDBS by an emulsifier SMA. This was done trying to evaluate whether xylene contributes to improving layer distribution between UV curable resin and PAAE within the core before shell formation. Data of microencapsulation of PAAE in UV curing acrylic resin are presented in Tables 17 and 18.

3.2.1.1. Characterization of PAAE microcapsules with UV curable shell

Size of microcapsules was evaluated using OM and SEM (Fig. 22-25). The microcapsules are round and of perfectly spherical structure. After lyophilization, most of the microcapsules were in powder form. Average size of microcapsules significantly depends on conditions of preparation and varies from 10 μm to 230 μm (Tables 17 and 18, Fig. 22-25). Core-to-shell ratio has low impact on the microcapsule size, and this is in accord with previous observations [136]. Microcapsule size highly depends on agitation speed being large at low agitation and much smaller at high agitation. The smallest microcapsules with the average diameter 10–30 μm were obtained at agitation speed 3000 rpm while the largest with the diameter 100–130 μm at agitation speed 500–750 rpm. Emulsifiers prevent agglomeration of microcapsules; thus, high concentration of emulsifiers is preferential for the formation of the microcapsules with smaller diameter. Solvents dilute viscous oil phase which facilitates formation of smaller microcapsules. The viscosity of xylene is more than 3 times lower compared to that of ethyl lactate, that is why dilution of the oil phase with xylene gives the smallest microcapsules and with narrower size distribution.

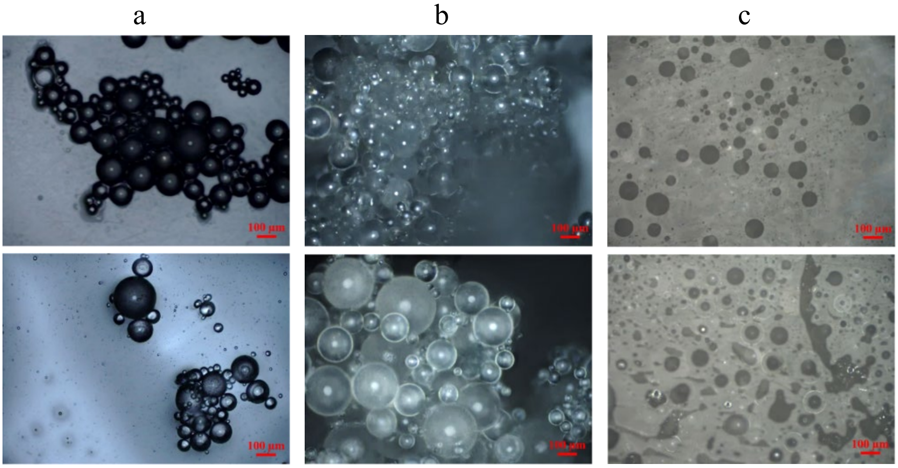

Fig. 22. OM micrographs of the microcapsules EA15 (upper line) and EA16 (bottom line), obtained in the presence of ethyl lactate as a solvent, in solution (a), dried (b) and ruptured (c).

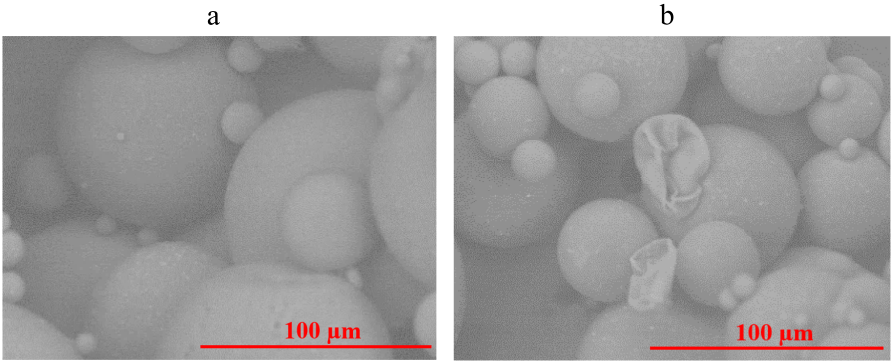

Fig. 23. SEM micrographs of dried (a) and ruptured (b) microcapsules EA16.

Upon pressing microcapsules between two glass panels, the healing agent PAAE is released and is seen as oil spatters on the glass. It was noticed that the microcapsules obtained using a mixture of emulsifiers PVA 2% / SDBS 1% were mostly tended to agglomeration, were unstable during lyophilization process and releasing lower amount of encapsulated PAAE after mechanical crush. Release of the core material PAAE after mechanical damage of the microcapsules was observed in Fig. 22c and 24c.

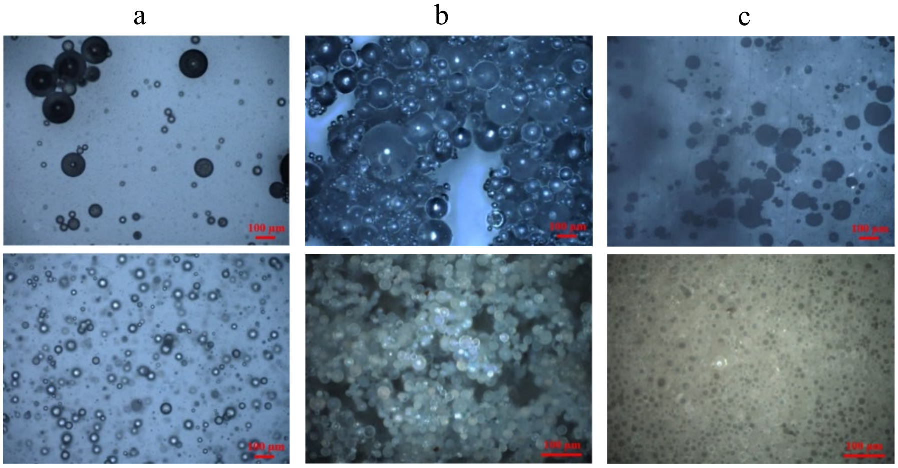

Fig. 24. OM micrographs of the microcapsules XA12 (upper line) and XA15 (bottom line), obtained in the presence of xylene as a solvent, in solution (a), dried (b) and ruptured (c).

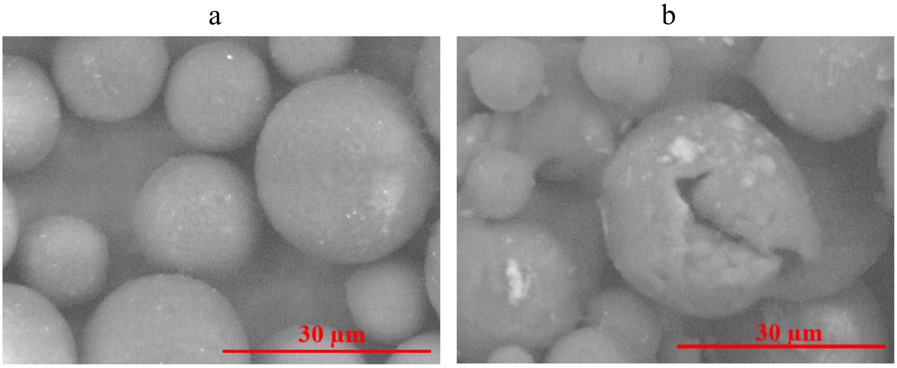

Fig. 25. SEM micrographs of dried (a) and ruptured (b) microcapsules XA15.

Under mechanical pressure, the microcapsules containing ethyl lactate as a solvent tend to shrink instead of breaking, which means that microcapsule shell is too elastic. In contrast, the microcapsules containing xylene as a solvent tend to break. We suppose, this phenomenon is related to volatility of the solvents: ethyl lactate remains mainly in the shell while xylene mainly evaporates making shell structure more fragile.

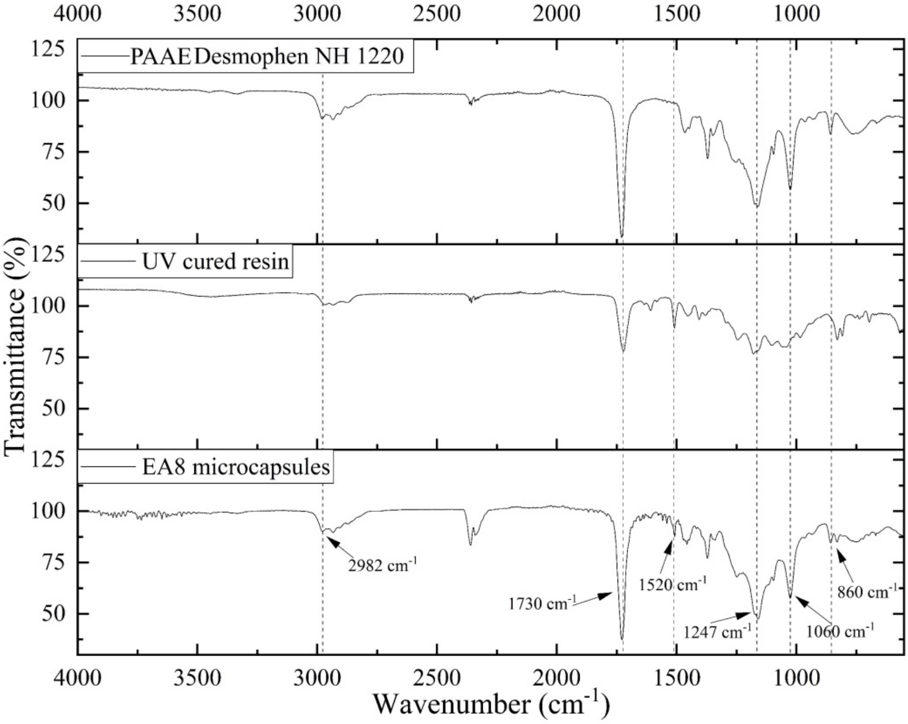

Fig. 26. FTIR spectra of PAAE, UV cured resin and EA8 microcapsules.

FTIR spectra of the cured acrylic resin (microcapsule shell), PAAE Desmophen NH 1220 (microcapsule core) and microcapsules containing encapsulated PAAE were recorded (Fig. 26). At several frequencies, the absorption bands of the core and shell materials overlapped due to the similarity of their functional groups. The absorption bands at approximately 2982 and 2870 cm^{-1} belong to asymmetric and symmetric vibrations of C–H bonds of CH_3 or CH_2 groups, respectively. Characteristic absorption band of C=O stretching vibrations at 1730 cm^{-1} is associated with both acrylic resin and PAAE [182]. Fortunately, PAAE C=O absorption band is stronger than that of the shell material, which enables to confirm encapsulation by increasing intensity of that band. A broad absorption band associated with hydroxyl groups of acrylates is observed at 3580-3200 cm^{-1}. The absorption band at 1520 cm^{-1} corresponds to C=C stretching vibration in aromatic epoxy resin. The absorption band at 1247 cm^{-1} is characteristic for the O=C–O–C ester bond in the polymeric acrylate [81]. Characteristic absorption bands of PAAE secondary amine are at 3340 cm^{-1} (–NH stretching vibrations), 860 cm^{-1} (–NH rocking vibrations), and 1030 cm^{-1} (–C–N stretching vibrations). In the spectra of microcapsules, in addition to the distinctive absorption bands attributed to the shell material, the absorption bands attributed to the core material were also present.

For determination of the core content in microcapsules, TGA of the core material, shell material, and microcapsules was done. Destruction and evaporation of the core material PAAE starts at approximately 200 °C and continues until approx. 300 °C. Degradation of the shell material proceeds at much higher temperatures, between 330 °C and 480 °C. As degradation of both materials occurs at distinct temperatures, determination of the core content in microcapsules is based on relative weight loss at temperatures until 320 °C.

Unfortunately, there is no possibility to discern between PAAE and solvent present in the core of microcapsules by TGA since these materials lose weight in the same temperature interval. Core content of the microcapsules was affected by many factors and was in the range from 6% to 72% (Tables 17 and 18). Very important that combining several parameters affecting microencapsulation process enabled to achieve high core content with the amount of encapsulated PAAE in microcapsules up to 60-70%.

3.2.1.2. Optimization of encapsulation of PAAE into UV curable shell

The SNR calculated using the Taguchi criterion larger-the-better as used for identification of the optimal conditions to achieve the maximum core content of the microcapsules, and the Taguchi criterion nominal-the-best to find conditions favorable for producing microcapsules with the average size of 50 μm. The impact of each parameter is presented in Fig. 27.

The highest SNR value (and the same, the highest core content) was at the core-to-shell ratio 4:1 when using ethyl lactate as the solvent, and at the core-to-shell ratio 3:1 when using xylene (Fig. 27A and 27B). Microcapsule size was closest to the target value of 50 μm at core-to-shell ratio 4:1 in the presence of ethyl lactate as the solvent, but this ratio was shifted to 5:1 in the presence of xylene (Fig. 27C and 27D).

The core content of microcapsules is the highest at low agitation speed (Fig. 27A and 27B). This phenomenon could be attributed to the formation of larger microcapsules, since faster agitation usually leads to smaller microcapsules. Furthermore, increasing the agitation speed may raise the likelihood of destruction of microcapsules with thinner shells and, the same, higher core content. The microcapsules with an average size of 50 μm (Fig.

27C and 27D) were produced at agitation speed of 1000 rpm, which was found to be optimal for both series.

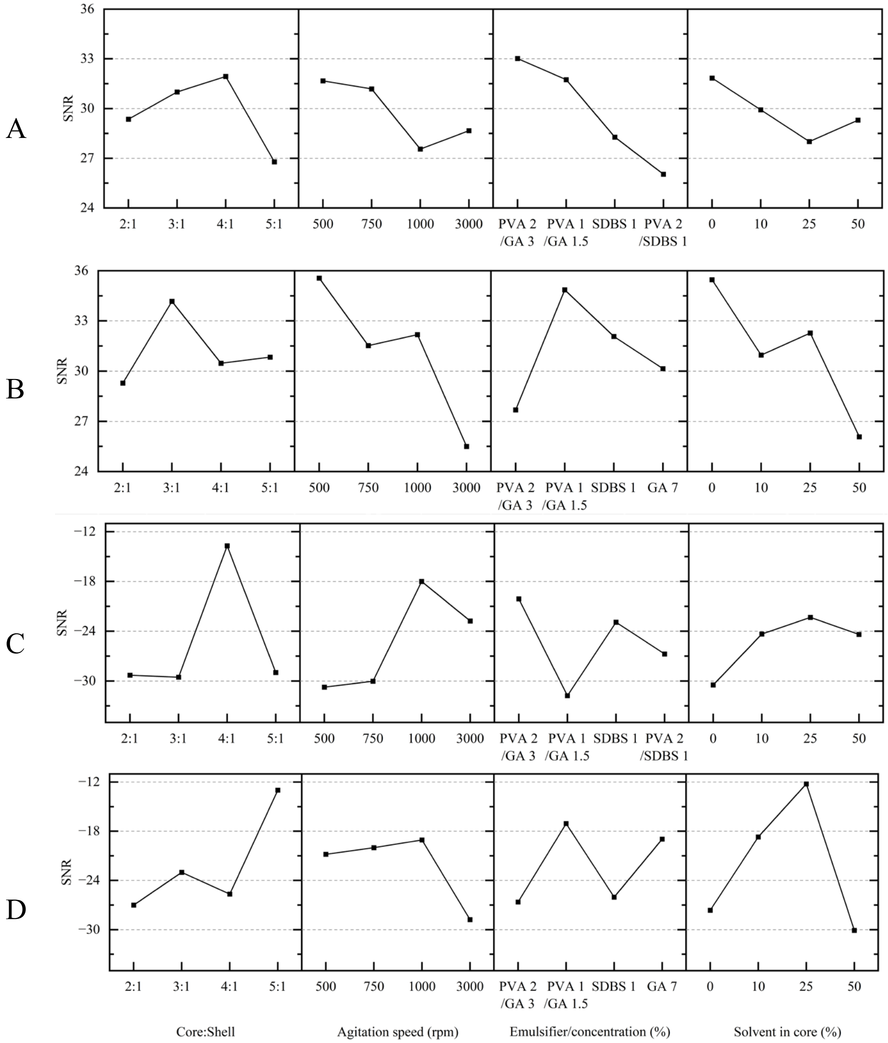

Fig. 27. SNR plots according to Taguchi method; the dependence of the microcapsule core content (A, B) and microcapsule size (C, D) on microencapsulation parameters core to shell ratio, agitation speed, type and concentration of emulsifier, and ethyl lactate (A, C) or xylene (B, D) content.

In the presence of ethyl lactate as the solvent, the highest core content of the microcapsules was achieved using a mixture of the emulsifiers PVA 2% and GA 3% (Fig. 27A). Meanwhile, when ethyl lactate was replaced by xylene, the optimal emulsifier concentration was lower – PVA 1% and GA 1.5%. The lower concentration of the emulsifiers PVA and GA also fits well for the compositions containing ethyl lactate (Fig. 27A). Optimal emulsifier for the microcapsules with the size of 50 µm in the presence of ethyl lactate is a mixture of PVA 2% and GA 3% (Fig. 27C); reasonably good results were obtained also using SDBS 1 % as an emulsifier. When xylene was used as the solvent, the optimal concentration of the emulsifiers was lower PVA 1% and GA 1.5% (Fig. 27D).

Table 19. Optimal conditions for microencapsulation of PAAE in UV curing resin in respect to the highest amount of the core content

	Core:shell	Agitation speed, rpm	Emulsifier and its concentration, %	Solvent content, %
First series EA1-EA16	4:1	500	PVA 2 / GA 3	-
Second series XA1-XA16	3:1	500	PVA 1 / GA 1.5	-

Table 20. Optimal conditions for microencapsulation of PAAE in UV curing resin in respect to the nominal microcapsule size of 50 µm

	Core:shell	Agitation speed, rpm	Emulsifier and its concentration, %	Solvent content, %
First series EA1-EA16	4:1	1000	PVA 2 / GA 3	Ethyl lactate, 25
Second series XA1-XA16	5:1	1000	PVA 1 / GA 1.5	Xylene, 25

Addition of the solvents either ethyl lactate or xylene to the oil phase before encapsulation decreases core content of the microcapsules. Thus, the optimal conditions for the microencapsulation of PAAE in respect to core content exclude both solvents. Dilution of PAAE by a certain amount of ethyl lactate or xylene (25%) was favorable in preparing microcapsules with an average size of 50 µm (Figs 27C and 27D). Optimal conditions for microencapsulation of PAAE in UV curing resin are presented in Tables 19 and 20.

Microencapsulation of PAAE into UV cured polyacrylate shell was done through oil-in-water emulsion polymerization triggered by UV light. The microencapsulation of PAAE in UV-curable acrylic resin was optimized using the Taguchi L16 parameter design approach, aiming to identify conditions that maximize core content while achieving a microcapsule size of 50 µm. The optimal conditions for highest core content was identified, which included a core-to-shell ratio of approximately 3:1 or 4:1, a low agitation speed of 500 rpm, the use of two polymeric emulsifiers mixture, PVA 1-2% / GA 1.5-3% in the absence of solvents. The microcapsules of optimal size 50 µm are formed by using 4:1 or 5:1 core content, agitation speed of 1000 rpm, emulsifier mixture of PVA 1-2% / GA 1.5-3%, and solvent content of 25%. The UV-initiated polymerization process significantly reduced processing time while enabling high core content and precise control over microcapsule size, offering a promising method for efficient encapsulation of active compounds.

3.2.2.Encapsulation of IPDI into PU shell

The microcapsules were produced through an oil-in-water emulsion, utilizing the interfacial polymerization reaction described in section 2.5.2. (Scheme 2). Two isocyanates, IPDI and 27% TIPTP solution in ethyl acetate (Desmodur RFE) were mixed and subsequently added to water-emulsifier solution to create an oil-in-water emulsion. A homogenizer was employed to achieve the desired oil droplet size. After emulsifying the isocyanates in the aqueous phase, the reactive amine TETA was added to initiate the interfacial polymerization reaction.

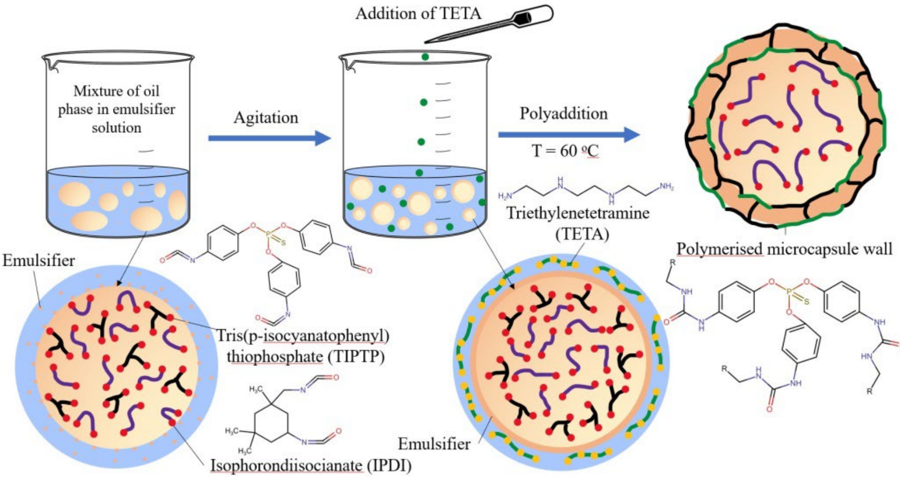

Scheme 2. IPDI encapsulation into PU shell

The reaction between TETA and the isocyanate groups led to the formation of a polymeric shell around the microcapsules, confined to the outer surface due to TETA's solubility in the aqueous phase and its insolubility in the oil phase. Since TIPTP is the more reactive of the two isocyanates, it is likely that TETA primarily reacted with this isocyanate, although some reaction with IPDI may have also taken place.

The encapsulation process was studied using L16 Taguchi method matrix, where 4 chosen parameters were changed throughout the synthesis. Three different signals were received and measured – content of the healing agent IPDI inside microcapsules (core content), microcapsule size and microcapsule yield. Synthesis parameters and the signals are given in Table 21.

Table 21. Data of microencapsulation of IPDI into PU shell

No	Core: shell	Agitation speed, rpm	Emulsifier and its concentration, %	Reaction time, min	Core content, %	Size range, µm	Average size, µm	Yield, %
IE1	2:1	3000	PVA 2 / GA 3	30	58.9	20-90	35	36.7
IE2	3:1	4000	PVA 1 / GA 1.5	45	64.1	20-90	45	58.9
IE3	4:1	5000	SDBS 1	60	72.3	10-40	20	74.3
IE4	5:1	6000	GA 7	90	78.6	20-90	60	26.9
IE5	2:1	4000	SDBS 1	90	52.2	10-20	10	84.3
IE6	3:1	5000	GA 7	30	61.7	15-110	60	56.0
IE7	4:1	6000	PVA 2 / GA 3	45	74.6	8-20	15	25.2
IE8	5:1	3000	PVA 1 / GA 1.5	60	76.1	30-120	80	32.6
IE9	2:1	5000	PVA 2 / GA 3	60	58.3	10-40	35	6.5
IE10	3:1	6000	PVA 1 / GA 1.5	90	65.8	20-60	40	12.6
IE11	4:1	3000	SDBS 1	30	66.4	10-60	25	6.0
IE12	5:1	4000	GA 7	45	69.7	30-60	50	29.4
IE13	2:1	6000	SDBS 1	45	49.9	10-20	10	71.5
IE14	3:1	3000	GA 7	60	74.6	20-70	50	48.9
IE15	4:1	4000	PVA 2 / GA 3	90	71.8	20-70	40	16.8
IE16	5:1	5000	PVA 1 / GA 1.5	30	73.1	20-80	40	19.3

Table 22. Stability of the synthesized microcapsules

No	Emulsifier/ concentration %	Stability in solution	Stability after lyophilization	Microcapsule size range, µm	Average microcapsule size, µm
IE1	PVA 2 / GA 3	Stable	Stable	20-90	35
IE2	PVA 1 / GA 1.5	Stable	Stable	20-90	45
IE3	SDBS 1	Agglomerated	Agglomerated	10-40	20
IE4	GA 7	Stable	Stable	20-90	60
IE5	SDBS 1	Agglomerated	Agglomerated	10-20	10
IE6	GA 7	Stable	Stable	15-110	60
IE7	PVA 2 / GA 3	Stable	Stable	8-20	15
IE8	PVA 1 / GA 1.5	Stable	Stable	30-120	80
IE9	PVA 2 / GA 3	Stable	Stable	10-40	35
IE10	PVA 1 / GA 1.5	Stable	Stable	20-60	40
IE11	SDBS 1	Agglomerated	Agglomerated	10-60	25
IE12	GA 7	Stable	Stable	30-60	50
IE13	SDBS 1	Agglomerated	Agglomerated	10-20	10
IE14	GA 7	Stable	Stable	20-70	50
IE15	PVA 2 / GA 3	Stable	Stable	20-70	40
IE16	PVA 1 / GA 1.5	Stable	Agglomerated	20-80	40

It was determined that some microcapsules tend to agglomerate more than others. During lyophilization, which proceeds under deep vacuum, some microcapsules with thin or defectively formed shells were deformed and even ruptured. After rupture, the core content of the microcapsules was released and spread among other microcapsules which invoked sticking them together and agglomerating. Agglomeration can also be caused by an unsuitable emulsifier chosen for the system. It was determined that the microcapsules obtained in the presence of SDBS as an emulsifier had higher tendency to agglomerate than those obtained using GA or PVA / GA solutions (Table 22). Moreover, using 1% SDBS as an emulsifier led to the smallest microcapsule size. It is known that small particles have a higher tendency to agglomeration which leads to the formation of much larger aggregates [184].

3.2.2.1. IPDI microcapsule with PU shell characterization

The prepared microcapsules were analyzed using OM and SEM to evaluate the microcapsule size, size distribution, stability in aqueous solution and in dry state, and resistance to rupture under applied force (Fig. 28-29).

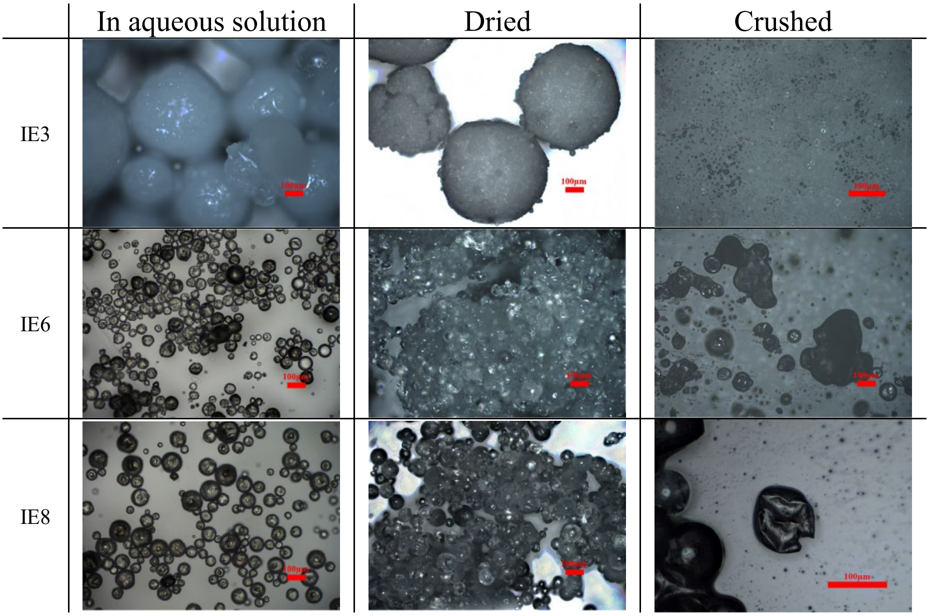

Fig. 28. Optical microscope images of the microcapsules IE3, IE6 and IE8

It was determined by OM that microcapsules synthesized in the presence of 1% SDBS as emulsifier were agglomerated both in water and when dried. The agglomerates measured 300-1000 µm in size were made up from 10-60 µm microcapsules stuck together and remained agglomerated even after washing and lyophilization. In contrast, the microcapsules synthesized using GA and GA / PVA as emulsifiers were stable, round and dispersed evenly. When pressed between two glass panels, the microcapsules underwent collapse, and the subsequently released healing agent was observed between the glass panels. This observation signifies a high efficiency in the encapsulation of the healing agent and suggests the presence of thin microcapsule walls that can be easily damaged.

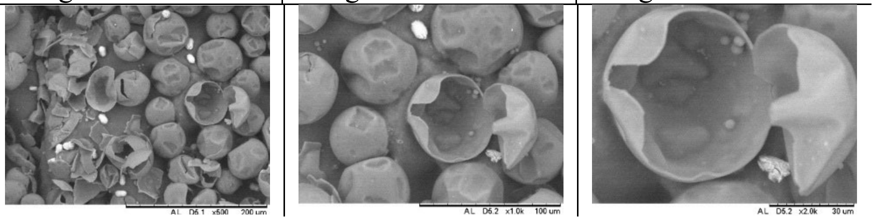
Magnification x500 | Magnification x1000 | Magnification x2000

IE4

Fig. 29. SEM images of the crushed microcapsules IE4

SEM was used to measure microcapsule size as well as visualize their surface, form, and determine approximate thickness of microcapsule shell (Fig. 29). Before the experiment, some microcapsules were crushed using metal spatula to examine the rupture picture and microcapsule shell thickness. As it is seen from SEM images, the microcapsule surface is smooth with slight indentations which could be caused by lyophilization process. It was determined that microcapsule shell was very thin, with the thickness of about 1-3 µm, that’s why it can be easily crushed.

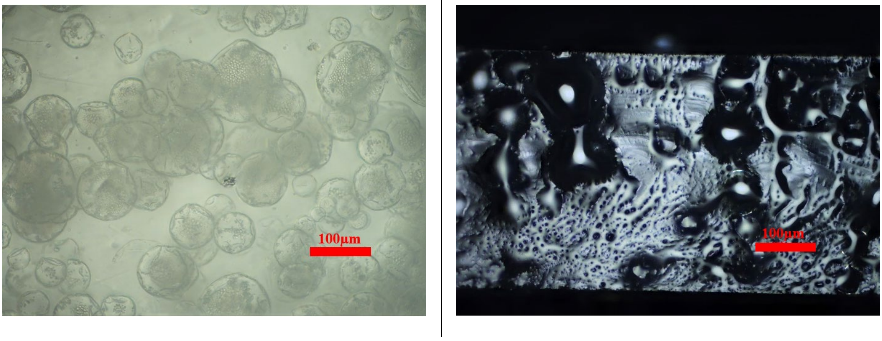
Microcapsules inside clear coating | Crosscut of coating

Fig. 30. Optical microscope images of microcapsules IE8 inside clear coating and coating crosscut

Microcapsules IE8 were added to PAAE/isocyanate through the coating which was cured. The clear coating was examined with an optical microscope trying to determine microcapsule dispersibility inside the coating as well as microcapsule ability to rupture when crack appears (Fig. 30).

The microcapsules inside the cured coating were dispersed evenly and did not agglomerate or rupture. The crosscut of coating showed that microcapsules were conjugated with the coating and split in two parts when coating was broken. A part of the healing agent is seen near the rupture place as oil splatter (Fig. 30).

FTIR spectra of IPDI (core material), PU shell and microcapsules IE14 were recorded and presented in Fig. 31. The absorption band of stretching vibrations of N–H at about 3350 cm^{-1} and absorption bands of C=O and N–H in carbamide group at about 1510 cm^{-1} and 1650 cm^{-1}, respectively, are characteristic to PU shell material and are seen in spectra of the shell material and microcapsule.

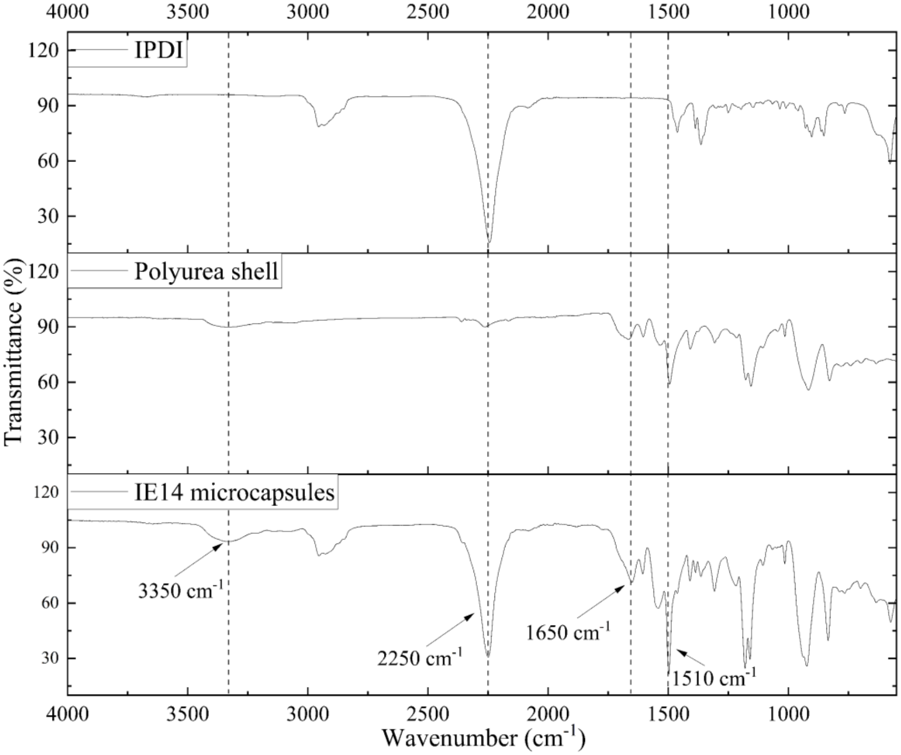

Fig. 31. FTIR spectra of IPDI as core material, polyurea shell, and microcapsules IE14

Intensive absorption band of stretching vibrations of N=C=O in isocyanate groups appears at about 2250 cm^{-1} in both spectra of IPDI and microcapsules IE14; this proves that the encapsulation of IPDI as core material was successful.

For determination of core content in microcapsules, TGA of the core material and microcapsules was done. IPDI evaporation and destruction starts at about 130 °C and continues until approx. 240 °C. The first stage of degradation of the shell material PU starts at about 150 °C and lasts until 200 °C; this part of degradation could be attributed to the destruction of unreacted shell material TETA, TIPTP and evaporation of ethyl acetate. The actual destruction of PU starts at about 250 °C and lasts until 550 °C and even further. The microcapsule IE4 analysis demonstrates that 79% of the microcapsule materials are destroyed at temperatures below 300 °C. This part of the weight loss could be contributed to IPDI. Slightly higher destruction temperature of IPDI in microcapsules is expected since IPDI is entrapped inside a PU shell, and destruction can only begin when the shell is damaged by rising pressure inside the microcapsule or under degradation. The core content of the microcapsules was in the range of 50% to 79%.

3.2.2.2. Optimization of encapsulation of IPDI into PU shell

The Taguchi method was employed to identify the optimal parameters to achieve the highest core content, a microcapsule size closest to 50 μm, and maximum microcapsule yield. The SNR was calculated using the larger-the-better criterion to discern optimal conditions for core content and yield, while the nominal-the-better criterion was applied for the optimization of microcapsule size. The results are summarized in Fig. 32.

The highest SNR value and significantly higher core content (Fig. 32A) was achieved using core-to-shell ratio 5:1. Agitation speed had small impact to the core content, but the best results were at the agitation speed 3000 rpm. Three emulsifiers – PVA 1 % / GA 1.5%, PVA 2% / GA 3% and GA 7% – had similar impact to the core content with small superiority of; GA 7%; anionic emulsifier SDBS was not suitable in achieving high core content. Reaction time also had rather small impact to the core content, although the highest core content was at the reaction time 60 min.

The optimal microcapsule size closest to 50 μm (Fig. 32B) was achieved at various combinations of the reaction parameters. Considering core-to-shell ratio, the optimal microcapsule size was at the ratio 3:1 and 5:1; at the ratio 2:1 and 4:1, the microcapsules tended to be either too large or too small. Agitation speed had lower impact on the microcapsule size while the optimal microcapsule size was at the agitation speed 4000 rpm. The emulsifier had a strong impact on the microcapsule size. Microcapsules of the optimal size were preferentially formed in the presence of GA 7% as an emulsifier. SDBS was not suitable as an emulsifier since it promoted agglomeration of the microcapsules. Reaction time had minimal impact on the microcapsule size, but the optimal time was 45 min.

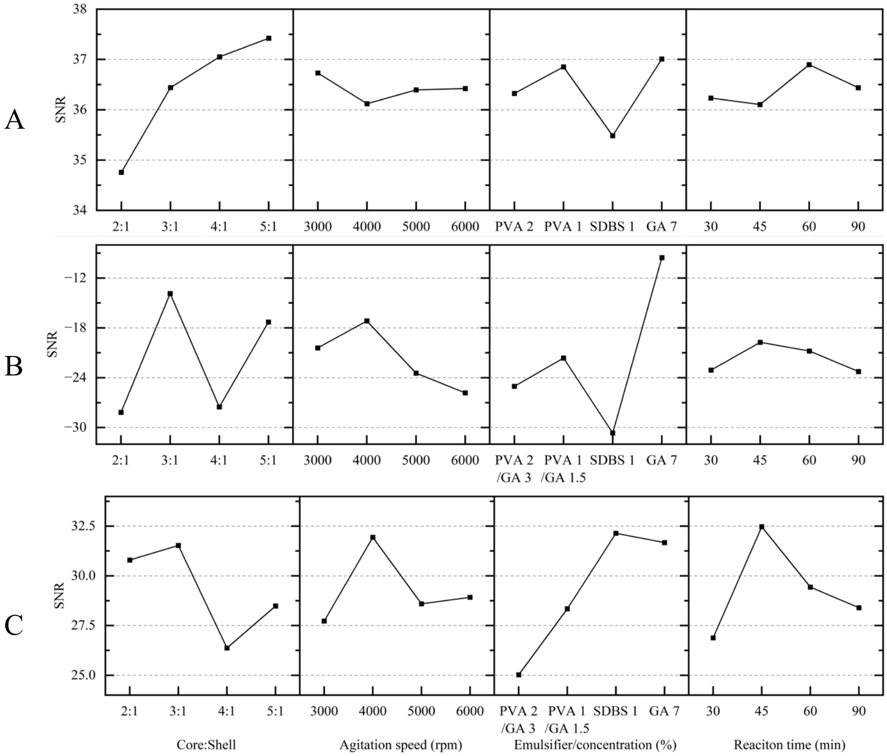

Fig. 32. SNR plots according to Taguchi method; the dependence of the microcapsule core content (A), microcapsule size (B) and microcapsule yield (C) on microencapsulation parameters core to shell ratio, agitation speed, type and concentration of emulsifier, and reaction time.

The highest yield of microcapsules (Fig. 32C) was obtained at the core-to-shell ratio 3:1; the ratio 4:1 was the most unfavorable. The optimal agitation speed regarding yield was 4000 rpm. The optimal emulsifier promoting the highest yield of microcapsules was SDBS 1%. Possibly, this could be explained by agglomeration of microcapsules in the presence of SDBS, since losses of large agglomerates during washing and lyophilization processes are minimal. The highest yield was achieved at the reaction time 45 min.

Optimal conditions for microencapsulation of IPDI in PU shell regarding the highest core content, optimal microcapsule size of 50 µm and the highest yield are presented in Table 23.

Table 23. Optimal conditions for microencapsulation of IPDI in PU shell

	Core:shell	Agitation speed, rpm	Emulsifier and its concentration, %	Reaction time, min
Highest core content	5:1	3000	GA 7	60
Optimal size of 50 µm	3:1	4000	GA 7	45
Highest yield	3:1	4000	SDBS 1	45

Microencapsulation of IPDI into PU shell was done by oil-in-water interfacial polymerization. The microencapsulation process was optimized using Taguchi L16 parameter design. Optimal conditions for the microencapsulation, to achieve all three – highest core content, highest yield and average microcapsule size of 50 µm, included the core-to-shell ratio 3:1, the agitation speed 3000 rpm, GA (7%) as an emulsifier and the reaction time 60 min. Under optimal conditions, the IPDI core content within the microcapsules was up to 74.6% and the microcapsule yield was up to 48.9%, with average microcapsule size of 50 µm.

3.3. Development of self-healing epoxy coatings

To prepare self-healing coatings, microcapsules EA8 with PAAE as healing agent (core content 71.1%) and polyacrylate shell, and microcapsules IE4 with IPDI as healing agent (core content 78.6%) and PU shell were dispersed in epoxy formulations. Two types of microcapsules were mixed at ratio 1:1 and added to epoxy formulation in different amounts given in Table 24.

Table 24. Epoxy formulations with added microcapsules

		EA8, %	IE4, %
Epoxy coating	2AE120-0	-	-
	2AE120-1	2.5	2.5
	2AE120-2	5.0	5.0
	2AE120-3	7.5	7.5

The epoxy coating used in this experiment was a zero-VOC, 100% solid formulation specifically designed for application in humid environments and for underwater curing. The coating is typically applied at a thickness of 200-500 µm, with an epoxy-to-amine ratio of 3:1 by weight. This formulation was selected for its zero-VOC characteristic, which eliminates potential solvent interactions with microcapsule systems and minimizes shrinkage during the curing process.

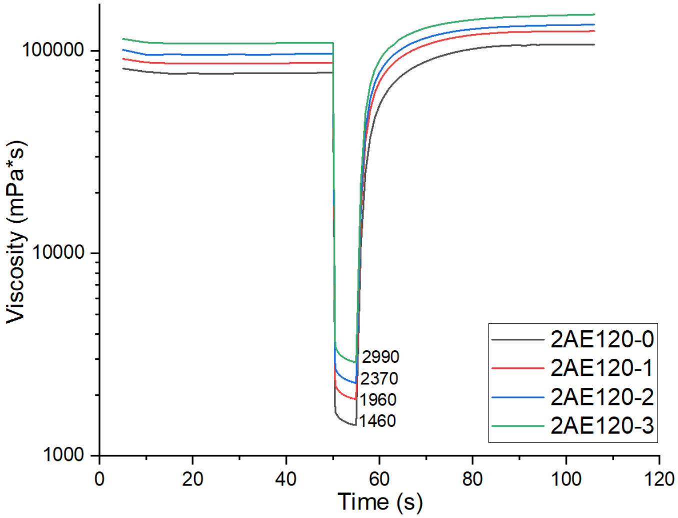

Fig. 33. Three interval rheology test of epoxy compositions, containing microcapsule EA8+IE4 mixtures of: 2AE120-0 – 0%; 2AE120-1 – 5%; 2AE120-2 – 10%; 2AE120-3 – 15%

The viscosity of formulations was tested using rheology three interval rheology test. Rheological analysis revealed that the addition of 5% (2.5% of each type) to 15% (7.5% of each type) of microcapsules to the epoxy composition increases the viscosity at both low shear rates (0.1 s^{-1}) and under simulated pressure conditions corresponding to the shear rate during the application process (1000 s^{-1}), regardless of the type of microcapsules used. In the dual microcapsule system, consisting of IPDI encapsulated in PU shell and PAAE encapsulated in polyacrylate shell, the initial viscosity increased from 106000 mPa·s to 125000 mPa·s, when 5% microcapsules (2.5% of each type) were added (2AE120-2). Similarly, at a shear rate of 1000 s^{-1}, the viscosity increased from 1460 mPa·s to 1960 mPa·s (Fig. 33).

The maximal viscosity was characteristic for the formulation containing 15% (7.5% of each type) microcapsules (2AE120-3), where the initial viscosity was 1.5 times higher, and the viscosity at a shear rate of 1000 s^{-1} was twice as high as for the composition without microcapsules (2AE120-0).

To assess the efficiency of microcapsule systems in promoting self-healing of epoxy coatings, selected epoxy formulations were combined with microcapsules in quantities detailed in Table 24. The resulting mixtures were applied to steel plates at a thickness of 400 µm and allowed to cure for one week. After curing, the coatings were deliberately damaged with a knife blade, left for microcapsule healing agent to cure for one day, and then subjected to salt spray exposure for one week. Rust formation was visually assessed (Fig. 34). Since no significant differences were observed at the damaged sites between the coatings with and without microcapsules, it was concluded that self-healing was either absent or the damaged area was too wide for microcapsules of this size and amount to fully heal.

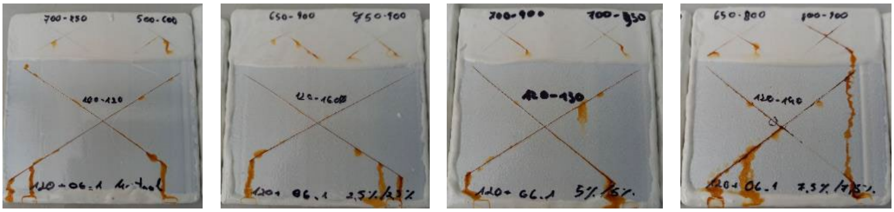

2AE120-0 2AE120-1 2AE120-2 2AE120-3

Fig. 34. Image of the steel plates coated in self-healing coating containing microcapsule mixture (EA8+IE4) after exposure in the salt spray chamber 2AE120-0 – 0%; 2AE120-1 – 5%; 2AE120-2 – 10%; 2AE120-3 – 15%

An additional experiment was conducted in which the samples, instead of being allowed to self-heal at room temperature, were placed in an oven at 80 °C for 1 hour. This thermal treatment was applied to enhance the self-healing performance by promoting the thermal activation of the damaged regions. The damaged areas were subsequently analyzed using OM. Evaluation of the self-healing properties of epoxy coatings utilizing a dual microcapsule system (Fig. 35) demonstrated a reduction in coating damage after 1 hour of thermal curing in all samples containing microcapsules, compared to the control coating without microcapsules. Before heat exposure, the metal surface beneath the damaged coating was visible. However, after exposure, the active components released from the microcapsules covered and sealed most of the damaged area, effectively hiding the metal surface. The highest self-healing effect, as observed under OM, was exhibited by the composition 2AE120-3, which contained the highest concentration of microcapsules (15%).

The dual microcapsule system investigated in this study shows considerable promise for improving the performance and durability of epoxy coatings. By releasing active agents upon mechanical damage, this system not only reduces the size of the damaged area but also has potential to prevent further rust formation, which is a common issue in coatings exposed to harsh environments.

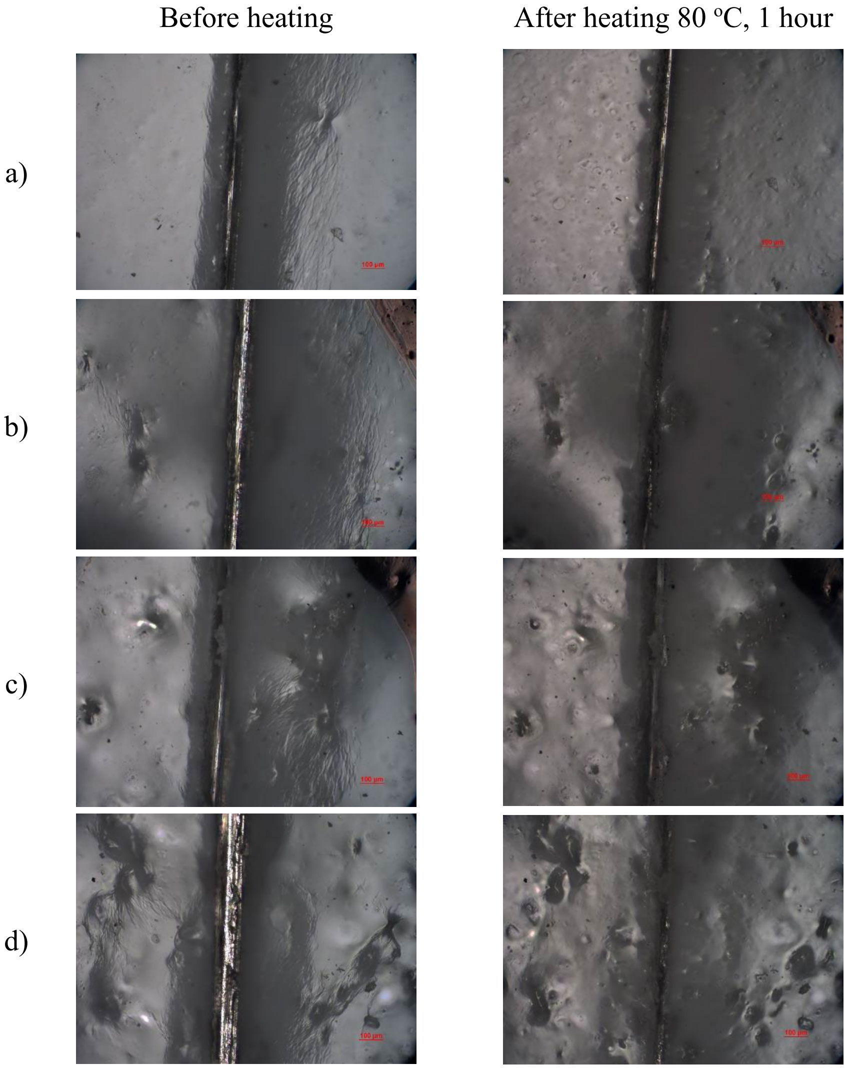

Fig. 35. OM images of epoxy coatings containing microcapsule mixtures (EA8+IE4) before and after heating 1 hour at 80 ºC: a) 2AE120-0 – 0% b) 2AE120-1 – 5%, c) 2AE120-2 – 10%, d) 2AE120-3 – 15%

The controlled release of repair agents ensures the restoration of protective properties, contributing to the coating's durability. However, further detailed studies are needed, as the results obtained are only preliminary. This approach could be pivotal in extending the lifespan of epoxy coatings, making them more efficient in maintaining structural integrity and reducing maintenance costs, particularly in industries where long-term protection is critical.

CONCLUSIONS

1. As determined by DSC and rheology experiments, curing of epoxy resins by phenalkamine based hardeners started at lower temperature, the cure temperature interval was broader, and the curing rates were slightly lower compared to those cured by low-molecular-weight amine hardeners. The curing of epoxy resins by PhA-based hardener NX-6019 was characterized by the lowest T_i and the shortest pot-life due to tertiary amine-based accelerators DMP and DMAPA used in composition. Due to TMD used in GX-6004 the curing of epoxy resin started later but proceeded with the highest rate and provided a possibility to increase T_g of formed coating up to 80-85 ^{o}C.
2. Oscillation, DSC and mechanical testing showed that reactive diluents influence both the curing process and the properties of epoxy coatings. Monofunctional RD C12-C14 alkyl glycidyl ether significantly reduced viscosity and slightly increased T_g of the cured coating, but also prolonged vitrification time. Difunctional reactive diluents 1,4-buthanediol and 1,6-hexandiol diglycidyl ethers led to the shortest gelation and vitrification times, moderate viscosity reduction, and noticeable improvements in coating hardness and abrasion resistance. Importantly, all studied formulations were VOC-free, as the reactive diluents remained chemically bound in the cured network, ensuring environmentally safer and solvent-free epoxy coating systems.
3. The new microencapsulation technique of PAAE into UV cured polyacrylate shell was developed through oil-in-water emulsion polymerization triggered by UV light. Synthesis parameters were optimized using Taguchi L16 parameter design approach. The optimal conditions for highest core content were identified, which included a core-to-shell ratio of approximately 3:1 or 4:1, a low agitation speed of 500 rpm, the use of two polymeric emulsifiers mixture, PVA 1-2% / GA 1.5-3% in the absence of solvents. The microcapsules of optimal size 50 μm are formed by using 4:1 or 5:1 core content, agitation speed of 1000 rpm, emulsifier mixture of PVA 1-2% / GA 1.5-3%, and solvent content of 25%.
4. Microencapsulation of IPDI into a PU shell was done by oil-in-water emulsion interfacial polymerization method. Optimal conditions for the microencapsulation, prepared by Taguchi L16 parameter design method to achieve all three – highest core content, highest yield and average microcapsule size of 50 μm, included the core-to-shell ratio

3:1, the agitation speed 3000 rpm, GA (7%) as an emulsifier and the reaction time 60 min. Under optimal conditions, the IPDI core content within the microcapsules was up to 74.6% and the microcapsule yield was up to 48.9%, with average microcapsule size of 50 µm.

5. Self-healing properties of advanced epoxy coatings utilizing a dual microcapsule system demonstrated a reduction in coating damage after 1 hour of thermal curing at 80 °C in all samples containing microcapsules, compared to the control coating without microcapsules. The highest self-healing effect, as observed under OM, was exhibited by the composition 2AE120-3, which contained the highest concentration of microcapsules (15%).

LIST OF PUBLICATIONS AND CONFERENCES PARTICIPATION

List of publications

1. J. Jonikaitė-Švėgždienė, L. Pastarnokienė, V. Juknevičiūtė, R. Makuška. Curing of epoxy resins by bio-based phenalkamines vs low-molecular-weight amines: study by DSC. Chemija 33(2) (2022) 54-63. https://doi.org/10.6001/chemija.v33i2.4709
2. L. Pastarnokienė, J. Jonikaitė-Švėgždienė, N. Lapinskaitė, R. Kulbokaitė, A. Bočkuvienė, T. Kochanė, R. Makuška. The effect of reactive diluents on curing of epoxy resins and properties of the cured epoxy coatings, J Coat Technol Res 20 (2023) 1207-1221. https://doi.org/10.1007/s11998-022-00737-4.
3. L. Pastarnokienė, E. Potapov, R. Makuška, T. Kochanė. Optimization of microencapsulation of polyaspartic acid ester into UV curable epoxy-acrylate resin using Taguchi method of experimental design. J. Appl. Polym. Sci. 141(15) (2024). https://doi.org/10.1002/app.55216
4. L. Pastarnokienė, E. Potapov, R. Makuška, T. Kochanė. Optimization of microencapsulation of isophorone diisocyanate into polyurea shell by oil-in-water interfacial polymerisation. Chemija, 35(2) (2024) 54-64. https://doi.org/10.6001/chemija.2024.35.2.4

The results of the thesis were presented at the following conferences

1. L. Pastarnokienė, T. Kochanė, R. Makuška. Improvement of anti-abrasion properties of anti-corrosive epoxy coating for industrial applications. International conference „Advanced Materials and Technologies 2021", Palanga, Lithuania.
2. L. Pastarnokienė, T. Kochanė, A. Jankauskytė, R. Makuška. Synthesis of microcapsules containing diisocyanate as a healing agent. International conference „Chemistry & Chemical Technology 2021", Vilnius, Lithuania.
3. L. Pastarnokienė, T. Kochanė, S. Žukaitytė. R. Makuška. Synthesis of microcapsules containing amines as healing agents. International conference „Baltic Polymer Symposium 2022", Tallinn, Estonia.
4. E. Potapov, L. Pastarnokienė, T. Kochanė, R. Makuška. Synthesis of microcapsules containing polyaspartic acid ester within UV curable shell. International conference „Chemistry & Chemical Technology 2023", Vilnius, Lithuania.
5. L. Pastarnokienė, T. Kochanė, E. Potapov, R. Makuška. Optimization of microencapsulation of isophorone diisocyanate in polyurea shell. International conference „Baltic Polymer Symposium 2023", Jelgava, Latvia.
6. T. Kochanė, A. Jankauskytė, L. Pastarnokienė. Optimization of microencapsulation conditions of polyaspartic acid esters. International conference „Baltic Polymer Symposium 2024", Birštonas, Lithuania.

CURRICULUM VITAE

PERSONAL INFORMATION

Name, Surname	Liepa Pastarnokienė
Email Address	liepa.pastarnokiene@chgf.vu.lt

EDUCATION AND QUALIFICATIONS

2020 to present	Doctoral studies. Department of Polymer Chemistry, Faculty of Chemistry and Geosciences, Institute of Chemistry, Vilnius University.
2018 – 2020	Master's degree in chemistry. Faculty of Chemistry and Geosciences, Vilnius University.
2014 – 2018	Bachelor of Chemistry. Faculty of Chemistry, Vilnius University.
2002 – 2014	Highschool. Vilnius Gabijos gymnasium.

WORK EXPERIENCE

2023-11 to present	UAB DG Dimense. Researcher in Inks group. Development of inks and liquids for inkjet printer technology.
2019-02 – 2023-11	UAB Litnobiles. Researcher. Development of new anti-corrosion coatings. Work in projects "Innovative anti-corrosion coatings for industrial and transport equipment and devices" Nr. J05-LVPA-K-03-0139 Work in projects "Polyaspartic coatings without volatile organic solvents for wood products" Nr. 01.2.1-LVPA-K-856-01-0089
2017-09 – 2017-11	Work practice European Institute of Membranes. Researcher. Development and characterization of novel biomimetic, biodegradable implants for drug delivery systems.

ACKNOWLEDGMENTS

I would like to express my sincere gratitude to:

My academic advisor and supervisor, Doc. Dr. Tatjana Kochanė, for guiding me through this polymeric journey, from my bachelor's degree to the completion of my doctoral studies. You have been the best teacher, colleague, role model, and friend I could have ever asked for. Thank you for your help and insight in writing all my publications and my doctoral thesis. Your support in correcting me, motivating me, pushing me to be better, and giving me the opportunity to test my own methods and theories has been invaluable. Your encouragement has helped shape me into the scientist and researcher I am today.

My academic supervisor and advisor, Prof. (HP) Dr. Ričardas Makuška, for inviting me to join the projects that form the foundation of this work. You have been an incredible motivator and role model, showing how to persevere even when research results do not always meet expectations.

Doc. Dr. Jūratė Jonikaitė-Švėgždienė, for being a wonderful colleague and friend, and for teaching me the fundamentals of DSC measurements. Thank you for co-authoring the first two publications we wrote together.

Doc. Dr. Alma Bočkuvienė, for being an excellent colleague and friend, and for motivating me by working alongside me on anticorrosion coatings.

Dr. Tatjana Kavleiskaja, for being a supportive colleague and friend, and for teaching me the fundamentals of rheology methods, which directly contributed to the results and discussions in the publications and this work.

Ernestas Potapov, for being a great colleague and friend on our shared journey to discover novel self-healing coatings. Your work and assistance with microcapsule synthesis – particularly in determining which methods work and which do not – have been invaluable.

Virginija Juknevičiūtė, Rūta Kulbokaitė, and Giedrius Navickas, for being amazing colleagues and friends while working together on anticorrosion coatings, and for making the experience enjoyable.

The Department of Polymer Chemistry, for providing me with the opportunity to explore the world of polymer chemistry throughout my four years of doctoral studies.

UAB Litnobiles, for giving me the chance to contribute to projects aimed at developing anticorrosion coatings and self-healing microcapsule systems.

Thank you all for your unwavering support, collaboration, and friendship throughout this journey.

REFERENCES

[1] Straits Research Private Limited - Garner Insights, ‘Anti-Corrosion coating market size to worth USD 48.69 billion by 2033 | Straits Research’. Accessed: Dec. 13, 2024. [Online]. Available: https://www.globenewswire.com/news-release/2024/10/15/2963432/0/en/Anti-Corrosion-Coating-Market-Size-to-Worth-USD-48-69-Billion-by-2033-Straits-Research.html

[2] H. Q. Pham and M. J. Marks, ‘Epoxy Resins’, in *Encyclopedia of Polymer Science and Technology*, Wiley, 2004. doi: 10.1002/0471440264.pst119.

[3] C. Verma *et al.*, ‘Epoxy resins as anticorrosive polymeric materials: A review’, *React Funct Polym*, vol. 156, p. 104741, Nov. 2020, doi: 10.1016/J.REACTFUNCTPOLYM.2020.104741.

[4] A. Kausar, ‘Performance of corrosion protective epoxy blend-based nanocomposite coatings: a review’, *Polymer-Plastics Technology and Materials*, vol. 59, no. 6, pp. 658–673, Apr. 2020, doi: 10.1080/25740881.2019.1673410.

[5] J. Guo and X. Zhang, ‘A latent curing agent for rapid curing of phenolic epoxy resin at low temperature’, *J Appl Polym Sci*, vol. 141, no. 39, Oct. 2024, doi: 10.1002/app.56003.

[6] H. Dodiuk and S. Kenig, ‘Low temperature curing epoxies for structural repair’, *Prog Polym Sci*, vol. 19, no. 3, pp. 439–467, Jan. 1994, doi: 10.1016/0079-6700(94)90002-7.

[7] P. Jia *et al.*, ‘Recent Development of Cardanol Based Polymer Materials-A Review’, *J Renew Mater*, vol. 7, no. 7, pp. 601–619, 2019, doi: 10.32604/jrm.2019.07011.

[8] J. Dai *et al.*, ‘Synthesis of bio-based unsaturated polyester resins and their application in waterborne UV-curable coatings’, *Prog Org Coat*, vol. 78, pp. 49–54, Jan. 2015, doi: 10.1016/j.porgcoat.2014.10.007.

[9] P. Samyn, J. Bosmans, and P. Cosemans, ‘Benchmark Study of Epoxy Coatings with Selection of Bio-Based Phenalkamine versus Fossil-Based Amine Crosslinkers’, *Molecules*, vol. 28, no. 11, p. 4259, May 2023, doi: 10.3390/molecules28114259.

[10] Cardolite, ‘Epoxy curing agents and performance benefits’. Accessed: Dec. 13, 2024. [Online]. Available: https://www.cardolite.com/products/epoxy-curing-agents/

[11] W. H. II. , P. E. Huifeng Qian, ‘A Novel VOC-Free Epoxy System for High Modulus Glass Fiber Reinforced Polymer Rebar’, in *SP-360: Proceedings of the 16th International Symposium on Fiber-Reinforced*

Polymer (FRP) Reinforcement for Concrete Structures (FRPRCS-16), American Concrete Institute, 2024. doi: 10.14359/51740631.

[12] B. Oktay, J. H. Türkcan, O. K. Özdemir, and N. Kayaman-Apohan, 'Vegetable oil-based epoxy coating materials for self-healing and anticorrosive applications', *Macromol Res*, vol. 31, no. 11, pp. 1077–1086, Nov. 2023, doi: 10.1007/s13233-023-00190-1.

[13] D. Wang *et al.*, 'Exploring Epoxy-Functionalized Polysulfide as a VOC-Free and Highly Effective Interfacial Modifier for Silica-Filled Rubber Composites', *Macromolecules*, vol. 57, no. 2, pp. 470–480, Jan. 2024, doi: 10.1021/acs.macromol.3c01972.

[14] K. Wutticharoenwong, J. Dziczkowski, and M. D. Soucek, 'Tung based reactive diluents for alkyd systems: Film properties', *Prog Org Coat*, vol. 73, no. 4, pp. 283–290, Apr. 2012, doi: 10.1016/j.porgcoat.2011.03.017.

[15] S. K. Yadav, K. M. Schmalbach, E. Kinaci, J. F. Stanzione, and G. R. Palmese, 'Recent advances in plant-based vinyl ester resins and reactive diluents', *Eur Polym J*, vol. 98, pp. 199–215, Jan. 2018, doi: 10.1016/j.eurpolymj.2017.11.002.

[16] A. R. Jagtap and A. More, 'Developments in reactive diluents: a review', *Polymer Bulletin*, vol. 79, no. 8, pp. 5667–5708, Aug. 2022, doi: 10.1007/s00289-021-03808-5.

[17] I. I. Udoh *et al.*, 'Active anticorrosion and self-healing coatings: A review with focus on multi-action smart coating strategies', *J Mater Sci Technol*, vol. 116, pp. 224–237, Jul. 2022, doi: 10.1016/j.jmst.2021.11.042.

[18] S. H. Cho, S. R. White, and P. V. Braun, 'Self-Healing Polymer Coatings', *Advanced Materials*, vol. 21, no. 6, pp. 645–649, Feb. 2009, doi: 10.1002/adma.200802008.

[19] M. Samadzadeh, S. H. Boura, M. Peikari, S. M. Kasiriha, and A. Ashrafi, 'A review on self-healing coatings based on micro/nanocapsules', *Prog Org Coat*, vol. 68, no. 3, pp. 159–164, Jul. 2010, doi: 10.1016/j.porgcoat.2010.01.006.

[20] ISO, *ISO 12944-5:2019 Paints and varnishes — Corrosion protection of steel structures by protective paint systems*. Geneva, Switzerland: International Organization for Standardization, 2019.

[21] P. A. Sørensen, S. Kiil, K. Dam-Johansen, and C. E. Weinell, 'Anticorrosive coatings: a review', *J Coat Technol Res*, vol. 6, no. 2, pp. 135–176, Jun. 2009, doi: 10.1007/s11998-008-9144-2.

[22] K. Pélissier and D. Thierry, 'Powder and High-Solid Coatings as Anticorrosive Solutions for Marine and Offshore Applications? A

Review', *Coatings*, vol. 10, no. 10, p. 916, Sep. 2020, doi: 10.3390/coatings10100916.

[23] A. K. Hussain, N. Seetharamaiah, M. Pichumani, and C. S. Chakra, 'Research progress in organic zinc rich primer coatings for cathodic protection of metals – A comprehensive review', *Prog Org Coat*, vol. 153, p. 106040, Apr. 2021, doi: 10.1016/J.PORGCOAT.2020.106040.

[24] R. N. Jagtap, P. P. Patil, and S. Z. Hassan, 'Effect of zinc oxide in combating corrosion in zinc-rich primer', *Prog Org Coat*, vol. 63, no. 4, pp. 389–394, Nov. 2008, doi: 10.1016/J.PORGCOAT.2008.06.012.

[25] G. Dillingham, 'Priming to improve adhesion', *Adhesion Science and Engineering*, pp. 433–464, 2002, doi: 10.1016/B978-044451140-9/50010-X.

[26] A. Verma *et al.*, 'Mechanism, Anti-Corrosion Protection and Components of Anti-Corrosion Polymer Coatings', in *Polymer Coatings: Technologies and Applications*, 1st Edition., Boca Raton: CRC Press, 2020.

[27] N. Akafuah, S. Poozesh, A. Salaimeh, G. Patrick, K. Lawler, and K. Saito, 'Evolution of the Automotive Body Coating Process—A Review', *Coatings*, vol. 6, no. 2, p. 24, Jun. 2016, doi: 10.3390/coatings6020024.

[28] B. Müller and U. Poth, *Coatings Formulation*. Vincentz Network, 2019. doi: 10.1515/9783748600268.

[29] R. Hsissou, 'Review on epoxy polymers and its composites as a potential anticorrosive coatings for carbon steel in 3.5% NaCl solution: Computational approaches', *J Mol Liq*, vol. 336, p. 116307, Aug. 2021, doi: 10.1016/J.MOLLIQ.2021.116307.

[30] F. L. Jin, X. Li, and S. J. Park, 'Synthesis and application of epoxy resins: A review', *Journal of Industrial and Engineering Chemistry*, vol. 29, pp. 1–11, Sep. 2015, doi: 10.1016/J.JIEC.2015.03.026.

[31] Y. Hao, F. Liu, and E.-H. Han, 'Protection of epoxy coatings containing polyaniline modified ultra-short glass fibers', *Prog Org Coat*, vol. 76, no. 4, pp. 571–580, Apr. 2013, doi: 10.1016/j.porgcoat.2012.11.012.

[32] M. N. Katariya, A. K. Jana, and P. A. Parikh, 'Corrosion inhibition effectiveness of zeolite ZSM-5 coating on mild steel against various organic acids and its antimicrobial activity', *Journal of Industrial and Engineering Chemistry*, vol. 19, no. 1, pp. 286–291, Jan. 2013, doi: 10.1016/j.jiec.2012.08.013.

[33] A. Gergely, I. Bertóti, T. Török, É. Pfeifer, and E. Kálmán, 'Corrosion protection with zinc-rich epoxy paint coatings embedded with various

amounts of highly dispersed polypyrrole-deposited alumina monohydrate particles', *Prog Org Coat*, vol. 76, no. 1, pp. 17–32, Jan. 2013, doi: 10.1016/j.porgcoat.2012.08.005.

[34] C.-H. Park, S.-W. Lee, J.-W. Park, and H.-J. Kim, 'Preparation and characterization of dual curable adhesives containing epoxy and acrylate functionalities', *React Funct Polym*, vol. 73, no. 4, pp. 641–646, Apr. 2013, doi: 10.1016/j.reactfunctpolym.2013.01.012.

[35] Y. Liu, G. Yang, H.-M. Xiao, Q.-P. Feng, and S.-Y. Fu, 'Mechanical properties of cryogenic epoxy adhesives: Effects of mixed curing agent content', *Int J Adhes Adhes*, vol. 41, pp. 113–118, Mar. 2013, doi: 10.1016/j.ijadhadh.2012.10.006.

[36] A. Kaboorani and B. Riedl, 'Nano-aluminum oxide as a reinforcing material for thermoplastic adhesives', *Journal of Industrial and Engineering Chemistry*, vol. 18, no. 3, pp. 1076–1081, May 2012, doi: 10.1016/J.JIEC.2011.12.001.

[37] H. V. Nguyen, E. Andreassen, H. Kristiansen, R. Johannessen, N. Hoivik, and K. E. Aasmundtveit, 'Rheological characterization of a novel isotropic conductive adhesive – Epoxy filled with metal-coated polymer spheres', *Materials & Design (1980-2015)*, vol. 46, pp. 784–793, Apr. 2013, doi: 10.1016/J.MATDES.2012.11.036.

[38] H. Jin *et al.*, 'Fracture behavior of a self-healing, toughened epoxy adhesive', *Int J Adhes Adhes*, vol. 44, pp. 157–165, Jul. 2013, doi: 10.1016/J.IJADHADH.2013.02.015.

[39] M. Shamsuddoha, M. M. Islam, T. Aravinthan, A. Manalo, and K. Lau, 'Characterisation of mechanical and thermal properties of epoxy grouts for composite repair of steel pipelines', *Materials & Design (1980-2015)*, vol. 52, pp. 315–327, Dec. 2013, doi: 10.1016/j.matdes.2013.05.068.

[40] K. Ahmed, S. S. Nizami, and N. Z. Raza, 'Characteristics of natural rubber hybrid composites based on marble sludge/carbon black and marble sludge/rice husk derived silica', *Journal of Industrial and Engineering Chemistry*, vol. 19, no. 4, pp. 1169–1176, Jul. 2013, doi: 10.1016/j.jiec.2012.12.014.

[41] D. Quang Dao, J. Luche, F. Richard, T. Rogaume, C. Bourhy-Weber, and S. Ruban, 'Determination of characteristic parameters for the thermal decomposition of epoxy resin/carbon fibre composites in cone calorimeter', *Int J Hydrogen Energy*, vol. 38, no. 19, pp. 8167–8178, Jun. 2013, doi: 10.1016/j.ijhydene.2012.05.116.

[42] M. M. Ayad, A. Abu El-Nasr, and J. Stejskal, 'Kinetics and isotherm studies of methylene blue adsorption onto polyaniline nanotubes

base/silica composite', *Journal of Industrial and Engineering Chemistry*, vol. 18, no. 6, pp. 1964–1969, Nov. 2012, doi: 10.1016/J.JIEC.2012.05.012.

[43] A. A. Azeez, K. Y. Rhee, S. J. Park, and D. Hui, 'Epoxy clay nanocomposites – processing, properties and applications: A review', *Compos B Eng*, vol. 45, no. 1, pp. 308–320, Feb. 2013, doi: 10.1016/j.compositesb.2012.04.012.

[44] N. Chand and A. Nigrawal, 'Development and electrical conductivity behavior of copper-powder-filled-epoxy graded composites', *J Appl Polym Sci*, vol. 109, no. 4, pp. 2384–2387, Aug. 2008, doi: 10.1002/app.28267.

[45] E. Kandare, B. K. Kandola, and P. Myler, 'Evaluating the influence of varied fire-retardant surface coatings on post-heat flexural properties of glass/epoxy composites', *Fire Saf J*, vol. 58, pp. 112–120, May 2013, doi: 10.1016/J.FIRESAF.2013.01.009.

[46] S. W. Suh, J. J. Kim, S. H. Kim, and B. K. Park, 'Effect of PI film surface on printing of Pd(II) catalytic ink for electroless copper plating in the printed electronics', *Journal of Industrial and Engineering Chemistry*, vol. 18, no. 1, pp. 290–294, Jan. 2012, doi: 10.1016/J.JIEC.2011.11.003.

[47] P. L. Teh, M. Jaafar, H. M. Akil, K. N. Seetharamu, A. N. R. Wagiman, and K. S. Beh, 'Thermal and mechanical properties of particulate fillers filled epoxy composites for electronic packaging application', *Polym Adv Technol*, vol. 19, no. 4, pp. 308–315, Apr. 2008, doi: 10.1002/pat.1014.

[48] M. A. Di Prima *et al.*, 'Cyclic compression behavior of epoxy shape memory polymer foam', *Mechanics of Materials*, vol. 42, no. 4, pp. 405–416, Apr. 2010, doi: 10.1016/j.mechmat.2010.01.004.

[49] D. You *et al.*, 'Microwave-assisted functionalization of polyurethane surface for improving blood compatibility', *Journal of Industrial and Engineering Chemistry*, vol. 19, no. 5, pp. 1587–1592, Sep. 2013, doi: 10.1016/j.jiec.2013.01.027.

[50] B. Ellis, *Chemistry and Technology of Epoxy Resins*. Dordrecht: Springer Netherlands, 1993. doi: 10.1007/978-94-011-2932-9.

[51] D. J. Weinmann, K. C. B. Dangayach, and C. Smith, 'Amine-functional curatives for low temperature cure epoxy coatings', *Journal of Coatings Technology*, vol. 68, pp. 29–37, 1996, [Online]. Available: https://api.semanticscholar.org/CorpusID:100749317

[52] M. Kaur and L. S. Jayakumari, 'Eco-friendly cardanol-based phenalkamine cured epoxy-cenosphere syntactic foams: Fabrication

and characterisation’, *J Appl Polym Sci*, vol. 133, no. 46, Dec. 2016, doi: 10.1002/app.44189.

[53] K. Wazarkar and A. S. Sabnis, ‘Phenalkamine curing agents for epoxy resin: characterization and structure property relationship’, *Pigment & Resin Technology*, vol. 47, no. 4, pp. 281–289, Aug. 2018, doi: 10.1108/PRT-08-2017-0071.

[54] F. A. Pfaff, ‘Growing more ductile epoxies: an essential work of fracture study’, *J Coat Technol Res*, vol. 4, no. 2, pp. 151–159, Jun. 2007, doi: 10.1007/s11998-007-9013-4.

[55] F. L. Jin, X. Li, and S. J. Park, ‘Synthesis and application of epoxy resins: A review’, *Journal of Industrial and Engineering Chemistry*, vol. 29, no. 25, pp. 1–11, 2015, doi: 10.1016/j.jiec.2015.03.026.

[56] S. Pradhan, P. Pandey, S. Mohanty, and S. K. Nayak, ‘Insight on the Chemistry of Epoxy and Its Curing for Coating Applications: A Detailed Investigation and Future Perspectives’, *Polymer - Plastics Technology and Engineering*, vol. 55, no. 8, pp. 862–877, 2016, doi: 10.1080/03602559.2015.1103269.

[57] C. Cui *et al.*, ‘Preparation and Research of Solvent-Free Epoxy Coating for Drinking Water Tank’, in *IOP Conference Series: Materials Science and Engineering*, 2020. doi: 10.1088/1757-899X/782/2/022064.

[58] U. U. T. Võ and M. P. Morris, ‘Nonvolatile, semivolatile, or volatile: Redefining volatile for volatile organic compounds’, *J Air Waste Manage Assoc*, vol. 64, no. 6, pp. 661–669, 2014, doi: 10.1080/10962247.2013.873746.

[59] E. David and V. C. Niculescu, ‘Volatile organic compounds (Vocs) as environmental pollutants: Occurrence and mitigation using nanomaterials’, *Int J Environ Res Public Health*, vol. 18, no. 24, p. 13147, 2021, doi: 10.3390/ijerph182413147.

[60] D. Nguyen Thuy, H. To Thi Xuan, A. Nicolay, Y. Paint, and M. G. Olivier, ‘Corrosion protection of carbon steel by solvent free epoxy coating containing hydrotalcites intercalated with different organic corrosion inhibitors’, *Prog Org Coat*, vol. 101, pp. 331–341, 2016, doi: 10.1016/j.porgcoat.2016.08.021.

[61] A. R. Jagtap and A. More, ‘Developments in reactive diluents: a review’, *Polymer Bulletin*, vol. 79, pp. 5667–5708, 2021, doi: 10.1007/s00289-021-03808-5.

[62] Z. K. Chen, G. Yang, J. P. Yang, S. Y. Fu, L. Ye, and Y. G. Huang, ‘Simultaneously increasing cryogenic strength, ductility and impact resistance of epoxy resins modified by n-butyl glycidyl ether’, *Polymer*

(Guildf), vol. 50, no. 5, pp. 1316–1323, 2009, doi: 10.1016/j.polymer.2008.12.048.

[63] Y. Li, B. Li, and W. Chen, ‘A study on the reactive diluent for the solvent-free epoxy anticorrosive coating’, *J Chem Pharm Res*, vol. 6, no. 7, pp. 2466–2469, 2014.

[64] A. Sinha, N. Islam Khan, S. Das, J. Zhang, and S. Halder, ‘Effect of reactive and non-reactive diluents on thermal and mechanical properties of epoxy resin’, *High Perform Polym*, vol. 8, no. 1, pp. 167–172, 2018, doi: 10.1177/0954008317743307.

[65] K. H. Zabel, R. P. Klaasen, W. J. Muizebelt, B. P. Gracey, C. Hallett, and C. D. Brooks, ‘Design and incorporation of reactive diluents for air-drying high solids alkyd paints’, *Prog Org Coat*, vol. 35, no. 1–4, pp. 255–264, 1999, doi: 10.1016/S0300-9440(99)00027-2.

[66] E. Ozeren Ozgul and M. H. Ozkul, ‘Effects of epoxy, hardener, and diluent types on the workability of epoxy mixtures’, *Constr Build Mater*, vol. 187, pp. 360–370, 2018, doi: 10.1016/j.conbuildmat.2017.10.008.

[67] Keiji Yurugi Akihiko Fukada Kenji Matsukawa, ‘Reactive diluent and curable resin composition’, US 6,767,980 B2, 2004

[68] M. Bakar, J. Szymanska, J. Rudecka, and J. Fitas, ‘Effect of reactive diluents and kaolin on the mechanical properties of epoxy resin’, *Polymers and Polymer Composites*, vol. 18, no. 9, pp. 503–510, 2010, doi: 10.1177/096739111001800905.

[69] J. J. Licari and D. W. Swanson, ‘Chemistry, Formulation, and Properties of Adhesives’, in *Adhesives Technology for Electronic Applications*, W. Andrews, Ed., New York, 2011, pp. 75–141. doi: 10.1016/b978-1-4377-7889-2.10003-8.

[70] D. A. Lakho, D. Yao, K. Cho, M. Ishaq, and Y. Wang, ‘Study of the Curing Kinetics toward Development of Fast-Curing Epoxy Resins’, *Polymer - Plastics Technology and Engineering*, vol. 56, no. 2, pp. 161–170, 2017, doi: 10.1080/03602559.2016.1185623.

[71] L. Núñez-Regueira, M. Villanueva, and I. Fraga-Rivas, ‘Effect of a reactive diluent on the curing and dynamomechanical properties of an epoxy-diamine system’, *J Therm Anal Calorim*, vol. 86, pp. 463–468, 2006, doi: 10.1007/s10973-005-7191-9.

[72] C. Li, M. H. Liu, Z. Y. Liu, M. L. Qing, and G. Wang, ‘DSC and curing kinetics of epoxy resin using cyclohexanediol diglycidyl ether as active diluents’, *J Therm Anal Calorim*, vol. 116, pp. 411–416, 2014, doi: 10.1007/s10973-013-3471-y.

[73] S. Montserrat, J. Málek, and P. Colomer, ‘Thermal degradation kinetics of epoxy-anhydride resins: I.: Influence of a silica filler’, *Thermochim Acta*, vol. 313, no. 1, pp. 83–95, 1998, doi: 10.1016/s0040-6031(97)00482-6.

[74] P. Vijayan P and M. Al-Maadeed, ‘Self-Repairing Composites for Corrosion Protection: A Review on Recent Strategies and Evaluation Methods’, *Materials*, vol. 12, no. 17, p. 2754, Aug. 2019, doi: 10.3390/ma12172754.

[75] E. M. Fayyad, M. A. Almaadeed, A. Jones, and A. M. Abdullah, ‘Evaluation Techniques for the Corrosion Resistance of SelfHealing Coatings’, *Int J Electrochem Sci*, vol. 9, no. 9, pp. 4989–5011, Sep. 2014, doi: 10.1016/S1452-3981(23)08147-6.

[76] X. Shi, B. M. D. Fernando, and S. G. Croll, ‘Concurrent physical aging and degradation of crosslinked coating systems in accelerated weathering’, *J Coat Technol Res*, vol. 5, no. 3, pp. 299–309, Sep. 2008, doi: 10.1007/s11998-008-9081-0.

[77] B. J. Blaiszik, S. L. B. Kramer, S. C. Olugebefola, J. S. Moore, N. R. Sottos, and S. R. White, ‘Self-Healing Polymers and Composites’, *Annu Rev Mater Res*, vol. 40, no. 1, pp. 179–211, Jun. 2010, doi: 10.1146/annurev-matsci-070909-104532.

[78] Nguyen J.K., ‘Dual microcapsule system for autonomous self-healing coatings’, University of New Hampshire, New Hampshire, 2008.

[79] K. S. Toohey, N. R. Sottos, J. A. Lewis, J. S. Moore, and S. R. White, ‘Self-healing materials with microvascular networks’, *Nat Mater*, vol. 6, no. 8, pp. 581–585, Aug. 2007, doi: 10.1038/nmat1934.

[80] D. Y. Zhu, M. Z. Rong, and M. Q. Zhang, ‘Self-healing polymeric materials based on microencapsulated healing agents: From design to preparation’, *Prog Polym Sci*, vol. 49–50, pp. 175–220, Oct. 2015, doi: 10.1016/j.progpolymsci.2015.07.002.

[81] M. Guo, Y. He, J. Wang, X. Zhang, and W. Li, ‘Microencapsulation of oil soluble polyaspartic acid ester and isophorone diisocyanate and their application in self-healing anticorrosive epoxy resin’, *J Appl Polym Sci*, vol. 137, no. 12, Mar. 2020, doi: 10.1002/app.48478.

[82] P. Cordier, F. Tournilhac, C. Soulié-Ziakovic, and L. Leibler, ‘Self-healing and thermoreversible rubber from supramolecular assembly’, *Nature*, vol. 451, no. 7181, pp. 977–980, Feb. 2008, doi: 10.1038/nature06669.

[83] H. Zhang and J. Yang, ‘Etched glass bubbles as robust micro-containers for self-healing materials’, *J. Mater. Chem. A*, vol. 1, no. 41, pp. 12715–12720, Sep. 2013, doi: 10.1039/C3TA13227G.

[84] Q. Li, Siddaramaiah, N. H. Kim, D. Hui, and J. H. Lee, ‘Effects of dual component microcapsules of resin and curing agent on the self-healing efficiency of epoxy’, *Compos B Eng*, vol. 55, pp. 79–85, Dec. 2013, doi: 10.1016/j.compositesb.2013.06.006.

[85] H. Wu *et al.*, ‘Hard, tough and fast self-healing thermoplastic polyurethane’, *Prog Org Coat*, vol. 159, p. 106409, Oct. 2021, doi: 10.1016/J.PORGCOAT.2021.106409.

[86] L. Zhang, T. Qiu, Z. Zhu, L. Guo, and X. Li, ‘Self-Healing Polycaprolactone Networks through Thermo-Induced Reversible Disulfide Bond Formation’, *Macromol Rapid Commun*, vol. 39, no. 20, Oct. 2018, doi: 10.1002/marc.201800121.

[87] K. S. Toohey, C. J. Hansen, J. A. Lewis, S. R. White, and N. R. Sottos, ‘Delivery of Two-Part Self-Healing Chemistry via Microvascular Networks’, *Adv Funct Mater*, vol. 19, no. 9, pp. 1399–1405, May 2009, doi: 10.1002/adfm.200801824.

[88] R. C. R. Gergely *et al.*, ‘Restoration of Impact Damage in Polymers via a Hybrid Microcapsule–Microvascular Self-Healing System’, *Adv Funct Mater*, vol. 28, no. 2, Jan. 2018, doi: 10.1002/adfm.201704197.

[89] M. A. Mohammadi, R. Eslami-Farsani, and H. Ebrahimnezhad-Khaljiri, ‘Experimental investigation of the healing properties of the microvascular channels-based self-healing glass fibers/epoxy composites containing the three-part healant’, *Polym Test*, vol. 91, p. 106862, Nov. 2020, doi: 10.1016/J.POLYMERTESTING.2020.106862.

[90] L. M. Dean, B. P. Krull, K. R. Li, Y. I. Fedonina, S. R. White, and N. R. Sottos, ‘Enhanced Mixing of Microvascular Self-Healing Reagents Using Segmented Gas–Liquid Flow’, *ACS Appl Mater Interfaces*, vol. 10, no. 38, pp. 32659–32667, Sep. 2018, doi: 10.1021/acsami.8b09966.

[91] S. Yang *et al.*, ‘Recyclable and self-healing polyurethane composites based on Diels-Alder reaction for efficient solar-to-thermal energy storage’, *Chemical Engineering Journal*, vol. 398, p. 125654, Oct. 2020, doi: 10.1016/j.cej.2020.125654.

[92] L. Yang, X. Lu, Z. Wang, and H. Xia, ‘Diels–Alder dynamic crosslinked polyurethane/polydopamine composites with NIR triggered self-healing function’, *Polym Chem*, vol. 9, no. 16, pp. 2166–2172, 2018, doi: 10.1039/C8PY00162F.

[93] S. J. Garcia, ‘Effect of polymer architecture on the intrinsic self-healing character of polymers’, *Eur Polym J*, vol. 53, no. 1, pp. 118–125, Apr. 2014, doi: 10.1016/J.EURPOLYMJ.2014.01.026.

[94] S. N. Khorasani and R. E. Neisiany, ‘Characterization of self-healing polymeric materials’, in *Self-Healing Polymer-Based Systems*, Elsevier, 2020, pp. 123–140. doi: 10.1016/B978-0-12-818450-9.00005-2.

[95] P. Yang, X. Gao, S. Wang, J.-F. Su, and L.-Q. Wang, ‘Novel waterproof bituminous coating using self-healing microcapsules containing ultraviolet light curing agent’, *Constr Build Mater*, vol. 329, p. 127189, Apr. 2022, doi: 10.1016/j.conbuildmat.2022.127189.

[96] J. Yang, M. W. Keller, J. S. Moore, S. R. White, and N. R. Sottos, ‘Microencapsulation of Isocyanates for Self-Healing Polymers’, *Macromolecules*, vol. 41, no. 24, pp. 9650–9655, Dec. 2008, doi: 10.1021/ma801718v.

[97] R. Dubey, ‘Microencapsulation Technology and Applications’, *Def Sci J*, vol. 59, pp. 82–95, 2009, [Online]. Available: https://api.semanticscholar.org/CorpusID:53339034

[98] J. D. Rule, E. N. Brown, N. R. Sottos, S. R. White, and J. S. Moore, ‘Wax-Protected Catalyst Microspheres for Efficient Self-Healing Materials’, *Advanced Materials*, vol. 17, no. 2, pp. 205–208, Jan. 2005, doi: 10.1002/adma.200400607.

[99] J.-S. Cho, A. Kwon, and C.-G. Cho, ‘Microencapsulation of octadecane as a phase-change material by interfacial polymerization in an emulsion system’, *Colloid Polym Sci*, vol. 280, no. 3, pp. 260–266, Mar. 2002, doi: 10.1007/s00396-001-0603-x.

[100] H. Jin, C. L. Mangun, A. S. Griffin, J. S. Moore, N. R. Sottos, and S. R. White, ‘Thermally Stable Autonomic Healing in Epoxy using a Dual-Microcapsule System’, *Advanced Materials*, vol. 26, no. 2, pp. 282–287, Jan. 2014, doi: 10.1002/adma.201303179.

[101] S. Neon Gan and N. Shahabudin, ‘Applications of Microcapsules in Self-Healing Polymeric Materials’, in *Microencapsulation - Processes, Technologies and Industrial Applications*, IntechOpen, 2019. doi: 10.5772/intechopen.83475.

[102] A. M. Bago Rodriguez and B. P. Binks, ‘Capsules from Pickering emulsion templates’, *Curr Opin Colloid Interface Sci*, vol. 44, pp. 107–129, Dec. 2019, doi: 10.1016/J.COCIS.2019.09.006.

[103] Y. Ren, G. Zhu, and J. Tang, ‘Synthesis of cement shell microcapsules via W/O Pickering emulsions’, *Colloids Surf A Physicochem Eng Asp*, vol. 584, p. 124073, Jan. 2020, doi: 10.1016/J.COLSURFA.2019.124073.

[104] F. Yu, H. Feng, L. Xiao, and Y. Liu, ‘Fabrication of graphene oxide microcapsules based on Pickering emulsions for self-healing water-

borne epoxy resin coatings', *Prog Org Coat*, vol. 155, p. 106221, Jun. 2021, doi: 10.1016/J.PORGCOAT.2021.106221.

[105] C. Li, J. Tan, J. Gu, L. Qiao, B. Zhang, and Q. Zhang, 'Rapid and efficient synthesis of isocyanate microcapsules via thiol-ene photopolymerization in Pickering emulsion and its application in self-healing coating', *Compos Sci Technol*, vol. 123, pp. 250–258, Feb. 2016, doi: 10.1016/J.COMPSCITECH.2016.01.001.

[106] H. Jiang, L. Liu, Y. Li, S. Yin, and T. Ngai, 'Inverse Pickering Emulsion Stabilized by Binary Particles with Contrasting Characteristics and Functionality for Interfacial Biocatalysis', *ACS Appl Mater Interfaces*, vol. 12, no. 4, pp. 4989–4997, Jan. 2020, doi: 10.1021/acsami.9b16117.

[107] K. Zhang, Q. Wang, H. Meng, M. Wang, W. Wu, and J. Chen, 'Preparation of polyacrylamide/silica composite capsules by inverse Pickering emulsion polymerization', *Particuology*, vol. 14, pp. 12–18, Jun. 2014, doi: 10.1016/J.PARTIC.2013.02.010.

[108] D. A. McIlroy, B. J. Blaiszik, M. M. Caruso, S. R. White, J. S. Moore, and N. R. Sottos, 'Microencapsulation of a Reactive Liquid-Phase Amine for Self-Healing Epoxy Composites', *Macromolecules*, vol. 43, no. 4, pp. 1855–1859, Feb. 2010, doi: 10.1021/ma902251n.

[109] Y. Jialan, Y. Chenpeng, Z. Chengfei, and H. Baoqing, 'Preparation Process of Epoxy Resin Microcapsules for Self - healing Coatings', *Prog Org Coat*, vol. 132, pp. 440–444, Jul. 2019, doi: 10.1016/J.PORGCOAT.2019.04.015.

[110] F. Safaei, S. N. Khorasani, H. Rahnama, R. E. Neisiany, and M. S. Koochaki, 'Single microcapsules containing epoxy healing agent used for development in the fabrication of cost efficient self-healing epoxy coating', *Prog Org Coat*, vol. 114, pp. 40–46, Jan. 2018, doi: 10.1016/J.PORGCOAT.2017.09.019.

[111] S. Parsaee, S. M. Mirabedini, R. Farnood, and F. Alizadegan, 'Development of self-healing coatings based on urea-formaldehyde/polyurethane microcapsules containing epoxy resin', *J Appl Polym Sci*, vol. 137, no. 41, Nov. 2020, doi: 10.1002/app.49663.

[112] H. Yi, Y. Deng, and C. Wang, 'Pickering emulsion-based fabrication of epoxy and amine microcapsules for dual core self-healing coating', *Compos Sci Technol*, vol. 133, pp. 51–59, Sep. 2016, doi: 10.1016/J.COMPSCITECH.2016.07.022.

[113] H. Jin, C. L. Mangun, D. S. Stradley, J. S. Moore, N. R. Sottos, and S. R. White, 'Self-healing thermoset using encapsulated epoxy-amine

healing chemistry', *Polymer (Guildf)*, vol. 53, no. 2, pp. 581–587, Jan. 2012, doi: 10.1016/J.POLYMER.2011.12.005.

[114] S. V. Karpov, V. P. Lodygina, V. V. Komratova, A. S. Dzhalmukhanova, G. V. Malkov, and E. R. Badamshina, 'Kinetics of urethane formation from isophorone diisocyanate: The catalyst and solvent effects', *Kinetics and Catalysis*, vol. 57, no. 4, pp. 422–428, Jul. 2016, doi: 10.1134/S0023158416040066.

[115] M. Huang and J. Yang, 'Facile microencapsulation of HDI for self-healing anticorrosion coatings', *J Mater Chem*, vol. 21, no. 30, p. 11123, 2011, doi: 10.1039/c1jm10794a.

[116] E. Koh, N.-K. Kim, J. Shin, and Y.-W. Kim, 'Polyurethane microcapsules for self-healing paint coatings', *RSC Adv.*, vol. 4, no. 31, pp. 16214–16223, 2014, doi: 10.1039/C4RA00213J.

[117] H. Li and X. Wang, 'Preparation of microcapsules with IPDI monomer and isocyanate prepolymer as self-healing agent and their application in self-healing materials', *Polymer (Guildf)*, vol. 262, p. 125478, Dec. 2022, doi: 10.1016/J.POLYMER.2022.125478.

[118] D. Sun, Y. B. Chong, K. Chen, and J. Yang, 'Chemically and thermally stable isocyanate microcapsules having good self-healing and self-lubricating performances', *Chemical Engineering Journal*, vol. 346, pp. 289–297, Aug. 2018, doi: 10.1016/J.CEJ.2018.04.046.

[119] A. H. Navarchian, N. Najafipoor, and F. Ahangaran, 'Surface-modified poly(methyl methacrylate) microcapsules containing linseed oil for application in self-healing epoxy-based coatings', *Prog Org Coat*, vol. 132, pp. 288–297, Jul. 2019, doi: 10.1016/J.PORGCOAT.2019.03.029.

[120] J. Li, H. Shi, F. Liu, and E. H. Han, 'Self-healing epoxy coating based on tung oil-containing microcapsules for corrosion protection', *Prog Org Coat*, vol. 156, p. 106236, Jul. 2021, doi: 10.1016/J.PORGCOAT.2021.106236.

[121] S. Lang and Q. Zhou, 'Synthesis and characterization of poly(urea-formaldehyde) microcapsules containing linseed oil for self-healing coating development', *Prog Org Coat*, vol. 105, pp. 99–110, Apr. 2017, doi: 10.1016/J.PORGCOAT.2016.11.015.

[122] S. Ray, U. Raychaudhuri, and R. Chakraborty, 'An overview of encapsulation of active compounds used in food products by drying technology', *Food Biosci*, vol. 13, pp. 76–83, Mar. 2016, doi: 10.1016/J.FBIO.2015.12.009.

[123] S. Then, G. S. Neon, and N. H. Abu Kasim, 'Performance of melamine modified urea–formaldehyde microcapsules in a dental host material',

J Appl Polym Sci, vol. 122, no. 4, pp. 2557–2562, Nov. 2011, doi: 10.1002/app.34361.

[124] Y. Wang and X. Yan, 'Preparation of Resin-Coated Waterborne Coating Microcapsules and Its Effect on the Properties of Waterborne Coating for Wood Surfaces', *Coatings*, vol. 12, no. 10, p. 1394, Sep. 2022, doi: 10.3390/coatings12101394.

[125] J. Kothari and J. O. Iroh, 'Self-Healing Poly(urea formaldehyde) Microcapsules: Synthesis and Characterization', *Polymers (Basel)*, vol. 15, no. 7, p. 1668, Mar. 2023, doi: 10.3390/polym15071668.

[126] M. Li, B. Cao, R. Shang, H. Mei, and L. Wang, 'Synthesis of poly(urea–formaldehyde) microcapsules for the <scp>self-healing</scp> system of silicone rubber insulating material', *J Appl Polym Sci*, vol. 139, no. 45, Dec. 2022, doi: 10.1002/app.53021.

[127] G. Farzi, A. Davoodi, A. Ahmadi, R. E. Neisiany, Md. K. Anwer, and M. A. Aboudzadeh, 'Encapsulation of Cerium Nitrate within Poly(urea-formaldehyde) Microcapsules for the Development of Self-Healing Epoxy-Based Coating', *ACS Omega*, vol. 6, no. 46, pp. 31147–31153, Nov. 2021, doi: 10.1021/acsomega.1c04597.

[128] A. Czeller and T. Czigány, 'Effect of healing agent-loaded microcapsules on the mechanical properties of self-healing epoxy composites', *ECCM 2012 - Composites at Venice, Proceedings of the 15th European Conference on Composite Materials*, Jan. 2012.

[129] W. Li, X. Zhu, N. Zhao, and Z. Jiang, 'Preparation and Properties of Melamine Urea-Formaldehyde Microcapsules for Self-Healing of Cementitious Materials', *Materials*, vol. 9, no. 3, p. 152, Mar. 2016, doi: 10.3390/ma9030152.

[130] M. Leskovšek, J. Kortnik, U. Stankovič Elesini, and B. Šumiga, 'Characterisation of melamine formaldehyde microspheres synthesised with prolonged microencapsulated reaction time', *Journal of Polymer Engineering*, vol. 42, no. 4, pp. 288–297, Apr. 2022, doi: 10.1515/polyeng-2021-0289.

[131] S. Sharma and V. Choudhary, 'Poly(melamine-formaldehyde) microcapsules filled with epoxy resin: effect of M/F ratio on the shell wall stability', *Mater Res Express*, vol. 4, no. 7, p. 075307, Jul. 2017, doi: 10.1088/2053-1591/aa7c8f.

[132] S. Furukawa, K. Hirasawa, Y. Tsuji, K. Suzuki, and M. Chiba, 'Self-Healing Coatings with Double-Layered Structure for Corrosion Protection of Aluminum Alloys', *Mater Trans*, vol. 64, no. 2, p. MT-LA2022050, Feb. 2023, doi: 10.2320/matertrans.MT-LA2022050.

[133] M. Madelatparvar, M. S. Hosseini, and C. Zhang, ‘Polyurea micro-/nano-capsule applications in construction industry: A review’, *Nanotechnol Rev*, vol. 12, no. 1, Feb. 2023, doi: 10.1515/ntrev-2022-0516.

[134] P. Canamas, N. Gozzi, J. Du, and P. Guichardon, ‘Interfacial Polymerization Kinetics of Polyurea Microcapsules Formed Using Hexamethylene Diisocyanate Biuret Low Viscosity Isocyanate’, *Chem Eng Technol*, vol. 46, no. 6, pp. 1115–1125, Jun. 2023, doi: 10.1002/ceat.202200543.

[135] M. F. Thorne, F. Simkovic, and A. G. Slater, ‘Production of monodisperse polyurea microcapsules using microfluidics’, *Sci Rep*, vol. 9, no. 1, p. 17983, Nov. 2019, doi: 10.1038/s41598-019-54512-4.

[136] F. Ahangaran, A. H. Navarchian, and F. Picchioni, ‘Material encapsulation in poly(methyl methacrylate) shell: A review’, *J Appl Polym Sci*, vol. 136, no. 41, Nov. 2019, doi: 10.1002/app.48039.

[137] F. Ahangaran, M. Hayaty, A. H. Navarchian, and F. Picchioni, ‘Micromechanical assessment of PMMA microcapsules containing epoxy and mercaptan as self-healing agents’, *Polym Test*, vol. 64, pp. 330–336, Dec. 2017, doi: 10.1016/J.POLYMERTESTING.2017.10.014.

[138] M. Araújo *et al.*, ‘Poly(methyl methacrylate) capsules as an alternative to the proof-of-concept’’ glass capsules used in self-healing concrete’, *Cem Concr Compos*, vol. 89, pp. 260–271, May 2018, doi: 10.1016/J.CEMCONCOMP.2018.02.015.

[139] X. You *et al.*, ‘Microfluidic-Assisted Fabrication of Monodisperse Core–Shell Microcapsules for Pressure-Sensitive Adhesive with Enhanced Performance’, *Nanomaterials*, vol. 10, no. 2, p. 274, Feb. 2020, doi: 10.3390/nano10020274.

[140] K. Wu, T. Gui, J. Dong, J. Luo, and R. Liu, ‘Synthesis of robust polyaniline microcapsules via UV-initiated emulsion polymerization for self-healing and anti-corrosion coating’, *Prog Org Coat*, vol. 162, p. 106592, Jan. 2022, doi: 10.1016/J.PORGCOAT.2021.106592.

[141] K. Wu *et al.*, ‘One-pot efficient preparation of microcapsules based on photopolymerization for self-healing coatings’, *Colloids Surf A Physicochem Eng Asp*, vol. 642, p. 128660, Jun. 2022, doi: 10.1016/J.COLSURFA.2022.128660.

[142] V. H. de Souza Rodrigues, A. Estêvão Carrara, S. S. Rossi, L. Mattos Silva, R. de Cássia Lazzarini Dutra, and J. C. N. Dutra, ‘Synthesis, characterization and qualitative assessment of self-healing capacity of PU microcapsules containing TDI and IPDI as a core agent’, *Mater*

Today Commun, vol. 21, p. 100698, Dec. 2019, doi: 10.1016/J.MTCOMM.2019.100698.

[143] M. Attaei *et al.*, ‘Autonomous self-healing in epoxy coatings provided by high efficiency isophorone diisocyanate (IPDI) microcapsules for protection of carbon steel’, *Prog Org Coat*, vol. 139, p. 105445, Feb. 2020, doi: 10.1016/J.PORGCOAT.2019.105445.

[144] J. L. Han, C. H. Yu, Y. H. Lin, and K. H. Hsieh, ‘Kinetic study of the urethane and urea reactions of isophorone diisocyanate’, *J Appl Polym Sci*, vol. 107, no. 6, pp. 3891–3902, Mar. 2008, doi: 10.1002/app.27421.

[145] Z. Chen, W. Yang, H. Yin, and S. Yuan, ‘Kinetics of water–isocyanate reaction in N,N-dimethylformamide’, *Chin J Chem Eng*, vol. 25, no. 10, pp. 1435–1441, Oct. 2017, doi: 10.1016/J.CJCHE.2017.03.012.

[146] S. Kumar, K. Jb, K. Park, K. Scholar, A. P. (Mech, and R. Sahai, ‘An Overview on Taguchi Method’, Aug. 2012. [Online]. Available: https://www.researchgate.net/publication/265282800

[147] N. Ghosh, P. K. Pal, and G. Nandi, ‘GMAW dissimilar welding of AISI 409 ferritic stainless steel to AISI 316L austenitic stainless steel by using AISI 308 filler wire’, *Engineering Science and Technology, an International Journal*, vol. 20, no. 4, pp. 1334–1341, Aug. 2017, doi: 10.1016/j.jestch.2017.08.002.

[148] P. A. R. P. H. N. P. Li, *Quality Control - Intelligent Manufacturing, Robust Design and Charts*. IntechOpen, 2021. doi: 10.5772/intechopen.87736.

[149] V. Nguyen, F. Altarazi, and T. Tran, ‘Optimization of Process Parameters for Laser Cutting Process of Stainless Steel 304: A Comparative Analysis and Estimation with Taguchi Method and Response Surface Methodology’, *Math Probl Eng*, vol. 2022, pp. 1–14, May 2022, doi: 10.1155/2022/6677586.

[150] N. H. Abdul Halim, C. H. Che Haron, J. Abdul Ghani, and M. F. Azhar, ‘Response Surface Methodology (RSM) based analysis for tool life optimization in cryogenic CO_2 milling of Inconel 718’, *IOP Conf Ser Mater Sci Eng*, vol. 606, no. 1, p. 012015, Aug. 2019, doi: 10.1088/1757-899X/606/1/012015.

[151] F. Zhang *et al.*, ‘Self-healing mechanisms in smart protective coatings: A review’, *Corros Sci*, vol. 144, pp. 74–88, Nov. 2018, doi: 10.1016/J.CORSCI.2018.08.005.

[152] A. N. Mustapha, Y. Zhang, Z. Zhang, Y. Ding, Q. Yuan, and Y. Li, ‘Taguchi and ANOVA analysis for the optimization of the microencapsulation of a volatile phase change material’, *Journal of*

Materials Research and Technology, vol. 11, pp. 667–680, Mar. 2021, doi: 10.1016/J.JMRT.2021.01.025.

[153] M. Mahmoudian, E. Nozad, M. G. Kochameshki, and M. Enayati, ‘Preparation and investigation of hybrid self-healing coatings containing linseed oil loaded nanocapsules, potassium ethyl xanthate and benzotriazole on copper surface’, *Prog Org Coat*, vol. 120, pp. 167–178, Jul. 2018, doi: 10.1016/J.PORGCOAT.2018.03.014.

[154] S. Sharma and V. Choudhary, ‘Parametric study for epoxy loaded PMMA microcapsules using Taguchi and ANOVA methods’, *Express Polym Lett*, vol. 11, no. 12, pp. 1023–1036, 2017, doi: 10.3144/expresspolymlett.2017.96.

[155] R. Bhavsar and S. Shreepathi, ‘Evolving empirical rheological limits to predict flow-levelling and sag resistance of waterborne architectural paints’, *Prog Org Coat*, vol. 101, pp. 15–23, Dec. 2016, doi: 10.1016/j.porgcoat.2016.07.016.

[156] A. Deka and N. Dey, ‘Rheological studies of two component high build epoxy and polyurethane based high performance coatings’, *J Coat Technol Res*, vol. 10, no. 3, pp. 305–315, May 2013, doi: 10.1007/s11998-012-9445-3.

[157] L. Xia, L. Zuo, S. Zha, S. Jiang, R. Guan, and D. Lu, ‘Kinetic research on low-temperature cure of epoxy adhesive’, *Int J Adhes Adhes*, vol. 50, pp. 255–264, Apr. 2014, doi: 10.1016/J.IJADHADH.2014.02.005.

[158] E. Özeren, ‘Effects of Epoxy Resin and Hardener Type on Durability and Mechanical Properties of Epoxy Mixes’, Istanbul Technical University, Istanbul, 2005.

[159] Thomas G. Mezger, *Applied Rheology*. 2014.

[160] S. Russo, S. L. Aggarwal, and G. Allen, *Comprehensive polymer science-second supplement*, 1st ed., vol. 34. SGA, 1997. doi: 10.1016/S0144-8617(97)87314-6.

[161] H. H. Winter, ‘Can the gel point of a cross-linking polymer be detected by the $G' - G''$ crossover?’, *Polym Eng Sci*, vol. 27, no. 22, pp. 1698–1702, Dec. 1987, doi: 10.1002/pen.760272209.

[162] H. Teil, S. A. Page, V. Michaud, and J. -A. E. Månson, ‘TTT-cure diagram of an anhydride-cured epoxy system including gelation, vitrification, curing kinetics model, and monitoring of the glass transition temperature’, *J Appl Polym Sci*, vol. 93, no. 4, pp. 1774–1787, Aug. 2004, doi: 10.1002/app.20631.

[163] J. Lange, N. Altmann, C. T. Kelly, and P. J. Halley, ‘Understanding vitrification during cure of epoxy resins using dynamic scanning

calorimetry and rheological techniques', *Polymer (Guildf)*, vol. 41, no. 15, pp. 5949–5955, Jul. 2000, doi: 10.1016/S0032-3861(99)00758-2.

[164] B. Lucio and J. L. de la Fuente, 'Rheological cure characterization of an advanced functional polyurethane', *Thermochim Acta*, vol. 596, pp. 6–13, Nov. 2014, doi: 10.1016/j.tca.2014.09.012.

[165] C. Russo, X. Fernández-Francos, and S. De la Flor, 'Rheological and Mechanical Characterization of Dual-Curing Thiol-Acrylate-Epoxy Thermosets for Advanced Applications', *Polymers (Basel)*, vol. 11, no. 6, p. 997, Jun. 2019, doi: 10.3390/polym11060997.

[166] A. Dotan, 'Handbook of Thermoset Plastics (Third Edition)', in *Handbook of Thermoset Plastics*, H. Dodiuk and S. H. Goodman, Eds., Elsevier, 2014.

[167] J. Zheng, 'Studies of PF Resole/Isocyanate Hybrid Adhesives', 2002.

[168] L. C. Thomas, 'Interpreting Unexpected Events and Transitions in DSC Results', *Gov Inf Q*, vol. 27, no. 4, pp. 423–430, 2010.

[169] Adriana Gregorova, 'Application of Differential Scanning Calorimetry to the Characterization of Biopolymers', in *Applications of Calorimetry in a Wide Context - Differential Scanning Calorimetry, Isothermal Titration Calorimetry and Microcalorimetry*, A. A. Elkordy, Ed., 2013. doi: 10.5772/53822.

[170] S. M. Hasan, J. E. Raymond, T. S. Wilson, B. K. Keller, and D. J. Maitland, 'Effects of Isophorone Diisocyanate on the Thermal and Mechanical Properties of Shape-Memory Polyurethane Foams', *Macromol Chem Phys*, vol. 215, no. 24, pp. 2420–2429, Dec. 2014, doi: 10.1002/macp.201400407.

[171] H. Choe and J. H. Kim, 'Reactivity of isophorone diisocyanate in fabrications of polyurethane foams for improved acoustic and mechanical properties', *Journal of Industrial and Engineering Chemistry*, vol. 69, pp. 153–160, Jan. 2019, doi: 10.1016/J.JIEC.2018.09.025.

[172] M. Ates, S. Karadag, A. A. Eker, and B. Eker, 'Polyurethane foam materials and their industrial applications', *Polym Int*, vol. 71, no. 10, pp. 1157–1163, Oct. 2022, doi: 10.1002/pi.6441.

[173] Marianne Gilbert, *Brydson's Plastics Materials*, Eighth Edition. Butterworth-Heinemann.

[174] C. Yu *et al.*, 'Role of Diisocyanate Structure on Self-Healing and Anticorrosion Properties of Waterborne Polyurethane Coatings', *Adv Mater Interfaces*, vol. 8, no. 10, May 2021, doi: 10.1002/admi.202100117.

[175] E. Spyrou, H. J. Metternich, and R. Franke, ‘Isophorone diisocyanate in blocking agent free polyurethane powder coating hardeners: analysis, selectivity, quantumchemical calculations’, *Prog Org Coat*, vol. 48, no. 2–4, pp. 201–206, Dec. 2003, doi: 10.1016/S0300-9440(03)00104-8.

[176] V. V. Gite, P. P. Mahulikar, and D. G. Hundiwale, ‘Preparation and properties of polyurethane coatings based on acrylic polyols and trimer of isophorone diisocyanate’, *Prog Org Coat*, vol. 68, no. 4, pp. 307–312, Aug. 2010, doi: 10.1016/J.PORGCOAT.2010.03.008.

[177] G. Xiang *et al.*, ‘Preparation and Self-Healing Application of Isocyanate Prepolymer Microcapsules’, *Coatings*, vol. 12, no. 2, p. 166, Jan. 2022, doi: 10.3390/coatings12020166.

[178] D.-M. Kim, Y.-J. Cho, J.-Y. Choi, B.-J. Kim, S.-W. Jin, and C.-M. Chung, ‘Low-Temperature Self-Healing of a Microcapsule-Type Protective Coating’, *Materials*, vol. 10, no. 9, p. 1079, Sep. 2017, doi: 10.3390/ma10091079.

[179] W. Li, Q. Wei, Q. Chen, and Z. Jiang, ‘Microencapsulation and evaluation of styrene maleic anhydride/epoxy for mechanical triggering self-healing of cementitious materials’, *Cem Concr Compos*, vol. 124, p. 104247, Nov. 2021, doi: 10.1016/J.CEMCONCOMP.2021.104247.

[180] T. Nesterova, K. Dam-Johansen, L. T. Pedersen, and S. Kiil, ‘Microcapsule-based self-healing anticorrosive coatings: Capsule size, coating formulation, and exposure testing’, *Prog Org Coat*, vol. 75, no. 4, pp. 309–318, Dec. 2012, doi: 10.1016/j.porgcoat.2012.08.002.

[181] M. Doble and A. K. Kruthiventi, ‘Alternate Solvents’, in *Green Chemistry and Engineering*, Elsevier, 2007, pp. 93–104. doi: 10.1016/B978-012372532-5/50006-7.

[182] G. Mashouf, M. Ebrahimi, and S. Bastani, ‘UV curable urethane acrylate coatings formulation: experimental design approach’, *Pigment & Resin Technology*, vol. 43, no. 2, pp. 61–68, Feb. 2014, doi: 10.1108/PRT-10-2012-0072.

[183] G. Yalcin, U. Yildiz, and A. Kayan, ‘Preparation of Al, Ti, Zr-perfluoroheptanoate compounds and their use in ring opening polymerization’, *Appl Catal A Gen*, vol. 423–424, pp. 205–210, May 2012, doi: 10.1016/J.APCATA.2012.02.042.

[184] T. Ogholaja, D. O. Njobuenwu, and M. Fairweather, ‘Particle Size Effects on Collision and Agglomeration in Turbulent Channel Flows’, *Computer Aided Chemical Engineering*, vol. 40, pp. 79–84, Jan. 2017, doi: 10.1016/B978-0-444-63965-3.50015-5.

SUMMARY IN LITHUANIAN

ĮVADAS

Korozija yra neišvengiamas ir dažnas procesas, keliantis didelių iššūkių metalinių paviršių ilgaamžiškumui ir struktūriniam vientisumui. Norint sumažinti drėgmės, cheminių medžiagų ir aplinkos druskų įtaką korozijos procesui yra naudojamos antikorozinės dangos. Šios dangos atlieka svarbų vaidmenį sudarydamos apsauginį barjerą, kuris neleidžia koroziją sukeliančioms medžiagoms prasiskverbti iki metalo paviršiaus ir taip prailgina metalinių konstrukcijų ir objektų tarnavimo trukmę. Antikorozinių dangų pagrindą sudaro įvairios polimerinės medžiagos, tokios kaip poliuretanai, alkidai, akrilai, epoksidai ir asparto rūgšties esteriai. Tinkamos sudėties kompozicijos užtikrina ne tik formuojamų dangų antikorozinį efektyvumą, bet ir cheminį, mechaninį ir terminį atsparumą.

Epoksidinės dangos išsiskiria savo daugiafunkcėmis apsauginėmis savybėmis. Jos užtikrina didelį paviršių atsparumą korozijai. Be to, gali pagerinti mechanines ir atsparumo įvairioms aplinkos sąlygoms savybes. Priklausomai nuo sudėties, šios dangos gali pasižymėti atsparumu smūgiams, itin dideliu kietumu, kuris savo ruožtu užtikrina didelį atsparumą nusitrynimui ir atmosferos veiksniams. Taip pat šios dangos gali būti hidrofobinės, atstumiančios drėgmę ir teršalus [2–4]. Epoksidinės dangos taip pat žinomos dėl puikaus cheminio ir šiluminio stabilumo, jomis paviršiai dengiami net ir žemose temperatūrose [5, 6]. Pažangios epoksidinės dangos apsaugo metalą ar kitus substratus iki 15-20 metų, užtikrindamos patvarumą ir ilgą eksploatavimą be reikšmingos degradacijos.

Šiomis dienomis vis daugiau dėmesio skiriama aplinkosaugai, todėl siekiama sumažinti pavojingų ir toksiškų medžiagų kiekį dangose. Pagrindinės toksiškos medžiagos epoksidinių dangų kompozicijose – mažamolekuliai aminai, naudojami epoksidervoms kietinti. Kaip alternatyva mažamolekuliams aminams gali būti naudojami mažiau toksiški kietikliai – biologinės kilmės fenalkaminai (*angl.* Phenalkamines, PhA), kurie sintetinami iš anakardžių riešutų kevalų (*angl.* Cashew nutshell liquid, CSNL) esančių medžiagų, pvz. kardanolio [7, 8]. Kardanolio pagrindo PhA kietikliai pasižymi hidrofobinėmis savybėmis yra tinkami kietinti epoksidines dervas net esant žemai temperatūrai ar drėgno klimato sąlygoms [8–10].

Dangų gamintojai privalo gaminti produktus, atsižvelgdami į griežtus aplinkosaugos reglamentus, kurių tikslas – sumažinti arba visiškai pašalinti lakiųjų organinių junginių (*angl.* Volatile organic compounds, VOC) kiekį dangų kompozicijose [11–13]. Pastebima tendencija pereiti prie didelio sausų ir rišančiųjų medžiagų kiekio turinčių dangų kompozicijų, kurių sudėtyje nėra lakiųjų komponentų, t.y. organinių tirpiklių, kurie formuojantis dangai išgaruoja, arba yra minimalus jų kiekis, taip sumažinant žalingą poveikį aplinkai ir žmogui. Tokiose dangų kompozicijose kaip alternatyva gali būti naudojami reaktyvūs skiedikliai (*angl.* Reactive diluent, RD), turintys aktyvias funkcines grupes, pvz, epoksi-. Todėl RD ne tik padeda sumažinti dangų kompozicijų klampą, bet ir yra priskiriami prie rišiklių, kadangi reaguoja su kitais dangų kompozicijose esančiais komponentais ir lieka „surišti“ dangoje [14–16].

Per pastaruosius du dešimtmečius labai sparčiai vystomas savaime užsigydančių (*angl.* self-healing) dangų, kurios leistų prailginti dengiamų medžiagų tarnavimo trukmę. Kuriant savaime užsigydančias dangas gali būti taikomi įvairūs jų pažeidimo užsigydymo mechanizmai. Šiuo metu vienas labiausiai tiriamų būdų, leidžiantis efektyviai spręsti pažangių dangų patvarumo ir tvarumo iššūkius, yra mikrokapsulių su aktyviomis medžiagomis įterpimas į dangą [19].

Šio darbo naujumas ir originalumas.

Šiame darbe siekiant sukurti išmanias epoksidines dangas buvo pritaikytos pažangios biologinės kilmės medžiagos – fenalkaminai, skirtingo funkcionalumo reaktyvūs skiedikliai ir ištirtas savaiminio dangų užsigydymo mikrokapsulėmis metodas.

Epoksidinėms dervoms sukietinti dažnai pasirenkama naudoti mažamolekulius aminus, gaunamus iš naftos produktų, kurie dėl didelio toksiškumo kenkia ne tik aplinkai, bet ir žmonėms. Siekiant sumažinti epoksidinių dangų kompozicijų toksiškumą ir padidinti ekologiškumą, buvo įvertintas fenalkaminų, biologinės kilmės aminų, veiksmingumas kietinant bisfenolio A pagrindo epoksidines dervas. Pirmą kartą ištirta reakcijų tarp bisfenolio A ir mažamolekulių aminų bei fenalkaminų pagrindo kietiklių kietinimo reakcijos kinetika, siekiant nustatyti ir palyginti jų terminį efektyvumą, sutinklinimo laipsnį ir darbinį laiką (*angl.* Pot-life), naudojantis diferencinės skenuojamosios kalorimetrijos (DSC) ir reologiniais metodais.

Neretai epoksidinių dangų kompozicijose yra naudojami lakūs organiniai tirpikliai dėl galimybės atpiginti ir suskystinti epoksidines kompozicijas. Šie lakūs epoksidinių dangų kompozicijų komponentai formuojantis dangai garuoja ir didina oro taršą bei kenkia žmogaus sveikatai. Siekiant sumažinti lakiųjų organinių junginių kiekį dangose, buvo naudojamos alternatyvios medžiagos – reaktyvūs epoksidiniai skiedikliai, kurie aktyviai dalyvauja poliadicijos reakcijoje, tapdami neatskiriama sukietėjusios dangos dalimi. Pirmą kartą buvo ištirtas skirtingo funkcionalumo reaktyviųjų epoksidinių skiediklių poveikis skystų epoksidinių dervų kietėjimui ir sukietėjusios epoksidinės dangos savybėms. Taip pat įvertintas jų poveikis reguliuojant kietinimo sistemos klampą ir gelėjimo trukmę. Atlikus dangų tyrimus įvertinta reaktyvių skiediklių įtaka mechaninėms dangų savybėms.

Sukurta inovatyvi danga, naudojant dviejų mikrokapsulių savaiminio užsigydymo sistemą. Pirmą kartą susintetintos poliasparto rūgšties esterių (PAAE) mikrokapsulės su UV šviesoje kietėjančiu poliakrilatinės dervos apvalkalu. UV polimerizacija mikrokapsulių formavimui suteikia didžiulį pranašumą dėl labai greito sintezės proceso. Patobulintas izoforondiizocianato (IPDI) įkapsuliavimo į poliurėjos (PU) apvalkalą sintezės procesas ir pasiektas didelis įkapsuliuotos aktyvios medžiagos kiekis. Siekiant optimizuoti PAAE ir IPDI mikrokapsulių sintezės sąlygas, pritaikytas Taguchi eksperimento dizaino metodas. Įvertintas mikrokapsulių poveikis savaiminiam dangų užsigydymui.

Šio darbo tikslas buvo sukurti betirpikles antikorozines dangas, naudojant aplinkai mažiau kenksmingus kietiklius, reaktyvius epoksidinius skiediklius ir ištirti dvigubos mikrokapsulių sistemos panaudojimą savaime užsigydančioms dangoms gauti. Šiam tikslui pasiekti buvo iškelti šie uždaviniai:

1. Įvertinti biologinės kilmės fenalkaminų kietiklių poveikį antikorozinių epoksidinių dangų kietėjimo kinetikai.
2. Įvertinti reaktyvių epoksidinių skiediklių poveikį dangų kietinimo procesui ir mechaninėms antikorozinių epoksidinių dangų savybėms.
3. Optimizuoti poliasparto rūgšties esterių įkapsuliavimo į UV kietinamą poliakrilatinį apvalkalą procesą, taikant Taguchi eksperimento dizaino metodą.
4. Optimizuoti izoforondiizocianato įkapsuliavimo į poliurėjos apvalkalą procesą, taikant Taguchi eksperimento dizaino metodą.
5. Sukurti savaime užsigydančias antikorozines epoksidines dangas, naudojant dvigubą mikrokapsulių sistemą.

EKSPERIMENTINĖ DALIS

Eksperimentinė dalis sudaryta iš šešių poskyrių. Pirmajame poskyryje yra išvardinti pagrindiniai komponentai, naudoti dangų kūrimo etape: epoksidinės dervos, RDs, PhA, mažamolekuliai aminai, pateiktos jų formulės bei fizikinės savybės. Antrame poskyryje pateiktos medžiagos, naudotos mikrokapsulių sintezėje, jų fizikiniai parametrai. Trečiame poskyryje nurodytos dangų kompozicijos, naudotos įvertinti RDs įtaką kietinamų dangų viskoelastinėms ir mechaninėms savybėms. Pateikiami DSC ir reologinių matavimų metodų aprašymai. Ketvirtame poskyryje pateikti mechaninių tyrimų aprašymai. Penktame poskyryje aprašyti PAAE ir IPDI įkapsuliavimo metodai. Taip pat nurodyti mikrokapsulių tyrimo metodai, aprašytas Taguchi metodas Šeštame poskyryje pateikta dangų savaiminio užsigydymo efektyvumo vertinimo metodika.

REZULTATAI IR JŲ APTARIMAS

1.1. Antikorozinių epoksidinių dangų kūrimas

1.1.1. Epoksidinių dervų kietinimas fenalkaminais

PhA yra palyginus nauja amininių kietiklių klasė, kuri turi keletą pranašumų prieš tradicinius mažamolekulius aminus. PhA pasižymi galimybe kietinti epoksidines dervas žemose temperatūrose (net iki 5 °C), jie gaunami iš atsinaujinančių gamtos šaltinių – CNSL, pasižymi hidrofobiškumu ir suteikia dangoms puikias antikorozines savybes [9, 52, 53].

Kinetiniams epoksidinių dervų kietinimo tyrimams buvo pasirinktos dvi bisfenolio A pagrindo dervos: Araldite GY-240 (mažesnės molekulinės masės) ir Araldite GY-2600 (didesnės molekulinės masės), kurios buvo kietinamos mažamolekuliais aminais: trietilentetraminu (TETA), 1,2-etandiaminu (EDA) ir polieteraminu (Jeffamine D-230), bei komerciniais PhA pagrindo kietikliais: Cardolite Lite-2002, Cardolite GX-6004 ir Cardolite NX-6019. Visi trys komerciniai PhA pagrindo kietikliai sudaryti iš 50-78 % kardanolio pagrindo PhA, 0-21 % CNSL ir 22-30 % mažamolekulių aminų – m-ksililendiamino (MXDA), tetraetilenpentamino (TEPA), 2,2,4-trimetilheksan-1,6-diamino (TMD), EDA, 2,4,6-tri[(dimetilamino)metil] fenolio (DMP) ir dimetilaminopropilamino (DMAPA). Tikslesnės šių komercinių PhA pagrindo kietiklių sudėtys pateikiamos eksperimentinėje dalyje 5 lentelėje.

Epoksidinių dervų kietinimas aminais buvo tiriamas DSC ir reologiniais metodais. DSC tyrimo metu nustatyti parametrai, apibūdinantys kietėjimo procesą: pradinė reakcijos temperatūra (T_i), kietėjimo temperatūros intervalas ($\Delta T = T_t - T_i$) ir kietėjimo reakcijos entalpija (ΔH_R). Atlikti reologiniai matavimai padeda nustatyti kietėjimo sistemos darbinį laiką (*angl.* Pot-life). Jis apibrėžiamas kaip laikas, per kurį epoksido-amino sistemos klampos vertė padvigubėja, lyginant su pradine iškart po komponentų sumaišymo.

Reakcija tarp epoksidinių dervų ir aminų/PhA pagrindo kietiklių yra egzoterminis procesas (1 pav.). Nustatyta, kad mažiausią T_i turi PhA pagrindo kietikliai NX-6019 ir GX-6004. PhA pagrindo kietiklio NX-6019 sudėtyje esantys DMP ir DMAPA yra tretiniai aminai, kurie naudojami kaip katalizatoriai. Jie greitina kietinimo reakciją ir sumažina T_i. Aukštos T_i, T_p ir T_t vertės, gautos kietinant epoksidines dervas su mažamolekuliu aminu Jeffamine D-230, rodo, kad mažamolekulis aminas Jeffamine D-230 yra mažiausiai aktyvus iš visų tirtų aminų. Kietinimo reakcijose naudoti mažamolekuliai aminai TETA ir Jeffamine D-230 lėmė didžiausią egzoterminį reakcijos efektą (ΔH_R 386-431 J/g) (1 lentelė).

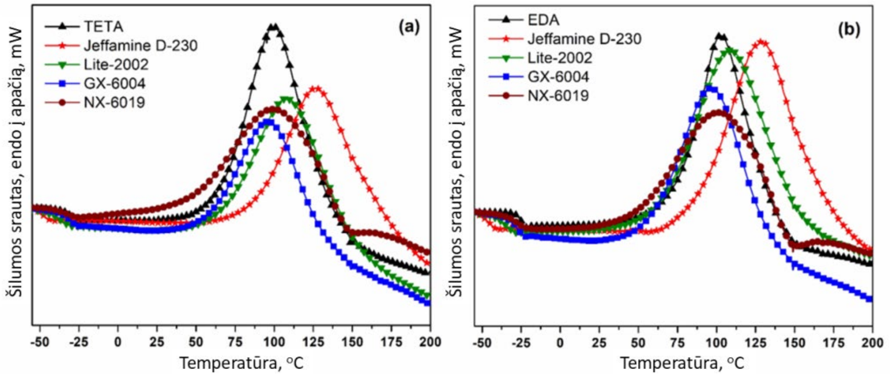

1 pav. Epoksidinių dervų GY-240 (a) ir GY-2600 (b) kietinimo skirtingais aminais DSC kreivės (pirmas kaitinimas)

1 lentelė. Epoksidinių dervų kietinimo skirtingais aminais DSC tyrimo parametrai

Aminų kietikliai	**T_i, °C**	**T_p, °C**	**T_t, °C**	**ΔT, °C**	**ΔH_R, J/g**	**T_g**
Epoksidinė derva GY-240						
EDA	72,6	100,9	132,7	60,1	-	76
TETA	64,7	100,0	142,7	78,0	431,4	-
Jeffamine D-230	85,2	126,5	188,9	103,7	386,0	80
Lite-2002	64,2	108,9	161,3	97,1	363,9	73
NX-6019	48,2	99,9	146,0	97,8	344,9	50
GX-6004	55,0	96,8	136,0	81,0	308,5	85
Epoksidinė derva GY-2600						
EDA	71,5	103,1	141,4	69,9	312,4	53
TETA	62,9	94,7	142,4	79,5	-	98
Jeffamine D-230	83,2	127,7	186,1	102,9	397,9	71
Lite-2002	63,9	108,9	158,0	94,1	335,1	76
NX-6019	47,1	103,0	146,9	99,8	276,8	53
GX-6004	55,5	96,8	137,2	81,7	291,4	82

Reakcijose, kuriose buvo naudojami PhA pagrindo kietikliai, ΔH_R vertės buvo mažesnės (ΔH_R = 277-364 J/g). PhA pagrindo kietikliai reaguoja su epoksidervomis esant žemesnei temperatūrai (T_i = 47-64 °C), nei mažamolekuliai aminai (T_i = 62-85 °C). Iš trumpiausio ΔT intervalo nustatyta, kad GX-6004 yra aktyviausias iš visų tirtų PhA pagrindo kietiklių. Šis fenomenas gali būti paaiškinamas didesniu aktyvių komponentų, kaip TMD [158], kiekiu PhA kompozicijoje.

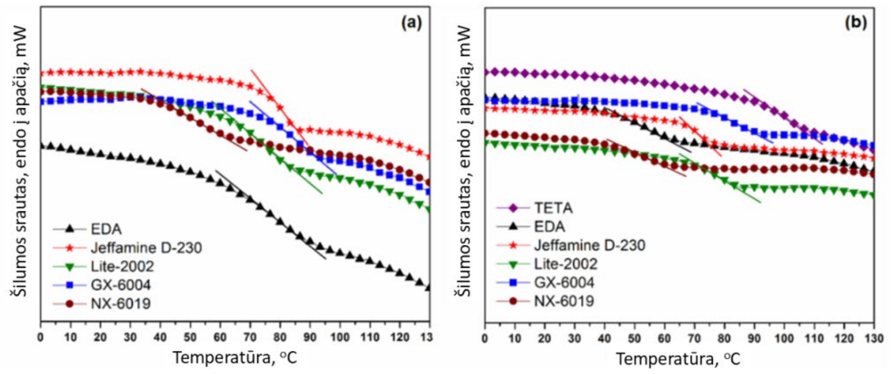

2 pav. Epoksidinių dervų GY-240 (a) ir GY-2600 (b) kietintų skirtingais aminais DSC kreivės (antras kaitinimas)

Epoksidinių dangų stiklėjimo temperatūra (T_g) priklauso nuo kompozicijos susitinklinimo tankio (2 pav.). Didžiausia T_g (98 °C) nustatyta, kai GY-2600 epoksidinė derva kietinta mažamolekuliu aminu TETA. Šiuo atveju didelis sutinklinimo tankis su aukšta T_g gautas dėl didelio TETA funkcionalumo ir mažų atstumų tarp aktyviųjų reaguojančių funkcinių grupių. PhA pagrindo kietikliais NX-6019 ir Lite-2002 sukietintos epoksidinės dangos pasižymi žemesnėmis T_g (50-76 °C) dėl retai išsidėsčiusių amino grupių bei PhA būdingų ilgų alifatinių grandinių, įsiterpiančių dangos struktūroje ir mažinančių dangos sutinklinimo tankį. Didesnė T_g (82-85 °C) nustatyta epoksidines dervas kietinant su PhA pagrindo kietikliu GX-6004, nes jis yra aktyviausias iš visų fenalkaminų.

Naudojantis rotaciniu reometru buvo nustatyti epoksidinių dervų reakcijos su aminais dinaminės klampos pokyčiai per 1-2 valandas nuo komponentų sumaišymo. Reaguojant epoksidinėms dervoms su aminais kompozicijos klampa nuolat didėja, o klampos padvigubėjimas yra fiksuojamas kaip darbinis laikas, (*angl.* Pot-life). Ilgiausias darbinis laikas nustatytas epoksidines dervas kietinant su mažiausiai aktyviu aminu Jeffamine D-230 (>120 min) (2 lentelė). Trumpiausias darbinis laikas (mažiau nei 20 min) nustatytas naudojant kietinimui aktyviausius PhA pagrindo kietiklius – NX-6019 ir GF-6004. Kietinant epoksidervas su PhA pagrindo kietikliais gauti trumpi darbiniai laikai koreliuoja su DSC tyrime nustatytomis žemomis T_i (1 lentelė), kurias nulemia mažamolekulių aminų (TMD) ir katalizatorių (DMP ir DMAPA) buvimas PhA pagrindo kietiklių sudėtyse. Atlikus reologinius tyrimus buvo pastebėta, kad reakcijos tarp epoksidinių dangų ir daugumos PhA pagrindo kietiklių turi trumpesnį darbinį laiką (*angl.* Pot-life) nei su mažamolekuliais aminais (2 lentelė).

2 lentelė. Epoksidinių dervų dinaminė klampa ir kompozicijų darbinis laikas, kietinant įvairiais aminų kietikliais

Aminų kietikliai	**Pradinė klampa, mPa·s**	**Darbinis laikas, min**	**Pradinė klampa, mPa·s**	**Darbinis laikas, min**
	Epoxy resin GY-240		**Epoxy resin GY-2600**	
EDA	1050	35,5	1500	30
TETA	1680	26,5	2490	24,5
Jeffamine D-230	530	>120	790	>120
Lite-2002	2320	30	2510	30
NX-6019	3960	12	3900	12,5
GX-6004	6010	15	7000	19

Įvertinus DSC tyrimo rezultatus nustatyta, kad PhA pagrindo kietikliais kietinant epoksidines dervas reakcija prasideda prie žemesnių T_i ir vyksta greičiau dėl PhA pagrindo kietiklių sudėtyse esančių mažamolekulių aminų ir katalizatorių. Sukietintų epoksidinių dervų stiklėjimo temperatūra (T_g) priklauso nuo naudojamo amino tipo ir gali svyruoti nuo 50 °C iki 98 °C. Toks T_g skirtumas parodo, kad priklausomai nuo mažamolekulių aminų esančių PhA pagrindo kietiklių kompozicijose, galima gauti didesnio ir mažesnio sutinklinimo tankio dangas, o tai leidžia reguliuoti dangų mechanines savybes ir pritaikymo galimybes.

Apibendrinant galima teigti, kad kietinant epoksidervas PhA pagrindo kietikliais, kurie turi tik dalį (22-30 %) mažamolekulių aminų (MXDA, TMD, TEPA, EDA) ir katalizatorių (DMP, DMAPA) galima pasiekti tokius pat ar geresnius sukietintų dangų rodiklius nei naudojant tradicinius mažamolekulius aminus. Dėl mažos T_i vertės PhA pagrindo kietikliai tinkami naudoti kietinti epoksidines dervas žemesnėje temperatūroje. Taip pat tai gali suteikti galimybę prailginti epoksidinių dangų kompozicijų darbinį laiką šaltuoju metų laiku. Epoksidinių dervų kietinimas PhA pagrindo kietikliais leidžia pasiekti sutinklintų dangų T_g reikšmes, panašias į tas, kurios gaunamos naudojant mažamolekulius aminus. Be to, PhA sudėtyje esančios ilgos alifatinės grandinės gali padidinti sukietintų epoksidinių dangų elastingumą, padidinti hidrofobiškumą ir sumažinti susitraukimą.

1.1.2.Reaktyvių skiediklių įtaka epoksidinių dangų formavimuisi ir savybėms

RDs – tai medžiagos, naudojamos vietoj VOC, siekiant sumažinti kompozicijų klampą, lakių komponentų kiekį ir padidinti sausų užpildų kiekį, išlaikant arba pagerinant mechanines dangų savybes. Darbe buvo ištirta RDs įtaka epoksidinių antikorozinių dangų formavimui, gelėjimui ir vitrifikacijos savybėms, bei sukietintų kompozicijų T_g. Taip pat įvertinta RDs funkcionalumo įtaka sukietintų epoksidinių dangų su užpildais ir be jų mechaninėms savybėms, tokioms kaip kietumas, atsparumas smūgiams, adhezija ir atsparumas nusitrynimui.

Norint pabrėžti RDs privalumus epoksidinėse kompozicijose, pasirinktos formuluotės, kurių sudėtyje naudota bisfenolio-A/-F derva (15 %), novolakinė derva (75 %) ir 10 % testuojamų RDs. Šiam eksperimentui pasirinkti RDs – trifunkcinis RD glicerolio propoksilatriglicidileteris (GPTE) naudotas kompozicijoje PA1, monofunkcinis RD C12-C14 alkilglicidileteris (AGE) kompozicijoje PA2, difunkcinis RD 1,4-butanedioldiglicidileteris (BDGE) kompozicijoje PA3 ir 1,6-heksandioldiglicidileteris (HDE) kompozicijoje PA4. Kompozicijos PA1-PA4 buvo kietintos su dviem pasirinktais kietikliais – PB1 ir PB2. Pagrindinis skirtumas tarp kietiklių – PB2 kompozicijoje naudotas tretinis aminas DMP, kuris veikia kaip tinklinimo reakcijos katalizatorius. Epoksidų ir aminų kompozicijos pateiktos eksperimentinėje dalyje 6 ir 7 lentelėse.

Viskoelastinėms dangų kietėjimo savybėms nustatyti pritaikytas reometro osciliacijos testas. Tyrimo metu nustatomas medžiagos pasipriešinimas, mėginį veikiant sinusoidine įtemptimi ir gaunami du parametrai – kaupimo modulis (*angl.* Storage modulus, G') kuris apibūdina struktūrinę, elastinę polimero dalį ir klampos nuostolių modulis (*angl.* Loss modulus, G'') kuris apibūdina klampią, takią polimero dalį. Šių parametrų santykis (G''/G') pateikia dar vieną parametrą – nuostolių faktorių (*angl.* Loss factor, $\tan\delta$). Vertinant šiuos modulius galima nustatyti epoksidinės kompozicijos, kietinamos aminais, reakcijos gelėjimo ir vitrifikacijos trukmes.

Epoksidinių dangų kompozicijų gelėjimo trukmė yra vertinama kaip polimero trimatės struktūros formavimas, kurio metu klampa išauga eksponentiškai iki begalybės [160]. Atliekant reometrinius matavimus, gelėjimo trukmė nustatoma G' ir G'' susikirtimo taške [161]. Sudėtingesnėse reakcijose gelėjimo trukmė randama nustačius $\tan\delta$ susikirtimo tašką esant skirtingiems dažniams [161–165].

Vitrifikacijos trukmė apibūdina polimero sutankėjimą pereinant iš elastinio į stikliškąjį būvį, kuriuo metu reakcija stipriai sulėtėja dėl sumažėjusio komponentų judrumo [166]. Vitrifikacijos trukmė randama nustačius G'' arba $\tan\delta$ kreivių aukščiausias reikšmes esant 1 Hz dažniui [167].

Nustatyta, kad epoksidinių dangų kompozicijų gelėjimo trukmė priklauso nuo naudoto RD. Trumpiausios gelėjimo trukmės nustatytos kompozicijose, kuriose naudoti difunkciniai RDs: BDGE (PA3) ir HDE (PA4) (3 lentelė). Difunkciniai BDGE ir HDE pasižymi didesniu aktyvumu dėl trumpesnių atstumų tarp epoksidinių grupių.

3 lentelė. Epoksidervų kietinimo metu nustatytos gelėjimo ir vitrifikacijos trukmės

Epoksidų/aminų sistemos	**Gelėjimo trukmė, min**		**Vitrifikacijos trukmė, min**	
	tanδ susikirtimo taškas, 1 Hz, 2 Hz, 4 Hz	G′ ir G″ susikirtimo taškas, 1 Hz	tanδ maksimalios vertės, 1 Hz	G″ maksimalios vertės, 1 Hz
PA1/PB1	111	132	120	152
PA1/PB2	51	59	88	112
PA2/PB1	85	90	140	173
PA2/PB2	49	59	100	126
PA3/PB1	67	75	110	134
PA3/PB2	45	49	90	111
PA4/PB1	66	76	120	147
PA4/PB2	45	49	83	102

Vitrifikacijos trukmės, nustatytos kompozicijose su difunkciniais BDGE (PA3), HDE (PA4) ir trufunkciniu GPTE (PA1) RDs, yra labai panašios. Tačiau monofunkcinis AGE (PA2) RD prailgina vitrifikacijos trukmę dėl ilgos alifatinės grandinės, kuri įsiterpia tarp aktyvių centrų reakcijos metu.

Visais atvejais epoksidnių dangų kompozicijų gelėjimo ir vitrifikacijos trukmės yra ženkliai trumpesnės naudojant aktyvesnį kietiklį PB2, kuris sudėtyje turi tretinio amino, DMP, greitinančio epoksidų-aminų reakciją.

Epoksidinių dangų T_g priklauso nuo pasirinktų kietiklių ir RDs. Epoksidinės dangos, kurios buvo gautos kietinant kietikliu PB2, pasižymi aukštesnėmis T_g nei PB1 (4 lentelė). Tai paaiškinama PB2 kietiklio sudėtyje esančiu DMP, kuris skatina epoksidų-aminų reakciją, taip padidindamas galutinį dangos sutinkilinimo tankį. Difunkciniai BDGE (PA3), HDE (PA4) ir trifunkcinis GPTE (PA1) didelės įtakos dangų stiklėjimo temperatūrai neturi. Tačiau kompozicijose su monofunkciniu AGE (PA2) matomas nežymus T_g padidėjimas (ΔT=3-7 °C). Toks T_g padidėjimas galimas dėl mažiausios monofunkcinio RD klampos, kas padeda funkcinėms grupėms lengviau reaguoti.

Norint įvertinti RDs įtaką epoksidinių dangų savybėms, buvo atlikti mechaniniai dangų tyrimai (4 lentelė). Tyrimo metu nustatyta, kad šiek tiek didesnis dangų kietumas gaunamas su difunkciniais BDGE (PA3), HDE (PA4) RDs ir kompozicijose kietintose su kietikliu kurio sudėtyje yra akseleratoriaus DMP (PB2). Didesnis dangų kietumas paaiškinamas mažesniu atstumu tarp difunkciniuose BDGE ir HDE esančių epoksigrupių.

Nustatyta, kad šiek tiek didesnis dangų atsparumas smūgiui gaunamas naudojant difunkcinius BDGE (PA3) ir HDE (PA4). Pastebimas šiek tiek mažesnis dangų atsparumas smūgiui, kai buvo naudotas PB2 kietiklis su katalizatoriumi,. Šie tyrimai koreliuoja su DSC nustatytomis T_g reikšmėmis. Aukštesnis T_g rodo didesnį dangos sutinklinimą, dėl to gaunamas ir didesnis dangų kietumas. Priešingai, dangų elastingumas, ir tuo pačiu metu atsparumas smūgiams yra mažesnis dėl didesnio dangos trapumo.

4 lentelė. Epoksidinių dangų su įvairiais RDs savybės

PA kompozicija	**PA1**		**PA2**		**PA3**		**PA4**	
Kietiklis	PB1	PB2	PB1	PB2	PB1	PB2	PB1	PB2
T_g, °C	51,9	60,0	58,2	64,4	-	-	51,3	61,9
Kietumas, Osc	88	103	83	96	101	104	102	103
Adhezija, MPa	20,3	19,8	19,7	22,1	17,3	23,3	23,0	19,8
Atsparumas smūgiui, J	4,5	4,5	5,0	4,5	6,0	5,5	6,0	5,0

Siekiant įvertinti RD poveikį realiose epoksidinėse antikorozinėse sistemose, buvo sukurtos dangų kompozicijos, pridedant vienodą kiekį užpildų ir įvairių priedų į prieš tai ištirtas epoksidinių dervų (PA1-PA4) ir kietiklių kompozicijas (5 lentelė).

Buvo įvertinta RDs įtaka kompozicijų klampai. Klampų tyrimas atliktas esant keliems skirtingiems šlyties greičiams, norint imituoti kompozicijų sandėliavimo sąlygas (mažas šlyties greitis, 0,1 cm^{-1}) ir darbines sąlygas purškimo ar dažymo metu (didelis šlyties greitis, 1000 cm^{-1}) (5 lentelė). Nustatyta, kad epoksidinių kompozicijų dinaminė klampa, esant dideliems šlyties greičiams, koreliuoja su RDs klampomis. Didžiausia klampa nustatyta PA1 kompozicijoje su trifunkciniu RD GPTE, o mažiausia – PA2 kompozicijoje su monofunkciniu RD AGE.

Nustatyta, kad dangų su užpildais ir specialiais priedais, adhezija, atsparumas smūgiui ir kietumas koreliuoja su minėtais parametrais, gautais dangose be užpildų. Užpildų pridėjimas pagerina atsparumą smūgiui dėl naudotų sausų priedų, tačiau papildomų užpildų įtakos nebuvo pastebėta. Taip pat nustatyta, kad dangos, kurių sudėtyje buvo difunkcinių RDs BDGE (PA3) ir HDE (PA4), pasižymi labai dideliu atsparumu nusitrynimui. Kietiklis su akseleratoriumi PB2 taip pat pagerina atsparumo nusitrynimui savybes.

5 lentelė. Epoksidinių sistemų su papildomai įdėtais užpildais ir specialiais priedais savybės

PA kompozicija	**PA1**		**PA2**		**PA3**		**PA4**	
Kietiklis	PB1	PB2	PB1	PB2	PB1	PB2	PB1	PB2
Klampa prie 0,1 cm^{-1} šlyties greičio, Pa·s	60,3	40,3	45,1	30,2	40,1	26,7	43,5	27,8
Klampa prie 1000 cm^{-1} šlyties greičio, Pa·s	2,65	3,47	1,69	2,42	1,89	2,63	2,24	2,65
Kietumas, Osc	94	95	93	97	90	105	97	107
Atsparumas trinčiai, mg	39	34	52	25	23	20	19	15
Adhezija, MPa	21,9	21,2	21,4	24,2	19,3	19,8	19,3	20,6
Atsparumas smūgiui, J	7	9	8	10	7	8	9	9

Skirtingo funkcionalumo RDs įtaka epoksidinių dervų kietėjimui yra akivaizdi, nors ir nėra didelė. Trumpiausia gelėjimo trukmė pasiekta kietinant epoksidines dervas, kurių sudėtyje yra difunkcinių RD. Difunkcinių BDGE, HDE ir trifunkcinių GPTE, turinčių epoksidinių dervų, kietinimo trukmė yra beveik identiška, o monofunkcinių RD, turinčių sudėtyje AGE, naudojimas padidina kietinimo trukmę. Monofunkcinio RD naudojimas turėjo didesnį poveikį dangų T_g, padidindamas T_g vertę 3-7 °C. Reaktyvūs epoksidiniai skiedikliai turėjo įtakos epoksidinių dangų be užpildų ir su užpildais savybėms. Monofunkcinis AGE labiausiai sumažino epoksidinių kompozicijų klampą, esant dideliam šlyties greičiui. Didžiausią įtaką turėjo dvifunkciniai BDGE ir HDE, kurie sumažino epoksidinių kompozicijų klampą ir padidino dangų su užpildais kietumą bei atsparumą nusitrynimui. Šis tyrimas parodė, kad RDs gali ne tik pakeisti tradicinius VOC, norint sumažinti kompozicijos klampą, bet ir pagerinti mechanines dangų savybes.

1.2. Reaktyvių komponentų įkapsuliavimo sąlygų optimizavimas savaime užsigydančioms epoksidinėms antikorozinėms dangoms gauti

Savaime užsigydančioms dangoms kurti pasirinktas dvigubų mikrokapsulių užsigydymo modelis. Buvo susintetintos dviejų tipų mikrokapsulės, kurias pažeidus, abu aktyvūs komponentai sureaguoja tarpusavyje, tokiu būdu užgydydami dangos pažeidimą.

Aminai yra vieni iš tinkamiausių komponentų savaiminio užgydymo mikrokapsulių sistemoms kaip aktyvios įkapsliuojamos medžiagos dėl jų gebėjimo reaguoti su izocianatais ir epoksidais sukuriant atsparią dangą. Tačiau jų įkapsuliavimas yra komplikuotas dėl jų hidrofiliškumo ir didelio pH [113]. Siekiant sukurti amino pagrindo mikrokapsules, PAAE buvo įkapsuliuotos į UV spinduliais kietinamą akrilatinės dervos apvalkalą.

PAAE pasirinktas dėl jo naujumo ir hidrofobinių savybių, kurios leidžia šį komponentą disperguoti vandenyje ir pritaikyti aliejus-vanduo emulsinės polimerizacijos metodą. Apvalkalo formavimas UV spinduliuotėje yra greitesnis ir efektyvesnis metodas, tačiau retai naudojamas mikrokapsuliavimo srityje.

Izocianato mikrokapsulėms pasirinkta įkapsuliuoti IPDI į PU apvalkalą. IPDI įkapsuliavimas yra plačiai aprašytas, IPDI mikrokapsulės yra naudojamos savaiminio užsigydymo dangų kūrime, tačiau retai izocianatai įkapsuliuojami į PU apvalkalą. Dėl gero izocianato grupių reaktingumo su amino grupėmis, IPDI tinkamas greitoms reakcijoms su PAAE (3 pav.), abiems komponentams susimaišius formuojama apsauginė danga, kuri pasižyminti cheminiu ir mechaniniu atsparumu.

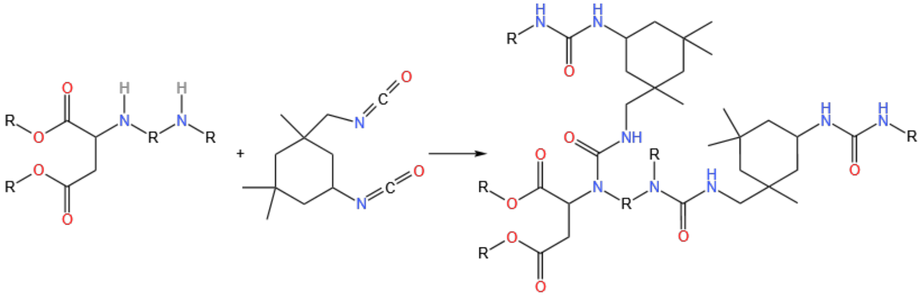

3 pav. PAAE reakcija su IPDI

1.2.1.PAAE įkapsuliavimas UV kietinamame poliakrilatiniame apvalkale

PAAE mikrokapsulės, gautos aliejus-vanduo emulsijos sistemoje, fotopolimerizacijos būdu, apvalkalą formuojant UV spinduliuotėje (1 schema). Mikrokapsulėms sintetinti aliejinė fazė sudaryta iš PAAE, tirpiklio ir UV spinduliuotėje kietinamos akrilatinės dervos buvo disperguota emulsiklio vandeninėje fazėje. Susidarius emulsijai, apvalkalas buvo formuotas iš akrilatų mišinio, polimerizaciją inicijuojant UV spinduliuotėje.

Sintezės sąlygoms optimizuoti buvo naudotas Taguchi L16 eksperimento dizaino metodas, kuris padeda sumažinti eksperimentų kiekį siekiant rasti tinkamas įkapsuliavimo sąlygas.

Kintamais reakcijos parametrais pasirinkti – įkapsuliuojamos medžiagos ir apvalkalo santykis, reakcijos mišinio maišymo greitis, emulsikliai ir jų koncentracija, bei tirpikliai ir jų kiekis (6-7 lentelės). Taguchi eksperimento tikslas buvo pasiekti kuo didesnį įkapsuliuoto PAAE kiekį, išlaikant mikrokapsulių dydį kuo artimesnį 50 µm [180].

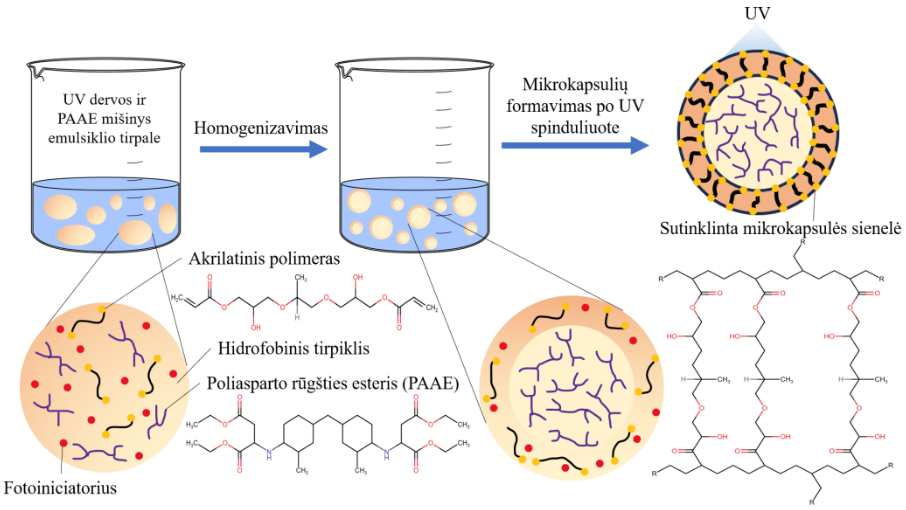

1 schema. PAAE įkapsuliavimas į UV kietinamą poliakrilatinį apvalkalą

Gautų mikrokapsulių dydis ir išvaizda buvo vertinami optiniu mikroskopu (OM) ir skenuojančiu elektroniniu mikroskopu (SEM) (4-5 pav.) Nustatyta, kad mikrokapsulės yra tolygios sferinės formos. Mikrokapsulių dydis varijuoja tarp 10-230 µm, priklausomai nuo pasirinktų parametrų (6 ir 7 lentelės). Mažiausi mikrokapsulių dydžių vidurkiai 10-30 µm gauti, esant didžiausiam maišymo greičiui 3000 apsk/min, o didžiausios – 100-130 µm – gautos, esant mažiausiems maišymo greičiams – 500-750 apsk/min.

6 lentelė. PAAE mikrokapsuliavimo rezultatai (etillaktatas naudotas kaip tirpiklis)

Nr.	Įk.:Apv. santykis	Maišymo greitis, apsk/min	Emulsiklis ir jo koncentracija, %	Etil-laktatas, %	Įkapsuliuotas kiekis, %	Mikro-kapsulių dydžiai, µm	Vid. mikro-kapsulių dydis, µm
EA1	2:1	500	PVA 2 / GA 3	50	40,3	30-270	70
EA2	3:1	750	PVA 1 / GA 1,5	25	51,2	20-260	130
EA3	4:1	1000	SDBS 1	10	21,0	5-160	50
EA4	5:1	3000	PVA 2 / SDBS 1	-	19,0	5-100	30
EA5	2:1	750	SDBS 1	-	47,6	10-1110	100
EA6	3:1	1000	PVA 2 / SDBS 1	50	10,3	5-110	40
EA7	4:1	3000	PVA 2 / GA 3	25	41,7	15-100	50
EA8	5:1	500	PVA 1 / GA 1,5	10	71,1	70-400	130
EA9	2:1	1000	PVA 2 / GA 3	10	37,5	10-140	70
EA10	3:1	3000	PVA 1 / GA 1,5	-	51,6	10-120	70
EA11	4:1	500	SDBS 1	50	43,7	30-280	70
EA12	5:1	750	PVA 2 / SDBS 1	25	14,2	5-150	60
EA13	2:1	3000	SDBS 1	25	13,2	5-110	10
EA14	3:1	500	PVA 2 / SDBS 1	10	58,1	20-330	100
EA15	4:1	750	PVA 2 / GA 3	-	63,7	40-180	80
EA16	5:1	1000	PVA 1 / GA 1,5	50	46,4	10-150	70

Emulsikliai apsaugo besiformuojančias mikrokapsules nuo aglomeravimo, be to smulkesnės mikrokapsulės gaunamos naudojant didesnę emulsiklio koncentraciją. Naudoti tirpikliai – etillaktatas ir ksilenas – taip pat padeda kontroliuoti mikrokapsulių dydį. Naudojami tirpikliai praskiedžia aliejaus fazę, dispergavimas tampa lengvesnis ir tokia aliejaus fazė yra lengviau išskaidoma į mikrolašelius. Naudojant ksileną gautos smulkiausios mikrokapsulės su siauresniu dalelių dydžio pasiskirstymu dėl mažesnės tirpiklio klampos.

7 lentelė. PAAE mikrokapsuliavimo rezultatai (ksilenas naudotas kaip tirpiklis)

Nr.	**Įk.:Apv. santykis**	**Maišymo greitis, apsk. min**	**Emulsiklis ir jo koncentracija, %**	**Ksilenas, %**	**Įkapsuliuotas kiekis, %**	**Mikro-kapsulių dydžiai, µm**	**Vid. mikro-kapsulių dydis, µm**
XA1	2:1	500	PVA 2 / GA 3	-	54,3	18-500	60
XA2	3:1	750	PVA 1 / GA 1.5	10	53,1	11-620	60
XA3	4:1	1000	SDBS 1	25	48.5	21-53	50
XA4	5:1	3000	SMA 1	50	6,0	9-28	15
XA5	2:1	750	SDBS 1	50	28,5	38-70	20
XA6	3:1	1000	SMA 1	-	57,4	18-280	70
XA7	4:1	3000	PVA 2 / GA 3	10	17,3	5-50	30
XA8	5:1	500	PVA 1 / GA 1,5	25	68,7	20-150	50
XA9	2:1	1000	PVA 2 / GA 3	25	15,6	8-25	20
XA10	3:1	3000	PVA 1 / GA 1,5	50	40,8	15-60	25
XA11	4:1	500	SDBS 1	-	63,1	30-390	230
XA12	5:1	750	SMA 1	10	56,8	16-240	50
XA13	2:1	3000	SDBS 1	10	29,8	9-130	22
XA14	3:1	500	SMA 1	25	54,8	23-210	60
XA15	4:1	750	PVA 2 / GA 3	50	23,5	5-35	15
XA16	5:1	1000	PVA 1 / GA 1,5	-	62,7	10-140	40

Siekiant įvertinti mikrokapsulių tvirtumą ir įkapsuliuotos medžiagos išsiliejimą, mikrokapsulės buvo sutraiškomos tarp dviejų stiklo plokštelių. Pažeidus mikrokapsules ant stiklo plokštelių stebima įkapsuliuotos medžiagos skysta fazė (4-5 pav.). Nustatyta, kad smulkesnės mikrokapsulės yra sunkiau mechaniškai pažeidžiamos nei stambesnės.

Sėkmingas aktyvios medžiagos įkapsuliavimas buvo patvirtintas FTIR spektroskopija. Signalas ties 1730 cm^{-1}, būdingas C=O ryšiams, esantiems tiek PAAE, tiek apvalkalo dervoje. Tačiau PAAE signalas yra ženkliai intensyvesnis PAAE ir mikrokapsulėse nei apvalkalo FTIR spektre. Mikrokapsulių spektre stebimi antriniams aminams būdingi signalai – 3340 cm^{-1} ir 860 cm^{-1} (–NH ryšio vibraciniai svyravimai), bei PAAE esančioms –C–N ryšio vibracijoms būdingas signalas ties 1060 cm^{-1}.

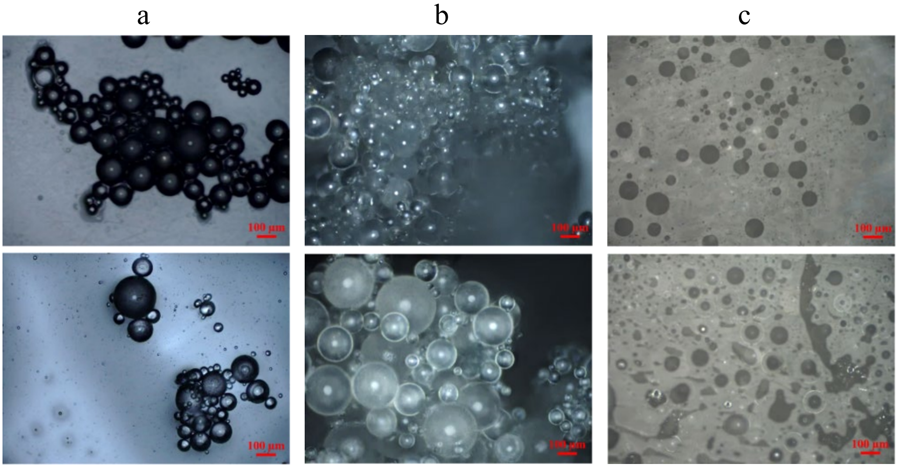

4 pav. Mikrokapsulių EA15 OM nuotraukos: vandenyje (a), džiovintos (b) traiškytos (c)

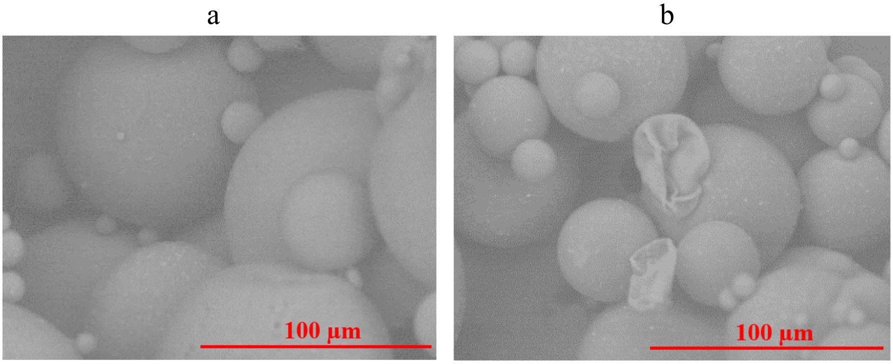

5 pav. Mikrokapsulių EA16 SEM nuotraukos: džiovintų (a) subliūškusių (b)

Mikrokapsulių terminės savybės ir įkapsuliuotos PAAE medžiagos kiekis mikrokapsulėse įvertintas iš termogravimetrinės analizės (TGA) duomenų. Nustatyta, kad PAAE skilimas ir garavimas prasideda ties 200 °C ir vyksta iki 300 °C, o apvalkalo skilimas vyksta nuo 330 iki 480 °C. Skirtingas temperatūrų intervalas leidžia tiksliai nustatyti įkapsuliuoto PAAE kiekį mikrokapsulėse. Įkapsuliuotas PAAE kiekis mikrokapsulėse svyruoja tarp 6 % ir 72 % (6-7 lentelės).

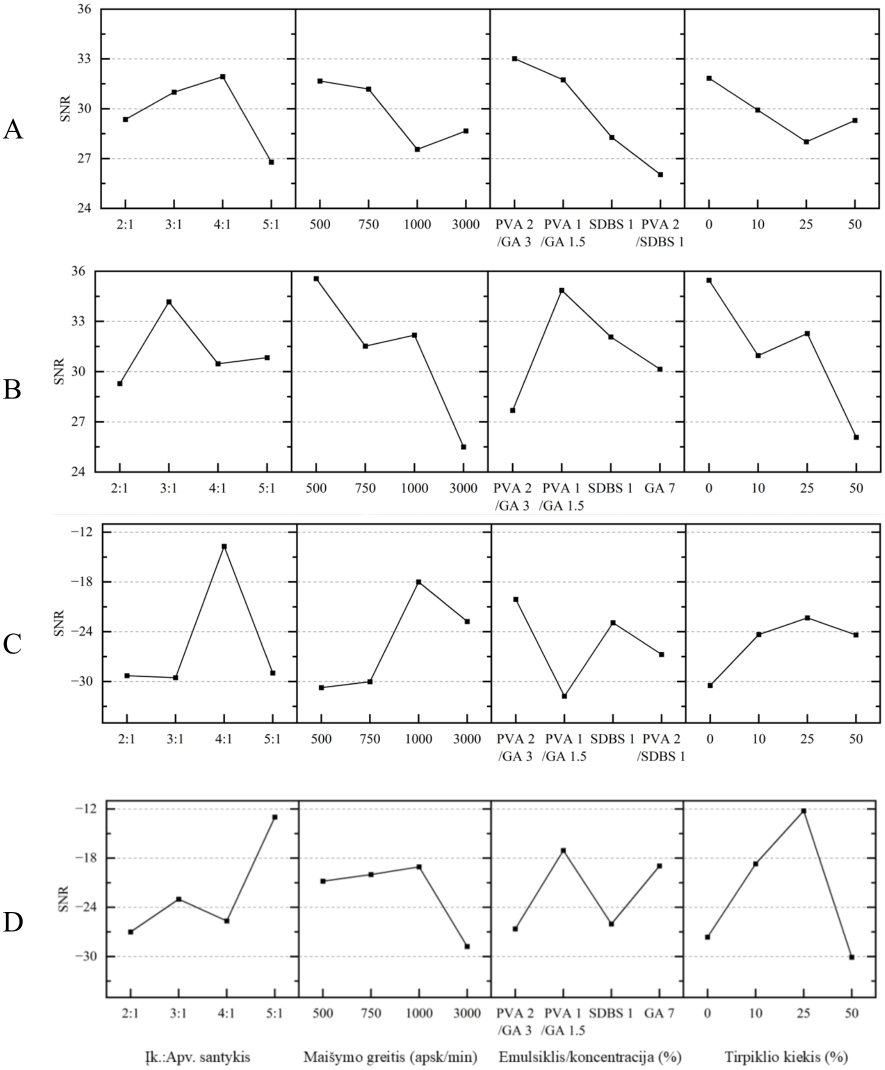

6 pav. Įkapsuliuotos medžiagos (A, B) ir mikrokapsulių dydžio (C, D) priklausomybė nuo įkapsuliavimo parametrų ir pasirinktų tirpiklių kiekio – etillaktato (A, C) ir ksileno (B, D)

Optimizuojant mikrokapsulių sintezės parametrus buvo vertinamas signalo ir triukšmo santykis (*angl.* Signal-to-noise, SNR), kuris rodo signalo (kokybės parametro) jautrumą triukšmui (veiksnių nuokrypiui). SNR dažniausiai yra naudojamas kaip tikslo funkcija optimaliam veikimo sąlygų rinkiniui nustatyti. Siekiant gauti didžiausią įkapsuliuojamos medžiagos kiekį ir optimalų jų dydį (50 µm) buvo pasirinkti Taguchi kriterijai didžiausias-geresnis (*angl.* Larger-the-better) ir nominalus-geriausias (*angl.* Nominal-the-best). Apskaičiavus SNR vertes gautos priklausomybės, parodančios, kurios iš pasirinktų parametrų reikšmių yra tinkamiausios ir kuris parametras daro didžiausią įtaką įkapsuliuotos medžiagos kiekiui ir mikrokapsulių dydžiui (6 pav.).

PAAE mišinio su etillaktatu įkapsuliavimo metu nustatyta, kad didžiausias įkapsuliuotos medžiagos kiekis gaunamas naudojant – 4:1 įkapsuliuojamos medžiagos ir apvalkalo santykį, mažiausią reakcijos mišinio maišymo greitį (500 apsk/min), emulsikliais pasirenkant 2 % polivinilalkoholio (PVA) / 3 % gumarabiko (GA), bei nenaudojant tirpiklio. Mikrokapsulės artimos 50 μm dydžiui gautos naudojant 4:1 įkapsuliuojamos medžiagos ir apvalkalo santykį, 1000 apsk/min maišymo greitį, 1 % PVA / 1,5 % GA emulsiklių mišinį ir 25 % tirpiklio.

PAAE mišinio su ksilenu įkapsuliavimo metu nustatyta, kad didžiausias įkapsuliuotos medžiagos kiekis gaunamas naudojant – 3:1 įkapsuliuojamos medžiagos ir apvalkalo santykį, mažiausią reakcijos mišinio maišymo greitį (500 apsk/min), emulsikliais pasirenkant 1 % PVA / 1,5 % GA, bei nenaudojant tirpiklio. Mikrokapsulės artimos 50 μm dydžiui gautos naudojant 5:1 įkapsuliuojamos medžiagos ir apvalkalo santykį, 1000 apsk/min maišymo greitį, 1 % PVA / 1,5 % GA emulsiklių mišinį ir 25 % tirpiklio.

Šiame darbe buvo atlikta PAAE mikrokapsulių su UV spinduliuote kietinamu poliakrilatiniu apvalkalu sintezė aliejus-vanduo emulsijoje. Sintezės parametrai optimizuoti naudojant Taguchi L16 parametrų metodą. Didžiausias įkapsuliuotos PAAE kiekis gautas naudojant įkapsuliuojamos medžiagos ir apvalkalo santykį 3:1 arba 4:1 ir mažiausią reakcijos mišinio maišymo greitį (500 apsk/min). PAAE įkapsuliavimas, nenaudojant tirpiklių, leidžia formuotis didesnio dydžio mikrokapsulėms dėl klampios aliejaus fazės. 50 μm dydžio mikrokapsulės gaunamos, naudojant įkapsuliuojamos medžiagos ir apvalkalo santykius 4:1 arba 5:1, reakcijos mišinio maišymo greitį 1000 apsk/min bei 25 % etillaktato ar ksileno tirpiklio aliejinei fazei praskiesti. Visais atvejais geriausi rezultatai pasiekti naudojant emulsiklių mišinį 1-2 % PVA / 1,5-3 % GA. Darbo metu pritaikytas UV inicijuojamos radikalinės polimerizacijos metodas ženkliai pagreitina mikrokapsulių sintezės procesą ir turi potencialų pritaikymą mikrokapsulių formavimo srityje.

1.2.2. IPDI įkapsuliavimas į PU apvalkalą

IPDI mikrokapsulės buvo gautos vykdant tarpfazinę polimerizaciją aliejus-vanduo emulsijoje (2 schema). Mikrokapsulėms gauti IPDI ir tri(4-izocianato fenil)tiofosfato (TIPTP) mišinys buvo disperguotas pasirinktame emulsiklio tirpale. Emulsijai susidarius, lašinamas TETA, kuris reaguodamas su TIPTP suformuoja PU apvalkalą.

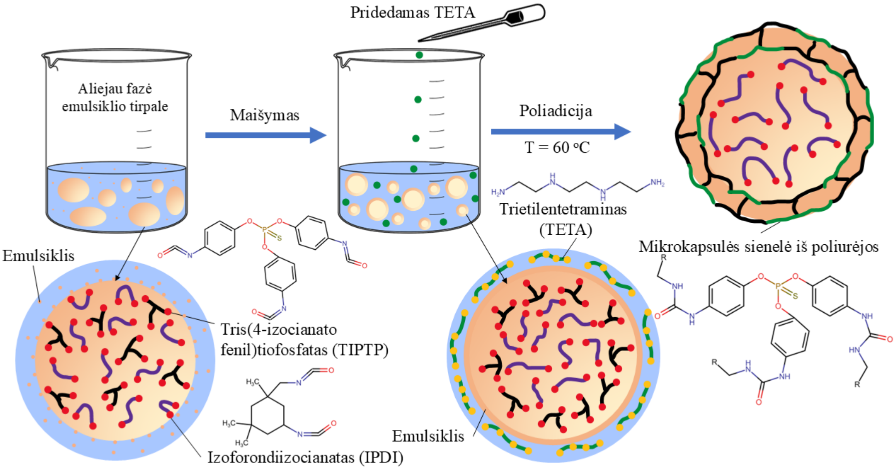

2 Schema. IPDI įkapsuliavimas į PU apvalkalą

Įkapsuliavimo parametrams optimizuoti pasirinktas Taguchi eksperimento dizaino metodas, siekiant gauti didžiausią įkapsuliuotą IPDI kiekį bei tinkamo dydžio mikrokapsules (50 µm). Įkapsuliavimo proceso parametrai ir rezultatai pateikti 8 lentelėje.

Nustatyta, kad dalis mikrokapsulių linkusios aglomeruotis. Panašu, kad išskiriant mikrokapsules liofilizavimo būdu, mikrokapsulės su plona apvalkalo sienele subliūkšta, o išsiliejusi įkapsuliuota medžiaga sulipina mikrokapsules tarpusavyje. Naudojant emulsikliu natrio dodecilbenzensulfonatą (SDBS) mikrokapsulių aglomeravimas buvo ženkliai dažnesnis. Taip pat, naudojant šį emulsiklį, buvo gautos mažiausios mikrokapsulės, kas skatina mikrokapsulių aglomeravimą ir didelių agregatų formavimąsi [184].

Mikrokapsulės tirpale, išdžiovintos liofilizavimo būdu ir mechaniškai pažeistos buvo tirtos OM ir SEM (7 pav.). Mikroskopo nuotraukose aiškiai matyti, kad mikrokapsulės IE3, kurių emulsijoms formuoti buvo naudotas SDBS, buvo mažos ir linkusios aglomeruotis. Kita vertus, mikrokapsulės, gautos naudojant GA ir PVA / GA emulsiklių mišinius, buvo stabilios, apvalios ir tolygiai pasiskirsčiusios.

8 lentelė. IPDI mikrokapsuliavimo į PU apvalkalą rezultatai

Nr	Įk.:Apv. santykis	Maiš. greitis, apsk/ min	Emulsiklis ir jo koncentracija, %	Reakc. laikas, min	Įk. medž. kiekis, %	Mikro-kapsulių dydžiai, µm	Vid. Mikro-kapsulių dydis, µm	Išeiga, %
IE1	2:1	3000	PVA 2 / GA 3	30	58,9	20-90	35	36,7
IE2	3:1	4000	PVA 1 / GA 1,5	45	64,1	20-90	45	58,9
IE3	4:1	5000	SDBS 1	60	72,3	10-40	20	74,3
IE4	5:1	6000	GA 7	90	78,6	20-90	60	26,9
IE5	2:1	4000	SDBS 1	90	52,2	10-20	10	84,3
IE6	3:1	5000	GA 7	30	61,7	15-110	60	56,0
IE7	4:1	6000	PVA 2 / GA 3	45	74,6	8-20	15	25,2
IE8	5:1	3000	PVA 1 / GA 1,5	60	76,1	30-120	80	32,6
IE9	2:1	5000	PVA 2 / GA 3	60	58,3	10-40	35	6,5
IE10	3:1	6000	PVA 1 / GA 1,5	90	65,8	20-60	40	12,6
IE11	4:1	3000	SDBS 1	30	66,4	10-60	25	6,0
IE12	5:1	4000	GA 7	45	69,7	30-60	50	29,4
IE13	2:1	6000	SDBS 1	45	49,9	10-20	10	71,5
IE14	3:1	3000	GA 7	60	74,6	20-70	50	48,9
IE15	4:1	4000	PVA 2 / GA 3	90	71,8	20-70	40	16,8
IE16	5:1	5000	PVA 1 / GA 1,5	30	73,1	20-80	40	19,3

Sutraiškius mikrokapsules tarp stiklo plokštelių, matomas įkapsuliuotos medžiagos ištekėjimas ir pastebimos subliūškusios mikrokapsulės (7 pav.). Mikrokapsulių sienelė yra ypač plona (1-3 µm), o mikrokapsulės paviršius susiraukšlėjęs, galimai dėl liofilizavimo metu naudoto gilaus vakuumo (8 pav.).

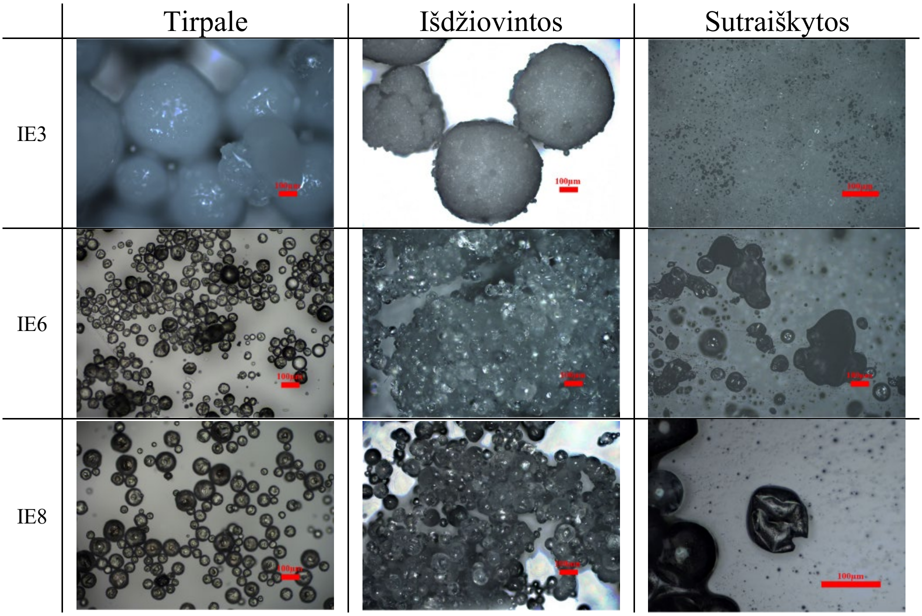

7 pav. Mikrokapsulių IE3, IE6 ir IE8 OM nuotraukos

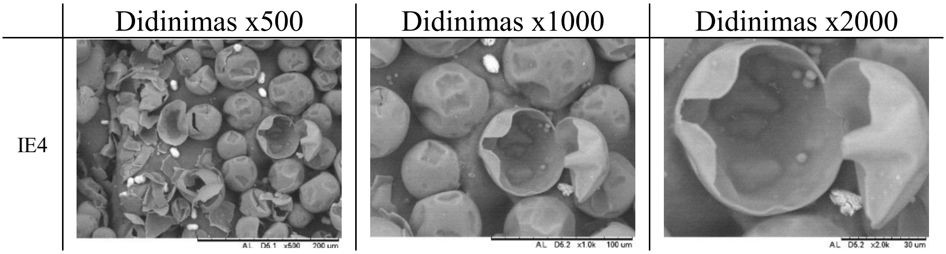

8 pav. Mikrokapsulių IE4 SEM nuotraukos

Sėkmingas aktyvios medžiagos, IPDI, mikrokapsuliavimas patvirtintas FTIR spektroskopija. Spektruose aiškiai matoma IPDI izocianato grupės N=C=O absorbcijos juosta ties 2250 cm^{-1} ir mikrokapsulių spektruose įrodo sėkmingą IPDI įkapsuliavimą.

Mikrokapsulių terminės savybės ir įkapsuliuotos medžiagos kiekis įvertintas iš TGA. IPDI garavimas ir destrukcija prasideda ties 130 ºC ir tęsiasi iki 240 ºC. PU apvalkalo skilimas prasideda ties 250 ºC ir tęsiasi iki 550 ºC. Gauti įkapsuliuoto IPDI kiekiai svyruoja nuo 50 % iki 79 %.

Siekiant optimizuoti mikrokapsulių sintezės parametru buvo pasitelktas Taguchi eksperimento dizaino metodas, o vertinant signalo ir triukšmo santykį SNR pasirinkti kriterijai didžiausias-geresnis (*angl.* Larger-the-better) didžiausiam įkapsuliuotos medžiagos kiekiui bei mikrokapsulių išeigai ir nominalus-geriausias (*angl.* Nominal-the-best) norimo 50 µm dydžio mikrokapsulėms gauti (9 pav.).

Įkapsuliuotos medžiagos kiekiui didžiausią įtaką turėjo įkapsuliuojamos medžiagos ir apvalkalo santykis. Naudojant didesnį įkapsuliuojamos medžiagos kiekį gautas didesnis įkapsuliuotos medžiagos mikrokapsulėse kiekis. Mikrokapsulės, gautos naudojant 5:1 pradinių medžiagų santykį, išlieka patvarios, kas rodo tvirtą PU apvalkalą.

Optimalus mikrokapsulių dydis, artimas 50 µm, gautas pasirinkus įkapsuliuojamos medžiagos ir apvalkalo santykius 3:1 ir 5:1, reakcijos maišymo greitį 4000 apsk/min ir 7 % GA emulsiklio. Reakcijos trukmė turėjo mažiausią įtaką mikrokapsulių dydžiui. Didžiausią įtaką gautiems rezultatams turėjo santykis tarp įkapsuliuojamos medžiagos ir apvalkalo bei emulsiklio tipas/kiekis.

Tinkami reakcijos parametrai didžiausiai kapsulių išeigai gauti: įkapsuliuojamos medžiagos ir apvalkalo santykiai 2:1 ir 3:1, 4000 apsk/min reakcijos mišinio maišymo greitis ir emulsiklių kiekis: 1 % SDBS arba 7 % GA. Optimali reakcijos trukmė didžiausiai išeigai pasiekti – 45 min.

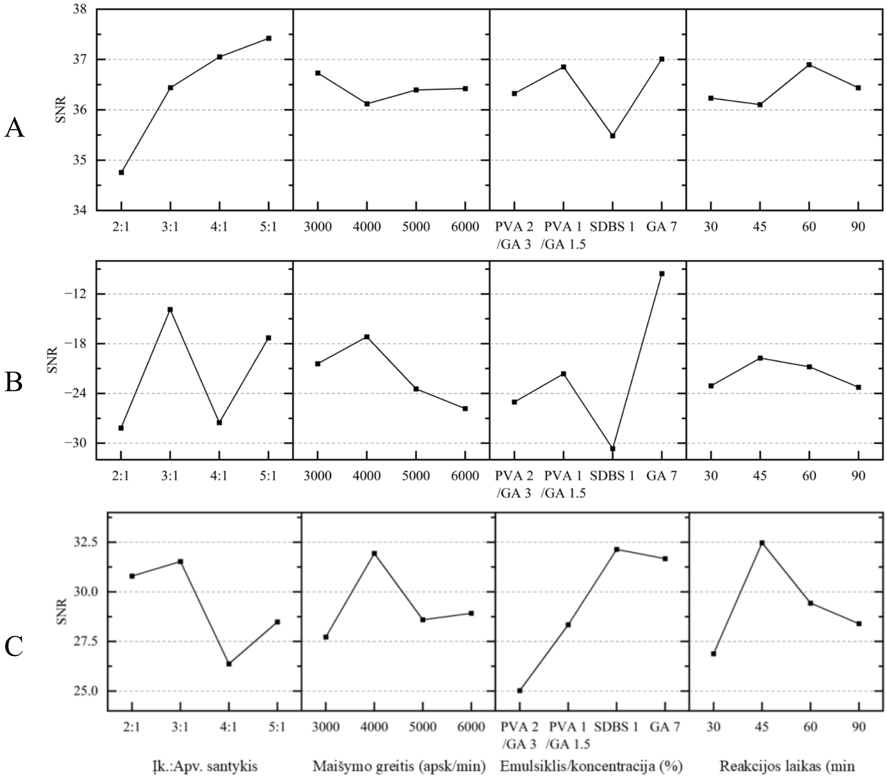

9 pav. SNR grafikai pagal Taguchi metodo skaičiavimus; įkapsuliuotos medžiagos kiekio (A), mikrokapsulių dydžio (B) ir mikrokapsulių išeigos (C) priklausomybė nuo pasirinktų įkapsuliavimo parametrų

Šiame darbe atliktas IPDI įkapsuliavimas į PU apvalkalą tarpfazinės polimerizacijos būdu. Procesas optimizuotas naudojantis Taguchi L16 parametrų metodu. Didžiausias nustatytas įkapsuliuotas IPDI kiekis – 78,6 %. (nustatyta TGA metodu). Didžiausia mikrokapsulių išeiga – 84,3 %. Įvertinta, kad norint gauti mikrokapsules artimas 50 µm, kurių sudėtyje būtų kuo didesnis įkapsuliuotos aktyvios medžiagos kiekis ir didžiausia mikrokapsulių išeiga, tinkamiausios sąlygos yra šios – 3:1 įkapsuliuojamos medžiagos ir apvalkalo santykis, 3000 apsk/min reakcijos mišinio maišymo greitis, 7 % GA emulsiklio ir 60 min reakcijos trukmė.

1.3. Pažangių antikorozinių epoksidinių dangų kūrimas ir tyrimas

Savaime užsigydančioms dangoms sukurti buvo pasirinktos EA8 mikrokapsulės su įkapsuliuotu PAAE (įkapsuliuotos medžiagos kiekis 71,1 %) ir mikrokapsulės IE4 su įkapsuliuotu IPDI (įkapsuliuotos medžiagos kiekis 78,6 %). Mikrokapsulės santykiu 1:1 buvo įdėtos į epoksidinę kompoziciją pridedant 5 % (po 2,5 % abiejų rūšių kapsulių), 10 % (po 5 % abiejų rūšių kapsulių) ir 15 % (po 7,5 % abiejų rūšių kapsulių) nuo bendros kompozicijos masės. Tyrimui pasirinkta betirpiklė epoksidinė kompozicija, tam, kad būtų išvengta tirpiklių įtakos ir dangos susitraukimų tyrimo metu.

Rotaciniu reometru ištirtos epoksidinių kompozicijų klampų priklausomybės nuo įvesto mikrokapsulių kiekio. Nustatyta, kad didinant mikrokapsulių kiekį klampos didėjimas yra proporcingas įvestam mikrokapsulių kiekiui. Kompozicijos, kuriose mikrokapsulių nebuvo, klampa esant 1000 s^{-1} šlyties greičiui siekė 1460 mPa·s, pridėjus 5 % mikrokapsulių klampa padidėjo iki 1960 mPa·s, 10 % – 2370 mPa·s ir 15 % – 2990 mPa·s.

Mikrokapsulių užsigydymo efektyvumui įvertinti, epoksidinės kompozicijos su 5, 10 ir 15 % mikrokapsulių buvo padengtos 400 μm storio sluoksniu ant metalinio substrato, sukietintos, pažeistos 100 μm storio metaliniu peiliu ir paliktos užgyti. Po užsigydymo dangos buvo perkeltos į druskos rūko kamerą ir po dienos buvo vertintas užsigydymo efektyvumas. Pastebėta, kad pilnas užsigydymas nebuvo pasiektas, dėl galimai per didelio pažeisto ploto (10 pav.).

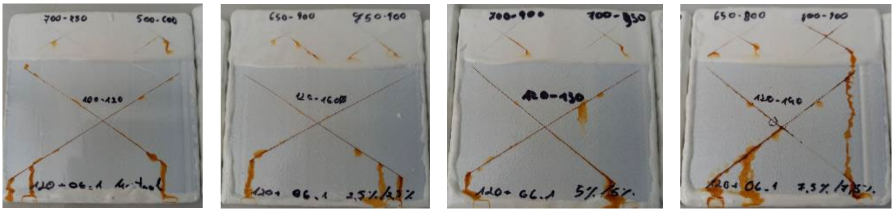

2AE120-0 2AE120-1 2AE120-2 2AE120-3

10 pav. Epoksidinių dangų su mikrokapsulių sistema (EA8+IE4) nuotraukos po druskos rūko korozijos tyrimo: 2AE120-0 – 0%; 2AE120-1 – 5%; 2AE120-2 – 10%; 2AE120-3 – 15%

Papildomai tyrimas atliktas plokšteles po pažeidimo pakaitinus 80 °C temperatūroje 1 valandą, siekiant pagreitinti ir pagerinti savaiminį dangos užsigydymą. Dangos užsigydymas buvo tirtas OM (11 pav.). Dangas pakaitinus 80 °C temperatūroje, pažeidimo vietoje akivaizdžiai matomas įpjovos susiaurėjimas ir dalinis metalo padengimas naujai susiformavusia plėvele. Geriausias efektas gautas naudojant 15 % mikrokapsulių epoksidinių dangų kompozicijoje.

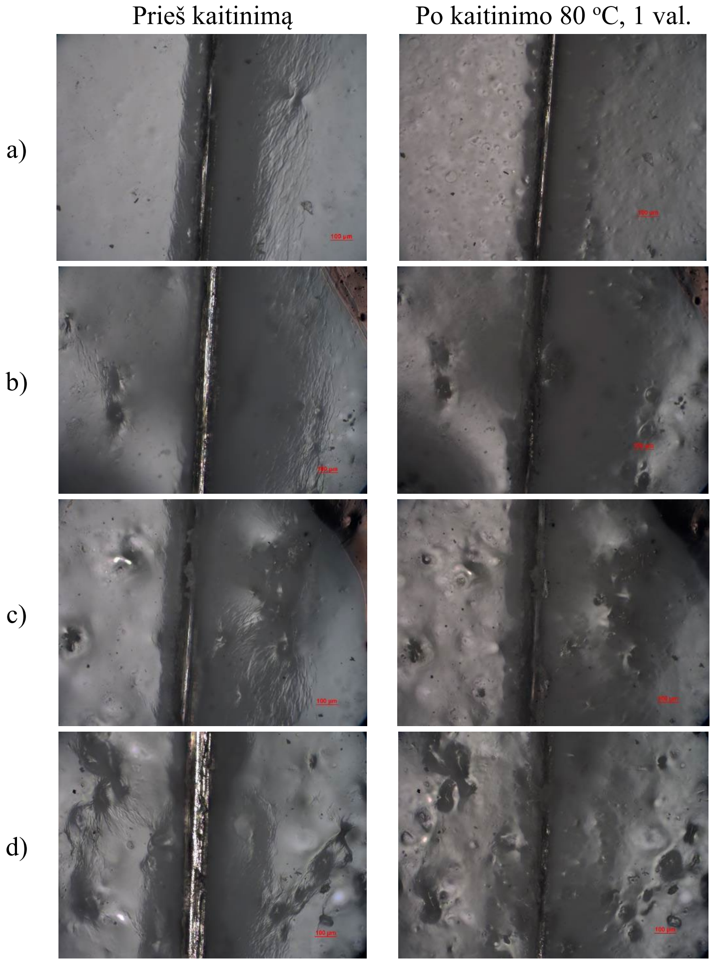

11 pav. Epoksidinių dangų su mikrokapsulių sistema (EA8+IE4) OM nuotraukos prieš ir po kaitinimo: a) 2AE120-0 – 0 % b) 2AE120-1 – 5 %, c) 2AE120-2 – 10 %, d) 2AE120-3 – 15 %

Apibendrinus pažangių antikorozinių kompozicijų ir iš jų formuojamų dangų tyrimą, nustatyta, kad dvigubos mikrokapsulių sistemos, sudarytos iš PAAE ir IPDI, įvedimas į epoksidinę kompoziciją kelia kompozicijos klampą proporcingai įvestų mikrokapsulių kiekiui. Suformuota danga turinti nuo 5 % iki 15 % mikrokapsulių sumažina pažeistos dangos plotą ir turi potencialo prailginti epoksidinių dangų naudojimo trukmę.

IŠVADOS

1. DSC ir reologiniai tyrimai parodė, kad reakcija tarp epoksidinių dervų ir fenalkaminų pagrindo kietiklių vyksta prie žemesnių temperatūrų, ir šiek tiek lėčiau nei su mažamolekuliais aminais. Fenalkaminų pagrindo kietiklis NX-6019 pasižymėjo žemiausia T_i ir trumpiausiu darbiniu laiku (*angl.* Pot-life) dėl jo sudėtyje esančių tretinių aminų DMP ir DMAPA kurie veikia kaip epoksidinių dervų tinklinimo reakcijos katalizatoriai. Naudojant GX-6004 fenalkaminų pagrindo kietiklį, turintį mažamolekulio TMD, stebėtas didžiausias kietinimo reakcijos greitis, o suformuota danga pasižymėjo aukšta (iki 80-85 ^{o}C) T_g.
2. Osciliaciniai, DSC ir mechaniniai tyrimai parodė, kad monofunkcinis reaktyvus skiediklis, C12-C14 alkilglicidileteris, prailgina kompozicijų vitrifikacijos trukmę, labiausiai sumažina jų klampas bei padidina sutinklintų dangų T_g. Difunkciniai reaktyvūs skiedikliai – 1,4-butanedioldiglicidileteris ir 1,6-heksandioldiglicidileteris – suteikia kompozicijoms trumpiausias gelėjimo ir vitrifikacijos trukmes, vidutiniškai sumažina klampas bei suteikia dangoms geriausias kietumo ir atsparumo nusitrynimams savybes, lyginant su kitais testuotais reaktyviais skiedikliais. Reaktyvūs skiedikliai buvo pritaikyti kaip lakių organinių junginių alternatyvos, taip sukuriant ekologiškesnes ir aplinkai mažiau kenksmingas epoksidinių dangų kompozicijas.
3. Sukurtas naujas PAAE mikrokapsulių su UV poliakrilatiniu apvalkalu sintezės aliejus-vanduo emulsijoje, inicijuojant apvalkalo radikalinę polimerizaciją UV spinduliuote, metodas. Nustatyta, kad norint gauti kapsules su kuo didesniu įkapsuliuotos aktyvios medžiagos kiekiu, tinkamiausios sąlygos yra – 3:1 ir 4:1 įkapsuliuotos medžiagos ir apvalkalo santykis, 500 apsk/min maišymo greitis, 1-2 % PVA / 1,5-3 % GA emulsiklių mišinys. Gautos artimos 50 µm dydžiui mikrokapsulės naudojant – 4:1 ir 5:1 įkapsuliuotos medžiagos ir apvalkalo santykius, 1000 apsk/min maišymo greitį, 1-2 % PVA / 1,5-3 % GA emulsiklių mišinį ir 25 % tirpiklių įkapsuliuojamos medžiagos sudėtyje.
4. Atliktas IPDI įkapsuliavimas į PU apvalkalą tarpfazinės polimerizacijos būdu. Nustatyta, kad norint gauti mikrokapsules, artimas 50 µm, kurių sudėtyje būtų kuo didesnis įkapsuliuotos aktyvios medžiagos kiekis, didžiausia mikrokapsulių išeiga, tinkamos sąlygos yra – 3:1 įkapsuliuojamos medžiagos ir apvalkalo santykis,

3000 apsk/min reakcijos mišinio maišymo greitis, 7 % emulsiklio GA ir 60 min reakcijos trukmė. Esant šioms sąlygoms, pasiektas 74,6 % IPDI įkapsuliavimas ir 48,9 % mikrokapsulių išeiga.

5. Sukurtos pažangios epoksidinės antikorozinės dangos su dviguba mikrokapsulių sistema sumažina pažeistą dangos plotą dangas pakaitinus 80 °C temperatūroje 1 val. Didžiausias pažeistų dangų užsigydymo efektas pastebėtas naudojant 2AE120-3 kompoziciją, ir esant didžiausiam mikrokapsulių kiekiui epoksidinių dangų kompozicijose (15 %).

PUBLIKACIJŲ SĄRAŠAS

Publikacijos žurnaluose

1. J. Jonikaitė-Švėgždienė, L. Pastarnokienė, V. Juknevičiūtė, R. Makuška. Curing of epoxy resins by bio-based phenalkamines vs low-molecular-weight amines: study by DSC. Chemija 33(2) (2022) 54-63. https://doi.org/10.6001/chemija.v33i2.4709
2. L. Pastarnokienė, J. Jonikaitė-Švėgždienė, N. Lapinskaitė, R. Kulbokaitė, A. Bočkuvienė, T. Kochanė, R. Makuška. The effect of reactive diluents on curing of epoxy resins and properties of the cured epoxy coatings, J Coat Technol Res 20 (2023) 1207-1221. https://doi.org/10.1007/s11998-022-00737-4.
3. L. Pastarnokienė, E. Potapov, R. Makuška, T. Kochanė. Optimization of microencapsulation of polyaspartic acid ester into UV curable epoxy-acrylate resin using Taguchi method of experimental design. J. Appl. Polym. Sci. 141(15) (2024). https://doi.org/10.1002/app.55216
4. L. Pastarnokienė, E. Potapov, R. Makuška, T. Kochanė. Optimization of microencapsulation of isophorone diisocyanate into polyurea shell by oil-in-water interfacial polymerisation. Chemija, 35(2) (2024) 54-64. https://doi.org/10.6001/chemija.2024.35.2.4

Konferencijų tezės

1. L. Pastarnokienė, T. Kochanė, R. Makuška. Improvement of anti-abrasion properties of anti-corrosive epoxy coating for industrial applications. Tarptautinė konferencija „Advanced Materials and Technologies 2021", Palanga, Lietuva.
2. L. Pastarnokienė, T. Kochanė, A. Jankauskytė, R. Makuška. Synthesis of microcapsules containing diisocyanate as a healing agent. Tarptautinė konferencija „Chemistry & Chemical Technology 2021", Vilnius, Lietuva.
3. L. Pastarnokienė, T. Kochanė, S. Žukaitytė. R. Makuška. Synthesis of microcapsules containing amines as healing agents. Tarptautinė konferencija „Baltic Polymer Symposium 2022", Talinas, Estija.
4. E. Potapov, L. Pastarnokienė, T. Kochanė, R. Makuška. Synthesis of microcapsules containing polyaspartic acid ester within UV curable shell. Tarptautinė konferencija „Chemistry & Chemical Technology 2023", Vilnius, Lietuva
5. L. Pastarnokienė, T. Kochanė, E. Potapov, R. Makuška. Optimization of microencapsulation of isophorone diisocyanate in polyurea shell. Tarptautinė konferencija „Baltic Polymer Symposium 2023", Jelgava, Latvia.
6. T. Kochanė, A. Jankauskytė, L. Pastarnokienė. Optimization of microencapsulation conditions of polyaspartic acid esters. Tarptautinė konferencija „Baltic Polymer Symposium 2024", Birštonas, Lietuva.

COPIES OF PUBLICATIONS

CHEMIJA. 2022. Vol. 33. No. 2. P. 54–63
© Lietuvos mokslų akademija, 2022

Curing of epoxy resins by bio-based phenalkamines vs low-molecular-weight amines: study by DSC

Jūratė Jonikaitė-Švėgždienė[1*],

Liepa Pastarnokienė[1, 2],

Virginija Juknevičiūtė[1],

Ričardas Makuška[1]

[1] *Department of Polymer Chemistry,*
Vilnius University,
24 Naugarduko Street,
03225 Vilnius, Lithuania

[2] *Litnobiles UAB,*
17 Kojelavičiaus Street,
11101 Vilnius, Lithuania

In this study, curing of BPA-based epoxy resins Araldite®GY-2600 and Araldite®GY-240 by low-molecular-weight amines EDA, TETA and Jeffamine D-230, and bio-based phenalkamines Cardolite®NX-6019, Cardolite®Lite-2002 and Cardolite®GX-6004 was studied by differential scanning calorimetry (DSC) and rheology measurements. DSC provided quantitative information on the overall reaction kinetics (the enthalpy of curing reaction, ΔH_R; cure degree, α; curing reaction rate, $d\alpha/dt$) and the glass transition temperature (T_g) of the cured product. It was demonstrated that the DSC curing of epoxy resins by phenalkamines started at lower temperature, and the curing rates were slightly lower compared to those cured by low-molecular-weight amine hardeners. The enthalpy of the curing by phenalkamines was lower, especially in the case of more viscous epoxy resin GY-2600. T_g of the cured epoxy resins varied from 50 to 98°C and was slightly lower when cured with cardanol-based phenalkamines. The results demonstrate that curing of epoxy resins by bio-based phenalkamines proceeds in a similar temperature interval like using low-molecular-weight amines as hardeners but with less exothermic effect, which could be an advantage.

Keywords: phenalkamines, epoxy resins, curing reaction, *pot-life*, DSC

INTRODUCTION

Phenalkamines (PA) are a relatively new class of curing agents for epoxy resins, widely used in protective coatings. Advantages of these curing agents are related to low/room temperature curing applications, a good moisture tolerance and a good surface appearance of the coatings [1–3]. PA are bio-based amines synthesised from cardanol refined from renewable material, Cashew nut shell liquid (CNSL) [3, 4]. CNSL has proven itself to be an invaluable resource for the development of a wide variety of products including not only epoxy curing agents but also other components of epoxy resins and polyurethanes, and much more [5].

Phenalkamines are Mannich base generally synthesised from equimolar quantities of cardanol, formaldehyde and polyamine (Scheme 1) [6].

The distinctive structure of PA has some effect on the properties of the resulting paints and coatings. Due to a long aliphatic alkyl side chain of cardanol, PA-containing paints are characterised by lower viscosity and surface tension, and improved wetting properties; the resulting coatings possess a good flexibility and hydrophobicity, and an improved water resistance. The aromatic backbone of PA gives an excellent chemical resistance. Side chains of PA containing amino- and imino-groups react easily with the epoxy groups giving highly cross-linked products. A high activity of PA even at ambient temperature as well as a good adhesion is related to the presence of the phenolic

---

[*] Corresponding author. Email: jurate.jonikaite-svegzdiene@chgf.vu.lt

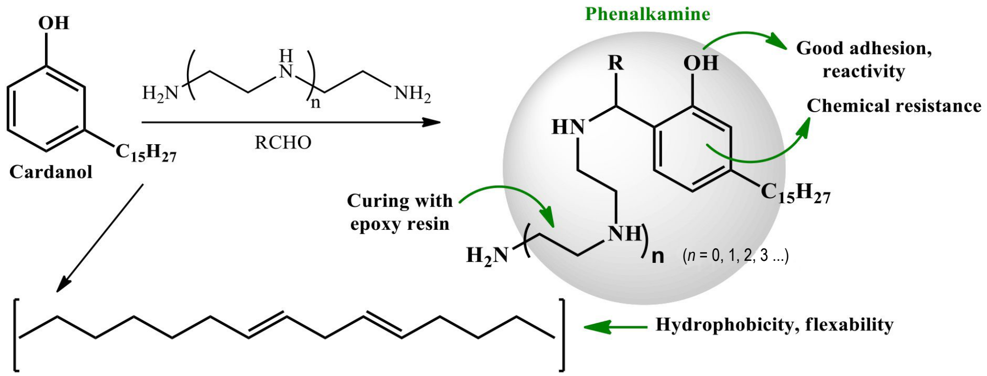

Scheme 1. The synthesis and structure–property relationship of phenalkamines [6]

hydroxyl group. Furthermore, PA hardeners are known for a low toxicity, which makes them eco-friendly.

Curing low-molecular-weight epoxy resins by amine hardeners, tightly cross-linked materials with high T_g are formed usually [7]. To reduce the brittleness (and the same, T_g) of the cured epoxy resins, phenalkamines can be successfully used in an eco-friendly way. The curing mechanism and properties of the epoxy coatings depend on the PA structure, molecular weight and amine value.

Differential scanning calorimetry (DSC) is a thermal analysis technique widely used to obtain a thorough understanding of the cure kinetics of various systems. A DSC calorimeter captures the exothermic heat flow which is released during the cross-linking process of a reactive polymer in respect of curing time under isothermal or non-isothermal conditions [8]. The curing kinetics of various epoxy-based systems has been extensively investigated by this method [9–15]. Furthermore, DSC is very useful to gain additional information about the extent of cross-linking by changes in glass transition temperature (T_g). Some authors declare that T_g is even more suited for monitoring of the cross-linking process than the cure degree α [16, 17].

Rheology is the science of deformation and the flow of matter and describes the interrelation between force, deformation and time. Flow properties of a fluid are usually characterised by a plot of the shear stress associated with the shear rate applied to the fluid. One of the important rheological terms is viscosity, which is a measure of its resistance to deformation at a given rate. The initial viscosity of epoxy resin–amine mixture is increasing with curing time, which could serve as an indicator of the curing rate [18–20].

The objective of the present work was to evaluate the kinetics of DSC curing of commonly used liquid epoxy resins by bio-based phenalkamines and compare with curing using typical low-molecular-weight amines. The further objective was to identify the specific features of curing of epoxy resins by cardanol-based phenalkamines in regard with the thermal effect, development of cure degree, and *pot-life* of the curing systems.

EXPERIMENTAL

Materials

Commercial epoxy resins and amine hardeners typically used in anti-corrosion epoxy-based coatings were used in this study. Bisphenol-A epoxy resins with commercial names Araldite® GY-240 (epoxy equivalent weight (EEW) 178–183 g/eq, viscosity (25°C) 7000–9000 mPa·s) and Araldite® GY-2600 (EEW 184–190 g/eq, viscosity (25°C) 12000-14000 mPa·s) were from Huntsman Co. Low-molecular-weight amines 1,2-ethanediamine (EDA, amine equivalent weight (AEW) 15 g/eq), triethylenetetramine (TETA, mixture of four ethyleneamines with similar boiling points including linear, branched and two cyclic, AEW = 24 g/eq) and amine-terminated polyoxypropylene glycol (polyetheramine) with the commercial name Jeffamine® D-230 (AEW = 60 g/eq) were provided by Huntsman Co. Cardanol-based phenalkamines with the commercial name Cardolite® were kindly donated by Cardolite Co. The commercial names and the composition of bio-based phenalkamines are given in Table 1.

Batches for DSC measurements were made by mixing 1 g of epoxy resin and the corresponding amount of an amine hardener. The mixing ratio of epoxy resin to a curing agent was stoichiometric. The amount of a hardener (g) required to cure 1 g of an epoxy resin was calculated by the equation [21]:

Table 1. **The composition of cardanol-based commercial phenalkamines***

Components	**Cardolite®**		
	Lite-2002, % (AEW = 104 eq/g)	**GX-6004, % (AEW = 76 eq/g)**	**NX-6019, % (AEW = 133 eq/g)**
Cardanol-based phenalkamine	72–78	50–62	68–75
1,1′-(1,3-Phenylene)di(methanamine) *m*-Xylylenediamine (MXDA) 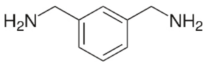	18–22	15–23	1–2
Cashew (*Anacardium occidentale*) nutshell extract, decarboxylated, distilled	–	16–20	18–21
N^1-(2-Aminoethyl)-N^2-{2-[(2-aminoethyl)amino]ethyl} ethane-1,2-diamine Tetraethylenepentamine (TEPA) 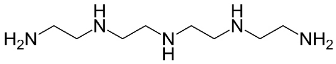	4–6	–	–
2,2,4-Trimethylhexane-1,6-diamine (TMD) 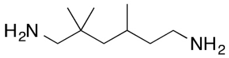	–	~7	–
2,4,6-Tris[(dimethylamino)methyl]phenol (DMP) 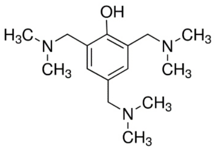	–	–	3–4
N^1,N^1-Dimethylpropane-1,3-diamine Dimethylaminopropylamine (DMAPA) 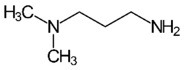	–	–	2–3
Phenol	–	–	0.6–0.9
Ethylenediamine (EDA)	–	–	0.6–0.9

* From the material safety data sheets (MSDS) of phenalkamines.

$$m_h = \frac{\mathrm{AEW} \cdot m_{\mathrm{epoxyresin}}}{\mathrm{EEW}}.$$

The general structure of BPA-based epoxy resins and amines used in this study is presented in Scheme 2.

DSC measurements

A calorimeter Perkin Elmer DSC8500 was used to study curing of epoxy resins by amines. A non-isothermal DSC test was performed under nitrogen atmosphere (rate 40 mL/min). A sealed empty aluminium pan was used as a reference. Samples of 3–5 mg were heated from –60 to 200°C at the rate of 10°C/min. and then kept at this temperature for additional 10 min. The heat flow curves were recorded, and the thermal data were further processed to determine the cure degree (α) and the curing reaction rate ($d\alpha/dt$). After the first heating, the temperature was decreased to –60°C and equilibrated for 3 min. Then the second heating at the rate 10°C/min to 200°C was performed, which was used for determination of the glass transition temperature (T_g) of the cured system.

Rheological measurements

A rheometer Anton Paar MCR302 was used to study the initial stage of curing and for the determination of *pot-life* of the curing system. The *pot-life* refers to the amount of time it takes for the product's initial mixed viscosity to double [22]. The measurements were performed at 25°C with a parallel-plate of diameter 50 mm and a distance between the parallel plate and the base mount of 1 mm, and the shear rate was kept constant at 0.25 s^{-1}. The viscosity (in mPa·s) was measured every 5 s.

RESULTS AND DISCUSSION

To demonstrate the curing progress of the epoxy resin–amine system, non-isothermal DSC tests were carried out. Some results of these tests presented in the form of DSC curves are shown in Fig. 1. The heat flow as a function of temperature was determined and the thermal data were further processed to determine the cure degree α (Fig. 2) as well as the rate of the curing reaction $d\alpha/dt$ (Figs. 3–4). The cure degree α was calculated by the ratio $\alpha = \Delta H_t/\Delta H_T$ [23], where ΔH_t represents the enthalpy of the curing reaction at time *t*, and ΔH_T is the total enthalpy of the curing reaction of the epoxy resin. ΔH_T was calculated by integrating the heat flow over the whole exothermic peak for a completely uncured sample. The curing reaction rate ($d\alpha/dt$) is proportional to the measured heat flow (dH/dt) [24] or, the same, to the changes in the cure degree. $d\alpha/dt$ was calculated by taking the derivatives of the curves presented in Fig. 2.

Evidently, the curing reaction is an exothermic process which is represented by one exothermic peak (Fig. 1). From the curing curves, the initial curing temperature (T_i), peak curing temperature (T_p), terminal curing temperature (T_t) [25] and enthalpy of the curing reaction (ΔH_R) were obtained and listed in Table 2. Some data were not processed due to the instability of the baseline (cases of EDA and TETA). The initial curing temperature T_i did not depend on the type of the epoxy resin

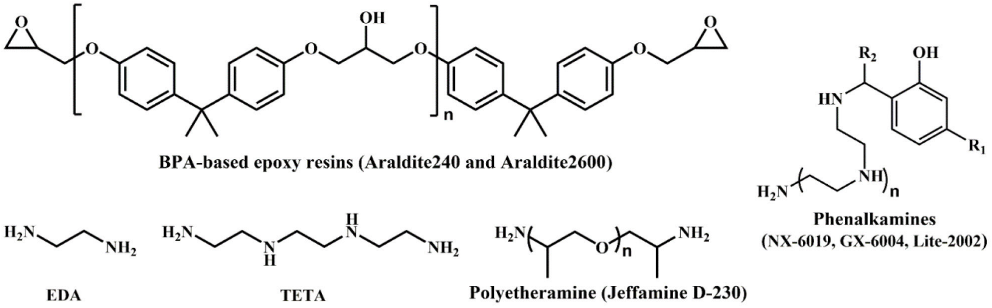

Scheme 2. Structure of the epoxy resins and amine hardeners used in the present study

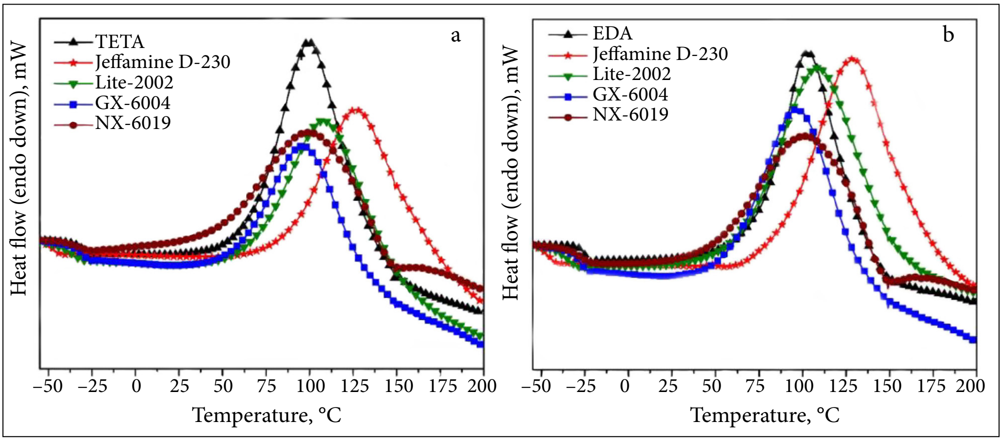

Fig. 1. DSC curing of the epoxy resins GY-240 (a) or GY-2600 (b) by different amines

but was dependent on the type of the hardener being the lowest for the phenalkamines NX-6019 and GX-6004 (Table 2). Curing by Jeffamine D-230 was evidently late, which was reflected in higher values of T_i, T_p and T_t. The peak curing temperature T_p obtained by using other hardeners including phenalkamines was similar and close to 100°C.

During curing, the cure degree α starts at 0 and can reach a maximum value of 1, representing the fully cured epoxy resin (Fig. 2). The relationship between the curing reaction rate ($d\alpha/dt$) and temperature is presented in Fig. 3. The curing rate in all the cases increases gently when the epoxy resin–amine system begins to cure. As the reaction progresses, the heat released by the curing reaction itself simultaneously accelerates the curing process. Thus, the internal system epoxy resin–amine most likely exhibits an autocatalytic curing reaction mechanism (Scheme 3) [9].

The maximal values of the curing reaction rate were reached at about 100°C with an exception for the mixture containing Jeffamine D-230. When most of the functional groups were reacted, the curing rate of the epoxy resin–amine system started to gradually decrease and at 150–200°C approached the values close to 0.

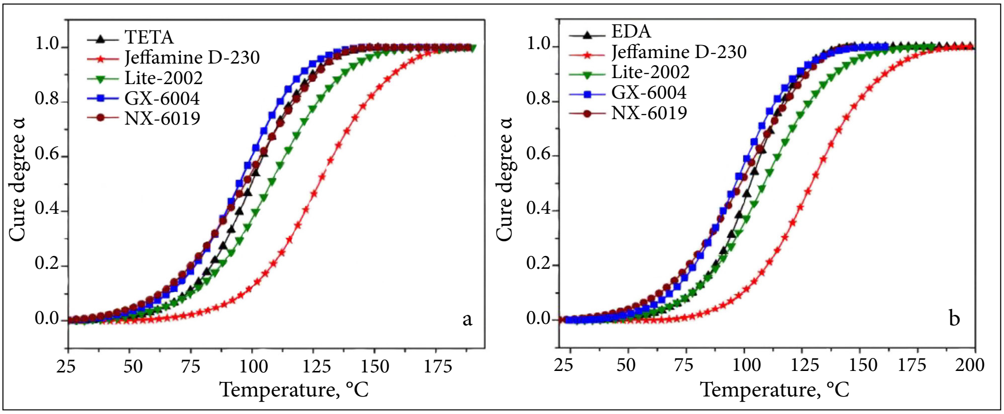

Fig. 2. The dependence of the cure degree α on temperature under DSC curing of the epoxy resins GY240 (a) and GY2600 (b) by different amines

Table 2. **Characteristic parameters of the DSC curing of epoxy resins by different amines**

Amine hardener	T_i, °C	T_p, °C	T_t, °C	$\Delta T = T_t - T_i$, °C	ΔH_R, J/g	T_g
Epoxy resin GY-240						
EDA	72.6	100.9	132.7	60.1	–	76
TETA	64.7	100.0	142.7	78.0	431.4	–
Jeffamine D-230	85.2	126.5	188.9	103.7	386.0	80
Lite-2002	64.2	108.9	161.3	97.1	363.9	73
NX-6019	48.2	99.9	146.0	97.8	344.9	50
GX-6004	55.0	96.8	136.0	81.0	308.5	85
Epoxy resin GY-2600						
EDA	71.5	103.1	141.4	69.9	312.4	53
TETA	62.9	94.7	142.4	79.5	–	98
Jeffamine D-230	83.2	127.7	186.1	102.9	397.9	71
Lite-2002	63.9	108.9	158.0	94.1	335.1	76
NX-6019	47.1	103.0	146.9	99.8	276.8	53
GX-6004	55.5	96.8	137.2	81.7	291.4	82

The relationship between the curing rate $d\alpha/dt$ and the cure degree α is given in Fig. 4. As the curing reaction progresses, the curing rate increases, reaches maximal values at the degree of curing 0.45–0.55 and then gradually decreases. There are no obvious differences in curing by low-molecular-weight amines and bio-based phenalkamines.

Enthalpy of the cure reaction of the epoxy resin GY-240 by various hardeners was slightly higher compared to that of GY-2600. Curing of the epoxy resins by low-molecular-weight amines TETA and Jeffamine D-230 was accompanied by the highest exothermic effect (ΔH_R about 386–431 J/g). The highest curing rates (more than 0.2 min^{-1}) were characteristic of the epoxy resins cured by low-molecular-weight amines EDA and TETA. Curing by these hardeners started at 63–73°C, and the cure interval was relatively narrow and ranged 60–80°C. Surprisingly, curing of the epoxy resins by polyetheramine Jeffamine D-230 proceeded at a significantly higher temperature. The curing rate of this system was lower (about 0.175 min^{-1}), irrespective of the epoxy resin used, and the full cure was reached at much higher temperature (at about 190°C).

The enthalpy of curing of the epoxy resins by phenalkamines Lite-2002, GX-6004 or NX-6019 was lower (ΔH_R 277–364 J/g). In these cases, the cure process started earlier (at about 47–64°C), and the cure interval was broader (about 80–100°C). The lowest curing rates were characteristic of the epoxy resins mixed with phenalkamines NX-6019 and Lite-2002, 0.15 min^{-1} and 0.175 min^{-1}, respectively (Fig. 3).

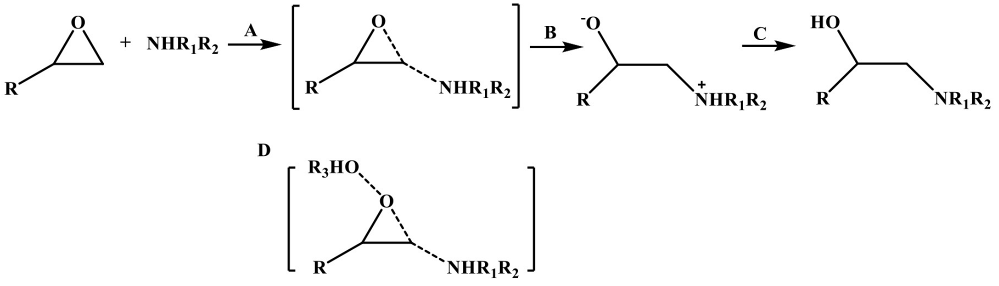

Scheme 3. The general mechanism presenting the autocatalytic nature of curing epoxy resins by amines: A, formation of an intermediate complex; B, ring-opening; C, proton transfer; D, the autocatalytic role of OH groups

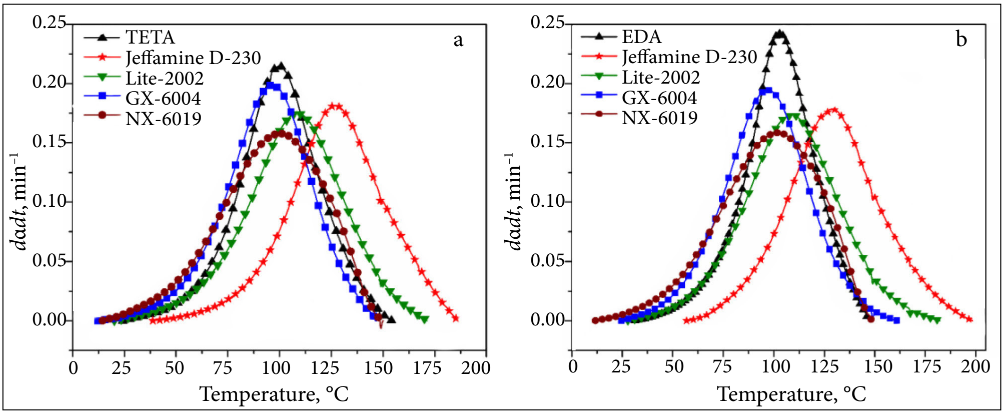

Fig. 3. The dependence of the curing reaction rate $d\alpha/dt$ on temperature under DSC curing of epoxy resins GY-240 (a) and GY-2600 (b) by different amines

Curing by the phenalkamine GX-6004 proceeded a little bit faster ($d\alpha/dt$ almost 0.2 min^{-1}) giving the lowest peak curing temperature (T_p 96.8°C). Thus, it seems that GX-6004 is the most active phenalkamine among all investigated. This phenomenon can be attributed to highly reactive 2,2,4-trimethylhexane-1,6-diamine (TMD) [26] present in the composition of this phenalkamine.

The glass transition temperature (T_g) of the cured epoxy resins is associated with the crosslinking density of the system (Fig. 5). T_g of the cured epoxy resins varied from 50 to 98°C and was dependent on the type of hardener (Table 2). The effect of the type of the epoxy resin (GY-240 or GY-2600) on T_g was much less. The highest T_g (98°C) was characteristic of the epoxy resin GY-2600 cured by TETA. Likely, a tightly crosslinked network was formed in this case due to a high functionality of TETA and short distances between active centers. Lower values of T_g were characteristic of the epoxy resins cured by EDA and Jeffamine D-230. The crosslinking density in the cured epoxy resins is expected to be lower in these cases due to a lower functionality of these hardeners. Lower T_g of the epoxy resins cured by phenalkamines NX-6019 and Lite-2002 (50–76°C) could be attributed to the long alkyl chains present

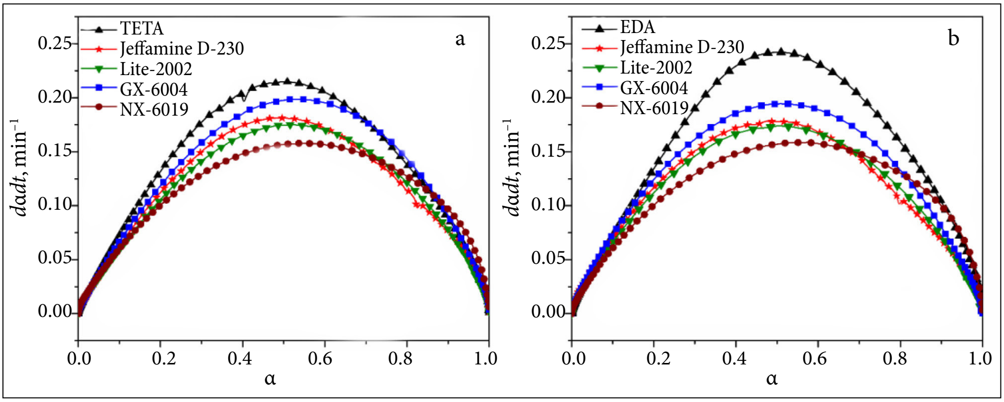

Fig. 4. The relationship between the curing rate $d\alpha/dt$ and the cure degree α under DSC curing of epoxy resins GY-240 (a) and GY-2600 (b) by different amines

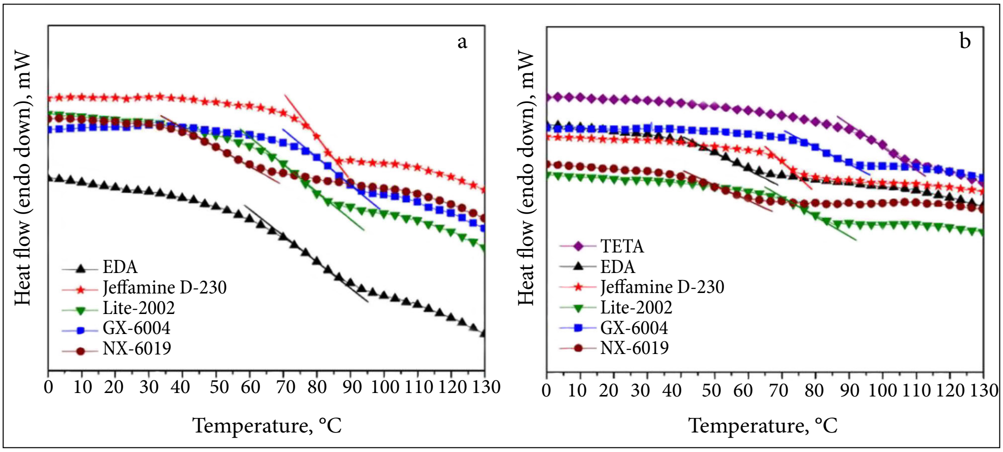

Fig. 5. DSC curves of the epoxy resins GY-240 (a) and GY-2600 (b) cured using different amines (second heating)

in the phenalkamines, which increase the flexibility and chain mobility in the cured system. Slightly higher T_g (82–85°C) was characteristic of the epoxy resins cured by phenalkamine GX-6004. This correlates well with a higher reactivity of this hardener demonstrated by DSC studies.

The curing of epoxy resins by amine hardeners results in a consistent increase in the viscosity of the system. The rate of viscosity changes could be an indicator of the activity of reacting components during the initial stage of curing. Changes in the viscosity of the curing epoxy resins at room temperature during 1–2 h after mixing were evaluated by a rotational rheometer. The *pot-life* of the curing systems was considered to be a quantitative parameter reflecting the rate of the cure process (Table 3). The curves presenting changes in the viscosity of the epoxy resins GY-240 and GY-2600 mixed with various amines show a similar trend (Fig. 6). The initial viscosity of the epoxy resins mixed with low-molecular-weight amines EDA and TETA, and phenalkamine Lite-2002 doubles in approx. 25–35 min. The *pot-life* of the epoxy resins mixed with Jeffamine D-230 is more than 120 min. This indicates that the activity of Jeffamine D-230 at room temperature is very low. Nevertheless, this amine could be used as a hardener for epoxy resins at higher temperatures, as it was shown by DSC studies. The shortest *pot-life* (less than 20 min) was characteristic of the systems comprising epoxy resins and phenalkamines NX-6019 and GX-6004. A high reactivity of the phenalkamine GX-6004 in curing epoxy resins was determined also by DSC studies (Fig. 3).

Table 3. **Dynamic viscosity and pot-life of the mixtures of epoxy resins and amine hardeners**

Amine hardener	**Initial viscosity, mPa·s**	***Pot-life*, min**	**Initial viscosity, mPa·s**	***Pot-life*, min**
	Epoxy resin GY-240		**Epoxy resin GY-2600**	
EDA	1050	35.5	1500	30
TETA	1680	26.5	2490	24.5
Jeffamine D-230	530	>120	790	>120
Lite-2002	2320	30	2510	30
NX-6019	3960	12	3900	12.5
GX-6004	6010	15	7000	19

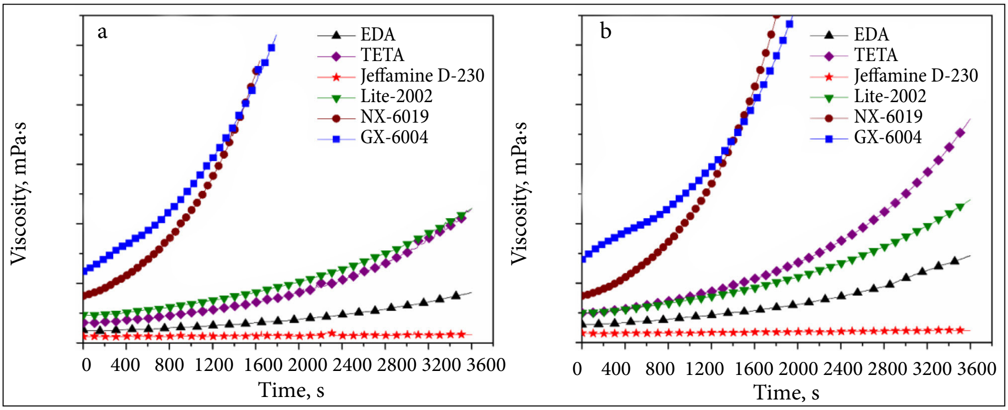

Fig. 6. Changes in the dynamic viscosity of the epoxy resins GY-240 (a) and GY-2600 (b) after mixing with various amine hardeners

A short *pot-life* of the systems containing epoxy resins and phenalkamine NX-6019 correlates well with the lowest initial curing temperature (at about 48°C) (Table 2), which means that the energetic barrier to start curing reactions is low. Thus, the DSC curing of epoxy resins by phenalkamine NX-6019 starts earlier and, regardless a lower curing rate, reaches full curing in approximately the same time as by using the most reactive phenalkamine GX-6004 (Fig. 2).

CONCLUSIONS

The curing of BPA-based epoxy resins Araldite®GY-2600 and Araldite®GY-240 by low-molecular-weight amines EDA, TETA and Jeffamine D-230, and bio-based phenalkamines Cardolite®NX-6019, Cardolite®Lite-2002 and Cardolite®GX-6004 was studied by DSC and rheology measurements. Usually, the DSC curing of epoxy resins by phenalkamines started at lower temperature, the cure temperature interval was broader, and the curing rates were slightly lower compared to those cured by low-molecular-weight amine hardeners. The enthalpy of the curing by phenalkamines was lower, especially in the case of more viscous epoxy resin GY-2600, which is an advantage. The curing of epoxy resins by phenalkamine NX-6019 was characterised by the lowest initial curing temperature and the shortest *pot-life* while curing by the phenalkamine GX-6004 started later but proceeded with the highest rate. The glass transition temperature T_g of the cured epoxy resins depended on the type of the hardener and varied from 50 to 98°C. Slightly lower T_g of the epoxy resins cured by phenalkamines is related to the long alkyl chains present in the composition of the phenalkamines, which increases the flexibility and chain mobility in the cured system. Nevertheless, the use of the most reactive phenalkamine GX-6004 provided a possibility to increase T_g of the cured epoxy resins to 80–85°C.

ACKNOWLEDGEMENTS

We gratefully acknowledge Huntsman Co. and Cardolite Co. for the donation of the materials. The financial support through Project No. S-J05-LVPA-K-03-0139 is gratefully acknowledged.

Received 25 February 2022
Accepted 11 March 2022

References

1. K. Wazarkar, A. S. Sabnis, *Pigment. Resin Technol.*, **47**, 281 (2018).
2. [https://www.cardolite.com/technology/phenalkamines/] and [https://www.cardolite.com/products/epoxy-curing-agents/].
3. M. Kathalewar, A. Sabnis, *Prog. Org. Coat.*, **84**, 79 (2015).
4. P. Jia, F. Song, Q. Li, et al., *J. Renewable Mater.*, **7**, 601 (2019).
5. S. Sami, *Cashew Nutshell Liquid (CNSL) Diols Bring Sustainability in PU* (2019) [https://adhesives.spe-

cialchem.com/tech-library/article/cashew-nut-shell-liquid-diols-bring-sustainability-in-pu].
6. K. Mandip, L. S. Jayakumari, *J. Appl. Polym.* Sci., **133**, 44189 (2016).
7. F. A. Pfaff, *J. Coat. Technol. Res.*, **4**, 151 (2007).
8. J. M. Barton, in: K. Dusek (ed.), *Epoxy Resins and Composites I. Advances in Polymer Science*, Vol. 72, Springer, Berlin, Heidelberg (1985).
9. G. B. Tezel, A. Sarmah, S. Desai, A. Vashisth, M. J. Green, *Carbon*, **175**, 1 (2021).
10. T. Zheng, H. Xi, Z. Wang, et al., *Polym. Test.*, **91**, 106781 (2020).
11. M. Jouyandeh, P. Zarrintaj, M. R. Ganjali, et al., *Prog. Org. Coat.*, **136**, 105245 (2019).
12. J. Yao, H. Zhan, Z. Zou, *Polym. Polym. Compos.*, **25**, 621 (2017).
13. J. Cheng, J. Li, J. Y. Zhang, *eXPRESS Polym. Lett.*, **3**, 501 (2009).
14. W. Zhan, X. Fu, F. Wang, et al., *J. Mater. Sci.*, **55**, 10558 (2020).
15. M. Jouyandeh, M. R. Ganjali, F. Seidi, H. Xiao, M. R. Saeb, *J. Compos. Sci.*, **55**, 1 (2020).
16. K. P. Pang, J. K. Gillham, *J. Appl. Polym. Sci.*, **39**, 909 (1990).
17. A. Bernath, L. Kärger, F. Henning, *Polymers*, **8**, 1 (2016).
18. I. Gorman, M. Henningsen, F. Hettche, et al. (2019) [https://www.pcimag.com/articles/105699-an-epoxy-curing-agent-with-superior-carbamate-stability].
19. S. J. Tucker, B. Fu, S. Kar, S. Heinz, J. S. Wiggins, *Compos. Part A*, **41**, 1441 (2010).
20. S. Jingjing, J. Zhaoxia, W. Junyan, et al., *Constr. Build. Mater.*, **176**, 165 (2018).
21. E. M. Petrie, *Epoxy Adhesive Formulations*, McGraw-Hill (2006).
22. [https://www.epotek.com/docs/en/Related/Tech%20Tip%2026%20Pot%20Life,%20Working%20Life%20and%20Gel%20Time%20of%20Epoxies.pdf].
23. C. Yi, P. Rostron, N. Vahdati, E. Gunister, A. Alfantazi, *Prog. Org. Coat.*, **124**, 165 (2018).
24. D. A. Lakho, D. Yao, K. Cho, M. Ishaq, Y. Wang, *Polym.-Plast. Technol. Eng.*, **56**, 161 (2017).
25. L. Xia, L. Zuo, S. Zha, S. Jiang, R. Guan, D. Lu, *Int. J. Adhes. Adhes.*, **50**, 255 (2014).
26. E. Özeren, *Effects of Epoxy Resin and Hardener Type on Durability and Mechanical Properties of Epoxy Mixes* (2005) [https://polen.itu.edu.tr/bitstream/11527/10263/1/3736.pdf].

Jūratė Jonikaitė-Švėgždienė, Liepa Pastarnokienė, Virginija Juknevičiūtė, Ričardas Makuška

EPOKSIDINIŲ DERVŲ KIETINIMO BIOLOGINĖS KILMĖS FENALKAMINAIS IR MAŽAMOLEKULIAIS AMINAIS TYRIMAS DSK METODU

Santrauka

Dviejų BPA tipo komercinių epoksidinių dervų *Araldite® GY-2600* ir *Araldite® GY-240* kietinimas (tinklinimas), naudojant mažos molekulinės masės aminus EDA, TETA ir *Jeffamine D-230*, taip pat iš kardanolio susintetintus fenalkaminus *Cardolite® NX-6019*, *Cardolite® Lite-2002* bei *Cardolite® GX-6004*, buvo tirtas diferencinės skenuojamosios kalorimetrijos (DSK) ir reologijos metodais. Nustatyti tokie svarbūs parametrai kaip epoksidinių dervų tinklinimo reakcijos entalpija ΔH_R, sutinklinimo laipsnis α ir tinklinimo greitis $d\alpha/dt$, taip pat sutinklintų epoksidinių dervų stiklėjimo temperatūra T_{st}. Naudojant fenalkaminus, tinklinimo reakcijos prasidėjo šiek tiek žemesnėje temperatūroje ir vyko šiek tiek mažesniu greičiu nei kietinimui naudojant mažamolekulius aminus. Tinklinimo fenalkaminais entalpijos pokyčiai buvo mažesni, ypač tinklinant didesnės klampos epoksidinę dervą *GY-2600*. Epoksidinių dervų ir fenalkamino *NX-6019* sistemai buvo būdinga mažiausia pradinė tinklinimo temperatūra ir trumpiausia darbo su kietinama derva trukmė, o tų pačių dervų tinklinimas fenalkaminu *GX-6004* prasidėjo vėliau, tačiau vyko didžiausiu greičiu. Iš kardanolio susintetintų fenalkaminų naudojimas epoksidinėms dervoms kietinti turi privalumų, nes reakcijos pakankamai greitai vyksta net ir kambario temperatūroje, pasiekiamas didelis sutinklinimo laipsnis ir išvengiama kietinamos sistemos perkaitimo. Sutinklintų epoksidinių dervų stiklėjimo temperatūra kito tarp 50 °C ir 98 °C, ir buvo šiek tiek žemesnė, kai tinklinimui buvo naudojami fenalkaminai. Norint stiklėjimo temperatūrą padidinti iki 80–85 °C, kietinimui reikia naudoti reaktingiausią fenalkaminą *GX-6004*.

J. Coat. Technol. Res.
https://doi.org/10.1007/s11998-022-00737-4

The effect of reactive diluents on curing of epoxy resins and properties of the cured epoxy coatings

Liepa Pastarnokienė, Jūratė Jonikaitė-Švėgždienė, Neringa Lapinskaitė, Rūta Kulbokaitė, Alma Bočkuvienė, Tatjana Kochanė, Ričardas Makuška

Received: 21 July 2022 / Revised: 4 November 2022 / Accepted: 8 November 2022
© American Coatings Association 2023

Abstract The effect of monofunctional, difunctional, and trifunctional reactive epoxy diluents (RDs) on curing of epoxy resins by amine hardeners was studied by DSC and oscillatory rheometry. It was determined that curing of the epoxy resins containing difunctional RD was characterized by the lowest activation energy E_a, and the cure reaction was of first order. The shortest gelation time under curing was characteristic for the epoxy resins containing difunctional RDs, while vitrification time of the cured epoxy resins containing difunctional or trifunctional RDs was similar. The use of difunctional RDs as a part of epoxy resins was the most advantageous since they facilitated curing process enabling to reach high degree of curing faster. The effect of RDs of various functionalities on glass transition temperature T_g of the cured epoxy resins and mechanical properties of the epoxy coatings was noticeable but small. Functionality of RDs had no noticeable effect on adhesion and flexibility of the epoxy coatings. Coatings of the cured epoxy resins containing difunctional RD were characterized by slightly higher hardness and increased abrasion resistance. Difunctional reactive epoxy diluents show great potential to be used in epoxy formulations by facilitating curing process and improving mechanical properties of the cured epoxy coatings.

Keywords Reactive diluents, Epoxy resins, Cure kinetics, DSC, Rheometry, Gelation time

Introduction

Epoxy resins are a versatile class of materials containing specific high reactivity and good mechanical, electrical, chemical, thermal, and anticorrosive properties.[1,2] Due to excellent properties, epoxy resins are used in different fields like paints and coatings,[3–5] adhesives,[6–9] industrial tooling, [10–12] aerospace industry,[13–15] electronic materials, [16–18] and biomaterial systems. [19–21] Due to very high reactivity, the epoxy resin prepolymers or polymers that contain epoxide groups in their molecular structures can react with various co-reactants such as high and low molecular weight aliphatic and aromatic amines, acid derivatives, amides, anhydrides, esters, thiols and form crosslinked structures.[22] However, successful application of such polymeric materials in coatings requires a proper balance between the crosslink density controlled by the curing conditions, and the processability characteristics of the resins.[23] Despite great properties, epoxy resins have some limitations such as high viscosity, high price, and tendency to high-density crosslinking, which limit the application of epoxy resins in some industrial and structural fields. These limitations can be eliminated to some extent by replacing a part of these resins with solvents or reactive diluents.[24–26]

Solventborne coatings are a vital part of the coating industry and are widely used in various segments.[1,27–29] Formulations for such coatings contain organic solvents, most of them with a relatively low boiling point, which are referred to as volatile organic compounds

---

Supplementary Information The online version contains supplementary material available at https://doi.org/10.1007/s11998-022-00737-4.

L. Pastarnokienė (✉), J. Jonikaitė-Švėgždienė,
N. Lapinskaitė, R. Kulbokaitė, A. Bočkuvienė,
T. Kochanė, R. Makuška
Department of Polymer Chemistry, Vilnius University,
Naugarduko Str. 24, 03225 Vilnius, Lithuania
e-mail: liepa.pastarnokiene@chgf.stud.vu.lt

L. Pastarnokienė
Litnobiles UAB, A. Kojelavičiaus Str. 17, 11101 Vilnius,
Lithuania

Published online: 08 February 2023

(VOC).[29] VOC are unsafe, harmful to the human body, and cause environmental pollution. Since environmental requirements are increasing, a demand for the coating's formulations with very low VOC and for the solvent-free coating systems is becoming essential. Solvent-free epoxy resin coatings not only solve environmental issues, but also improve some coatings properties like stability and strength.[30,31]

To avoid problems associated with VOC, the use of reactive diluents in solventborne coatings instead of organic solvents was proposed and realized.[32] Reactive diluents (RDs) are substances that contain reactive groups and take part in reactions with a hardener becoming an integral part of a coating during curing.[33] The essential requirements to RDs are low viscosity, compatibility with the base resin, low volatility, nontoxicity, and the ability to participate in the curing process.[26,34,35] The addition, RDs reduce viscosity of resins, allows the addition of more fillers, improves the wetting behavior, and facilitates film-forming process. RDs are categorized as monofunctional and polyfunctional. Most monofunctional diluents are excellent in reducing viscosity but cause a decrease in the crosslink density of the resin, which affects mechanical properties of the coatings. Reaction behavior of polyfunctional RDs are considered to be similar to that of the basic epoxy components, which means that they do not affect the crosslink density.[36–38] Among the RDs, those with epoxy groups are the most important for VOC-free (or very low VOC) epoxy coatings. Usually, they are compatible with the base resin, do not produce VOC during curing, and therefore are more environmentally friendly than nonreactive diluents.[39]

There is a lot of information about the use of RDs in epoxy coatings. The effect of several monofunctional RDs including aliphatic glycidyl ether (AGE), butyl glycidyl ether (BGE), and phenyl glycidyl ether (PGE) on viscosity of epoxy resins and thermal properties of epoxy coatings was studied.[40] Viscosity of the epoxy resins decreased with increasing the amount of RD and depended on molecular weight of RD. Thermal stability of the epoxy coatings depended on chemical structure of the monofunctional RD being the best when using PGE; the presence of PGE increased the value of T_g of the coatings, while the presence of BGE decreased it.

The effect of difunctional reactive diluents 1,4-butandioldiglicidylether (BDGE), cyclohexandiol diglycidyl ether (CHDGE), and diglycidyl aniline (DGA) on epoxy systems was studied by DSC.[41–44] It was determined that the presence of DGA decreased the apparent activation energy of the curing process. Contrarily, addition of BDGE increased the value of E_a and the reaction exponent. Moreover, the addition of BDGE increased the efficacy of the curing process, curing degree, and T_g of the cured coatings.[43] It was shown by DMA that the presence of BDGE in an epoxy resin reduced the storage modulus and glassy state region but had no effect on gelling time.

In order to evaluate the effect of functionality of RDs, rheological behavior and curing of RDs containing epoxy resins as well as mechanical and physical properties of epoxy coatings were investigated.[36] As additives to epoxy resin formulations, three RDs were used: monofunctional C12-14 alkyl glycidyl ether (AGE), difunctional 1,6-hexandiol diglycidyl ether (HDE), and trifunctional trimethyl propane glycidyl ether (TMGE). The highest viscosity was characteristic for the epoxy resin mixture containing trifunctional TMGE, while the viscosity of the mixtures containing AGE or HDE was similar and lower. Addition of RDs improved workability and usually increased pot-life of the epoxy resins; in some cases, addition of the trifunctional TMGE slightly reduced pot-life of the system. The longest pot-life of the epoxy system was obtained using monofunctional AGE. The presence of difunctional HDE and trifunctional TMGE significantly increased compressive and flexural strength of the epoxy coatings. Addition of RDs irrespective of their functionality decreased adhesion of the epoxy coatings.

The same RDs were used in another study[26] evaluating their effect on viscosity of the epoxy resins, and physical and mechanical properties of the epoxy coatings. The fastest curing of the epoxy resin and the shortest film drying time were characteristic for the epoxy mixture containing trifunctional TMGE. The best mechanical properties of the epoxy coatings were obtained using epoxy mixtures containing 12% RDs, irrespective of functionality. The presence of difunctional HDE increased molecular chain flexibility and impact strength of the coatings, while the presence of TMGE increased brittleness and decreased impact resistance of the coatings.

The published data about the effect of RDs on properties of epoxy resins and epoxy coatings are not numerous and, in some cases, contradictive. The main purpose of the present study was to evaluate the effect of reactive epoxy diluents of different functionality on curing of liquid epoxy resins and properties of the cured epoxy coatings. A further objective was to control viscosity and gelling time of the curing systems, and also hardness and elasticity of the epoxy coatings.

Experimental

Materials

Commercial epoxy resins and amine hardeners typical for anticorrosion epoxy coatings were used in this study. Bisphenol-A/-F and novolac epoxy resins with commercial names Araldite® GY 783 and Araldite® GY 289, respectively, reactive epoxy diluents Araldite® DY-L, Araldite® DY-E, Araldite® DY-D, and Araldite® DY-H as well as components of the amine hardeners Aradur 450, DETA (diethylenetriamine) and Accelerator 960-1 were kindly donated by Huntsman Co. Other amine hardeners LUNACURE PACM-20 and LUNACURE MACM-F were obtained from DKSH. Composition of the mixtures of the epoxy resins (PA) and amine hardeners (PB) is presented in Tables 1 and 2. Structure of the epoxy resins, amine hardeners, and reactive epoxy diluents is presented in Schemes 1, 2, and 3, respectively.

The mixture of epoxy resins was chosen by anticipated properties of the epoxy coatings foreseen for particular applications. Novolac resin Araldite GY 289 was chosen as a nonviscous epoxy resin that has high reactivity and produces high crosslinking density providing coatings with excellent chemical resistance. A certain amount (15% in all cases) of the epoxy resin Araldite GY 783 was added for dilution of the novolac resin and increasing flexibility of the coatings.

Amine hardeners used in this study were based on polyaminoamine adduct (Aradur 450), 4,4′-methylenebis (cyclohexylamine) (LUNACURE PACM-20), 4,4′-methylenebis (2-methylcyclo-hexylamine) (LUNACURE MACM-F) and DETA (diethylenetriamine). Mixture of the hardeners was chosen from the practical point of view seeking to reduce curing time and improve mechanical properties of the coatings. Commercial hardener polyaminoamine Aradur 450, which is oligomeric and moderately reactive, was chosen as the main hardener. Addition of more reactive low molecular weight amines PACM, MACM, and DETA to PB was predetermined by intention to increase the curing rate and crosslinking density and improve hardness and adhesion of the coatings.

Reactive diluents used in this study contained different amounts of epoxy functional groups: Araldite® DY-L—trifunctional RD based on glycerol propoxylated triglycidylether, Araldite® DY-D and Araldite® DY-H—difunctional RDs based on diglycidylether of butanediol and 1,6-hexanediol, respectively, and Araldite® DY-E—monofunctional RD based on monoglycidylether alcohol.

Methods

DSC measurements

A calorimeter DSC8500 (*PerkinElmer)* was used to study curing of epoxy resin mixtures PA1, PA2, and PA4 by amine hardeners PB1 or PB2. PA and PB were preweighed in stoichiometric proportions and mixed just before DSC experiment. Amine hydrogen equivalent weight (AHEW) of amine blends, epoxy equivalent weight (EEW) of epoxy blends, and weight of curing agent per 100 parts of epoxy resin (phr) are calculated using equations (1)–(3). Nonisothermal DSC test was performed under nitrogen atmosphere (rate 40 mL/min). A sealed empty aluminum pan was used as a reference. Samples of 3–5 mg were heated from 0 °C to 200 °C at heating rates 5, 10, 15, and 20 °C/min. The heat flow curves were recorded, and the thermal data were further processed to determine the total reaction heat (ΔH_R), cure degree (α), curing reaction rate ($\mathrm{d}\alpha/\mathrm{d}t$), enthalpy of the reaction (E_a), preexponential factor (A), and the experimental reaction order (n). For determination of the glass transition temperature (T_g) of the fully cured systems, mixed epoxy-amine samples were cured at room temperature for 2 weeks, and then, nonisothermal DSC test was performed heating from 0 to 200 °C at the rate of 10 °C/min.

$$\text{AHEW of Amine Blend} = \frac{\text{Total Weight of Amine Blend}}{\frac{\text{Weight }A}{\text{AHEW}_A} + \frac{\text{Weight }B}{\text{AHEW}_B} + \ldots} \tag{1}$$

$$\text{EEW of Epoxy Resin Blend} = \frac{\text{Total Weight of Epoxy Resin Blend}}{\frac{\text{Weight }A}{\text{EEW}_A} + \frac{\text{Weight }B}{\text{EEW}_B} + \ldots} \tag{2}$$

$$\text{phr} = \frac{\text{AHEW of Amine}}{\text{EEW of Epoxy Resin}} \times 100 \tag{3}$$

Rheological measurements

Rheological properties of the epoxy/amine mixtures during isothermal curing at 50 °C were studied by the oscillatory shear measurements using a rheometer MCR302 (*Anton Paar*). Parallel-plate measuring system with diameter of 25 mm and a gap between measuring plates of 0.5 mm was used to perform the

Table 1: Composition of epoxy resins (PA)

Epoxy system	EEW (g/eq)	PA1 (%) EEW = 183.5	PA2 (%) EEW = 177.5	PA3 (%) EEW = 162.8	PA4 (%) EEW = 167.0
Araldite® GY 783	189	15	15	15	15
Araldite® GY 289	167	75	75	75	75
Araldite® DY-L	606	10	–	–	–
Araldite® DY-E	278	–	10	–	–
Araldite® DY-D	118	–	–	10	–
Araldite® DY-H	143	–	–	–	10

Table 2: Composition of amine hardeners (PB)

Hardener system	PB1 (%); AHEW = 66.2 g/eq	PB2 (%); AHEW = 67.9 g/eq
Aradur 450	52	70
PACM	33	20
MACM	9	–
DETA	6	5
Accelerator 960-1	–	5

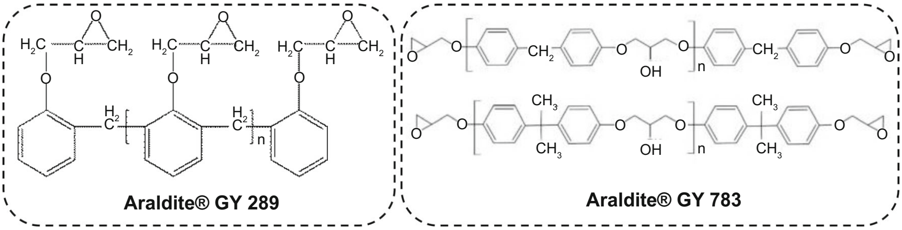

Scheme 1: Structure of the epoxy resins

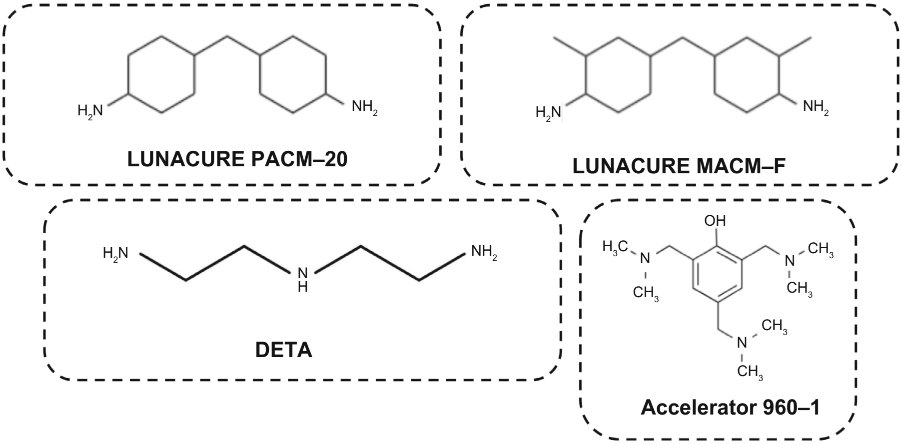

Scheme 2: Structure of the amine hardeners

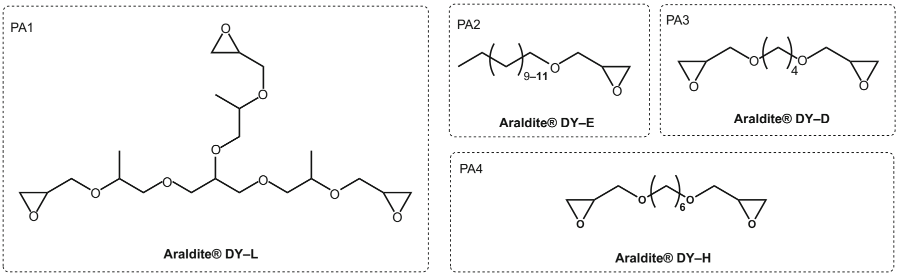

Scheme 3: Structure of the reactive epoxy diluents

Table 3: Metal substrates used for mechanical tests

Substrate type	Steel plates, smooth surface, thickness 1 mm	Aluminum-coated flexible plates	Blasted plates, roughness 50 to 85 μm, thickness 5 mm
Coating method	Automatic, BYK byko-drive XL, thickness 200 μm, speed 3 mm/s	Automatic, BYK byko-drive XL, thickness 200 μm, speed 3 mm/s	Coating by hand with spatula
Mechanical tests	Coating hardness (BYK Pendulum Hardness Tester), direct impact resistance (TQC Impact Tester)	Coating flexibility (BYK Conical Mandrel Tester)	Adhesion, resistance to abrasion (PosiTest AT-A Automatic)

shear oscillation sweep test. All experiments were carried out with amplitude of oscillation 0.1% and an angular frequency of 1 Hz, 2 Hz, and 4 Hz. Sinusoidal stress was used in all experiments, which is the basis for calculating the storage modulus (G'), the loss modulus (G''), and the loss factor tanδ. Components of PA and PB were used as received and carefully mixed at the stoichiometric ratio. After preparing the sample, it was immediately placed in the plate–plate geometry assembly and quickly heated (60 °C/min) to the target curing temperature (50 °C).

The three-interval thixotropy test (3ITT) was performed to determine the thixotropic behavior of the mixed compositions PA + PB using a rheometer MCR302 (*Anton Paar*). Parallel-plate measuring system with diameter of 50 mm with a gap between measuring plates of 1 mm and constant 25 °C temperature was used to perform the 3ITT test. The low–high-low shear test regime of 3ITT test closely resembles brush/roller/spray loading, brushing/rolling/spraying, and subsequent drying of paint, respectively.[45] During the first interval, the sample was subjected to low shear rate (0.1 s^{-1}) for 50 s, and then, for 5 s, a higher (1000 s^{-1}) shear rate is applied and finally back to low shear rate for 200 s. The low–high–low shear rate test of 3ITT resembles the application process of composition. During this process, the internal structure of composition is broken down using high shear rates and the recovery pre- and postapplication of high shear was measured by tracking the change in viscosity. The recovery rate of viscosity at given time after removal of high shear was used to predict the sagging and leveling characteristics of coating systems.[46]

Preparation of the samples for testing of mechanical properties of coatings

PA and PB were mixed at stoichiometric ratio, and three different metal substrates were coated immediately by the curing epoxy resins (Table 3). The steel smooth plates were used for hardness and impact resistance tests, aluminum-coated flexible plates for flexibility tests, and blasted plates of high roughness for adhesion tests. The steel smooth plates and flexible aluminum-coated plates were coated using BYK byko-drive XL and a film applicator with 4 gaps from 50 to 200 μm. The thickness chosen for the coating application was 200 μm, and the applicator was pushed at 3 mm/s speed to assure good coating spread. The blasted plates were coated by hand using spatula, spreading and leveling the coating across the plate surface.

Hardness test

Hardness of the epoxy coatings was evaluated by the König pendulum method according to ASTM D4366 (*BYK* König Pendulum Hardness Tester). The test was performed on a coating with the thickness of 200 μm on a steel surface. The pendulum hardness of the coating surface was measured with respect to the pendulum oscillation time from 6° to 3° at 23 ± 1 °C and 50 ± 2% R.H. The number of oscillations is recorded. Three replicates were made for each treatment group.

Direct impact test

Coatings resistance to cracking or peeling from the metal substrate was evaluated according to ISO 6272-1:2011 using the impact resistance testing device *TQC*. The test was performed on coatings with the thickness 200 μm on a steel surface. The minimum height of fall for 20 mm diameter 1 kg weight was measured under normalized conditions, in order to damage tested coatings. Impact resistance is defined as the impact energy (J) that a coating can withstand without visual damage. Three replicates were made for each treatment group.

Flexibility test

Flexibility of coatings with the thickness of 200 μm on a flexible aluminum plate was evaluated according to ASTM D5221. The coating on the plate was cut into even pieces every 2 cm. Conical mandrel bend tests were performed by bending the coated panels on a conical mandrel tester (*BYK* Conical Mandrel Tester) up to 135° over a period of 3 s. For the test, three coated aluminum specimens from each coating with dimensions of 150 × 100 × 0.5 mm^3 were used. The diameter of the cone varied from 38 to 3 mm. The coating was considered flexible if there was no crack on its surface.

Adhesion test

Determination of the adhesion to a metal surface is performed according to ATSM D4541 using a PosiTest® AT-A (*DeFelsko*). The pull-off test was carried out by gluing a 14-mm diameter dollies to the abrased with sandpaper coating using a two-part epoxy glue. After 24 h, a pull-off test was conducted by applying a tensile stress perpendicular to the surface. The tensile stress was applied until the coating was torn from the metal surface and the magnitude of the stress measured was recorded in N/mm^2 (MPa). On completion of the test, the dolly was visually examined to determine if the failure had occurred at the interface (cohesion) or in the substrate (adhesion). Three replicates were made for each treatment group, and the average of results is reported.

Antisagging test

Antisagging properties were determined according to ASTM D4400 using a BYK Sag Meter. The multiple-notched applicators with varying clearances spanning medium range (3–12 mils) and high range (4–24 mils) were used. For the measurements, approximately 10 mL of the mixed composition PA + PB was transferred onto a flexible smooth metal plate. The multiple-notched applicator was drawn down across the metal plate, which formed a series of evenly spaced stripes. The plate was then quickly hanged vertically and left to dry at room conditions. The coating samples were monitored visually after drying and rated for an antisagging measure. The antisagging index is defined as the thickest thickness (mm) of dry coating stripe remained without sagging.

Abrasion test

The abrasion resistance of the coatings was determined according to ASTM D4060 using Taber Abrasion Tester. In a Taber test, a coating is mounted on a turntable platform that rotates on a vertical axis at a fixed speed. Two standard CS17 Taber abrasive wheels, each applied with 1000 g load, are lowered onto the specimen surface. 1000 cycles of abrasive wear action were produced. The reducing of the coating weight (mg) after abrasion was evaluated. Two replicates were made for each treatment group, and the average of results is reported.

Results and discussion

The effect of reactive diluents on the curing of the epoxy/amine systems

In order to understand the effect of the reactive diluents on the curing of epoxy resins, the cure process was monitored by DSC and oscillatory rheometry. Despite differences in conditions of the above methods (nonisothermal DSC and rheological measurements at 50 °C), they are providing different and complementary information about the cure process allowing evaluating the effect of reactive epoxy diluents.

Differential scanning calorimetry (DSC) is providing quantitative information on overall reaction kinetics[47] including the enthalpy of curing reaction, ΔH_R, cure degree, α, curing reaction rate, $d\alpha/dt$, the activation energy, E_a, Arrhenius preexponential factor, A, and reaction order, n. The nonisothermal method to study kinetics of exothermic reactions is more popular because of its versatility and a broad range of temperatures, in which some changes of materials could be efficiently observed.[48] So far, the curing kinetics of various epoxy systems has been extensively investigated by nonisothermal DSC method.[49–56]

Figure 1 presents nonisothermal DSC curves of epoxy/amine mixtures PA4/PB1 (a) and PA4/PB2 (b) recorded by curing the mixtures at different heating rates. DSC curves of PA1 and PA2 cured by PB1 and PB2 are provided in SI. Obviously, the curing reaction is an exothermic process which is represented by one exothermic peak. At higher heating rates (β), the exothermic peak becomes stronger and shifts to higher temperature. From the curing curves, the characteristic peak temperature (T_p) and the total reaction heat (ΔH_R) were obtained and are listed in Table 4. T_p slightly depends on the type of hardener being lower when using PB2. This difference is attributed to the tertiary amine accelerator present in the hardener system PB2: Accelerated curing proceeds faster reaching the peak temperature T_p earlier. The total reaction heat ΔH_R was calculated by integrating the heat flow over the whole exothermic peak. This was done by Pyris software processing data in the coordinates heat flow (W/g) vs time (s) (see SI). Average values of ΔH_R for PA1, PA2 and PA4 cured by PB1 are 296.4, 312.6 and 319.1 J/g, respectively, and for the same epoxy systems cured by PB2 are 286.5, 318.8 and 318.8 J/g, respectively. The total reaction heat ΔH_R slightly depends on the epoxy system being the highest for PA4 which contains difunctional RD; the lowest values of ΔH_R are characteristic for the epoxy system PA1 which contains trifunctional RD.

Nonisothermal DSC thermographs (Fig. 1) were converted into dependencies of the cure degree (α)

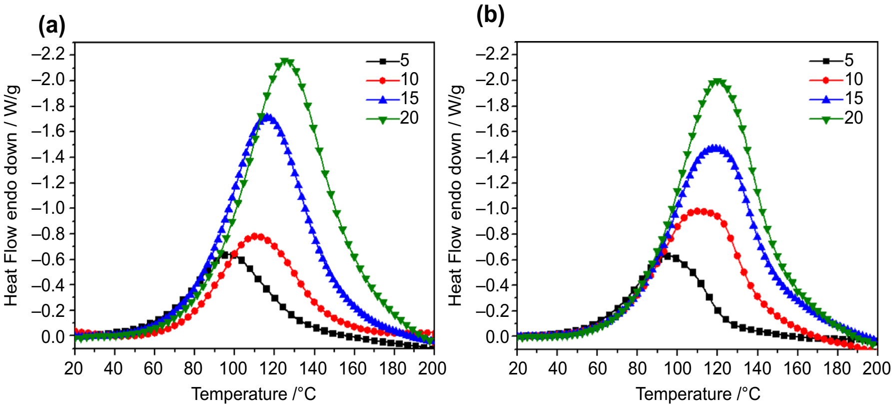

Fig. 1: Nonisothermal DSC curves of epoxy/amine mixtures PA4/PB1 (a) and PA4/PB2 (b) recorded at heating rates 5, 10, 15, and 20 °C/min

Table 4: Characteristic parameters of DSC curing of epoxy resins by different amines

PA system	Heating rate β (K/min)	T_p (K)		R_p (min^{-1})		ΔH_R (J/g)	
		PB1	PB2	PB1	PB2	PB1	PB2
PA1	5	371.4	368.6	0.093	0.119	– 342.6	– 288.1
	10	386.0	383.2	0.195	0.201	– 311.5	– 294.3
	15	391.5	389.7	0.362	0.300	– 258.0	– 286.5
	20	400.1	393.0	0.349	0.400	– 273.4	– 277.0
PA2	5	374.6	373.2	0.102	0.100	– 364.3	– 342.0
	10	387.5	382.4	0.205	0.203	– 258.6	– 331.4
	15	395.0	391.4	0.283	0.279	– 306.9	– 313.2
	20	401.2	396.5	0.369	0.358	– 320.7	– 288.6
PA4	5	369.9	367.9	0.104	0.106	– 360.9	– 336.8
	10	383.2	383.5	0.208	0.189	– 220.5	– 308.3
	15	389.3	391.5	0.297	0.272	– 347.3	– 323.4
	20	398.8	393.9	0.372	0.388	– 347.6	– 306.6

on isoconversional temperatures (Fig. 2). The same dependencies for the systems PA1/PB1, PA1/PB2, PA2/PB1, and PA2/PB2 are provided in SI. The cure degree α was calculated by the ratio $\alpha = \Delta H_t/\Delta H_R$,[55] where ΔH_t represents the heat of the curing reaction at time t, and ΔH_R is the total reaction heat of the curing process. ΔH_R was calculated by integrating the heat flow over the whole exothermic peak for a completely uncured sample. During DSC curing, the cure degree α starts at 0 and at a certain temperature is reaching maximal value equal to 1 which corresponds to fully cured epoxy resin (Fig. 2). At higher heating rates, the dependencies of the cure degree α on temperature are shifted to higher temperatures. This is explained by diffusion control of the process, i.e., deficiency of the reacting species in the reaction site at higher temperatures.[57]

The curing reaction rate ($d\alpha/dt$) is proportional to the measured heat flow (dH/dt)[41] or, the same, to the changes in the cure degree α. $d\alpha/dt$ was calculated by taking the derivatives of the curves α versus time. The relationship between the curing reaction rate ($d\alpha/dt$) and temperature is presented in Fig. 3. The same dependencies for the systems PA1/PB1, PA1/PB2, PA2/PB1, and PA2/PB2 are provided in SI. At about 50 °C, and the curing rate starts to increase and later increases gently reaching maximal values at about 100–130 °C. The maximal values of the DSC curing rate R_p for various epoxy/amine systems are presented in Table 4. Evidently, they strongly depend on the heating rate but are almost unvarying in respect to the epoxy system and the hardener. When most of the functional groups were reacted, the curing rate R_p of the epoxy resin/amine system started gradually de-

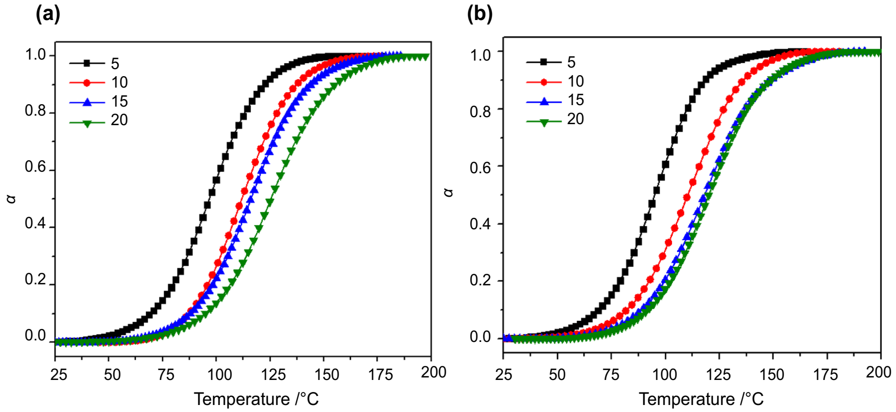

Fig. 2: The dependence of the cure degree α on temperature under DSC curing of epoxy resin PA4 by the hardeners PB1 (a) and PB2 (b) at heating rates 5, 10, 15, and 20 °C/min

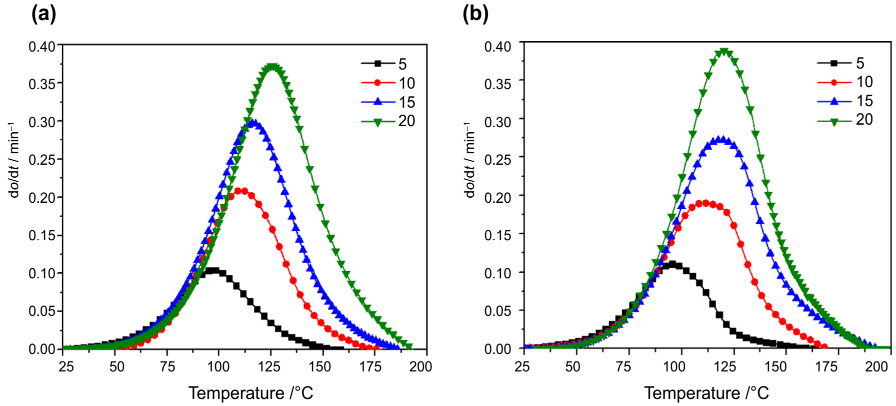

Fig. 3: The dependence of the reaction rate dα/d*t* on temperature under DSC curing of epoxy resin PA4 by the hardeners PB1 (a) and PB2 (b) at heating rates 5, 10, 15, and 20 °C/min

crease and at 150–190 °C approached the values close to 0.

The characteristic peak temperatures T_p listed in Table 4 were used to calculate activation energy E_a of the cure process, Arrhenius preexponential factor A, and the cure reaction order n. These parameters were calculated by the methods of Kissinger,[58] Ozawa[59] and Crane[60] used before for similar curing processes. Basics of these methods and formulas as well as Kissinger, Ozawa, and Crane plots for the studied epoxy/amine systems are presented in SI. Kinetic parameters calculated using Kissinger, Ozawa, and Crane plots are listed in Table 5.

The apparent activation energy E_a for the studied epoxy/amine systems is similar to that of typical epoxy-amine cure reactions (50–70 kJ/mol).[55] E_a calculated by the Ozawa method is higher than that calculated by the Kissinger method, irrespective of the epoxy/amine system. Activation energy E_a for the accelerated curing (cured by PB2) is higher irrespective of the epoxy system. Possibly, higher E_a values for the curing reactions taking place in the presence of the hardener PB2 containing tertiary amines are related to formation of tridimensional molecular network at early stages of the curing and higher viscosity of the system, which impedes further development of the reaction.

Activation energy E_a of curing of the epoxy system PA4 containing difunctional RD is the lowest in the studied set; moreover, its value (about 40 kJ/mol for nonaccelerated curing) is below typical values of E_a for

Table 5: Kinetic parameters for the DSC curing of epoxy/amine systems

PA system	E_a (kJ/mol) (Kissinger)		A (min^{-1}) (Kissinger)		n (Kissinger-Crane)		E_a (kJ/mol) (Ozawa)		n (Ozawa-Crane)	
	PB1	PB2	PB1	PB2	PB1	PB2	PB1	PB2	PB1	PB2
PA1	55.4	59.9	1.7×10^6	7.8×10^7	0.893	0.903	61.7	66.3	0.995	0.999
PA2	49.7	58.6	2.1×10^6	4.7×10^7	0.902	0.909	52.2	64.1	0.947	0.995
PA4	39.9	54.8	1.0×10^5	1.4×10^7	0.902	0.895	44.3	61.2	1.000	0.999

epoxy-amine cure reactions.[55] Low values of E_a for curing the epoxy system containing difunctional RD suggest that such RD facilitates curing process enabling to reach high degree of curing faster.

Activation energy is the energy required for a reaction to occur and determines its rate. The higher the activation energy, the slower the chemical reaction will be. Activation energy for a chemical reaction depends upon nature and environment of reacting groups. Likely, difunctional RD containing flexible alkyl chain and terminal epoxy groups not impeding each other is favorable for the development of the curing reaction. The use of trifunctional RD stimulates formation of tridimensional molecular network at early stages of the curing and higher viscosity of the system, which impedes further development of the reaction. Slightly higher activation energy values of curing reaction of the epoxy system PA2, compared to that of the epoxy system PA4 are, possibly, predetermined by monofunctionality of RD, which partly terminates curing reactions.

Preexponential factor A (Arrhenius factor) is a constant for each chemical reaction that defines the rate due to the frequency of collisions in the correct orientation. Preexponential factor A is larger for the accelerated curing (using the hardener PB2) indicating that the number of collisions is higher in that case (Table 5). Preexponential factor is almost independent on composition of PA (i.e., on type of RD). Reaction order *n* calculated by two different methods is in the range 0.9–1.0, which demonstrates that the cure process is first-order reaction irrespective of the used hardener system.

Complementary information about the cure process was received studying the same epoxy/amine systems by oscillatory rheometry. Rheological analysis of the oscillatory test gave a total curing profile, which provided information about the curing behavior in terms of the measured storage modulus G', the loss modulus G'', and the loss factor $\tan\delta$. Evolution of these parameters during curing of the epoxy system PA4 by amine hardeners PB1 and PB2 is presented in Fig. 4. Similar dependencies for the systems PA1/PB1, PA1/PB2, PA2/PB1, PA2/PB2, PA3/PB1, and PA3/PB2 are provided in SI.

Evolution and trend of the parameters G', G'' and $\tan\delta$ during curing of epoxy resins present important information about the cure process, more specifically, provide gelation and vitrification times. There is no generally accepted criterion for the detection of the gelation and vitrification times. One criterion is that gelation occurs when viscosity increases exponentially to infinity.[61] The problem is that infinite viscosity is very difficult to detect. The most generally accepted criterion for gelation is the crossover point of the shear storage modulus G' and loss modulus G''.[1] For other, more complicated networks, the gel point can be found by detecting loss factor $\tan\delta$ at different frequencies and determining their crossover point during cure.[62–66] Vitrification time is defined as the point at which the molecular weight or crosslink density of the curing polymer exceeds that which is thermodynamically stable as a rubber to a glass, at which point the reaction dramatically slows due to the reduced mobility of the reactants.[67] Thus, vitrification is a reversible change of the viscous liquid state to crosslinked glassy state for a gelled system. Vitrification can be determined from the maximum $\tan\delta$ peak at 1 Hz, the maximum G'' peak at 1 Hz, the onset of frequency dependence in G', and with the end of frequency dependence in G'.[68]

In the present study, gelation time of the curing epoxy systems was determined by crossover of the parameters G' and G'', and crossover of $\tan\delta$ at different frequencies. Vitrification time was determined from the maximum $\tan\delta$ peak at 1 Hz and the maximum G'' peak at 1 Hz. These parameters are presented in Table 6.

Epoxy-amine systems behave like solids at the beginning of the curing process ($G' > G''$) due to entrapped air bubbles during mixing of the epoxy system and a hardener together. After 10–15 min, the loss modulus G'' becomes larger than the storage modulus G' since the system shows liquid-type behavior (Fig. 4). As the reaction proceeds, both G' and G'' increase and at a certain time intersect; the crossover point indicates equilibrium between viscous and elastic behavior, and after this point gelation occurs. Later-on, when curing reaction progresses and elastic behavior dominates, G' becomes larger than G'' and tends to approach its maximum value, whereas G'' reaches a peak and starts to decrease. In this zone, vitrification occurs.

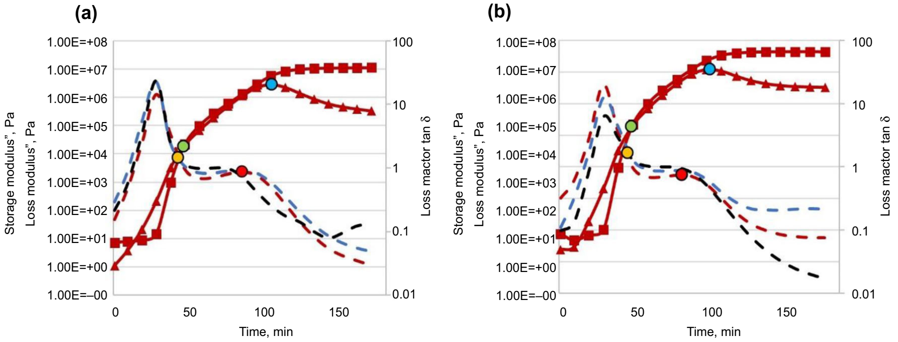

Fig. 4: **Evolution of storage modulus G' (-■-) and loss modulus G'' (-▲-) (angular frequency 1 Hz), and loss factor tanδ (—) (angular frequencies 1 Hz (---); 2 Hz (---); 4 Hz (—)) during curing of the epoxy system PA4 by amine hardeners PB1 (a) and PB2 (b) at 50 °C. Filled circles indicate tanδ crossover (●), crossover of G' and G'' (●), peak of G'' (●), and second peak of tan δ at 1 Hz (●) (Color figure online)**

Table 6: **Gelation and vitrification time of the curing epoxy resins determined by oscillatory rheometry**

Epoxy/amine system	Gelation time (min)		Vitrification time (min)	
	tanδ crossover, 1 Hz, 2 Hz, 4 Hz	G' and G'' crossover, 1 Hz	tanδ peak, 1 Hz	G'' peak, 1 Hz
PA1/PB1	111	132	120	152
PA1/PB2	51	59	88	112
PA2/PB1	85	90	140	173
PA2/PB2	49	59	100	126
PA3/PB1	67	75	110	134
PA3/PB2	45	49	90	111
PA4/PB1	66	76	120	147
PA4/PB2	45	49	83	102

Gelation time and vitrification time determined by tanδ crossover and tanδ peak, respectively, are shorter compared to those determined by G' and G'' crossover, and G'' peak, respectively (Table 6). As it was discussed before,[61–65] more reliable data are considered to be received from the dependencies of tanδ. It is evident from Table 6 that gelation time and vitrification time of the epoxy system under curing by the accelerator-containing hardener PB2 were significantly shorter compared to those received under curing by the accelerator-free hardener PB1. This confirms that curing of epoxy systems in the presence of the accelerator proceeds much faster.

Gelation time is affected by the type of the epoxy system, more specifically, by the used reactive diluent. The shortest gelation time is characteristic for the epoxy systems PA3/PB1(PB2) and PA4/PB1(PB2) containing difunctional RDs (Table 6). Higher reactivity of difunctional RDs in curing reactions could be related to lower epoxy equivalents and low molecular weight of these RDs compared to monofunctional and trifunctional RDs (Table 1). Epoxy systems containing monofunctional (PA2) and trifunctional (PA1) RDs were less reactive. Monofunctional RD has long aliphatic chain of C_{12}–C_{14} and only one epoxy group, which makes it less reactive and impeding crosslinking reactions. Trifunctional RD has the highest molecular weight and branched structure, which could reduce flexibility of the compound and make some reactive groups inaccessible.

Vitrification time of the epoxy systems containing difunctional and trifunctional reactive diluents is very close (Table 6). The presence of monofunctional RD makes vitrification time longer; possibly, this could be related to plasticizing effect of this RD containing long aliphatic chain.

The data got from DSC analysis and rheological measurements on curing of epoxy systems containing various reactive epoxy diluents suggest that the use of difunctional RD facilitates curing process enabling to reach high degree of curing faster. By contrast, trifunctional RD increases activation energy of the process and retards curing.

The effect of reactive diluents on properties of the cured epoxy coatings

The effect of reactive diluents in epoxy resin mixtures, on glass transition of the cured epoxy resins and properties of the cured epoxy coatings were studied. DSC curves of the epoxy resin mixtures containing various RDs cured by two amine hardeners are presented in Fig. 5. DSC curves show endothermic transition at about 60–75 °C. This transition appears like a part of an endothermic peak which is caused by the thermal history of the cured epoxy systems and should be ignored.[69,70] Glass transition temperature T_g of the cured samples determined from the DSC curves is presented in Table 7. T_g of the cured epoxy resins depends on the type of hardener being higher for the systems cured by the accelerator-containing hardener PB2. Apparently, it is related to higher degree of crosslinking taking place in the presence of tertiary amine. T_g of the cured epoxy resins containing difunctional and trifunctional reactive diluents (PA4 and PA1, respectively) is very close. Monofunctional reactive diluent (PA2) had more remarkable effect on the glass transition raising its value by 3–7 °C. This could be attributed to lower viscosity of the epoxy system PA2 (Table 8), which makes it easier for network structure to form and create higher crosslinking during formation of the coatings. Nevertheless, differences in T_g of the cured epoxy resins containing reactive diluents of different functionality are rather small and hardly deserve attention.

Mechanical properties of the naked epoxy coatings (without fillers and various additives) prepared from the epoxy resin mixtures containing RDs and cured by the hardeners with and without accelerator are listed in Table 7. Hardness of the coatings is rather high, about 100 Osc. Slightly higher hardness is characteristic for the coatings containing difunctional reactive diluents (PA3 and PA4) and also cured by the hardener containing an accelerator (PB2). This could be predetermined by rather short aliphatic chains between epoxy groups in PA2, which creates tighter crosslinking of the coatings. Flexibility of the coatings is fair and almost independent of the used reactive diluent. Curing of the coatings by the hardener-containing accelerator (PB2) increases flexibility of the coatings. Adhesion of the coatings is good and does not depend on the used RDs and amine hardeners. Impact resistance of the coatings is rather good and is slightly affected by composition of PA and PB. Slightly higher impact resistance is characteristic for the coatings containing difunctional reactive diluents (PA3 and PA4). Curing of the coatings by the hardener-containing accelerator (PB2) slightly reduces impact resistance.

Table 8 presents properties of anticorrosion epoxy coatings containing not only RDs but also fillers and various additives. Coatings containing fillers and various additives were used to evaluate the effect of reactive diluents on properties of coatings in real formulations. Quartz, glass flakes, and silicon carbide were used as fillers. Quartz is a filler increasing mechanical properties of coatings such as abrasion resistance, hardness and impact resistance and also decreasing coatings cost.[71] The diameter of the quartz particles used in the present compositions was between 20 and 60 μm. Glass flakes are known to improve corrosion resistance as well as decrease water and chemical permeability through coatings by creating barrier.[72] Glass fillers are often used in lining systems and marine coatings that require the highest mechanical properties, resistance to both heat and cold, and great chemical resistance. Silicon carbide particles were chosen to improve abrasion resistance of the coatings. Coatings were pigmented by titanium dioxide that is widely used to increase whiteness and hiding power of coatings. The amount of pigments/fillers and solvents in PA was 30% and 2%, respectively. Commercial defoamers, rheology additives, and leveling agents were used to reduce bubble formation, control viscosity, and improve leveling.

It should be noted that the content of fillers and additives is the same in all compositions. Hardness and

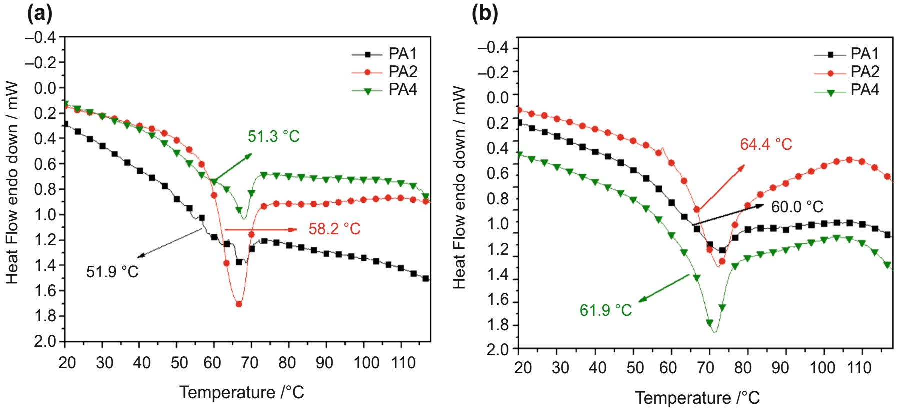

Fig. 5: DSC curves of the epoxy resins PA1, PA2, and PA4 cured by the amine hardeners PB1 (a) and PB2 (b)

Table 7: Properties of the cured epoxy coatings containing reactive diluents of various functionalities

Epoxy resin	PA1		PA2		PA3		PA4	
Hardener	PB1	PB2	PB1	PB2	PB1	PB2	PB1	PB2
T_g (°C)	51.9	60.0	58.2	64.4	–	–	51.3	61.9
Hardness (Osc)	88	103	83	96	101	104	102	103
Flexibility (°)	12.3	23.0	16.2	22.6	9.2	14.6	12.3	15.7
Adhesion (MPa)	20.3	19.8	19.7	22.1	17.3	23.3	23.0	19.8
Impact resistance (J)	4.5	4.5	5.0	4.5	6.0	5.5	6.0	5.0

Table 8: Properties of the cured epoxy coatings containing various reactive diluents, fillers, and additives

Epoxy resin	PA1		PA2		PA3		PA4	
Hardener	PB1	PB2	PB1	PB2	PB1	PB2	PB1	PB2
Viscosity at shear rate 0.1 cm^{-1} (Pa·s)	60.3	40.3	45.1	30.2	40.1	26.7	43.5	27.8
Viscosity at shear rate 1000 cm^{-1} (Pa·s)	2.65	3.47	1.69	2.42	1.89	2.63	2.24	2.65
Hardness (Osc)	94	95	93	97	90	105	97	107
Abrasion resist. (mg)	39	34	52	25	23	20	19	15
Adhesion (MPa)	21.9	21.2	21.4	24.2	19.3	19.8	19.3	20.6
Impact resistance (J)	7	9	8	10	7	8	9	9

adhesion of the filled coatings are comparable to those of unfilled and do not depend on RDs (see SI for illustration). Impact resistance of the filled epoxy coatings is much higher due to special fillers such as glass flakes and quartz but also do not depend on RDs. The filled coatings are characterized by very high abrasion resistance, especially, those containing difunctional RDs (PA3 and PA4) due to tighter crosslinking of the coatings. The use of the amine hardener containing an accelerator (PB2) increases abrasion resistance.

Very important characteristic of the mixed epoxy compositions is dynamic viscosity at low shear rate ($0.1\ s^{-1}$) mimicking storage state and at high shear rate ($1000\ s^{-1}$) mimicking airless spray (Table 8). Low viscosity of the mixed compositions is desirable. Dynamic viscosity of the mixed compositions at high shear rates was in correlation with the viscosity of RDs. The highest viscosity is characteristic for the composition containing trifunctional RD (PA1). Viscosity of the compositions containing difunctional RD is the lowest, especially, at low shear rate. Mixing with the hardener containing an accelerator (PB2) reduces viscosity at low shear rate but evidently increases viscosity of the compositions at high shear rate.

Conclusions

The effect of reactive epoxy diluents (RDs) of various functionalities on curing of epoxy resins is noticeable but small. Curing of the epoxy resin containing trifunctional RDs is characterized by the largest activation energy E_a, while curing of the epoxy resin containing difunctional RDs by the lowest. Cure process of the epoxy resins by amine hardeners is the first-order reaction irrespective of the RDs used. The shortest gelation time under curing is characteristic for the epoxy resins containing difunctional RDs. Vitrification time of the cured epoxy resins containing difunctional and trifunctional RDs is very close, but the presence of monofunctional RDs makes vitrification time longer. The data got from DSC analysis and rheological measurements on curing of epoxy resins containing reactive diluents of various functionalities suggest that the use of difunctional RDs facilitates curing process enabling to reach high degree of curing faster. By contrast, trifunctional RDs increases activation energy of the process and retards curing.

Reactive epoxy diluents had some effect on properties of the cured naked and filled epoxy coatings. Adhesion and flexibility of the coatings did not depend on functionality of RDs. The use of trifunctional RD increased viscosity of the epoxy formulations and had no positive effect on mechanical properties of the coatings. Monofunctional RD helped to decrease viscosity of the epoxy formulations at high shear rate and increase flexibility of the coatings. The most noticeable effect had difunctional RDs decreasing viscosity of the epoxy formulations and increasing hardness and abrasion resistance of the filled coatings.

Difunctional reactive epoxy diluents show great potential to be used in epoxy formulations by facilitating curing process and improving mechanical properties of the cured epoxy coatings.

Acknowledgments We gratefully acknowledge Huntsman Co. for donation of the materials. Financial support through the Project No. S-J05-LVPA-K-03-0139 is gratefully acknowledged.

References

1. Jin, FL, Li, X, Park, SJ, "Synthesis and Application of Epoxy Resins: A Review." *J. Ind. Eng. Chem.*, **29** 1–11 (2015)
2. Hsissou, R, "Review on Epoxy Polymers and Its Composites as a Potential Anticorrosive Coatings for Carbon Steel in 3.5% NaCl Solution: Computational Approaches." *J. Mol. Liq.*, **336** 116307 (2021)
3. Hao, Y, Liu, F, Han, EH, "Protection of Epoxy Coatings Containing Polyaniline Modified Ultra-Short Glass Fibers." *Prog. Org. Coat.*, **76** 571–580 (2013)
4. Katariya, MN, Jana, AK, Parikh, PA, "Corrosion Inhibition Effectiveness of Zeolite ZSM-5 Coating on Mild Steel Against Various Organic Acids and Its Antimicrobial Activity." *J. Ind. Eng. Chem.*, **19** 286–291 (2013)
5. Gergely, A, Bertóti, I, Török, T, Pfeifer, É, Kálmán, E, "Corrosion Protection with Zinc-Rich Epoxy Paint Coatings Embedded with Various Amounts of Highly Dispersed Polypyrrole-Deposited Alumina Monohydrate Particles." *Prog. Org. Coat.*, **76** 17–32 (2013)
6. Nguyen, HV, et al. "Rheological Characterization of a Novel Isotropic Conductive Adhesive—Epoxy Filled with Metal-Coated Polymer Spheres." *Mater. Des.*, **46** 784–793 (2013)
7. Park, CH, Lee, SW, Park, JW, Kim, HJ, "Preparation and Characterization of Dual Curable Adhesives Containing Epoxy and Acrylate Functionalities." *React. Funct. Polym.*, **73** 641–646 (2013)
8. Liu, Y, Yang, G, Xiao, HM, Feng, QP, Fu, SY, "Mechanical Properties of Cryogenic Epoxy Adhesives: Effects of Mixed Curing Agent Content." *Int. J. Adhes. Adhes.*, **41** 113–118 (2013)
9. Kaboorani, A, Riedl, B, "Nano-aluminum Oxide as a Reinforcing Material for Thermoplastic Adhesives." *J. Ind. Eng. Chem.*, **18** 1076–1081 (2012)
10. Jin, H, et al. "Fracture Behavior of a Self-healing, Toughened Epoxy Adhesive." *Int. J. Adhes. Adhes.*, **44** 157–165 (2013)
11. Shamsuddoha, M, Islam, MM, Aravinthan, T, Manalo, A, Lau, KT, "Characterisation of Mechanical and Thermal Properties of Epoxy Grouts for Composite Repair of Steel Pipelines." *Mater. Des.*, **52** 315–327 (2013)
12. Ahmed, K, Nizami, SS, Raza, NZ, "Characteristics of Natural Rubber Hybrid Composites Based on Marble Sludge/Carbon Black and Marble Sludge/Rice Husk Derived Silica." *J. Ind. Eng. Chem.*, **19** 1169–1176 (2013)
13. Quang Dao, D, et al. "Determination of Characteristic Parameters for the Thermal Decomposition of Epoxy Resin/Carbon Fibre Composites in Cone Calorimeter." *Int. J. Hydrog. Energy*, **38** 8167–8178 (2013)
14. Ayad, MM, Abu El-Nasr, A, Stejskal, J, "Kinetics and Isotherm Studies of Methylene Blue Adsorption onto Polyaniline Nanotubes Base/Silica Composite." *J. Ind. Eng. Chem.*, **18** 1964–1969 (2012)
15. Azeez, AA, Rhee, KY, Park, SJ, Hui, D, "Epoxy Clay Nanocomposites - Processing, Properties and Applications: A Review." *Compos. Part B Eng.*, **45** 308–320 (2013)
16. Chand, N, Nigrawal, A, "Development and Electrical Conductivity Behavior of Copper-powder-filled-epoxy Graded Composites." *J. Appl. Polym. Sci.*, **109** 2384–2387 (2008)
17. Kandare, E, Kandola, BK, Myler, P, "Evaluating the Influence of Varied Fire-retardant Surface Coatings on Post-heat Flexural Properties of Glass/Epoxy Composites." *Fire Saf. J.*, **58** 112–120 (2013)
18. Suh, SW, Kim, JJ, Kim, SH, Park, BK, "Effect of PI Film Surface on Printing of Pd(II) Catalytic Ink for Electroless Copper Plating in the Printed Electronics." *J. Ind. Eng. Chem.*, **18** 290–294 (2012)
19. Teh, PL, et al. "Thermal and Mechanical Properties of Particulate Fillers Filled Epoxy Composites for Electronic Packaging Application." *Polym. Adv. Technol.*, **19** 308–315 (2008)
20. Di Prima, MA, et al. "Cyclic Compression Behavior of Epoxy Shape Memory Polymer Foam." *Mech. Mater.*, **42** 405–416 (2010)
21. You, D, et al. "Microwave-assisted Functionalization of Polyurethane Surface for Improving Blood Compatibility." *J. Ind. Eng. Chem.*, **19** 1587–1592 (2013)
22. Zhang, HH, et al. "Functionalization of Nanodiamond with Epoxy Monomer." *Chin. Chem. Lett.*, **22** 485–488 (2011)
23. Verma, C, et al. "Epoxy Resins as Anticorrosive Polymeric Materials: A Review." *React. Funct. Polym.*, **156** 104741 (2020)
24. Berdasco, NAM, Waechter, JM, "Epoxy Compounds: Aromatic Diglycidyl Ethers, Polyglycidyl Ethers, Glycidyl Esters, and Miscellaneous Epoxy Compounds." In: *Patty's Toxicology*, pp. 491–528. Wiley. https://doi.org/10.1002/0471435139.tox083.pub2 (2012)
25. Aras, Ö, Kaya, Y, "Effect of Reactive and Non-Reactive Diluent on Mechanical Properties of Epoxy Resin." *Bilecik Şeyh Edebali Üniversitesi Fen Bilim. Derg.*, **8** *167–172 (2021)*
26. Li, Y, Li, B, Chen, W, "A Study on the Reactive Diluent for the Solvent-Free Epoxy Anticorrosive Coating." *J. Chem. Pharm. Res.*, **6** 2466–2469 (2014)
27. Pradhan, S, Pandey, P, Mohanty, S, Nayak, SK, "Insight on the Chemistry of Epoxy and Its Curing for Coating Applications: A Detailed Investigation and Future Perspectives." *Polym. Plast. Technol. Eng.*, **55** 862–877 (2016)
28. Cui, C, et al. "Preparation and Research of Solvent-Free Epoxy Coating for Drinking Water Tank." *IOP Conf. Ser. Mater. Sci. Eng.*, https://doi.org/10.1088/1757-899X/782/2/022064 (2020)
29. Võ, UUT, Morris, MP, "Nonvolatile, Semivolatile, or Volatile: Redefining Volatile for Volatile Organic Compounds." *J. Air Waste Manag. Assoc.*, **64** 661–669 (2014)
30. David, E, Niculescu, VC, "Volatile Organic Compounds (VOCs) as Environmental Pollutants: Occurrence and Mitigation Using Nanomaterials." *Int. J. Environ. Res. Public Health*, **18** 13147 (2021)
31. Nguyen Thuy, D, To Thi Xuan, H, Nicolay, A, Paint, Y, Olivier, MG, "Corrosion Protection of Carbon Steel by Solvent Free Epoxy Coating Containing Hydrotalcites Intercalated with Different Organic Corrosion Inhibitors." *Prog. Org. Coat.*, **101** 331–341 (2016)
32. Jagtap, AR, More, A, "Developments in Reactive Diluents: A Review." *Polym. Bull.*, **79** 5667–5708 (2021)
33. Chen, ZK, et al. "Simultaneously Increasing Cryogenic Strength, Ductility and Impact Resistance of Epoxy Resins Modified by n-Butyl Glycidyl Ether." *Polymer*, **50** 1316–1323 (2009)
34. Sinha, A, Islam Khan, N, Das, S, Zhang, J, Halder, S, "Effect of Reactive and Non-reactive Diluents on Thermal and

Mechanical Properties of Epoxy Resin.” *High Perform. Polym.*, **8** 167–172 (2018)

35. Zabel, KH, et al. “Design and Incorporation of Reactive Diluents for Air-Drying High Solids Alkyd Paints.” *Prog. Org. Coat.*, **35** 255–264 (1999)
36. Ozeren Ozgul, E, Ozkul, MH, “Effects of Epoxy, Hardener, and Diluent Types on the Workability of Epoxy Mixtures.” *Constr. Build. Mater.*, **187** 360–370 (2018)
37. Yurugi, K, Fukada, A, Matsukawa, K, “Reactive Diluent and Curable Resin Composition.” (2004)
38. Bakar, M, Szymanska, J, Rudecka, J, Fitas, J, “Effect of Reactive Diluents and Kaolin on the Mechanical Properties of Epoxy Resin.” *Polym. Polym. Compos.*, **18** 503–510 (2010)
39. Licari, JJ, Swanson, DW, “Chemistry, Formulation, and Properties of Adhesives.” In: Andrews, W (ed.) *Adhesives Technology for Electronic Applications*, pp. 75–141. Elsevier. https://doi.org/10.1016/b978-1-4377-7889-2.10003-8 (2011)
40. Hong, IK, Yoon, YS, Lee, SB, “Selection of Thinner for Epoxy Type Resins for Neon Transformer Housing.” *J. Ind. Eng. Chem.*, **18** 1997–2003 (2012)
41. Lakho, DA, Yao, D, Cho, K, Ishaq, M, Wang, Y, “Study of the Curing Kinetics Toward Development of Fast-Curing Epoxy Resins.” *Polym. Plast. Technol. Eng.*, **56** 161–170 (2017)
42. Núñez-Regueira, L, Villanueva, M, Fraga-Rivas, I, “Effect of a Reactive Diluent on the Curing and Dynamomechanical Properties of an Epoxy-Diamine System.” *J. Therm. Anal. Calorim.*, **86** 463–468 (2006)
43. Li, C, Liu, MH, Liu, ZY, Qing, ML, Wang, G, “DSC and Curing Kinetics of Epoxy Resin Using Cyclohexanediol Diglycidyl Ether as Active Diluents.” *J. Therm. Anal. Calorim.*, **116** 411–416 (2014)
44. Montserrat, S, Málek, J, Colomer, P, “Thermal Degradation Kinetics of Epoxy-Anhydride Resins: I.: Influence of a Silica Filler.” *Thermochim. Acta*, **313** 83–95 (1998)
45. Bhavsar, R, Shreepathi, S, “Evolving Empirical Rheological Limits to Predict Flow-Levelling and Sag Resistance of Waterborne Architectural Paints.” *Prog. Org. Coat.*, **101** 15–23 (2016)
46. Deka, A, Dey, N, “Rheological Studies of Two Component High Build Epoxy and Polyurethane Based High Performance Coatings.” *J. Coat. Technol. Res.*, **10** (3) 305–315 (2013)
47. Barton, JM, “The Application of Differential Scanning Calorimetry (DSC) to the Study of Epoxy Resin Curing Reactions.” In: Dusek, K (ed.) *Advances in Polymer Science*. Springer, Berlin. https://doi.org/10.1007/3-540-15546-5_5 (1985)
48. Zhang, X, “Applications of Kinetic Methods in Thermal Analysis: A Review.” *Eng. Sci.*, **14** 1–13 (2021)
49. Tezel, GB, Sarmah, A, Desai, S, Vashisth, A, Green, MJ, “Kinetics of Carbon Nanotube-Loaded Epoxy Curing: Rheometry, Differential Scanning Calorimetry, and Radio Frequency Heating.” *Carbon*, **175** 1–10 (2021)
50. Ding, J, Peng, W, Luo, T, Yu, H, “Study on the Curing Reaction Kinetics of a Novel Epoxy System.” *RSC Adv.*, **7** 6981–6987 (2017)
51. Jouyandeh, M, Ganjali, MR, Seidi, F, Xiao, H, Saeb, MR, “Nonisothermal Cure Kinetics of Epoxy/Polyvinylpyrrolidone Functionalized Superparamagnetic Nano-Fe_3O_4 Composites: Effect of Zn and Mn Doping.” *J. Compos. Sci.*, **4** 55 (2020)
52. Zhan, W, et al. “Effect of Aromatic Amine Modified Graphene Aerogel on the Curing Kinetics and Interfacial Interaction of Epoxy Composites.” *J. Mater. Sci.*, **55** 10558–10571 (2020)
53. Zheng, T, et al. “The Curing Kinetics and Mechanical Properties of Epoxy Resin Composites Reinforced by PEEK Microparticles.” *Polym. Test.*, **91** 106781 (2020)
54. Jonikaitė-Švėgždienė, J, Pastarnokienė, L, Juknevičiūtė, V, Makuška, R, “Curing of Epoxy Resins by Bio-Based Phenalkamines vs Low-Molecular-Weight Amines: Study by DSC.” *Chemija*, **33** 54–63 (2022)
55. Yi, C, Rostron, P, Vahdati, N, Gunister, E, Alfantazi, A, “Curing Kinetics and Mechanical Properties of Epoxy Based Coatings: The Influence of Added Solvent.” *Prog. Org. Coat.*, **124** 165–174 (2018)
56. Ran, Z, Liu, X, Jiang, X, Wu, Y, Liao, H, “Study on Curing Kinetics of Epoxy-Amine to Reduce Temperature Caused by the Exothermic Reaction.” *Thermochim. Acta*, **692** 178735 (2020)
57. Zhu, L, Wang, Z, Bin Rahman, M, Shen, W, Zhu, C, “The Curing Kinetics of E-Glass Fiber/Epoxy Resin Prepreg and the Bending Properties of its Products.” *Materials*, **14** 4673 (2021)
58. Kissinger, HE, “Variation of Peak Temperature with Heating Rate in Differential Thermal Analysis.” *J. Res. Natl. Bur. Stand.*, **1934** (57) 217–221 (1956)
59. Ozawa, T, “A New Method of Analyzing Thermogravimetric Data.” *Bull. Chem. Soc. Jpn.*, **38** 1881–1886 (1965)
60. Crane, LW, Dynes, PJ, Kaelble, DH, “Analysis of Curing Kinetics in Polymer Composites.” *J. Polym. Sci. Polym. Lett. Ed.*, **11** 533–540 (1973)
61. Russo, S, Sundar, L, Aggarwat, SGA, “Comprehensive Polymer Science-Second Supplement.” *Carbohydr. Polym.*,. https://doi.org/10.1016/s0144-8617(97)87314-6 (1997)
62. Winter, HH, “Can the Gel Point of a Cross-Linking Polymer be Detected by the G′–G″ Crossover?” *Polym. Eng. Sci.*, **27** 1698–1702 (1987)
63. Teil, H, Page, SA, Michaud, V, Månson, JAE, “TTT-cure Diagram of an Anhydride-Cured Epoxy System Including Gelation, Vitrification, Curing Kinetics Model, and Monitoring of the Glass Transition Temperature.” *J. Appl. Polym. Sci.*, **93** 1774–1787 (2004)
64. Lange, J, Altmann, N, Kelly, CT, Halley, PJ, “Understanding Vitrification During Cure of Epoxy Resins Using Dynamic Scanning Calorimetry and Rheological Techniques.” *Polymer (Guildf).*, **41** 5949–5955 (2000)
65. Lucio, B, De La Fuente, JL, “Rheological Cure Characterization of an Advanced Functional Polyurethane.” *Thermochim. Acta*, **596** 6–13 (2014)
66. Russo, C, Fernández-Francos, X, De la Flor, S, “Rheological and Mechanical Characterization of Dual-Curing Thiol-Acrylate-Epoxy Thermosets for Advanced Applications.” *Polymers*, **11** 997 (2019)
67. Dotan, A, “Handbook of Thermoset Plastics.” In: Dodiuk, H, Goodman, SH (eds.) *Handbook of Thermoset Plastics*, 3rd edn. Elsevier, Berlin (2014)
68. Zheng, J, “Studies of PF Resole/Isocyanate Hybrid Adhesives.” *Virginia Polytechnic Institute and State University.* (2002)
69. Thomas, LC, “Interpreting Unexpected Events and Transitions in DSC Results.” *Gov. Inf. Q.*, **27** 423–430 (2010)
70. Gregorova, A, “Application of Differential Scanning Calorimetry to the Characterization of Biopolymers.” In:

Elkordy, AA (ed.) *Applications of Calorimetry in a Wide Context - Differential Scanning Calorimetry, Isothermal Titration Calorimetry and Microcalorimetry*. IntechOpen (2013)

71. Kouloumbi, N, Ghivalos, LG, Pantazopoulou, P, ‘‘Effect of Quartz Filler on Epoxy Coatings Behavior.’’ *J. Mater. Eng. Perform.*, **12** 135–140 (2003)
72. Yan, G, Wang, M, Sun, T, Li, X, Wang, G, Yin, W, ‘‘Anticorrosion Property of Glass Flake Reinforced Chemically Bonded Phosphate Ceramic Coatings.’’ *Materials*, **12** 2082 (2019)

Publisher’s Note Springer Nature remains neutral with regard to jurisdictional claims in published maps and institutional affiliations.

Springer Nature or its licensor (e.g. a society or other partner) holds exclusive rights to this article under a publishing agreement with the author(s) or other rightsholder(s); author self-archiving of the accepted manuscript version of this article is solely governed by the terms of such publishing agreement and applicable law.

Check for updates

Received: 18 October 2023 | Revised: 20 December 2023 | Accepted: 31 December 2023
DOI: 10.1002/app.55216

RESEARCH ARTICLE

Journal of Applied Polymer Science WILEY

Optimization of microencapsulation of polyaspartic acid ester into UV curable epoxy-acrylate resin using Taguchi method of experimental design

L. Pastarnokienė[1,2] | **E. Potapov**[1,2] | **R. Makuška**[1] | **T. Kochanė**[1]

[1]Department of Polymer Chemistry, Vilnius University, Vilnius, Lithuania
[2]R&D Department, JSC Litnobiles, Vilnius, Lithuania

Correspondence
L. Pastarnokienė, Department of Polymer Chemistry, Vilnius University, Naugarduko str. 24, LT-03225 Vilnius, Lithuania.
Email: liepa.pastarnokiene@chgf.stud.vu.lt

Abstract

Due to fast reaction with isocyanates, polyaspartic acid esters (PAAE) can be used for the development of microcapsules for self-healing coatings. Microcapsules with encapsulated PAAE into shell formed by UV-cured commercial epoxy-acrylate resin were produced through oil-in-water emulsion polymerization triggered by UV light. The obtained microcapsules were characterized by FTIR, TGA, optical microscopy, and SEM. Various encapsulation parameters, including core to shell ratio, agitation speed, emulsifier type and concentration, solvent type and its concentration in the oil phase, have been selected at four different levels. Microencapsulation was optimized using Taguchi L16 parameter design approach for determination of desired outcome as larger is better (maximal core content) and nominal is better (microcapsule diameter of 50 μm). It was determined that conditions to prepare microcapsules with the highest core content and the microcapsule size close to 50 μm are rather similar requiring core-to-shell ratio at about 4:1, low agitation speed of 500–1000 rpm, and the use of two polymeric emulsifiers poly(vinyl alcohol) and Gum Arabic at concentration of about 2%. Primary benefits of UV-induced shell formation during microencapsulation of active compounds are remarkably shorter time of the process and possibilities to reach high core content and prepare microcapsules of desirable size.

KEYWORDS

epoxy-acrylate resin, microencapsulation, polyaspartic acid ester, Taguchi method, UV curing

1 | INTRODUCTION

Encapsulation is an effective preservation method to cover an active compound with a protective shell. The protective shell provides stabilization of the active compounds, allowing them to maintain their chemical, physical, and biological properties, as well as release of active compounds or delivery under specified or desired conditions.[1,2] Microcapsules with active agent have been successfully produced using various techniques such as interfacial polymerization, in situ polymerization, coacervation, meltable dispersion, or physical wall formation.[3] Core–shell microcapsules have also been prepared by inverse emulsion (w/o), Pickering stabilization,[4–7] inverse Pickering stabilization,[8–10] and multiple emulsions,[3] and so forth. The correct choice of the wall material is very important since it influences the encapsulation efficiency and stability of the microcapsules. The ideal wall material

J Appl Polym Sci. 2024;141:e55216.
https://doi.org/10.1002/app.55216

© 2024 Wiley Periodicals LLC.

10974628, 2024, 15, Downloaded from https://onlinelibrary.wiley.com/doi/10.1002/app.55216 by Vilnius University, Wiley Online Library on [08/09/2024]. See the Terms and Conditions (https://onlinelibrary.wiley.com/terms-and-conditions) on Wiley Online Library for rules of use; OA articles are governed by the applicable Creative Commons License

should have good rheological properties at high concentrations, chemical non-reactivity with the active core materials, ability to seal and hold the active material within its structure during processing or storage, ability for providing maximum protection to the active material against oxygen, heat, light, and humidity, and other environmental conditions.[11] The advantages and benefits of encapsulation technology have been applied in various areas of applications, such as textile, cosmetics, wastewater treatment, food, pharmaceutical, chemical industry, corrosion inhibition, and so forth.[1]

In the last two decades, extensive studies were directed toward microcapsules providing self-healing capabilities. The encapsulation of reactive components not only prolongs pot-life of active materials, but it also serves for their controlled release as required for practical applications. Self-healing polymeric materials have a great potential to be explored and utilized in many applications such as engineering and surface coating. The prevailing technique often employed involves the integration of microcapsules filled with an active agent into the primary polymer matrix. When cracks develop within the polymer matrix, the microcapsules rupture, enabling the release of the active agent. The active agent then triggers cross-linking processes, enabling the repair and restoration of the cracked areas. Numerous polymer materials are appropriate for creating the shell of the capsules. The most popular shells for microcapsules formation are poly(urea formaldehyde),[12–17] poly(melamine formaldehyde),[18–20] poly(urea melamine formaldehyde),[19,21] polyurethane,[22] polyurea,[23–25] poly(methyl methacrylate),[26–29] and others.

Among others, UV curable materials are promising to be used for encapsulation of active compounds. UV curable shell of microcapsules can be formed from various materials subject to the specific requirements of an application. UV-curable resins or polymers, such as acrylates, epoxies, or urethanes, can be used to form the shell. These materials are designed to undergo polymerization and cross-linking upon exposure to UV light, resulting in a solid and durable shell. A microfluidic device was employed to produce monodisperse water-in-oil-in-water (W/O/W) double-emulsion droplets of controllable size.[12] Under UV irradiation, ethoxylated trimethylolpropane triacrylate prepolymer was cross-linked to form the shell of microcapsules.[30] Tung oil as a self-healing agent was encapsulated into photo-crosslinkable polyacrylic shell.[31] The oil phase contained tung oil, photopolymerization monomer glycidyl methacrylate, and crosslinker 1,6-hexanediol diacrylate. Upon UV irradiation, glycidyl methacrylate and 1,6-hexanediol diacrylate were polymerized along the inner side of the oil droplets, leading to the formation of cross-linked poly(glycidyl methacrylate) shell. The microcapsules exhibited good mechanical properties, allowing them to maintain their integrity even under high shear forces encountered during agitation and further dispersion within water-based epoxy coating.[31] Photopolymerization technology combined with solvent evaporation technique was employed to prepare microcapsules containing linseed oil as an active agent for self-healing purposes.[13] Polyurethane acrylate with four active sites was used for shell formation. The initial emulsion was directly irradiated by UV light for the polymerization of UV-curable prepolymer of polyurethane acrylate, and then the co-solvent was removed to prepare microcapsules. Water-borne epoxy coatings formulated with microcapsules exhibited good self-healing properties, enabling full recovery of scratches with a microcapsule concentration of 15 wt%.[32]

Polyaspartic acid esters (PAAE) are essential for the development of polyaspartic coatings. PAAE is used as co-reactants in the two-component polyurea system, along with an isocyanate component.[14] During NCO-amine reaction, a crosslinked polyurea network is formed, providing the coating unique properties, such as exceptional chemical resistance, abrasion resistance, flexibility, and fast curing. Due to fast reaction with isocyanates, PAAE can be used for the development of microcapsules for self-healing coatings. However, to our knowledge, there are only a couple publications on encapsulation of PAAE. PAAE was encapsulated in poly(melamine-formaldehyde) shell via in situ polymerization method.[15] It was determined, however, that the reaction between the amino groups of PAAE and hydroxyl groups of the melamine-formaldehyde prepolymer occurred during the shell formation leading to reduced size of microcapsules.[16] It was reported that smaller microcapsules were less likely to rupture during the scratch process providing worse self-healing properties to the coating.[15]

The successful microencapsulation process depends on numerous controlled and uncontrolled parameters within the preparation process, which are interconnected in a synergistic manner. The Taguchi orthogonal array is a robust and systematic experimental design technique employed to minimize the influence of uncontrollable factors and determine the optimal combination of process parameters. Taguchi experimental design method utilizes two major tools: orthogonal array for experiment design and analysis of data using signal-to-noise ratio (SNR). Orthogonal arrays are fractional factorial design of experiments where only a fraction of the total possible combinations of variables are considered. The SNR indicates the sensitivity of signal (characteristic of quality) to noise (deviation in factors). The SNR is mainly used as an objective function to determine the most optimum set of operating conditions. There are three main types of SNRs used in the Taguchi method: smaller-the-better (used when the goal is to minimize the response), larger-the-better (used when the goal is to maximize the response) and nominal-the-better (used when the aim is to achieve a target value for the response).[33] Two characteristics such as higher loading and optimal size of microcapsules are the most desirable for optimization of encapsulation processes. Different parameters can be varied in obtaining both characteristics. Usually, such parameters as agitation speed, surfactant type and concentration, reaction time, reaction temperature, and core to shell ratio are chosen as affecting loading and size of microcapsules.[28,34–38]

The purpose of the present study was to demonstrate the possibilities of encapsulation of PAAE into UV-cured epoxy-acrylate shell produced through oil-in-water emulsion polymerization triggered by UV light. Another objective was optimization of the encapsulation process using Taguchi's L16 parameter design approach enabling to find optimal encapsulation parameters ensuring desired outcome as larger is better (maximal core content) and nominal is better (microcapsules size of 50 μm).

2 | EXPERIMENTAL

2.1 | Materials and methods

The UV printing resin Anycubic Colored UV Resin containing epoxy resin and (1-methyl-1,2-ethanediyl)bis[oxy(methyl-2,1-ethanediyl)]diacrylate was purchased from ANYCUBIC 3D Printing. The epoxy-acrylate resin is characterized by low viscosity, short curing time, low shrinkage after curing, and appropriate hardness. Polyaspartic acid ester Desmophen® NH 1220 (PAAE) was purchased from Covestro AG, xylene was supplied by Eurochemicals, ethyl lactate was obtained from TCI, and sodium dodecylbenzenesulfonate (SDBS) was acquired from Eurochemicals. Gum Arabic (GA) was purchased from Thermo Fisher Scientific, while styrene maleic anhydride copolymer (SMA) and polyvinyl alcohol (PVA, deacetylation degree 85%) were obtained from Sigma-Aldrich.

2.2 | Encapsulation of polyaspartic acid ester

Microcapsules containing encapsulates PAAE were obtained by an oil-in-water emulsion polymerization method. General procedures and an example of the used materials are presented below. To make microcapsules EA1, the oil phase was prepared by mixing UV curable epoxy-acrylate resin (1.67 g), PAAE Desmophen NH 1220 (1.67 g), and solvent ethyl lactate (1.67 g). An emulsifier solution was prepared by dissolving and stirring overnight PVA (3 g) and GA (4.5 g) in deionized water (142.5 g) to make PVA 2%/GA 3% solution. The oil phase (5 g) was then added to 150 g of aqueous emulsifier solution (Tables 1 and 2) and stirred at a given speed by Ultra Turrax homogenizer for 10 min. The resulting emulsion was subjected to photo-irradiation with 48 W UV light for 3 min at a distance of 10 cm. The microcapsules obtained were washed with deionized water and separated by freeze-drying.

2.3 | Characterization of microcapsules

FT-IR spectra of the microcapsules were recorded using a Jasco FT-IR 4600 spectrometer in the range 550–4000 cm^{-1}. The amount of PAAE plus solvent as a core of microcapsules was determined by thermogravimetric analysis (TGA) using Hitachi STA200 instrument, with a heating rate of 40°C/min until 150°C, and then 10°C/min until 550°C under a nitrogen gas flow. The average microcapsule size was determined by optical microscope Nikon Eclipse LV100ND. Size, form, and rupture of the microcapsules were further characterized by scanning electron microscope (SEM) Hitachi TM3000.

2.4 | Design of experiment by Taguchi method

It was determined in preliminary studies that there are four key parameters that have the potential impact to the core content and size of microcapsules. These parameters are the core-to-shell ratio, agitation speed, type and amount of emulsifier, and type and amount of solvent for the oil phase. The selected parameters and their levels are presented in Tables 1 and 2. The range of levels was chosen during preliminary experiments.

The Taguchi design methodology was utilized in this study to determine the optimal process parameters through the use of SNR analysis.[24] The larger-the-better criterion (Equation 1) was used to identify the optimal conditions to achieve the maximum core content of the microcapsules, while the nominal-the-best criterion (Equation 2) was used to find conditions favorable for producing microcapsules with the size of 50 μm.

$$\frac{S}{N} = -10 \cdot \log\left(\frac{1}{n}\sum\frac{1}{y^2}\right), \tag{1}$$

Larger-the-better.

10974628, 2024, 15, Downloaded from https://onlinelibrary.wiley.com/doi/10.1002/app.55216 by Vilnius University, Wiley Online Library on [08/09/2024]. See the Terms and Conditions (https://onlinelibrary.wiley.com/terms-and-conditions) on Wiley Online Library for rules of use; OA articles are governed by the applicable Creative Commons License

TABLE 1 Taguchi design parameters and their selected levels for the experiment using ethyl lactate as a solvent.

	Levels			
Parameter, units	**1**	**2**	**3**	**4**
Core-to-shell ratio	2:1	3:1	4:1	5:1
Agitation speed, rpm	500	750	1000	3000
Emulsifier and its concentration, %	PVA 2/GA 3	PVA 1/GA 1.5	SDBS 1	PVA 2/SDBS 1
Ethyl lactate, % of the core content	50	25	10	–

Abbreviations: GA, Gum Arabic; PVA, polyvinyl alcohol; SDBS, sodium dodecylbenzenesulfonate.

TABLE 2 Taguchi design parameters and their selected levels for the experiment using xylene as a solvent.

	Levels			
Parameter, units	**1**	**2**	**3**	**4**
Core-to-shell ratio	2:1	3:1	4:1	5:1
Agitation speed, rpm	500	750	1000	3000
Emulsifier and its concentration, %	PVA 2/GA 3	PVA 1/GA 1.5	SDBS 1	SMA 1
Xylene, % of the core content	–	10	25	50

Abbreviations: GA, Gum Arabic; PVA, polyvinyl alcohol; SDBS, sodium dodecylbenzenesulfonate.

$$\frac{S}{N} = -10 \cdot \log \frac{\bar{y}^2}{s^2}, \tag{2}$$

Nominal-the-best.

3 | RESULTS AND DISCUSSION

3.1 | Encapsulation of PAAE into UV curable resin

Dual-component microcapsules are commonly employed to attain favorable self-healing characteristics. Polyaspartic acid ester (PAAE) was chosen as a healing agent based on its high reactivity with isocyanates and good compatibility with matrix. The resulting product polyurea offers numerous advantages, such as good leveling performance, alkali and acid resistance, water and wear resistance.

Schematic representation of encapsulation process is presented in Scheme 1. The oil phase, containing UV curable resin, PAAE and a solvent, was dispersed in an aqueous phase, containing an emulsifier. After full homogenization and UV curing, crosslinking through the units of (1-methyl-1,2-ethanediyl)bis[oxy(methyl-2,1-ethanediyl)]diacrylate along the inner side of the oil droplets occurred, resulting in formation of microcapsule shells. Encapsulation of PAAE into UV cured shell enabled to prepare mechanically stable microcapsules within extremely short time (3 min).

Successful encapsulation depends on many factors, with emulsification being the primary and most influential factor. The emulsification depends on the selected emulsifier, agitation speed, temperature, and duration of the process. The emulsifier ensures generation of new oil droplets in the dispersed phase and subsequent stabilization of these droplets. Polymeric and charge-containing emulsifiers (stabilizers) were used for stabilization of the emulsions. Mixture of poly(vinyl alcohol) and Gum Arabic (PVA-GA), a copolymer of styrene and maleic anhydride (SMA) or sodium dodecyl benzyl sulphonate (SDBS) were used as stabilizers. Gum Arabic demonstrated good stabilization ability in many studies on microencapsulation.[39,40] Combining two polymeric stabilizers, PVA and GA, gave even better results, increasing efficiency of microencapsulation. SMA was also often used for stabilization of emulsions containing encapsulating materials.[41,42] Hydrolyzed SMA possesses hydrophilic carboxyl groups alongside hydrophobic aryl groups, enabling it to self-assemble into a dual-layered structure. This emulsifier combines both polymeric and ionic stabilization. Low molecular weight charge-containing emulsifier SDBS exhibits good stabilization by the formation of micellar layer on hydrophobic droplets.

It is known,[43] that increasing size of microcapsules usually worsens their mechanical properties but improves healing efficiency. Obviously, there is an optimal microcapsule size that can effectively balance both properties. When the size of microcapsules approaches the thickness of a coating, it leads to compromised mechanical and visual characteristics of the coating. In the present study, obtaining of microcapsules with the size of 50 μm was projected, since microcapsules of such dimensions are appropriate for the coatings with the thickness of 150–200 μm.

Two series of experiments were carried out to synthesize microcapsules differing in size and core content.

10974628, 2024, 15, Downloaded from https://onlinelibrary.wiley.com/doi/10.1002/app.55216 by Vilnius University, Wiley Online Library on [08/09/2024]. See the Terms and Conditions (https://onlinelibrary.wiley.com/terms-and-conditions) on Wiley Online Library for rules of use; OA articles are governed by the applicable Creative Commons License

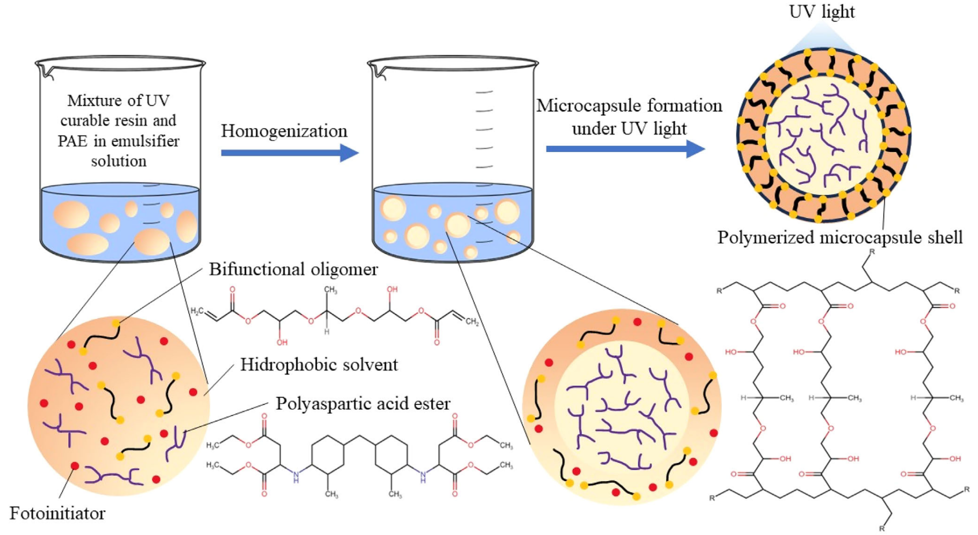

SCHEME 1 Schematic representation of polyaspartic acid esters encapsulation into UV cured epoxy-acrylate shell. [Color figure can be viewed at wileyonlinelibrary.com]

Four key parameters such as core-to-shell ratio, agitation speed, emulsifier type and concentration, and amount of solvents ethyl lactate or xylene were chosen to govern core content and size of microcapsules. In the first series (Table 1), solvent for the oil phase ethyl lactate was used to enhance layer separation during emulsification. Ethyl lactate is a biodegradable solvent with high solvency power, low vapor pressure, low surface tension, and high boiling point. The substitution of solvents like toluene or acetone with ethyl lactate has led to a notably safer working environment.[44] In the second series (Table 2), the solvent for the oil phase ethyl lactate was replaced by xylene, and the emulsifier mixture PVA/SDBS by an emulsifier SMA. This was done trying to evaluate whether xylene contributes to improving layer distribution between UV curable resin and PAAE within the core before shell formation. Data of microencapsulation of PAAE in UV curing epoxy-acrylate resin are presented in Tables 3 and 4.

3.2 | Characterization of the prepared microcapsules

Size of microcapsules was evaluated using optical microscopy (OM) and SEM (Figures 1–4). The microcapsules are round and of perfectly spherical structure, which size distribution depends on experimental conditions. After drying, most of the microcapsules were in powder form. Average size of microcapsules significantly depends on conditions of preparation and varies from 10 to 230 μm (Tables 4 and 5, Figures 1–4). Core-to-shell ratio has low impact on the microcapsule size, and this is in accord with previous observations.[28] Microcapsule size highly depends on agitation speed being large at low agitation and much smaller at high agitation. The smallest microcapsules with the average diameter 10–30 μm were obtained at agitation speed 3000 rpm while the largest with the diameter 100–130 μm at agitation speed 500–750 rpm. Emulsifiers prevent agglomeration of microcapsules, thus high concentration of emulsifiers is preferential for the formation of the microcapsules with smaller diameter. Solvents dilute viscous oil phase, which facilitates formation of smaller microcapsules. Viscosity of xylene is more than three times lower compared to that of ethyl lactate, which is why dilution of the oil phase with xylene gives the smallest microcapsules and with narrower size distribution.

Upon pressing microcapsules between two glass panels, the healing agent PAAE is released and is seen as oil spatters on the glass. It was noticed that the microcapsules obtained using a mixture of emulsifiers PVA 2%/SDBS 1% were mostly tended to agglomeration, were unstable during drying process and releasing lower

10974628, 2024, 15, Downloaded from https://onlinelibrary.wiley.com/doi/10.1002/app.55216 by Vilnius University, Wiley Online Library on [08/09/2024]. See the Terms and Conditions (https://onlinelibrary.wiley.com/terms-and-conditions) on Wiley Online Library for rules of use; OA articles are governed by the applicable Creative Commons License

TABLE 3 Data of microencapsulation of PAAE in UV-curing resin: first series—ethyl lactate as a solvent.

No	Core: Shell	Agitation speed, rpm	Emulsifier and its concentration, %	Ethyl lactate in core, %	Core content, %	Microcapsule size range, μm	Average microcapsule size, μm
EA1	2:1	500	PVA 2/GA 3	50	40.3	30–270	70
EA2	3:1	750	PVA 1/GA 1.5	25	51.2	20–260	130
EA3	4:1	1000	SDBS 1	10	21	5–160	50
EA4	5:1	3000	PVA 2/SDBS 1	-	19	5–100	30
EA5	2:1	750	SDBS 1	-	47.6	10–1110	100
EA6	3:1	1000	PVA 2/SDBS 1	50	10.3	5–110	40
EA7	4:1	3000	PVA 2/GA 3	25	41.7	15–100	50
EA8	5:1	500	PVA 1/GA 1.5	10	71.1	70–400	130
EA9	2:1	1000	PVA 2/GA 3	10	37.5	10–140	70
EA10	3:1	3000	PVA 1/GA 1.5	-	51.6	10–120	70
EA11	4:1	500	SDBS 1	50	43.7	30–280	70
EA12	5:1	750	PVA 2/SDBS 1	25	14.2	5–150	60
EA13	2:1	3000	SDBS 1	25	13.2	5–110	10
EA14	3:1	500	PVA 2/SDBS 1	10	58.1	20–330	100
EA15	4:1	750	PVA 2/GA 3	-	63.7	40–180	80
EA16	5:1	1000	PVA 1/GA 1.5	50	46.4	10–150	70

Abbreviations: GA, Gum Arabic; PAAE, polyaspartic acid esters; PVA, polyvinyl alcohol; SDBS, sodium dodecylbenzenesulfonate.

TABLE 4 Data of microencapsulation of PAAE in UV-curing resin: second series – xylene as a solvent.

No	Core: Shell	Agitation speed, rpm	Emulsifier and its concentration, %	Xylene in core, %	Core content, %	Microcapsule size range, μm	Average microcapsule size, μm
XA1	2:1	500	PVA 2/GA 3	-	54.3	18–500	60
XA2	3:1	750	PVA 1/GA 1.5	10	53.1	11–620	60
XA3	4:1	1000	SDBS 1	25	48.5	21–53	50
XA4	5:1	3000	SMA 1	50	6	9–28	15
XA5	2:1	750	SDBS 1	50	28.5	38–70	20
XA6	3:1	1000	SMA 1	-	57.4	18–280	70
XA7	4:1	3000	PVA 2/GA 3	10	17.3	5–50	30
XA8	5:1	500	PVA 1/GA 1.5	25	68.7	20–150	50
XA9	2:1	1000	PVA 2/GA 3	25	15.6	8–25	20
XA10	3:1	3000	PVA 1/GA 1.5	50	40.8	15–60	25
XA11	4:1	500	SDBS 1	-	63.1	30–390	230
XA12	5:1	750	SMA 1	10	56.8	16–240	50
XA13	2:1	3000	SDBS 1	10	29.8	9–130	22
XA14	3:1	500	SMA 1	25	54.8	23–210	60
XA15	4:1	750	PVA 2/GA 3	50	23.5	5–35	15
XA16	5:1	1000	PVA1/GA 1.5	-	62.7	10–140	40

Abbreviations: GA, Gum Arabic; PAAE, polyaspartic acid esters; PVA, polyvinyl alcohol; SDBS, sodium dodecylbenzenesulfonate.

amount of encapsulated PAAE after mechanical crush. Release of the core material PAAE after mechanical damage of the microcapsules was observed by SEM (Figures 2b and 4b). Under mechanical pressure, the microcapsules containing ethyl lactate as a solvent tend to shrink instead of breaking, which means that

10974628, 2024, 15, Downloaded from https://onlinelibrary.wiley.com/doi/10.1002/app.55216 by Vilnius University, Wiley Online Library on [08/09/2024]. See the Terms and Conditions (https://onlinelibrary.wiley.com/terms-and-conditions) on Wiley Online Library for rules of use; OA articles are governed by the applicable Creative Commons License

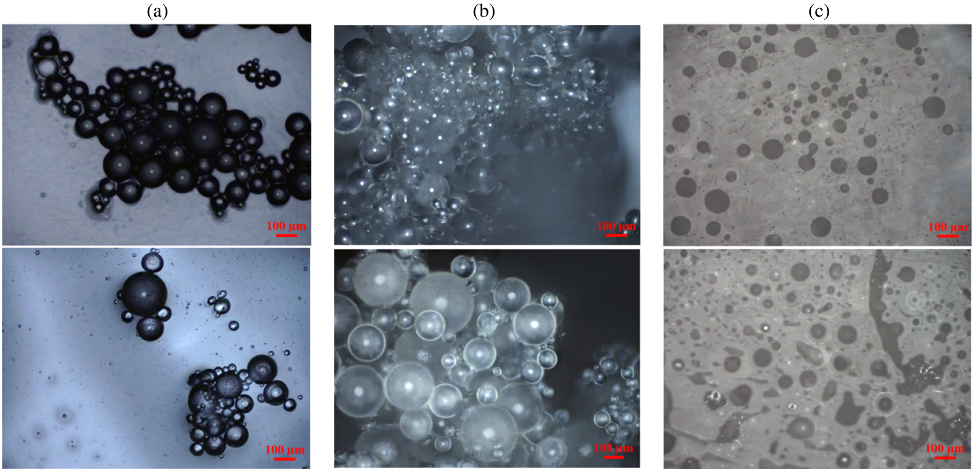

FIGURE 1 OM micrographs of the microcapsules EA15 (upper line) and EA16 (bottom line), obtained in the presence of ethyl lactate as a solvent, in solution (a), dried (b), and ruptured (c). OM, optical microscopy. [Color figure can be viewed at wileyonlinelibrary.com]

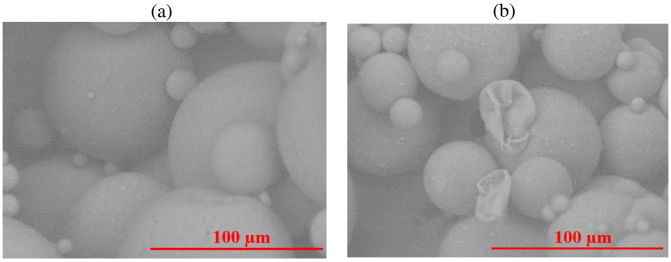

FIGURE 2 Scanning electron microscope micrographs of dried (a) and ruptured (b) microcapsules EA16. [Color figure can be viewed at wileyonlinelibrary.com]

microcapsule shell is too elastic. In contrast, the microcapsules containing xylene as a solvent tend to break. We suppose, this phenomenon is related to volatility of the solvents: methyl lactate remains mainly in the shell while xylene mainly evaporates making shell structure more fragile.

FTIR spectra of the cured epoxy-acrylate resin (microcapsule shell), PAAE Desmophen NH 1220 (microcapsule core) and microcapsules containing encapsulated PAAE were recorded (Figure 5). At several frequencies, the absorption bands of the core and shell materials overlapped due to the similarity of their functional groups. The absorption bands at approximately 2982 and 2870 cm^{-1} belong to asymmetric and symmetric vibrations of C—H bonds of CH_3 or CH_2 groups, respectively. Characteristic absorption band of C═O stretching vibrations at 1730 cm^{-1} is associated with both epoxy-acrylate resin and PAAE.[45] Fortunately, PAAE C═O absorption band is stronger than that of the shell material, which enables to confirm encapsulation by increasing intensity of that band. A broad absorption band associated with hydroxyl groups of epoxy-acrylate is observed at 3580–3200 cm^{-1}. The absorption band at 1520 cm^{-1} corresponds to C═C stretching vibration in aromatic epoxy resin. The absorption band at 1247 cm^{-1} is characteristic for the O═C—O—C ester bond in the polymeric acrylate.[46] The absorption peak at 1060 cm^{-1} demonstrates the presence of an aromatic ether group.[47] Characteristic absorption bands of PAAE secondary amine are at 3340 cm^{-1} (—NH stretching vibrations), 860 cm^{-1} (—NH rocking vibrations), and 1030 cm^{-1} (—C—N stretching vibrations). In the spectra of microcapsules, in addition to the distinctive absorption bands attributed to the shell material, the absorption bands attributed to the core material were also present.

10974628, 2024, 15, Downloaded from https://onlinelibrary.wiley.com/doi/10.1002/app.55216 by Vilnius University, Wiley Online Library on [08/09/2024]. See the Terms and Conditions (https://onlinelibrary.wiley.com/terms-and-conditions) on Wiley Online Library for rules of use; OA articles are governed by the applicable Creative Commons License

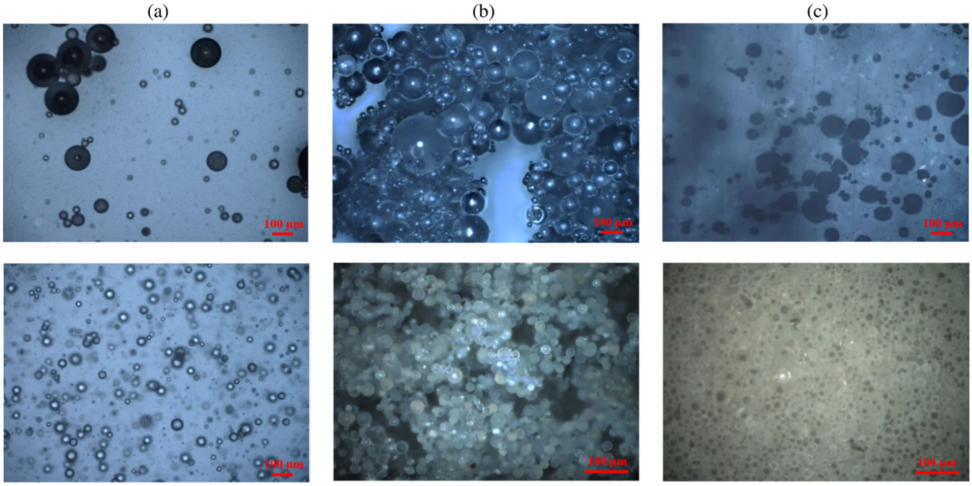

FIGURE 3 OM micrographs of the microcapsules XA12 (upper line) and XA15 (bottom line), obtained in the presence of xylene as a solvent, in solution (a), dried (b), and ruptured (c). OM, optical microscopy. [Color figure can be viewed at wileyonlinelibrary.com]

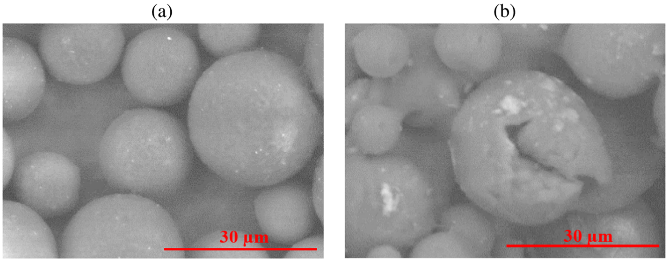

FIGURE 4 Scanning electron microscope micrographs of dried (a) and ruptured (b) microcapsules XA15. [Color figure can be viewed at wileyonlinelibrary.com]

TABLE 5 Optimal conditions for microencapsulation of PAAE in UV curing resin in respect to the highest amount of the core content.

	Core: Shell	Agitation speed, rpm	Emulsifier and its concentration, %	Solvent content
First series EA1-EA16	4:1	500	PVA 2/GA 3	-
Second series XA1-XA16	3:1	500	PVA 1/GA 1.5	-

Abbreviations: GA, Gum Arabic; PAAE, polyaspartic acid esters; PVA, polyvinyl alcohol; SDBS, sodium dodecylbenzenesulfonate.

For determination of the core content in microcapsules, TGA of the core material, shell material, and microcapsules was done (Figure 6). Destruction and evaporation of the core material PAAE starts at approximately 200°C and continues until approximately 300°C. Degradation of the shell material proceeds at much higher temperatures, between 330°C and 480°C. As degradation of both materials occurs at distinct temperatures, determination of the core content in microcapsules is based on relative weight loss at temperatures until 320°C. Unfortunately, there is no possibility to discern between PAAE and solvent present in the core of microcapsules by TGA since these materials lose weight in the same temperature interval. Core content of the microcapsules was affected by many factors and was in the range from 6% to 72% (Tables 3 and 4). Very importantly, combining several parameters affecting microencapsulation process enabled to achieve high core content with the

10974628, 2024, 15, Downloaded from https://onlinelibrary.wiley.com/doi/10.1002/app.55216 by Vilnius University, Wiley Online Library on [08/09/2024]. See the Terms and Conditions (https://onlinelibrary.wiley.com/terms-and-conditions) on Wiley Online Library for rules of use; OA articles are governed by the applicable Creative Commons License

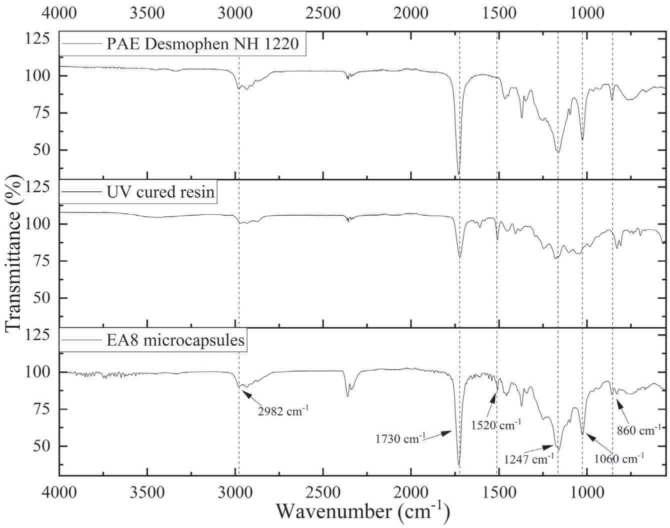

FIGURE 5 FTIR spectra of PAAE Desmophen NH 1220, UV cured resin and EA8 microcapsules.

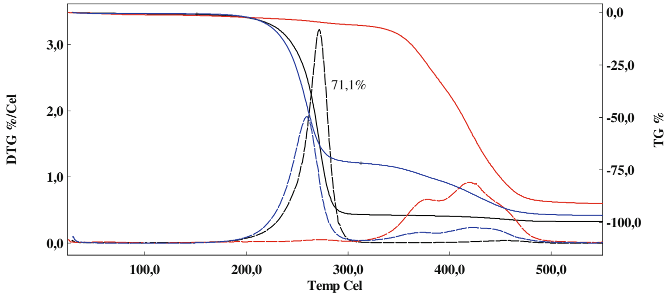

FIGURE 6 TGA and DTG curves of the core material PAAE (black), shell material cured epoxy-acrylate resin (red) and microcapsules XA8 (blue). [Color figure can be viewed at wileyonlinelibrary.com]

amount of encapsulated PAAE in microcapsules up to 60–70%.

3.3 | Optimization of the encapsulationn process

The SNR calculated using the Taguchi criterion larger-the-better as used for identification of the optimal conditions to achieve the maximum core content of the microcapsules, and the Taguchi criterion nominal-the-best to find conditions favorable for producing microcapsules with the average size of 50 μm. The impact of each parameter is presented in Figure 7.

The highest SNR value (and the same, the highest core content) was at the core-to-shell ratio 4:1 when using ethyl lactate as the solvent, and at the core-to-shell ratio 3:1 when using xylene (Figure 7a,b). Microcapsule size was closest to the target value of 50 μm at core-to-shell ratio 4:1 in the presence of ethyl lactate as the solvent, but this ratio was shifted to 5:1 in the presence of xylene (Figure 7c,d).

The core content of microcapsules is the highest at low agitation speed (Figure 7a,b). This phenomenon could be attributed to the formation of larger microcapsules, since faster agitation usually leads to smaller microcapsules.[3] Furthermore, increasing the agitation speed may raise the likelihood of destruction of microcapsules with thinner shells and, the same, higher core content. The microcapsules with an average size of 50 μm (Figure 7c,d) were produced at agitation speed of 1000 rpm, which was found to be optimal for both series.

10974628, 2024, 15, Downloaded from https://onlinelibrary.wiley.com/doi/10.1002/app.55216 by Vilnius University, Wiley Online Library on [08/09/2024]. See the Terms and Conditions (https://onlinelibrary.wiley.com/terms-and-conditions) on Wiley Online Library for rules of use; OA articles are governed by the applicable Creative Commons License

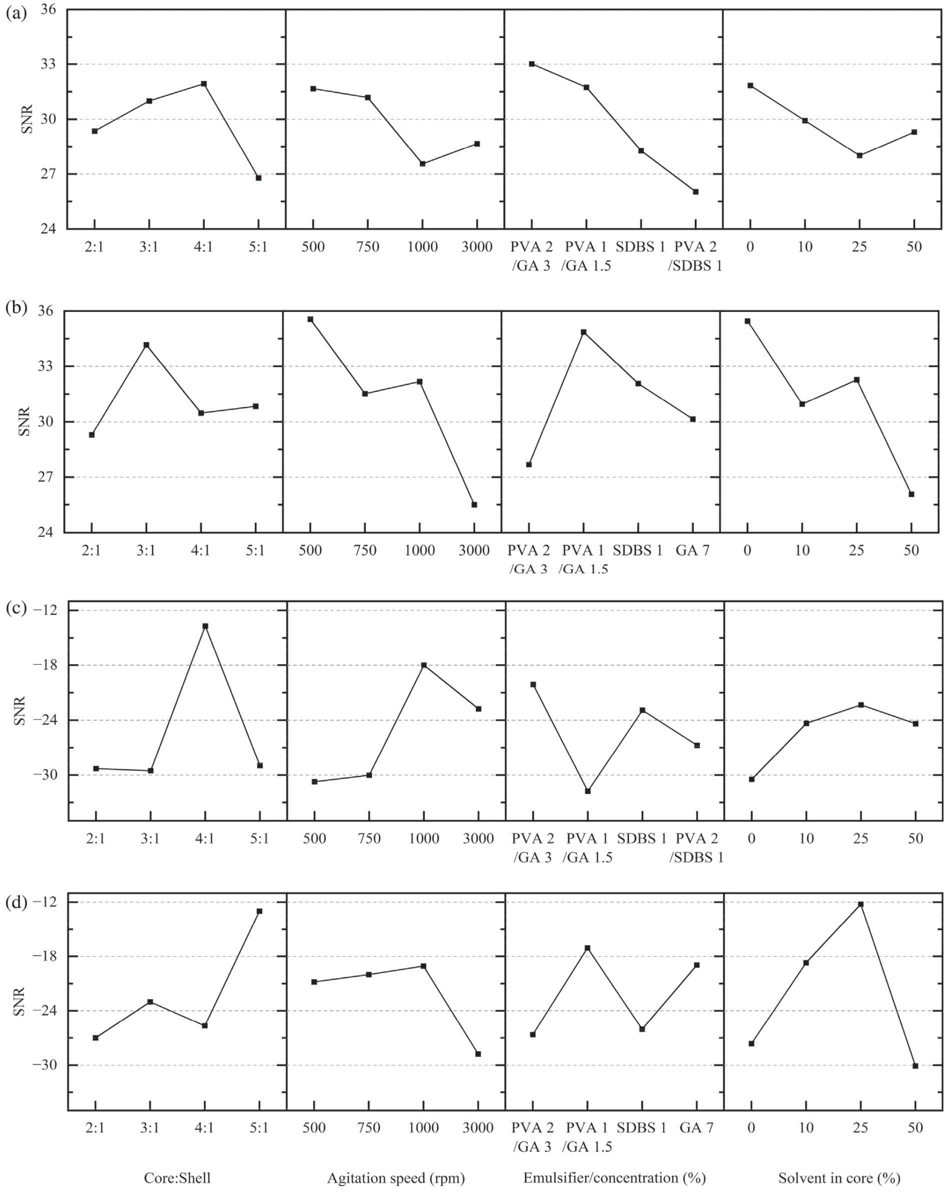

FIGURE 7 SNR plots according to Taguchi method; the dependence of the microcapsule core content (a,b) and microcapsule size (c,d) on microencapsulation parameters core to shell ratio, agitation speed, type and concentration of emulsifier, and ethyl lactate (a,c) or xylene (b,d) content.

10974628, 2024, 15, Downloaded from https://onlinelibrary.wiley.com/doi/10.1002/app.55216 by Vilnius University, Wiley Online Library on [08/09/2024]. See the Terms and Conditions (https://onlinelibrary.wiley.com/terms-and-conditions) on Wiley Online Library for rules of use; OA articles are governed by the applicable Creative Commons License

TABLE 6 Optimal conditions for microencapsulation of PAAE in UV curing resin in respect to the nominal microcapsule size of 50 μm.

	Core: Shell	Agitation speed, rpm	Emulsifier and its concentration, %	Solvent content, %
First series EA1-EA16	4:1	1000	PVA 2/GA 3	Ethyl lactate, 25
Second series XA1-XA16	5:1	1000	PVA 1/GA 1.5	Xylene, 25

Abbreviations: GA, Gum Arabic; PAAE, polyaspartic acid esters; PVA, polyvinyl alcohol; SDBS, sodium dodecylbenzenesulfonate.

In the presence of ethyl lactate as the solvent, the highest core content of the microcapsules was achieved using a mixture of the emulsifiers PVA 2% and GA 3% (Figure 7a). Meanwhile, when ethyl lactate was replaced by xylene, the optimal emulsifier concentration was lower—PVA 1% and GA 1.5%. Lower concentration of the emulsifiers PVA and GA also fits well for the compositions containing ethyl lactate (Figure 7a). Optimal emulsifier for the microcapsules with the size of 50 μm in the presence of ethyl lactate is a mixture of PVA 2% and GA 3% (Figure 7c); reasonably good results were obtained also using SDBS 1% as an emulsifier. When xylene was used as the solvent, the optimal concentration of the emulsifiers was lower PVA 1% and GA 1.5% (Figure 7d).

Addition of the solvents either ethyl lactate or xylene to the oil phase before encapsulation decreases core content of the microcapsules. Thus, the optimal conditions for the microencapsulation of PAAE in respect to core content exclude both solvents. Dilution of PAAE by a certain amount of ethyl lactate or xylene (25%) was favorable in preparing microcapsules with an average size of 50 μm (Figure 7c,d**)**. Optimal conditions for microencapsulation of PAAE in UV curing resin are presented in Tables 5 and 6.

4 | CONCLUSIONS

Microencapsulation of polyaspartic acid ester (PAAE) into UV cured epoxy-acrylate shell was done through oil-in-water emulsion polymerization triggered by UV light. Microencapsulation of PAAE into UV curable epoxy-acrylate resin was optimized using Taguchi L16 parameter design approach trying to find conditions favorable to prepare microcapsules with the highest core content and the microcapsule size of 50 μm. The highest amount of encapsulated PAAE as a core of the microcapsules (up to 70%) is obtained at core-to-shell ratio 4:1 to 3:1, low agitation speed of 500 rpm, using a mixture of the emulsifiers poly(vinyl alcohol) (PVA) 1–2% and Gum Arabic (GA) 1.5–3%, and in the absence of solvents for the oil phase. The optimal microcapsule size of 50 μm is formed at core-to-shell ratio 4:1 to 5:1, agitation speed of 1000 rpm, using a mixture of the emulsifiers PVA 1–2% and GA 1.5–3%, and the solvents for the oil phase ethyl lactate or xylene at concentration 25%. Thus, conditions to prepare microcapsules with the highest core content and the microcapsule size close to 50 μm are rather similar requiring core-to-shell ratio at about 4:1, low agitation speed of 500–1000 rpm, the use of two polymeric emulsifiers PVA and GA at concentration of about 2%. Primary benefits of UV-induced shell formation during microencapsulation of active compounds are remarkably shorter time of the process and possibilities to reach high core content and prepare microcapsules of desirable size.

AUTHOR CONTRIBUTIONS

L. Pastarnokienė: Data curation (lead); formal analysis (equal); methodology (equal); visualization (equal); writing – original draft (equal); writing – review and editing (equal). **E. Potapov:** Data curation (equal); formal analysis (equal); investigation (equal); resources (equal). **R. Makuška:** Project administration (lead); supervision (lead); writing – review and editing (lead). **T. Kochanė:** Formal analysis (equal); methodology (lead); resources (lead); supervision (equal); visualization (equal); writing – original draft (equal); writing – review and editing (equal).

ACKNOWLEDGMENTS

Financial support through project No 13.1.1-LVPA-K-856-01-0104 is gratefully acknowledged.

DATA AVAILABILITY STATEMENT

The data that support the findings of this study are available from the corresponding author upon reasonable request.

ORCID

L. Pastarnokienė https://orcid.org/0000-0003-1994-2121

REFERENCES

[1] S. H. Sonawane, B. A. Bhanvase, M. Sivakumar, *Encapsulation of Active Molecules and Their Delivery System*, Elsevier, Amsterdam, Netherlands **2020**.

[2] D. J. McClements, *Nanoparticle- and Microparticle-Based Delivery Systems: Encapsulation Protection and Release of Active Compounds*, CRC Press, Boca Raton, Florida, US **2014**.

[3] S. N. Gan, N. Shahabudin, in *Microencapsulation* (Ed: F. Salaün), IntechOpen, London, UK **2019**. https://doi.org/10.5772/intechopen.83475

10974628, 2024, 15, Downloaded from https://onlinelibrary.wiley.com/doi/10.1002/app.55216 by Vilnius University, Wiley Online Library on [08/09/2024]. See the Terms and Conditions (https://onlinelibrary.wiley.com/terms-and-conditions) on Wiley Online Library for rules of use; OA articles are governed by the applicable Creative Commons License

[4] A. M. Bago Rodriguez, B. P. Binks, *Curr. Opin. Colloid Interface Sci.* **2019**, *44*, 107.
[5] Y. Ren, G. Zhu, J. Tang, *Colloids Surf., A* **2020**, *584*, 124073.
[6] F. Yu, H. Feng, L. Xiao, Y. Liu, *Prog. Org. Coat.* **2021**, *155*, 106221.
[7] C. Li, J. Tan, J. Gu, L. Qiao, B. Zhang, Q. Zhang, *Compos. Sci. Technol.* **2016**, *123*, 250.
[8] D. A. McIlroy, B. J. Blaiszik, M. M. Caruso, S. R. White, J. S. Moore, N. R. Sottos, *Macromolecules* **2010**, *43*, 1855.
[9] K. Zhang, Q. Wang, H. Meng, M. Wang, W. Wu, J. Chen, *Particuology* **2014**, *14*, 12.
[10] H. Jiang, L. Liu, Y. Li, S. Yin, T. Ngai, *ACS Appl. Mater. Interfaces* **2020**, *12*, 4989.
[11] S. Ray, U. Raychaudhuri, R. Chakraborty, *Food Biosci.* **2016**, *13*, 76.
[12] S. Then, G. S. Neon, *J. Appl. Polym. Sci.* **2011**, *122*, 2557.
[13] Y. Wang, X. Yan, *Coatings* **2022**, *12*, 1394.
[14] J. Kothari, J. O. Iroh, *Polymer* **2023**, *15*, 1668.
[15] M. Li, B. Cao, R. Shang, H. Mei, L. Wang, *J. Appl. Polym. Sci.* **2022**, *139*, e53021.
[16] G. Farzi, A. Davoodi, A. Ahmadi, R. E. Neisiany, M. K. Anwer, M. A. Aboudzadeh, *ACS Omega* **2021**, *6*, 31147.
[17] S. Lang, Q. Zhou, *Prog. Org. Coat.* **2017**, *105*, 99.
[18] M. Leskovšek, J. Kortnik, U. Stankovič Elesini, B. Šumiga, *J. Polym. Eng.* **2022**, *42*, 288.
[19] W. Li, X. Zhu, N. Zhao, Z. Jiang, *Materials* **2016**, *9*, 152.
[20] A. Czeller, T. Czigány, *Mater. Sci. Forum* **2012**, *729*, 205.
[21] S. Sharma, V. Choudhary, *Mater. Res. Express* **2017**, *4*, 075307.
[22] S. Furukawa, K. Hirasawa, Y. Tsuji, K. Suzuki, M. Chiba, *Mater. Trans.* **2023**, *64*, 473.
[23] M. F. Thorne, F. Simkovic, A. G. Slater, *Sci. Rep.* **2019**, *9*, 17983.
[24] P. Canamas, N. Gozzi, J. Du, P. Guichardon, *Chem. Eng. Technol.* **2023**, *46*, 1115.
[25] M. Madelatparvar, M. Hosseini, C. Zhang, *Nanotechnol. Rev.* **2023**, *12*, 20220516.
[26] M. Araújo, S. Chatrabhuti, S. Gurdebeke, N. Alderete, K. Van Tittelboom, J.-M. Raquez, V. Cnudde, S. Van Vlierberghe, N. De Belie, E. Gruyaert, *Cem. Concr. Compos.* **2018**, *89*, 260.
[27] F. Ahangaran, A. Navarchian, M. Hayaty, K. Esmailpour, *Smart Mater. Struct.* **2017**, *25*, 25.
[28] F. Ahangaran, A. H. Navarchian, F. Picchioni, *J. Appl. Polym. Sci.* **2019**, *136*, 48039.
[29] R. Jahadi, H. Beheshti, M. Heidari-Rarani, A. H. Navarchian, *Smart Structures and Systems* **2021**, *27*, 1001.
[30] X. You, B. Wang, S. Xie, L. Li, H. Lu, M. Jin, L. Shui. Microfluidic-Assisted Fabrication of Monodisperse Core–Shell Microcapsules for Pressure-Sensitive Adhesive with Enhanced Performance. *Nanomaterials* **2020**, *10*, 274 .
[31] K. Wu, T. Gui, J. Dong, J. Luo, R. Liu, *Prog. Org. Coat.* **2022**, *162*, 106592.
[32] K. Wu, Z. Wei, Y. Dong, Y. He, H. Liu, G. Sun, J. Luo, *Colloids Surf., A* **2022**, *642*, 128660.
[33] P. Li, P. A. R. Pereira, H. Navas, *Quality Control–Intelligent Manufacturing Robust Design and Charts*, IntechOpen, London, UK **2021**. https://doi.org/10.5772/intechopen.87736
[34] Ç. Özada, M. Ünal, E. Kuzu Şahin, H. Özer, A. R. Motorcu, M. Yazıcı, *Multidiscip. Model. Mater. Struct.* **2022**, *18*, 1049.
[35] A. N. Mustapha, Y. Zhang, Z. Zhang, Y. Ding, Q. Yuan, Y. Li, *J. Mater. Res. Technol.* **2021**, *11*, 667.
[36] F. Zhang, P. Ju, M. Pan, D. Zhang, Y. Huang, G. Li, X. Li, *Corros. Sci.* **2018**, *144*, 74.
[37] N. H. Abdul Halim, C. Haron, J. Ghani, M. Azhar, *J. Mech. Eng.* **2019**, *16*, 1.
[38] V. Nguyen, F. Altarazi, T. Tran, *Math. Probl. Eng.* **2022**, *2022*, 6677586.
[39] G. Xiang, J. Tu, H. Xu, J. Ji, L. Liang, H. Li, H. Chen, J. Tian, X. Guo, *Coatings* **2022**, *12*, 166.
[40] D.-M. Kim, Y.-J. Cho, J.-Y. Choi, B.-J. Kim, S.-W. Jin, C.-M. Chung, *Materials* **2017**, *10*, 1079.
[41] W. Li, Q. Wei, Q. Chen, Z. Jiang, *Cem. Concr. Compos.* **2021**, *124*, 104247.
[42] H. Ghazali, K. Ghazali, R. Yusoff, *IOP Conf. Ser.: Mater. Sci. Eng.* **2022**, *1217*, 12017.
[43] J. Yang, M. W. Keller, J. S. Moore, S. R. White, N. R. Sottos, *Macromolecules* **2008**, *41*, 9650.
[44] M. Doble, A. Kruthiventi, *Green Chemistry and Engineering*. Academic Press, Cambridge **2007**, p. 93. https://doi.org/10.1016/B978-012372532-5/50006-7
[45] G. Mashouf, M. Ebrahimi, S. Bastani, *Pigm. Resin Technol.* **2014**, *43*, 61.
[46] M. Guo, Y. He, J. Wang, X. Zhang, W. Li, *J. Appl. Polym. Sci.* **2019**, *137*, 48478.
[47] G. Yalcin, U. Yildiz, A. Kayan, *Appl. Catal., A* **2012**, *423-424*, 205.

How to cite this article: L. Pastarnokienė, E. Potapov, R. Makuška, T. Kochanė, *J. Appl. Polym. Sci.* **2024**, *141*(15), e55216. https://doi.org/10.1002/app.55216

10974628, 2024, 15, Downloaded from https://onlinelibrary.wiley.com/doi/10.1002/app.55216 by Vilnius University, Wiley Online Library on [08/09/2024]. See the Terms and Conditions (https://onlinelibrary.wiley.com/terms-and-conditions) on Wiley Online Library for rules of use; OA articles are governed by the applicable Creative Commons License

CHEMIJA
2024. Vol. 35. No. 2. P. 54–64

ISSN 0235-7216 eISSN 2424-4538
DOI: https://doi.org/10.6001/chemija.2024.35.2.4

Optimisation of microencapsulation of isophorone diisocyanate into polyurea shell by oil-in-water interfacial polymerisation

Liepa Pastarnokienė*,

Ernest Potapov,

Ričardas Makuška,

Tatjana Kochanė

Department of Polymer Chemistry,
Vilnius University,
24 Naugarduko Street,
03225 Vilnius, Lithuania

In this work, microcapsules containing isophorone diisocyanate (IPDI) encapsulated within a polyurea (PU) shell were synthesised via an oil-in-water emulsion interfacial polymerisation reaction involving tris(4-isocyanato phenyl)thiophosphate (TIPTP) and triethylenetetramine (TETA). Characterisation of the resulting microcapsules was conducted using Fourier transform infrared spectroscopy (FTIR), thermogravimetric analysis (TGA), optical microscopy and scanning electron microscopy (SEM). Various encapsulation parameters such as core-to-shell ratio, agitation speed, emulsifier type and concentration, and reaction time were systematically varied at four different levels. Optimisation of microencapsulation was performed using a Taguchi L16 parameter design approach, aiming to maximise desired outcomes (i.e. maximal core content and yield) while keeping the targeted microcapsule diameter of 50 μm. Under optimal conditions, the IPDI core content within microcapsules was up to 75% and the microcapsule yield was up to 49%.

Keywords: microencapsulation, isophorone diisocyanate, polyurea, interfacial polymerisation, Taguchi method

INTRODUCTION

Coatings are engineered with the primary objective of safeguarding the coated region against environmental and mechanical impairments, corrosion, and consequently extending the lifespan of the coated object significantly. Within the category of coatings, self-healing coatings exhibit a unique capability to autonomously repair mechanical damage or microcracks that may occur during their operational service. Numerous healing systems have undergone extensive testing over the years, with one such system involving the incorporation of microcapsules into the coating formulation [1–5]. These microcapsules contain healing agents such as epoxy resins [6–8], amines [9, 10], isocyanates [11–15] and various kinds of oils [16–18]. If the coating is damaged, either through mechanical force or its inclination to shrink and crack, the microcapsules release healing agents into the affected area. This action forms a new barrier against the environment and seals the damaged area.

IPDI is a cycloaliphatic diisocyanate known for its two reactive isocyanate groups, which display distinct reactivity between primary and secondary NCO groups. This distinctive property imparts a high selectivity in reacting with hydroxyl-bearing compounds. It is commonly used in polyurethane foam formation [19–22] and polyurethane coatings [23–25]. IPDI is a great candidate for self-healing systems because of its low curing speed, low viscosity and good reactivity when mixed with alcohols, polyols, amines or water if catalysed [26–28].

---

* Corresponding author. Email: liepa.pastarnokiene@chgf.stud.vu.lt

The selection of shell materials holds significant importance as it can exert influence on both the core composition of the microcapsule and its integration into the coating system. Isocyanates can be encapsulated into several different shells like PU [29], polyurethane (PUR) [30], double walled – polyurea/melamine-formaldehyde (PU/MF) [31], polyurethane/urea-formaldehyde (PUR/UF) [32], or even biodegradable shell from polycaprolactone (PCL) [33]. In the referenced studies, microcapsules demonstrated variations in mechanical properties alongside differences in size, shell thickness, porosity and structure. Attaei et al. [29] described a synthesis technique for producing PU microcapsules using Desmodur RFE containing tris(p-isocyanatophenyl) thiophosphante (TIPTP) at 27 wt.% in ethyl acetate, IPDI and diethylenetriamine (DETA). PU microcapsules typically exhibited an average diameter of 10 μm with a shell thickness of 1.5 μm, presenting a smooth, nearly spherical morphology. Kardar et al. [30] investigated microcapsules with PUR shell material derived from various polyols. Morphological analysis revealed that the capsules synthesised using glycerol exhibited a wrinkled outer surface compared to those synthesised using 1,4-butanediol and 1,6-hexanediol. To enhance the mechanical properties of microcapsules, Du et al. [31] and Cruso et al. [32] developed microcapsules with a double shell. Double shell PU/MF microcapsules displayed elastomeric characteristics under small deformations (5.06%) and could recover after the applied force. However, under conditions of larger deformation (>14.53%), the microcapsules exhibited a viscoelastic behaviour and could not recover. In the case of PUR microcapsules coated with a second layer of UF, TGA indicated improved thermal stability compared to single-wall microcapsules.

Several methods can be employed to create microcapsules for self-healing coatings including in situ polymerisation [34, 35], interfacial polymerisation [36–38], the solvent evaporation method [33, 39] and spray drying [40, 41]. In situ polymerisation and interfacial polymerisation are methods most commonly used in production of self-healing coating microcapsules from UF, MF, PU, PUR and others mainly due to the high active ingredient loading, moderately fast reaction, high yield and controllable synthesis process [42]. In comparison, the solvent evaporation technique usually tends to have lower active ingredient loading, lower yield, and thicker microcapsule shell formation [39, 42], although it can form more durable and more chemically resistant shells made from PCL [33] or with better interfacial interaction made from poly(methyl methacrylate) (PMMA) [18].

The purpose of the present study was to improve the process of microencapsulation of IPDI by interfacial polymerisation into a PU shell reaching a very high IPDI core content (Scheme 1). Another objective was optimisation of the microencapsulation process using the Taguchi's L16 parameter design approach enabling to find optimal parameters ensuring the maximal core content and, at the same, the formation of microcapsules with a size of 50 μm.

EXPERIMENTAL

MATERIAL AND METHODS

Isophorone diisocyanate (IPDI, NCO content 37.5%) and polyisocyanate under commercial name Desmodur RFE (27% solution of tris(4-isocyanato phenyl)thiophosphate (TIPTP) in ethyl acetate, NCO content of 7.2%) were supplied by Covestro AG. Triethylenetetramine (TETA)

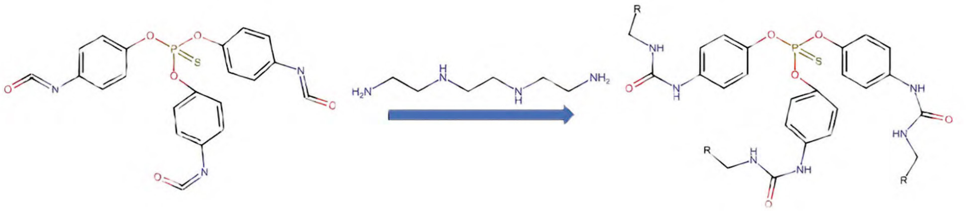

Scheme 1. Chemical reaction between TIPTP and TETA that leads to formation of PU microcapsule shells

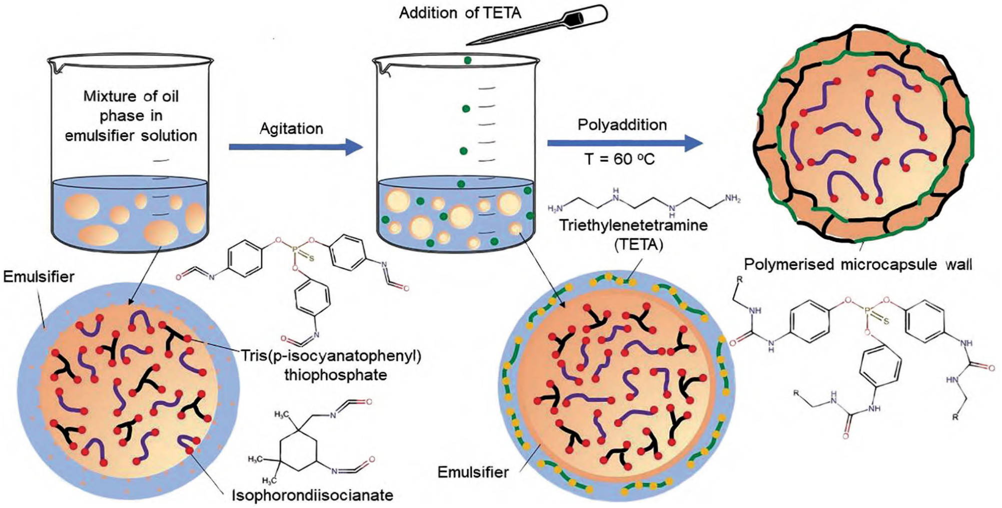

Scheme 2. Schematic representation of IPDI encapsulation into PU shell

was supplied by Huntsman. Sodium dodecylbenzenesulfonate (SDBS) was acquired from Eurochemicals. Gum Arabic (GA) was purchased from Thermo Fisher Scientific, while polyvinyl alcohol (PVA, deacetylation degree 85%) was obtained from Sigma-Aldrich.

Encapsulation of IPDI into PU shell

An example of the encapsulation of IPDI into a PU shell (experiment No. IE1)

The solution of the emulsifiers PVA 2%/GA 3% was prepared by dissolving PVA (3 g) and GA (4.5 g) in deionized water (142.5 g) and stirring overnight. The oil phase was prepared by mixing IPDI (13.3 g) with the solution of Desmodur RFE (15.6 g). The oil phase (28.9 g) was then added to the emulsifier solution (150 g) and stirred at 3000 rpm for 5 min. The resulting emulsion was set to stir at the constant speed of 1000 rpm while the temperature was increased up to 60°C. When the temperature reached the intended value, TETA was slowly added to the emulsion, and the emulsion was stirred at 1000 rpm for 30 min. To remove unreacted materials, the obtained microcapsules were washed with deionized water 4–5 times. Finally, the microcapsules were separated by freeze-drying at −55°C and 0.2 mbar.

Characterisation of microcapsules

The assessment of average microcapsule size, size distribution, and stability was conducted using an optical microscope Nikon Eclipse LV100ND. Further characterisation of microcapsule size, morphology and rupture was performed utilising a scanning electron microscope (SEM) Hitachi TM3000. The analysis of the microcapsules using FT-IR spectra within a range of 550–4000 cm^{-1} was carried out by a Jasco FT-IR 4600 spectrometer. The determination of the isophorone diisocyanate (IPDI) content within the microcapsules was executed through thermogravimetric analysis (TGA) using a Hitachi STA200 instrument. The TGA involved a heating rate of 40°C/min until reaching 150°C, followed by 10°C/min until 550°C, all under a nitrogen gas flow.

Design of experiment by Taguchi method

In the preliminary investigation it was identified that four pivotal parameters have the biggest potential to influence the core content, size of microcapsules and microcapsule yield. These parameters are the core-to-shell ratio, agitation speed, type and quantity of emulsifier, and reaction time. The chosen parameters and their respective levels are given in Table 1, with the range of levels determined through preliminary experimental assessments.

Table 1. **Taguchi design parameters and their selected levels**

Parameter, units	Levels			
	1	2	3	4
Core-to-shell ratio	2:1	3:1	4:1	5:1
Agitation speed, rpm	3000	4000	5000	6000
Emulsifier and its concentration, %	PVA 2/GA 3	PVA 1/GA 1.5	SDBS 1	GA 7
Reaction time, min	30	45	60	90

In this study, the Taguchi design methodology was employed to find the optimal process parameters using signal-to-noise ratio (SNR) analysis [43, 44]. The larger-the-better criterion (Eq. 1) was applied to discern the optimal conditions for attaining the maximum core content of the microcapsules and the highest reaction yield. Simultaneously, the nominal-the-best criterion (Eq. 2) was utilised to identify conditions conducive to the production of microcapsules with a size of 50 µm:

$$\frac{S}{N} = -10 \cdot \log\left(\frac{1}{n}\sum\frac{1}{y^2}\right) \qquad \frac{S}{N} = -10 \cdot \log\frac{\overline{y}^2}{s^2}.$$

Larger-the-better Nominal-the-best

In the equations, y represents the measured value of the core content (%) or the microcapsule average size (µm), n is the number of measurements in a trial, and s is the nominal value.

RESULTS AND DISCUSSION

Encapsulation of IPDI into PU shell

The encapsulation process was studied using the L16 Taguchi method matrix, where 4 chosen parameters were changed throughout the synthesis. Three different signals were received and measured – the content of the healing agent IPDI inside microcapsules (core content), the microcapsule size and the microcapsule yield. Synthesis parameters and the signals are given in Table 2.

It was determined that some microcapsules tend to agglomerate more than others. During freeze-drying, which proceeds under deep vacuum, some microcapsules with thin or defectively formed shells were deformed and even ruptured.

Table 2. **Data of microencapsulation of IPDI into PU shell**

No.	Core: shell	Agitation speed, rpm	Emulsifier and its concentration, %	Reaction time, min	Core content, %	Microcapsule size range, µm	Average microcapsule size, µm	Microcapsule yield, %
IE1	2:1	3000	PVA 2/GA 3	30	58.9	20–90	35	36.7
IE2	3:1	4000	PVA 1/GA 1.5	45	64.1	20–90	45	58.9
IE3	4:1	5000	SDBS 1	60	72.3	10–40	20	74.3
IE4	5:1	6000	GA 7	90	78.6	20–90	60	26.9
IE5	2:1	4000	SDBS 1	90	52.2	10–20	10	84.3
IE6	3:1	5000	GA 7	30	61.7	15–110	60	56.0
IE7	4:1	6000	PVA 2/GA 3	45	74.6	8–20	15	25.2
IE8	5:1	3000	PVA 1/GA 1.5	60	76.1	30–120	80	32.6
IE9	2:1	5000	PVA 2/GA 3	60	58.3	10–40	35	6.5
IE10	3:1	6000	PVA 1/GA 1.5	90	65.8	20–60	40	12.6
IE11	4:1	3000	SDBS 1	30	66.4	10–60	25	6.0
IE12	5:1	4000	GA 7	45	69.7	30–60	50	29.4
IE13	2:1	6000	SDBS 1	45	49.9	10.0–20	10	71.5
IE14	3:1	3000	GA 7	60	74.6	20–70	50	48.9
IE15	4:1	4000	PVA 2/GA 3	90	71.8	20–70	40	16.8
IE16	5:1	5000	PVA 1/GA 1.5	30	73.1	20–80	40	19.3

After the rupture, the core content of the microcapsules was released and spread among other microcapsules which invoked sticking them together and agglomerating. Agglomeration can also be caused by an unsuitable emulsifier chosen for the system. It was determined that the microcapsules obtained in the presence of SDBS as an emulsifier had higher tendency to agglomerate than those obtained using GA or PVA/GA solutions (Table 3). Moreover, using 1% SDBS as an emulsifier led to the smallest microcapsule size. It is known that small particles have a higher tendency to agglomeration which leads to formation of much larger aggregates [45].

Characterisation of the prepared microcapsules

The prepared microcapsules were analysed using optical microscopy and scanning electron microscopy to evaluate the microcapsule size, size distribution, stability in an aqueous solution and in a dry state, and resistance to rupture under applied force (Figs 1, 2).

It was determined by optical microscopy that the microcapsules synthesised in the presence of 1% SDBS as emulsifier were agglomerated both in water and when dried. The agglomerates measured 300–1000 μm in size were made up from 10–60 μm microcapsules stuck together and remained agglomerated even after washing and freeze-drying. In contrast, the microcapsules synthesised using GA and GA/PVA as emulsifiers were stable, round and dispersed evenly. When pressed between two glass panels, the microcapsules underwent collapse, and the subsequently released healing agent was observed between the glass panels. This observation signifies a high efficiency in the encapsulation of the healing agent and suggests the presence of thin microcapsule walls that can be easily damaged.

Scanning electron microscopy (SEM) was used to measure the microcapsule size as well as visualise their surface and form, and determine the approximate thickness of microcapsule shell (Fig. 2). Before the experiment, some microcapsules were crushed using a metal spatula to examine the rupture picture and microcapsule shell thickness. As it is seen from the SEM images, the microcapsule surface is smooth with slight indentations which could be caused by freeze-drying process. It was determined that the microcapsule shell was very thin, with the thickness of about 1–3 μm, that is why it can be easily crushed.

Microcapsules IE8 were added to polyaspartic acid ester/isocyanate through the coating which was cured. The clear coating was examined with an optical microscope trying to determine

Table 3. **Stability of the synthesised microcapsules**

No.	Emulsifier/concentration, %	Stability in solution	Stability after drying	Microcapsule size range, μm	Average microcapsule size, μm
IE1	PVA 2/GA 3	Stable	Stable	20–90	35
IE2	PVA 1/GA 1.5	Stable	Stable	20–90	45
IE3	SDBS 1	Agglomerated	Agglomerated	10–40	20
IE4	GA 7	Stable	Stable	20–90	60
IE5	SDBS 1	Agglomerated	Agglomerated	10–20	10
IE6	GA 7	Stable	Stable	15–110	60
IE7	PVA 2/GA 3	Stable	Stable	8–20	15
IE8	PVA 1/GA 1.5	Stable	Stable	30–120	80
IE9	PVA 2/GA 3	Stable	Stable	10–40	35
IE10	PVA 1/GA 1.5	Stable	Stable	20–60	40
IE11	SDBS 1	Agglomerated	Agglomerated	10–60	25
IE12	GA 7	Stable	Stable	30–60	50
IE13	SDBS 1	Agglomerated	Agglomerated	10–20	10
IE14	GA 7	Stable	Stable	20–70	50
IE15	PVA 2/GA 3	Stable	Stable	20–70	40
IE16	PVA 1/GA 1.5	Stable	Agglomerated	20–80	40

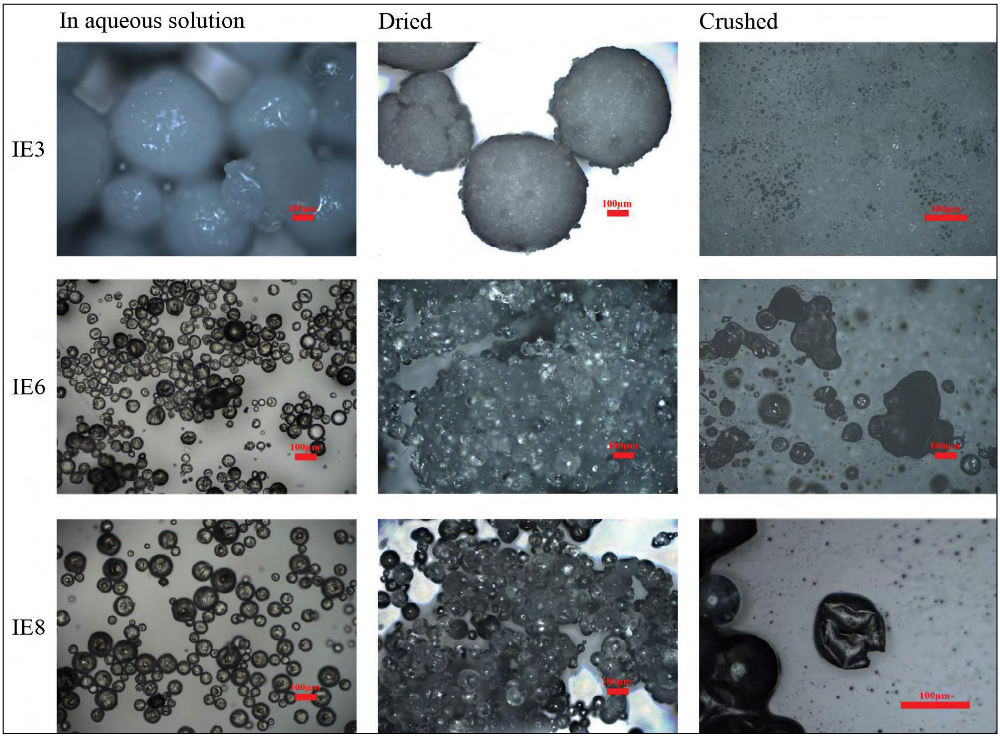

Fig. 1. Optical microscope images of the microcapsules IE3, IE6 and IE8

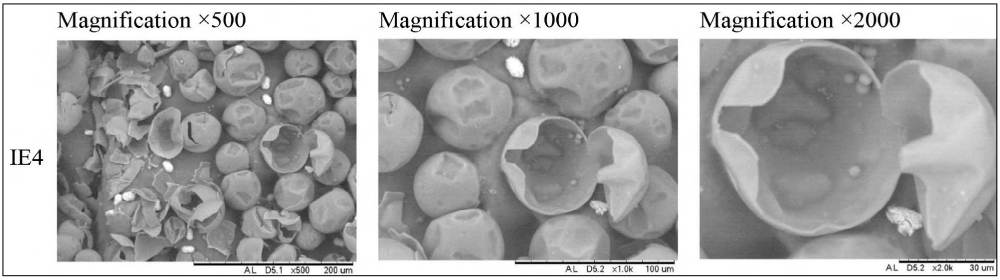

Fig. 2. SEM images of the crushed microcapsules IE4

microcapsule dispersibility inside the coating as well as microcapsule ability to rupture when a crack appears (Fig. 3).

The microcapsules inside the cured coating were dispersed evenly and did not agglomerate or rupture. The crosscut of coating showed that microcapsules were conjugated with the coating and split in two parts when the coating was broken. A part of the healing agent is seen near the rupture place as oil splatter (Fig. 3).

FTIR spectra of IPDI (core material), RFE+TETA (cured shell material) and microcapsules IE14 were recorded and presented in Fig. 4. The absorption band of the stretching vibrations of N–H at about 3350 cm^{-1} and the absorption bands of C=O and N–H in the carbamide group

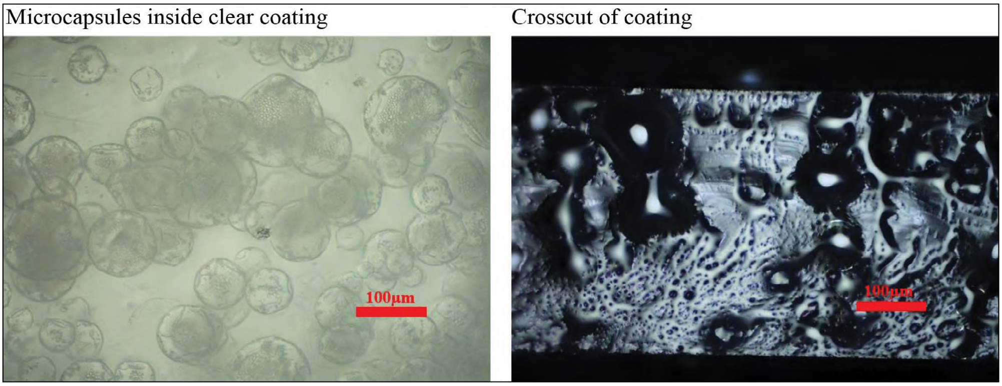

Fig. 3. Optical microscope images of microcapsules IE8 inside a clear coating and a coating crosscut

at about 1510 and 1650 cm^{-1}, respectively, are characteristic of PU shell material and are seen in the spectra of the shell material and microcapsule. An intensive absorption band of the stretching vibrations of N=C=O in isocyanate groups appears at about 2250 cm^{-1} in both spectra of IPDI and microcapsules IE14; this proves that the encapsulation of IPDI as core material was successful.

For the determination of core content in microcapsules, the thermogravimetric analysis (TGA) of the core material and microcapsules was done (Fig. 5). IPDI evaporation and destruction

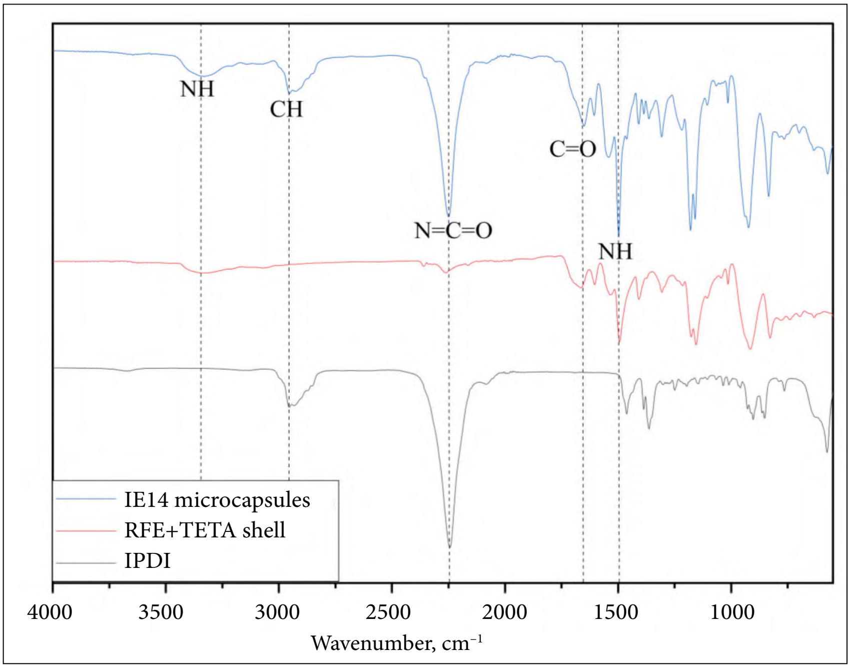

Fig. 4. FTIR spectra of IPDI as core material, RFE+TETA as microcapsule shell, and microcapsules IE14

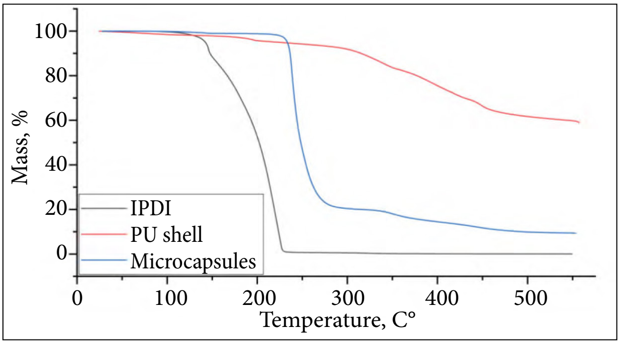

Fig. 5. TGA curves of the core material IPDI, shell material PU and microcapsules IE4

start at about 130°C and continues until approx. 240°C. The first stage of degradation of the shell material PU starts at about 150°C and lasts until 200°C; this part of degradation could be attributed to the destruction of unreacted shell material TETA, TIPTP and the evaporation of ethyl acetate. The actual destruction of PU starts at about 250°C and lasts until 550°C and even further. The microcapsule IE 4 analysis demonstrates that 79% of the microcapsule materials are destroyed at temperatures below 300°C. This part of the weight loss could be contributed to IPDI. Slightly higher destruction temperature of IPDI in microcapsules is expected since IPDI is entrapped inside a PU shell, and destruction can only begin when the shell is damaged by rising pressure inside the microcapsule or under degradation. The core content of the microcapsules was in a range of 50 to 79%.

Optimisation of the encapsulation process

The Taguchi method was employed in this study to identify the optimal parameters to achieve the highest core content, a microcapsule size closest to 50 μm, and the maximum microcapsule yield. Four distinct synthesis parameters, namely the core-to-shell ratio, agitation speed, emulsifier type and concentration, and reaction time, were systematically varied throughout the experimental process. The signal-to-noise ratio (SNR) was calculated using the larger-the-better criterion to discern optimal conditions for the core content and yield, while the nominal-the-best criterion was applied for the optimisation of microcapsule size. The results are summarised in Fig. 6.

The highest SNR value and significantly higher core content (Fig. 6a) were achieved using the core-to-shell ratio 5:1. The agitation speed had a small impact to the core content, but the best results were at the agitation speed 3000 rpm. Three emulsifiers – PVA 1%/GA 1.5%, PVA 2%/GA 3% and GA 7% – had a similar impact on the core content with a small superiority of GA 7%; anionic emulsifier SDBS was not suitable in achieving a high core content. The reaction time also had a rather small impact to the core content, although the highest core content was at the reaction time 60 min. Considering four key parameters, the core-to-shell ratio and the choice of emulsifiers had the highest impact on the microcapsule core content (Fig. 7).

The optimal microcapsule size closest to 50 μm (Fig. 6b) was achieved at various combinations of the reaction parameters. Considering the core-to-shell ratio, the optimal microcapsule size was at the ratio 3:1 and 5:1; at the ratio 2:1 and 4:1, the microcapsules tended to be either too large or too small. The agitation speed had lower impact on the microcapsule size while the optimal microcapsule size was at the agitation speed 4000 rpm. The emulsifier had a strong impact on the microcapsule size. Microcapsules of the optimal size were preferentially formed in the presence of GA 7% as an emulsifier. SDBS was not suitable as an emulsifier since it promoted agglomeration of the microcapsules. The reaction time had a minimal impact on the microcapsule size, but the optimal time was 45 min. Considering the four reaction parameters, the choice of emulsifiers and the core-to-shell ratio had the highest impact on the microcapsule size (Fig. 6).

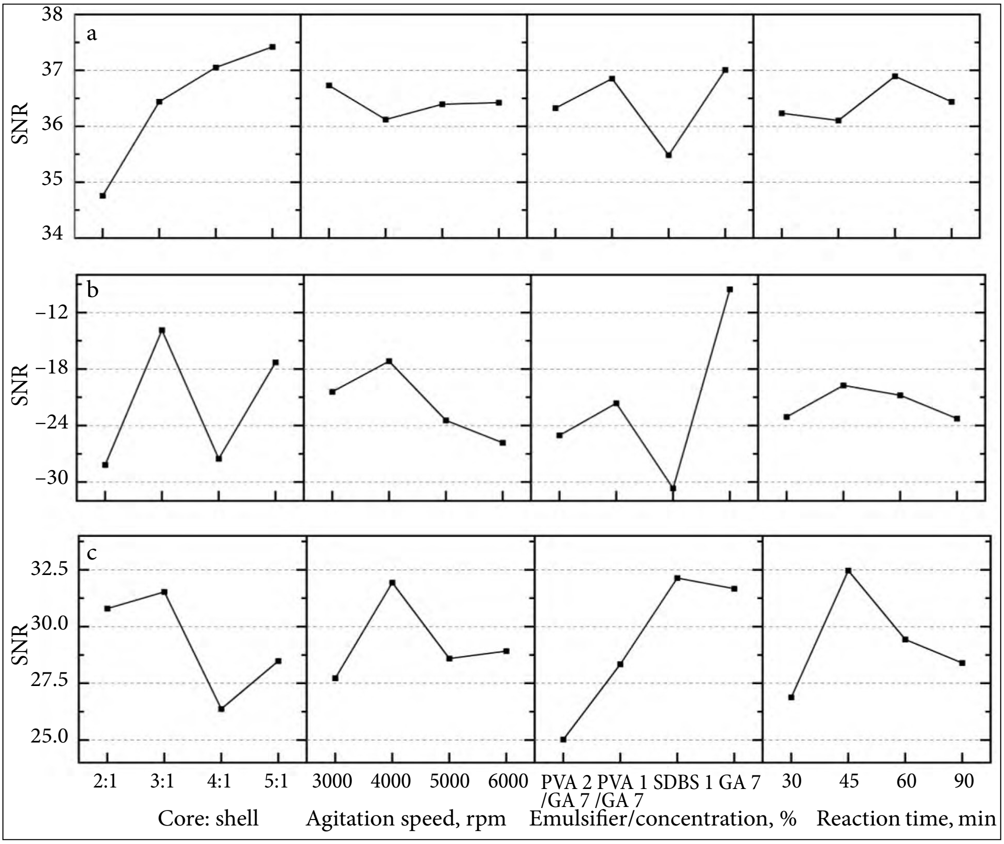

Fig. 6. SNR plots according to the Taguchi method; the dependence of the microcapsule core content (a), microcapsule size (b) and microcapsule yield (c) on the microencapsulation parameters: core-to-shell ratio, agitation speed, type and concentration of emulsifier, and reaction time

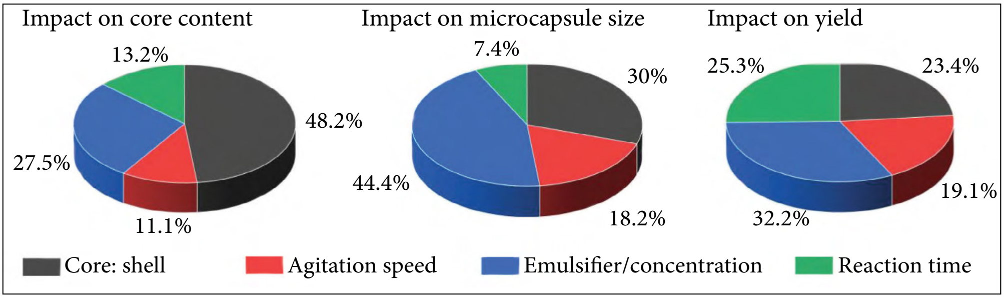

Fig. 7. Impact of the reaction parameters on the microcapsule core content, size and yield

The highest yield of microcapsules (Fig. 6c) was obtained at the core-to-shell ratio 3:1; the ratio 4:1 was the most unfavourable. The optimal agitation speed regarding yield was 4000 rpm. The optimal emulsifier promoting the highest yield of microcapsules was SDBS 1%. Possibly, this could be explained by agglomeration of microcapsules in the presence of SDBS, since losses of large agglomerates during washing and drying processes are minimal. The highest yield was achieved at the reaction time 45 min. The impact of the four parameters on the yield of microcapsules was similar (Fig. 7), moreover, the yield is very much dependent on the time given for the microcapsules to settle before they are separated from liquid after washing. Optimal conditions for the microencapsulation of IPDI in the PU shell regarding the highest core content, optimal microcapsule size of 50 μm and the highest yield include the core-to-shell ratio 3:1, the agitation speed 3000 rpm, Gum Arabic (7%) as an emulsifier and the reaction time 60 min.

CONCLUSIONS

Microencapsulation of IPDI into a PU shell was done by oil-in-water emulsion interfacial polymerisation. The microencapsulation process was optimised using the Taguchi L16 parameter design with four chosen parameters – core-to-shell ratio, agitation speed, emulsifier/concentration and reaction time – and three signals – core content, microcapsule size and reaction yield. Optimal conditions for the microencapsulation of IPDI into the PU shell regarding the highest core content, optimal microcapsule size of 50 μm and the highest yield include the core-to-shell ratio 3:1, the agitation speed 3000 rpm, Gum Arabic (7%) as an emulsifier and the reaction time 60 min. Under optimal conditions, the IPDI core content within the microcapsules was up to 75% and the microcapsule yield was up to 49%. The Taguchi's experimental design enabled the efficient optimisation of the IPDI microencapsulation process with a reduced number of experiments. The synthesised IPDI microcapsules could potentially be used in self-healing coatings, whether in single or double capsule systems.

Received 5 July 2024
Accepted 30 August 2024

References

1. Y. Zhao, W. Zhang, L. Liao, S. Wang, W. Li, *Appl. Surf. Sci.*, **258(6)**, 1915 (2012).
2. X. Liu, H. Zhang, J. Wang, Z. Wang, S. Wang, *Surf. Coat. Tech.*, **206(23)**, 4976 (2012).
3. C. Zhang, H. Wang, Q. Zhou, *Prog. Org. Coat.*, **125**, 403 (2018).
4. D. Sun, H. Zhang, X. Tang, J. Yang., *Polymer*, **91**, 33 (2016).
5. T. Siva, S. Sathiyanarayanan, *Prog. Org. Coat.*, **82**, 57 (2015).
6. Y. Jialan, Y. Chenpeng, Z. Chengfei, H. Baoqing, *Prog. Org. Coat*, **132**, 440 (2019).
7. F. Safaei, S. N. Khorasani, H. Rahnama, R. E. Neisiany, M. S. Koochaki, *Prog. Org. Coat*, **114**, 40 (2018).
8. S. Parsaee, S. M. Mirabedini, R. Farnood, F. Alizadegan, *J. Appl. Polym. Sci.*, **137(41)**, 49663 (2020).
9. H. Yi, Y. Deng, C. Wang, *Compos. Sci. Technol.*, **133**, 51 (2016).
10. H. Jin, C. L. Mangun, D. S. Stradley, J. S. Moore, N. R. Sottos, S. R. White, *Polymer*, **53(2)**, 581 (2012).
11. D. Sun, Y. B. Chong, K. Chen, J. Yang, *Chem. Eng. J.*, **346**, 289 (2018).
12. H. Li, X. Wang, *Polymer*, **262**, 125478 (2022).
13. E. Koh, N. Kim, J. Shin, Y. Kim, *RSC Adv.*, **4(31)**, 16214 (2014).
14. M. Huang, J. Yang, *J. Mater. Chem.*, **21(30)**, 11123 (2011).
15. S. V. Karpov, V. P. Lodygina, V. V. Komratova, A. S. Dzhalmukhanova, G. V. Malkov, E. R. Badamshina, *Kinet. Catal.*, **57(4)**, 422 (2016).
16. S. Lang, Q. Zhou, *Prog. Org. Coat*, **105**, 99 (2017).
17. J. Li, H. Shi, F. Liu, E. Han, *Prog. Org. Coat*, **156**, 106236 (2021).
18. A. H. Navarchian, N. Najafipoor, F. Ahangaran, *Prog. Org. Coat*, **132**, 288 (2019).
19. H. Choe, J. H. Kim, *J. Ind. Eng. Chem.*, **69**, 153 (2018).
20. S. M. Hasan, J. E. Raymond, T. S. Wilson, B. K. Keller, D. J. Maitland, *Macromol. Chem. Phys.*, **215(24)**, 2420 (2014).
21. R. Heath, *R. Brydson's Plastics Materials*, 799 (2017).
22. M. Ates, S. Karadag, A. A. Eker, B. Eker, *Polym. Int.*, **71(10)**, 1157 (2022).
23. V. V. Gite, P. P. Mahulikar, D. G. Hundiwale, *Prog. Org. Coat*, **68(4)**, 307 (2010).
24. E. Spyrou, H. Metternich, R. Franke, *Prog. Org. Coat*, **48(2)**, 201 (2003).
25. C. Yu, M. Salzano de Luna, A. Russo, et al., *Adv. Mater. Interfaces*, **8(10)**, 2100117 (2021).
26. Y. Wei, X. Jiang, S. Li, X. Z. Kong, *Eur. Polym. J.*, **115**, 384 (2019).
27. M. Guo, W. Li, N. Han, et al., *Polymers*, **10(3)**, 319 (2018).
28. S. V. Karpov, V. P. Lodygina, V. V. Komratova, A. S. Dzhalmukhanova, G. V. Malkov, E. R. Badamshina, *Kinet. Catal.*, **57(3)**, 319 (2016).
29. M. Attaei, L. M. Calado, M. G. Taryba, et al., *Prog. Org. Coat*, **139**, 105445 (2019).

30. P. Kardar, *Prog. Org. Coat*, **89**, 271 (2015).
31. G. Du, J. Hu, J. Zhou, et al., *Chin. J. Chem. Eng.*, **28(5)**, 1459 (2020).
32. M. M. Caruso, B. J. Blaiszik, H. Jin, et al., *ACS Appl. Mater. Interfaces*, **2(4)**, 1195 (2010).
33. M. V. Loureiro, M. Vale, R. Galhano, S. Matos, J. C. Bordado, I. Pinho, A. C. Marques, *ACS Appl. Polym. Mater*. **2(11)**, 4425 (2020).
34. E. Katoueizadeh, S. M. Zebarjad, K. Janghorban, *J. Mater. Res. Technol.*, **8(1)**, 541 (2018).
35. H. Zhang, W. Li, R. Huang, N. Wang, J. Wang, X. Zhang, *New J. Chem.*, **41(23)**, 14696 (2017).
36. X. Ji, J. Li, W. Hua, Y. Hu, B. Si, B. Chen, *Constr. Build. Mater*, **289**, 123179 (2021).
37. F. Yu, Y. Wang, Y. Zhao, J. Chou, X. Li, *Materials*, **14(13)**, 3753 (2021).
38. F. Ricardo, D. Pradilla, R. Luiz, O. A. Solano, *Polymers*, **13(4)**, 644 (2021).
39. J. Fan, Y. Zheng, Y. Xie, et al., *Compos. Sci. Technol.*, **138**, 80 (2017).
40. E. Assadpour, S. M. Jafari, *Annu. Rev. Food Sci. Technol.*, **10(1)**, 103 (2019).
41. S. Shamaei, S. S. Seiiedlou, M. Aghbashlo, E. Tsotsas, A. Kharaghani, *Innov. Food Sci. Emerg. Technol.*, **39**, 101 (2017).
42. D. Y. Zhu, M. Z. Rong, M. Q. Zhang, *Prog. Polym. Sci.*, **49–50**, 175 (2015).
43. Ç. Özada, M. Ünal, E. K. Şahin, H. Özer, A. R. Motorcu, M. Yazıcı, *Multidiscip. Model. Mater. Struct.*, **18(6)**, 1049 (2022).
44. A. N. Mustapha, Y. Zhang, Z. Zhang, Y. Ding, Q. Yuan, Y. Li, *J. Mater. Res. Technol.*, **11**, 667 (2021).
45. T. Ogholaja, D. O. Njobuenwu, M. Fairweather, *Proceedings of ESCAPE-27*, 79 (2017).

Liepa Pastarnokienė, Ernest Potapov, Ričardas Makuška, Tatjana Kochanė

IZOFORONO DIIZOCIANATO ĮKAPSULIAVIMO Į POLIKARBAMIDO APVALKALĄ, NAUDOJANT TARPFAZINĘ POLIMERIZACIJĄ, OPTIMIZAVIMAS

Santrauka

Mikrokapsulės, sudarytos iš įkapsuliuoto izoforono diizocianato (IPDI) ir polikarbamido (PU) apvalkalo, buvo gautos tarpfazinės polimerizacijos metodu kaip reagentus naudojant tris(4-izocianatofenil)tiofosfatą (TIPTP) ir trietilentetraminą (TETA). Mikrokapsulės buvo apibūdintos naudojant FTIR spektroskopiją, termogravimetrinę analizę (TGA), optinę mikroskopiją ir skenuojančią elektroninę mikroskopiją (SEM). Vykdant mikrokapsuliavimą buvo sistemingai keturiais lygiais keičiami didžiausią įtaką procesui turintys parametrai, tokie kaip įkapsuliuojamos medžiagos ir apvalkalo santykis, maišymo greitis, emulsiklio tipas ir koncentracija bei reakcijos trukmė. Siekiant gauti maksimalų rezultatą – didžiausią santykinę įkapsuliuotos medžiagos dalį mikrokapsulėse ir didžiausią mikrokapsulių išeigą, išlaikant tikslinį 50 µm mikrokapsulių skersmenį, – mikrokapsuliavimo procesas buvo optimizuotas naudojant Taguchi metodą L16 parametrų. Mikrokapsuliavimą vykdant optimaliomis sąlygomis, IPDI kiekis mikrokapsulėse siekė 75 %, o mikrokapsulių išeiga – 49 %.

Vilnius University Press
Saulėtekio Ave. 9, Building III, LT-10222 Vilnius
Email: info@leidykla.vu.lt, www.leidykla.vu.lt
bookshop.vu.lt, journals.vu.lt
Print run copies 20.